Cranfield University

Masoud Kavosh

Process engineering and development of post-combustion CO_2 separation from fuels using limestone in CaO-looping cycle

School of Applied Sciences
Centre for Energy and Resource Technology

PhD

Cranfield University

School of Applied Sciences
Centre for Energy and Resource Technology

PhD THESIS

2011

Masoud Kavosh

Process engineering and development of post-combustion CO_2 separation from fuels using limestone in CaO-looping cycle

Supervisor: Prof. John Oakey

Co-supervisor: Dr Kumar Patchigolla

Academic Year 2008 to 2011

This thesis is submitted in partial fulfilment of the requirements for the degree of PhD

ABSTRACT

Global CO_2 emissions produced by energy-related processes, mainly power plants, have increased rapidly in recent decades; and are widely accepted as the dominant contributor to the greenhouse gas (GHG) effect and consequent climate changes. Among countermeasures against the emissions, CO_2 capture and storage (CCS) is receiving much attention. Capture of CO_2 is the core step of CCS as it contributes around 75% of the overall cost, and may increase the production costs of electricity by over 50%. The reduction in capture costs is one of the most challenging issues in application of CCS to the energy industry. Using limestone in CaO-looping cycles is a promising capture technology to provide a cost-effective separation process to remove CO_2 content from power plants operations. Limestone has the advantage of being relatively abundant and cheap, and that has already been widely used as a sorbent for sulphur capture. However, this technology suffers from a critical challenge caused by the decay in the sorbent capture capacity during cyclic carbonation/calcination, which results in the need for more sorbent make-up; hence a reduction in cost efficiency of the technology. The performance of sorbent influenced by several operating and reaction conditions. Therefore, much research involves investigation of influencing factors and different methods to reduce the sorbent deactivation.

This project aimed at studying factors which influence the performance of limestone used for CO_2 capture purposes in a solid looping cycle separation process; in particular for coal-based post-combustion systems. A three-part experimental programme was carried out to investigate the effects of steam, SO_2, and pressurised calcination on cyclic calcination-carbonation of limestone, using bubbling fluidized bed reactor. The idea of co-capturing process of CO_2 and SO_2 has also been assessed.

In the first part, the results showed that steam-diluted calcination could enhance the capacity of sorbents to capture CO_2. In addition, steam-diluted calcination could result in energy saving in the separation process by lowering the reaction temperature. It seems that steam could be used to dilute the calciner atmosphere; particularly considering its ease of separation from CO_2 by condensation. The results of the carbonation step showed that increasing the steam percentage in the carbonation atmosphere improved the capture capacity of sorbents, which have been calcined in conditions with a lower steam dilution.

The results in the second part demonstrated that the presence of SO_2 in the calcination atmosphere reduces the CO_2 capture capacity of the CaO sorbent. Carbonation of CaO particles in the presence of SO_2 revealed that the ability of the sorbent to capture CO_2 decreased at a higher rate, proportional to the SO_2 concentration. The results did not support the use of the co-capture process, as the presence of SO_2 caused a decrease not only in CO_2 capture capacity but in total Ca-utilisation as well.

In the third part, the results indicated that carbonation conversions of calcined particles decrease significantly by increasing the level of pressure in calcination step. The results also demonstrated that pressurised calcination, which requires higher temperature and longer times than those for lower pressure, caused an increase in sorbent sintering; and consequently, reduced the capture capacity of sorbents.

Keywords:

CO_2 capture; CO_2 separation; Carbon capture and storage; Limestone; CaO-looping cycle; Calcination-carbonation; Global warming; Climate changes; Greenhouse gas emissions; fossil fuels

ACKNOWLEDGEMENTS

I am deeply grateful to my supervisor, Professor John Oakey, Head of Centre for Energy and Resources Technology (CERT). His wide knowledge, logical way of thinking and understanding has been of great value to me.

Sincere thanks to Dr Kumar Patchigolla for his kind assistance and helpful advice during the work.

I am also grateful to all members of staff and students at CERT for being supportive throughout the accomplishment of this task. My warm thanks go to engineers and technicians at CERT for their patience and kind support over my long time in the laboratory.

I would like to convey thanks to Cranfield University and EPSRC H2 Network for their financial support for this project.

I owe my loving thanks to my wife Farah, my daughters Newsha and Mojan for their continuous support and patience. They have lost a lot due to my research work. Without their encouragement and understanding it would have been impossible for me to finish this task.

TABLE OF CONTENTS

TABLE OF FIGURES

TABLE OF TABLES

LIST OF PUBLICATIONS

Journals:

Yongping Yang, Rongrong Zhai, Liqiang Duan, **Masoud Kavosh**, Kumar Patchigolla and John Oakey, Integration and evaluation of a power plant with a CaO-based CO_2 capture system. *International Journal of Greenhouse Gas Control*, Volume 4, Issue 4, July 2010, Pages 603-612.

Masoud Kavosh, Kumar Patchigolla, John Oakey. Investigation of CO_2 capture by limestone looping cycle with Steam-Diluting calcination and carbonation reactions *(ready to submit).*

Masoud Kavosh, Kumar Patchigolla, John Oakey. Performance of limestone looping cycles for CO_2 removal with SO_2 present in calcination and carbonation *(ready to submit).*

Masoud Kavosh, Kumar Patchigolla, John Oakey. Pressurised calcination in limestone looping cycle for CO_2 capture *(ready to submit).*

Conferences:

John Oakey, Rongrong Zhai, **Masoud Kavosh,** Kumar Patchigolla, and Paul Kilgallon. CO_2 capture research at Cranfield University. *1st Meeting of the High Temperature Solid Looping Cycles Network*, 15-17 September 2009 Oviedo, Spain.

Masoud Kavosh, Kumar Patchigolla, John Oakey. Efficient CO_2 capture by Ca-based sorbent with steam presence. *The 2nd Meeting on High Temperature Solid Looping Cycle,* September 15-17, Alkmaar, the Netherlands.

Masoud Kavosh, Kumar Patchigolla, John Oakey. Effect of SO_2 on Multi Cycle Carbonation-Calcination of Limestone for CO_2 Capture. *Fifth International Conference on Clean Coal Technologies*, 8-12 May 2011, Zaragoza, Spain.

Masoud Kavosh, Kumar Patchigolla, John Oakey. Effects of SO_2 and steam on limestone calcination-carbonation for CO_2 capture. *10th Annual conference on carbon capture and sequestration 2011*, May 2-5 2011, Pennsylvania, USA.

Alissa Cotton, Kumar Patchigolla, **Masoud Kavosh**, John Oakey. Engineering Issues for Carbon Capture via Calcium Looping in a 25 kW_{th} Reactor *Fifth International Conference on Clean Coal Technologies*, 8-12 May 2011, Zaragoza, Spain.

Alissa Cotton, Kumar Patchigolla, **Masoud Kavosh**, John Oakey. Calcium Looping Cycle Technology Developments at Cranfield University. *The 3rd Meeting on High Temperature Solid Looping Cycle,* August 30-31, Vienna University of Technology, Austria

ABBREVIATIONS

BET	Brunauer-Emmett-Teller
BJH	Barrett-Joyner-Halenda
CCS	CO_2 Capture and Storage
CLC	Chemical Looping Combustion
ESRL	Earth System Research Laboratory
FBC	Fluidised Bed Combustion
FBR	Fluidised Bed Reactor
FGD	Flue Gas Desulphurisation
GHG	Green House Gas
GTSP	Global Energy Technology and Strategy Programme
IEA	International Energy Agency
IGCC	Integrated Gasification Combined Cycle
IPCC	Intergovernmental Panel on Climate Change
MEA	Monoethaloamine
NGCC	Natural Gas Combined-Cycle
PC	Pulverised Coal
PF	Pulverised Fuel
PSA	Pressure Swing Adsorption
PTGA	Pressurised Thermogravimetric Analyses
SEM	Scanning Electron Microscopy
TGA	Thermogravimetric Analyses
TSA	Temperature Swing Adsorption
XRD	X-ray Diffraction

CHAPTER 1

Introduction

Chapter 1 : Introduction

1.1 CO_2 emissions and climate changes

Arrhenius's paper (1896) was the first study to quantify the contribution of CO_2 to the greenhouse effect, and its contribution to long-term climate changes. The growing trend of CO_2 concentration in the atmosphere subsequent to the industrial revolution, demonstrated in Figure 1.1, has changed the relatively balanced amount of carbon between the lithosphere, atmosphere and biosphere [1].

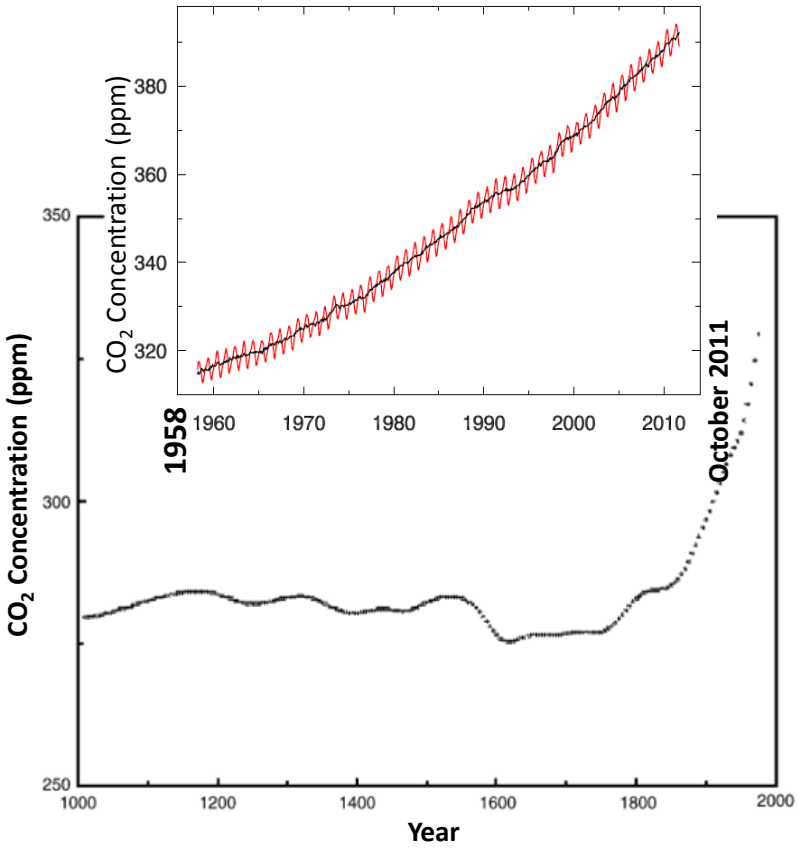

Figure 1.1: CO_2 concentrations in the atmosphere during 1000–2011 based on the analysis of ice cores and actual data logged. Red lines depict the monthly records; black lines show the seasonal corrected amounts by moving averages over seven month periods, centered by each month [2; 3].

Carbon dioxide is a naturally occurring gas that helps to keep the temperature agreeable on earth. In this role, CO_2 and other greenhouse gases (GHG), as a protecting layer, prevent most of the outgoing long-wave radiation from leaving earth's atmosphere. The problem that has been recognised in the past five decades is the increase in atmospheric of CO_2 levels, which is believed to cause global warming. Figure 1.1 shows the concentration of CO_2 in the atmosphere over the years between 1000 and 2011 (derived from: analysis of Antarctica ice core data for 1000-1958, and actual data logged in Hawaii after 1958). It reveals that atmospheric CO_2 levels increased from 280 ppm in 1000 to 295 ppm in 1900; then increased to 315 ppm in 1958, augmented to 377 ppm in 2004, and finally rose to more than 390 ppm by October 2011.

However, according to the trend of CO_2 and other GHG emissions, several projections for future climate changes have been presented. The International Panel on Climate Change (IPCC, 1995) predicted a rise in CO_2 concentrations in the atmosphere up to 570 ppmv by the year 2100, causing a mean global temperature rise of around 1.9°C and consequently an increase in mean sea level of 38 cm [4]. A later projection by IPCC, 2007 [5], predicts 1.1- 6.4°C increase in global temperature causing 18-59 cm raise in sea-level in the current century (both temperature and sea-level relative to 1980-1999). Recently, the Copenhagen Diagnosis (December 2009) [6], estimated that by 2100 the rise in global sea-levels is likely to be twice that projected by IPCC (2007); and even for unmitigated emissions the rise may well exceed 1 metre. Figure 1.2 shows these predictions for temperature (a), and sea-level (b).

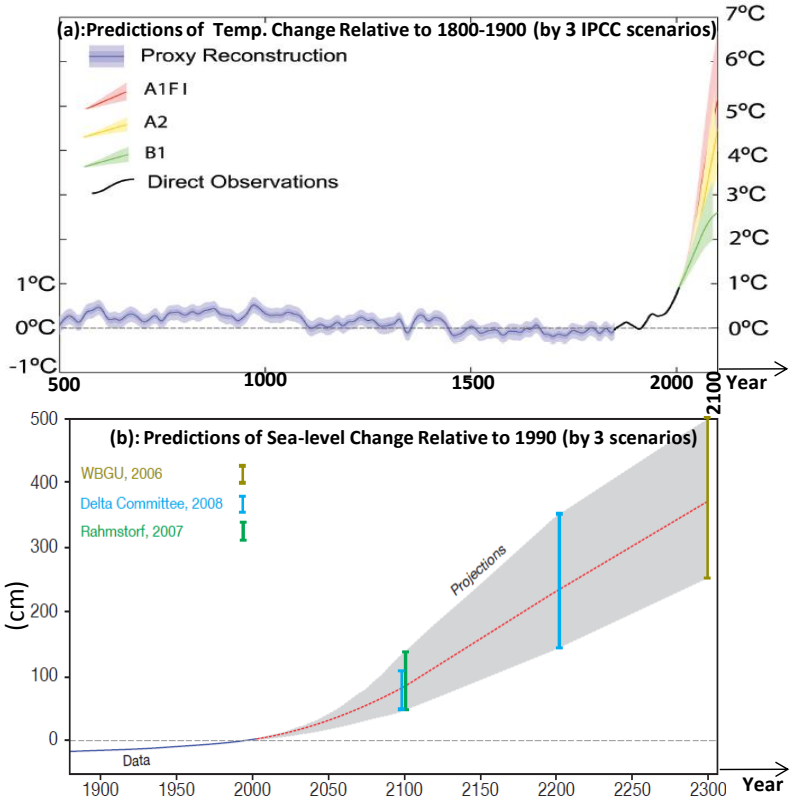

Figure 1.2: Predictions for changes in temperature by three IPCC (2007) scenarios (a), and for sea-level according to three different presented scenarios (b) [6].

The ranges of the presented projections exist due to the different scenarios for technologies, population, energy resources, and mitigation status over the estimation period.

Figure 1.3 presents the status of energy and CO_2 emissions, extracted from IEA-2011 statistics [7]. These data reveal that: **(a)** fossil-fuelled energy supply in 1971 doubled by 2009; **(b)** since 1870 CO_2 annual emissions have risen exponentially; **(c)** in developed countries, the energy sector is the source of 83% of GHGs, and CO_2 is the dominant contributor to anthropogenic GHG contributing 92%; **(d)** more than 40% of CO_2 is emitted by electricity and heat generation.

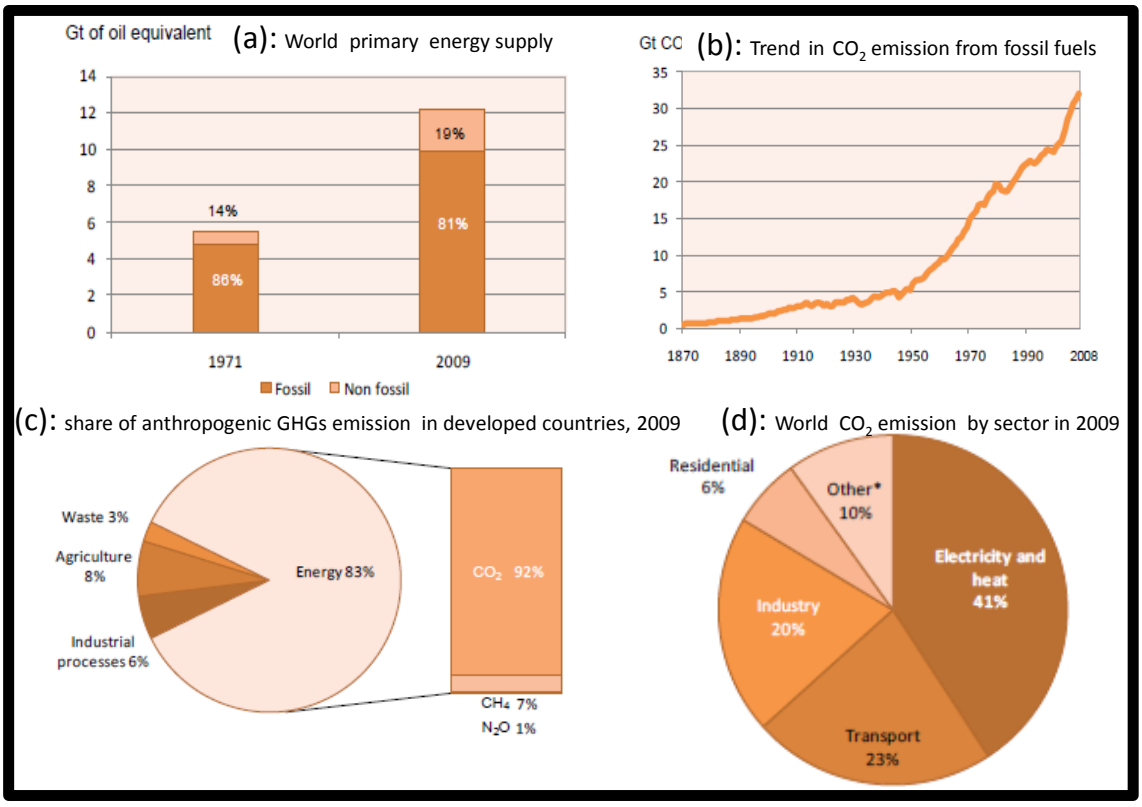

Figure 1.3: (a) world energy supply, **(b)** trend in CO_2 emission from fossil fuels, **(c)** share of GHGs emission in developed countries, **(d)** world CO_2 emissions by sector [7].

Furthermore, the fast rise in global population and the industrialisation of more countries will cause to an increase in energy needs. Currently, fossil fuels provide more than 85% of electricity to meet this growing demand [8]. EIA (U.S. Energy Information Administration) predicts that world energy consumption will also increase by 53% from 2008 to 2035 (EIA, 2011) [9]. Given this growing energy intensive lifestyle, the scale of the problem is evident.

To fight the subsequent global climate changes, mitigation strategies have been schemed targeting the actions of countries, through international agreements such as the Kyoto Protocol. It has been found necessary to develop cost-effective CO_2 mitigation systems to meet these intended schemes. The mitigation measures to reduce the total CO_2 emission into the atmosphere can be classified in three options: to reduce energy intensity, to reduce carbon intensity, and to enhance the capture and storage of CO_2. The first option requires improvement in energy efficiency, thus involves a long term development in energy technologies. The second option requires switching to less carbon-intensive (or non-fossil) fuels, such as nuclear and renewable energy sources, which is not economical since the current infrastructure is greatly dependant on plentiful and cheap fossil fuels. The third option involves the development of technologies to capture and store CO_2. Therefore, most mitigation scenarios project that fossil fuels will continue to be the dominant source of energy at least by the middle of the 21st century

[10]. As a result, in the interim phase to a low-carbon society following the first and/or second option, Carbon dioxide Capture and Storage (CCS) is receiving much attention to reduce CO_2 emissions.

1.2 CO_2 capture and storage (CCS)

CO_2 capture and storage (CCS) is a three-step process: (i) capture of CO_2 from industrial emissions before theses enter the atmosphere, and compression of the separated CO_2 to 110 bars; (ii) CO_2 transportation through pipeline or by tanker ships; (iii) and finally geological storage or other industrial application. Figure 1.4 illustrates the possible CCS systems including sources, transportation and storage options. Applying CCS concept, CO_2 can be captured from large point sources such as power plants, cement production, iron and steel industry, refineries, petrochemical industry, oil and gas processing.

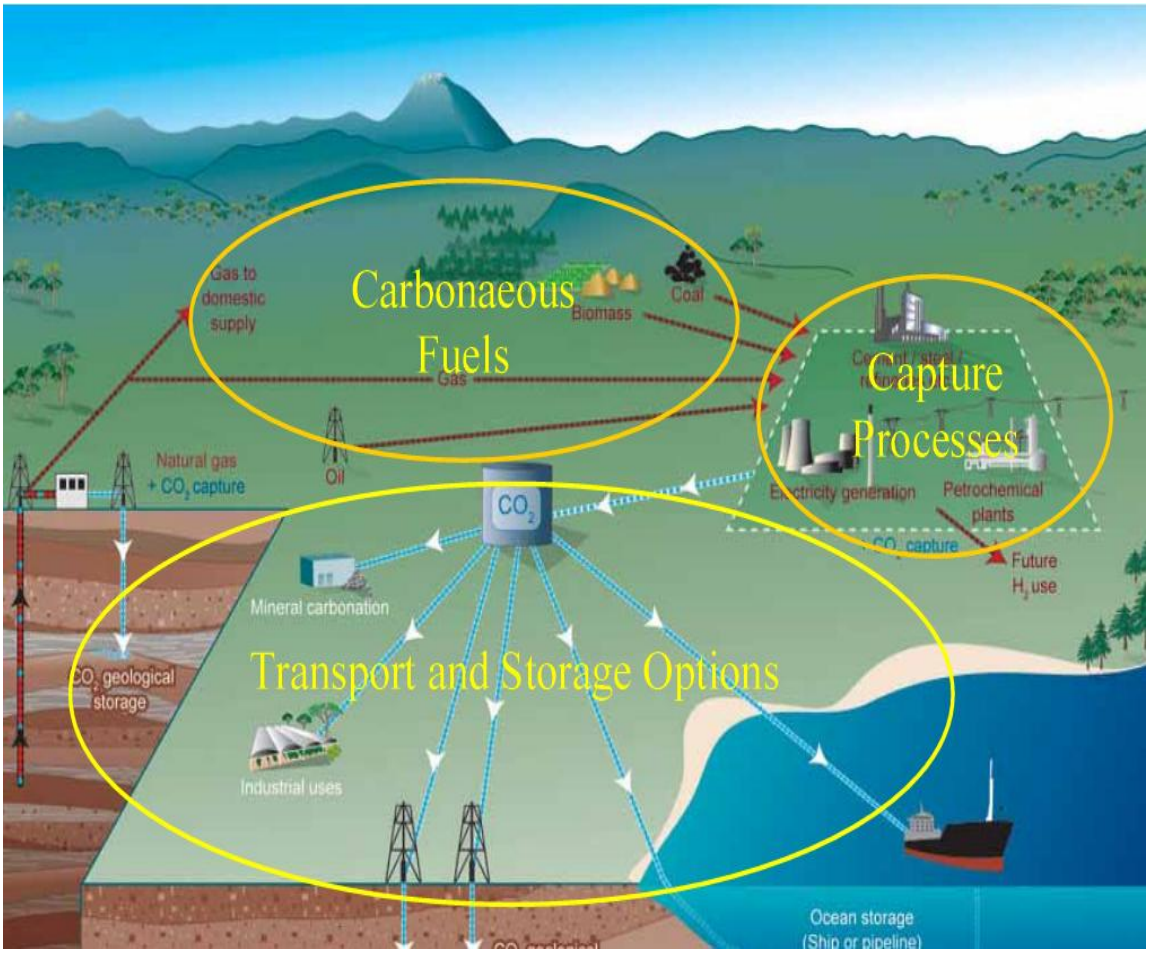

Figure 1.4: Schematic diagram of possible CCS systems [11].

Worldwide, there are about 8000 large point CO_2 emission sources, most of which are power plants [10; 12]. Large sources associate to points with CO_2 emission greater than 0.1 million ton per year. Table 1.1 presents the profile of these large stationary points by their processes [10].

Table 1.1: Worldwide large CO_2 sources with emissions of more than 0.1millione ton ($MtCO_2$)/year.

Process	**Number of sources**	**Emissions** ($MtCO_2\ yr^{-1}$)
Fossil Fuel		
Power plants	4,942	10,539
Cement production	1,175	932
Iron and steel industry	638	798
Refineries	269	646
Petrochemical industry	470	379
Oil and gas processing	Not available	50
Other sources	90	33
Biomass		
Bioethanol and bioenergy	303	91
Total	**7,887**	**13,466**

The above processes could conceivably adopt CCS technology to mitigate CO_2 emissions. However, the vast majority of these existing facilities have not adopted CCS systems.

1.3 CO_2 capture process systems

Three process pathways are proposed that can be practiced for CO_2 capture from large stationary emission sources. These consist of post-combustion process, pre-combustion process (or CO-shift, or water-gas shift), and oxy-fuel (or O_2/CO_2 firing, or denitrogenation process). A schematic of processes in these three methods is illustrated in Figure 1.5.

1.3.1 Post-combustion

This process system involves separation of CO_2 from the flue gases, after a normal combustion step, and just before they are vented to atmosphere. In general, after a normal combustion flue gases are at low pressure (1 bar), low CO_2-content (ranges 3-15% from natural gas combined cycle, NGCC, to coal-fired), containing a mixture of other gases such as nitrogen (about 80%), oxygen, and also impurities such as SO_x, NO_x and particulates [13];[14]. The impact of these impurities on CO_2 capturing performance needs to be taken into account as well. The great advantage with a post-combustion process is that the CO_2 separation equipment can be added to an existing coal-fired power generation or other industrial plants, which are considered as the main contributors to emissions. However, low CO_2 partial pressure in flue gases and the subsequent low thermodynamic driving force is a technical challenge for this system [15].

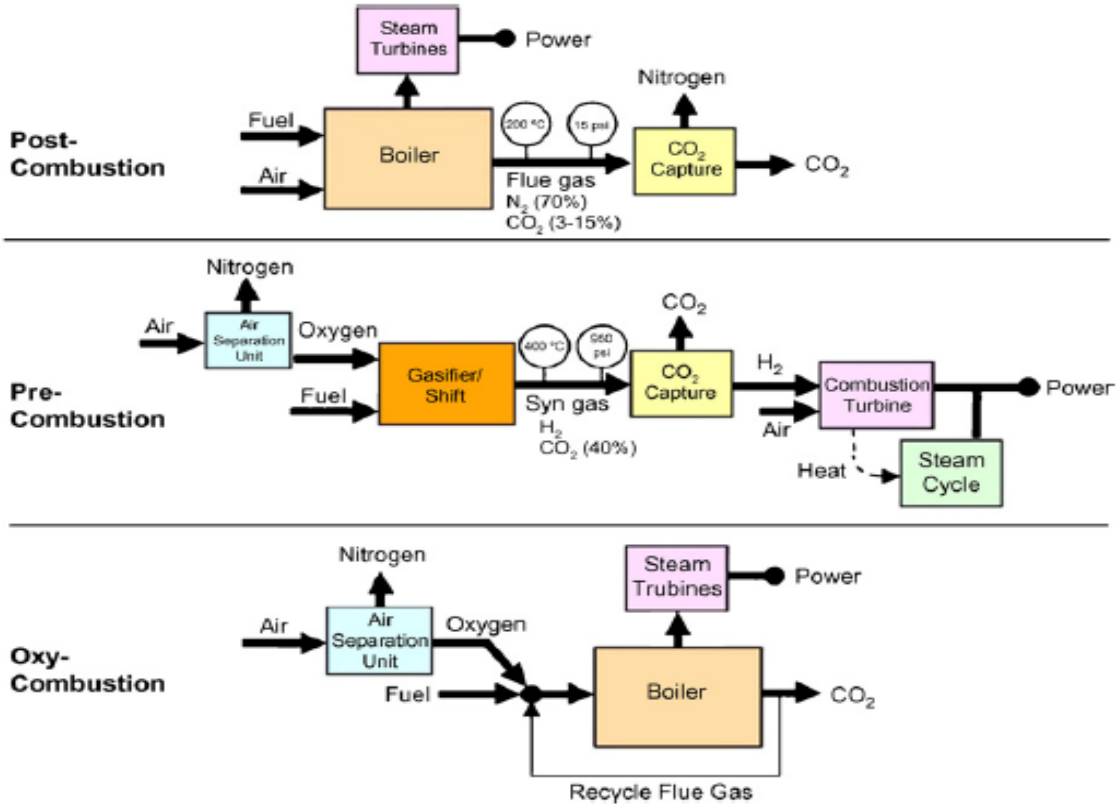

Figure 1.5: Block diagram demonstrating CO_2 capture process systems [15].

1.3.2 Pre-combustion

In pre-combustion or CO-shift process, CO_2 is captured from fuel before burning. Here prior to CO_2 capture, O_2 and usually some steam are used to convert the fuel to synthesis gas (syngas), which is a mixture of CO_2, CO, H_2O and H_2. The conversion takes place through partial combustion processes, namely gasification of coal, or reforming of oil and natural gas. This mixture is then converted to CO_2 and H_2 (as $CO+H_2O \leftrightarrow CO_2+H_2$) in a shift reactor. The converted mixture consists of H_2 and medium CO_2-content (15%-60% dry basis) at a high total pressure (20-70 bars) [10]. Finally, the CO_2 is separated from this stream, and H_2 can be burned in a modified gas turbine as the fuel. Pre-combustion system can be considered only for new plant projects. The long-term target for pre-combustion systems is to reduce the electricity cost penalty to 10% [16], from the initial value of 25% estimated by DOE in 2000 [17]. Furthermore, hydrogen production would also be possible by means of this system [16].

1.3.3 Oxy-fuel

The oxy-fuel or denitrogenization process prevents the presence of nitrogen in flue gases by using oxygen instead of air in the combustion step. This system combines the combustion unit (boiler) with the air separation device and the CO_2 recycling system. The combustion environment may be pure O_2 or a mixture of O_2 and CO_2, the latter being recycled from flue gas to obtain more CO_2 concentration in the final output gases. The exhaust gases include CO_2, H_2O, O_2, which results in some advantages such as

lowering the amount of flue gases to be treated and avoiding the formation of NO_x. The flue gas is then cooled down to 50 °C or lower, to concentrate the steam and remove it as water, and to condense the CO_2 gas to approximately 95% [18]. However, the cost of air separation units, an energy penalty of 23% to 37%, high capital costs, higher risk of corrosion in equipment due to higher SO_x concentration subsequent to flue gas recycling have been raised as disadvantages [16]. A further significant problem is the potential for air ingress from the atmosphere, which causes contamination in the CO_2 produced. This system is also appropriate for new plant projects.

1.4 CO_2 capture technologies

Separation of CO_2 is the core step in the CCS chain, in view of its energy and cost demand. The CO_2 separation step contributes to about 75% of CCS cost; hence it determines the overall cost of the system [13]. CO_2 separation technologies from gas streams are based on chemical and physical absorption, adsorption, membrane, and cryogenic distillation concept. Chapter 2 will review these different CO_2 capture technologies.

1.5 Economical issues of CCS

Deploying the CCS system to a power plant will increase energy input per electricity unit of output, due to the energy demanded for capture, transport and storage steps. Consequently, this yields more CO_2 per unit of plant production (i.e. CO_2/ kWh electricity). Therefore, to determine the CO_2 reduction by CCS, the CO_2 emissions (per kWh) can be compared for a plant with and without CCS. This difference is referred to as CO_2 avoided, as shown in Figure 1.6. Cost of CO_2 avoided and efficiency penalty are appropriate metrics to compare the economics performance of different CO_2 capture technologies and systems.

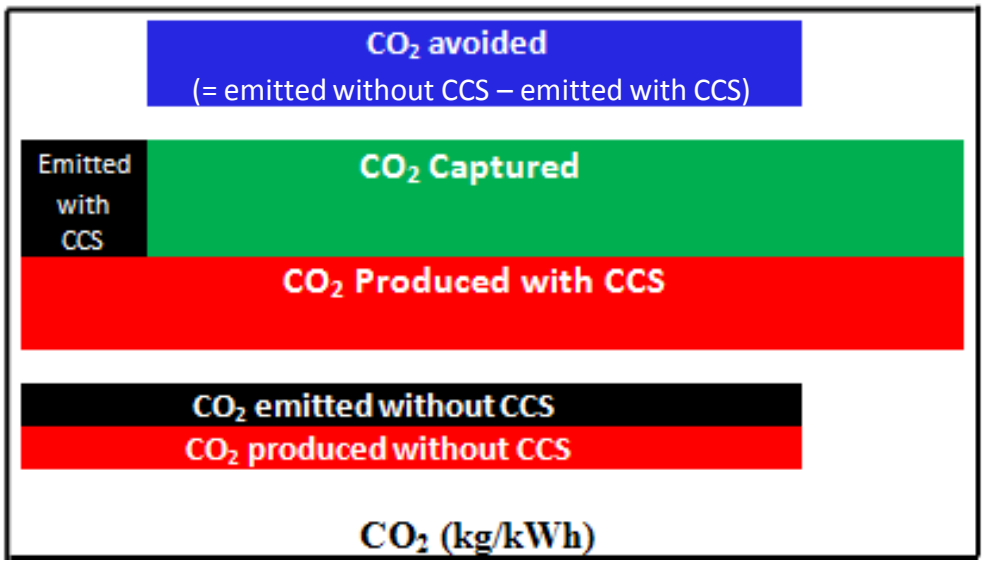

Figure 1.6: Graphical representation of the CO_2 generated, emitted and avoided.

The cost of CCS considerably depends on factors such as: CO_2 separation technology, CO_2 capture process system, characteristics and design of the power plant (or other industries) that indicate flue gas conditions and CO_2 concentration [10]. Costs of CO_2 avoided and efficiency penalties for variety of power plant types, fuels, CO_2 capture technologies and systems were reported by IEA ,2011 [19]. A summary of extracted data is presented in Table 1.2. The costs and efficiencies cover only CO_2 capture and compression.

Table 1.2: Economics performance of different power plants deployed by various CO_2 capture [19].

Fuel	**Coal**			**Natural Gas**
CO_2 capture system	Post-combustion	Pre-combustion	Oxy-fuel	Post-combustion
CO_2 capture technology	Amine (MEA)			Amine (MEA)
Plant technology	**PC**	**IGCC**	**PC**	**NGCC**
Relative ave. efficiency penalty	25%	20%	23%	15%
Net efficiency penalty (% point)	8.7% - 12%	5.5% - 11.4%	7.9% - 12.2%	6% - 10.7%
Cost of CO_2 avoided ($/t$CO_2$)	40 - 74	26 - 62	35 - 72	60 - 128
Cost of CO_2 avoided-av.($/t$CO_2$)	58	43	52	80

For the pulverized coal-fired plants (PC), cost of CO_2 avoided by post-combustion CO_2 capture using amines solvents range 40-74 $/t$CO_2$. Net efficiency penalty between 8.7 and 12 percentage points are estimated, which is an average 25% reduction in relative efficiency. However, a key research objective to develop the application of CCS will be cost reduction, particularly for CO_2 separation [20].

1.6 Aims and objectives

Using limestone to remove CO_2 content from power plants flue gases is a promising capture technology to provide a cost-effective separation process. Deploying post-combustion CO_2 capture systems (including CaO-looping cycle as the capture technology) to the numerous existent large emission sources is considered as the likely measure to mitigate CO_2 emissions to the atmosphere.

1.6.1 Aim

The overall aim of this project was to study factors that could influence the performance of limestone used for CO_2 capture purposes in a solid looping cycle separation process, in particular for post-combustion systems. This general aim will be met through the following objectives.

1.6.2 Objectives

To determine the effect of flue gas conditions for post-combustion capture from a coal-based combustion process on the sorbent performance; in particular, to explore the effect of presence of SO_2 on CO_2 capture capacity

To determine the effect of operating conditions in the carbonation and calcination steps on the sorbent performance; in particular, to explore the effect of the presence of steam (in carbonation and calcination). In addition, to investigate the impact of using a high pressure calcination (with close-to-atmospheric pressure carbonation) on CO_2 capture capacity and overall cycle performance

To study the opportunity for limestone to be used for a co-capture process for both CO_2 and $SO_{2;}$ and to investigate the application of steam to dilute the calcination atmosphere

1.6.3 Project designation

Process engineering and development of post-combustion CO_2 separation from fuels using limestone in CaO-looping cycle

CHAPTER 2

CO_2 capture technologies

Chapter 2 : CO_2 capture technologies

2.1 Introduction to CO_2 separation technologies

This chapter reviews different technologies for CO_2 separation from gas streams. There are several different technologies to capture CO_2 from gas streams founded on absorption, adsorption, membranes, and cryogenic techniques, as categorised in Figure 1.

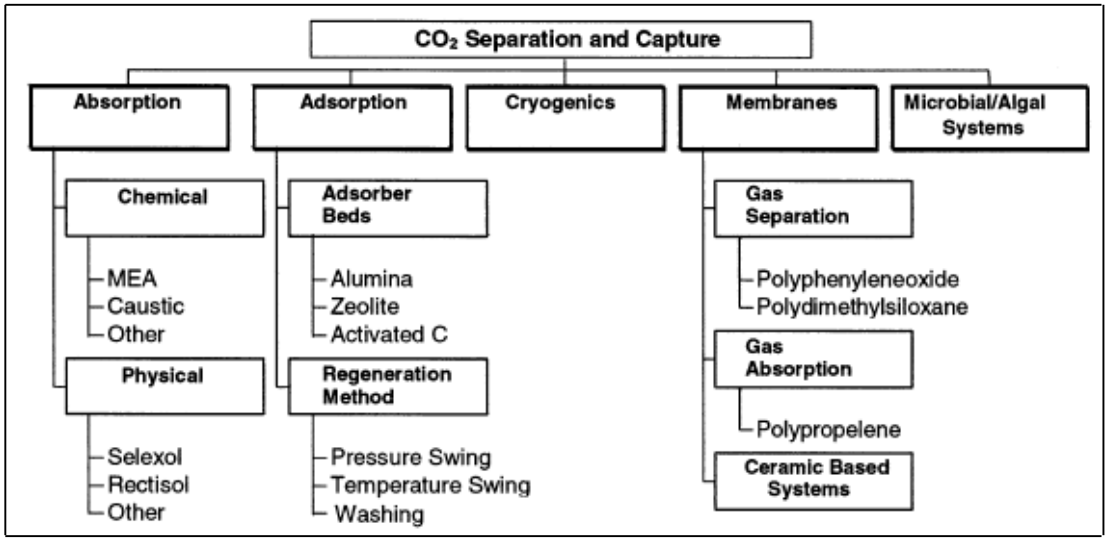

Figure 2.1: Classification of different CO_2 separation technologies [21].

These technologies differ in operational conditions and waste material, which determine their advantages, disadvantages and limitations. Some factors such as the partial pressure of CO_2 in the gas stream, presence of other impurities, environmental impacts (waste or by-products production), and capital and operating costs, influence the selection of capture technology [22]. Some of these technologies involve similar basic process concepts. Figure 2.2 presents an overall schematic of the separation processes.

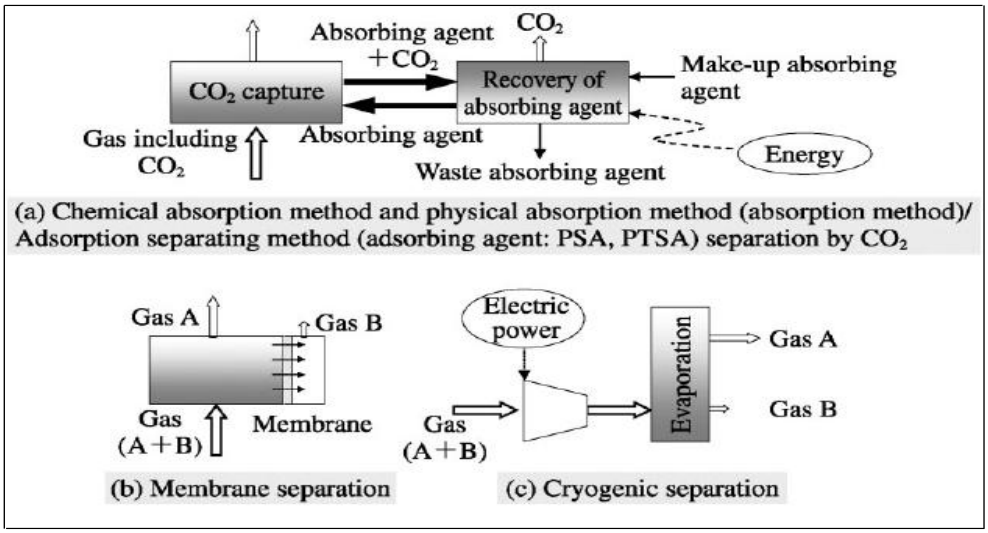

Figure2.2: Overall schematic of the different separation processes [18]

2.1.1 Chemical absorption technologies

In chemical absorption technologies the absorbing solvent reacts with the existing CO_2 in the gas stream to take CO_2 into the solution through gas-liquid contact. The solvent with the CO_2 is then sent to the regeneration reactor where the solution is heated to release CO_2, as shown in Figure 2.2(a). Examples of commercially available chemical solvents, which are mainly used in gas cleaning processes and to a limited extent for CO_2-removal from flue gases, are presented in Table 2.1, [23].

Table 2.1: Commercially available chemical solvent processes.

Type of solvent	Example
Primary amines	Monoethanolamine (MEA), Diglycolamine (DIPA)
Secondary amines	Diethanolamine (DEA), Diisopropanolamine (DIPA)
Tertiary amines	Methyldiethanolamine (MDEA), Triethanolamine (TEA)
Alkaline salt solutions	Potassium carbonate

Chemical absorption by liquid solvents, particularly monoethaloamine (MEA), is considered as an available and well-developed technology for CO_2 capture in post-combustion systems [10; 23-25]. Although this chemisorption has been widely used in gas and chemical industries to capture CO_2 for more than 60 years, it is very energy intensive in the regeneration step, which will result in increasing electricity costs by ~70% if it is deployed to power plants [17]. Relatively high solvent makeup is required to attain a high rate of CO_2 capture due to oxidative degradation of the solvent [26]. Solvent consumption has been reported between 0.35 and 2.0 kg/tCO_2 captured [23]. Therefore, increasing the absorption capacity requires a concentration of MEA greater than 20-30%, which results in corrosion problems [22]. High temperatures (100 °C or more) will cause degradation in MEA solubility of CO_2 [27]. Formation of corrosive salts by irreversible reactions between amines and flue gas impurities such as SO_2, SO_3, NO_2, and fly ash [27]; sorption loss due to solvent degradation owing presence of high amount of O_2 (about 2%) [28-30] high cost of solvent (i.e. MEA about $1250/tonne) [21], are considered as further limitations of the technologies.

2.1.2 Physical absorption technologies

In the physical absorption technology, CO_2 is separated by dissolving CO_2 in an absorbing solution. Here, chemical reactions may or may not take place. In the regeneration reactor, the solution pressure is lowered to release the CO_2 from the solvent. Physical solvent processes claim to be applicable to capture CO_2 from gas streams that have high CO_2 partial pressures, i.e. about 7 bars. Therefore, these processes are mostly applicable to remove CO_2 from the mixed stream of CO_2 and H_2 that comes from the shift reaction (following the gasification process) in pre-combustion systems [10].

2.1.3 Adsorption technologies

In the adsorbing separation method, CO_2 is adsorbed in an adsorbing agent. After adsorption, the pressure of the entire adsorbing reactor is lowered to release CO_2 for capturing. This method is called Pressure Swing Adsorption (PSA). The CO_2 may also be released by increasing the reaction temperature using technology known as Temperature Swing Adsorption (TSA). The schematic of this technology is similar to absorption, as presented in Figure 2.2(a).

This technology is considered as a competitive option for other CO_2 separation technologies. Recent investigation on adsorbents has led to of promising materials for CO_2 removal under pressures of up to 45 bars [31]. Adsorption technologies require high CO_2 concentrations in the gas streams and hence, are more appropriate for pre-combustion systems. These technologies have been used for CO_2 removal from syngas for hydrogen production but have not achieved a commercial stage for application in post-combustion systems [10].

2.1.4 Membrane technologies

In membrane separation technology CO_2 is separated using thin barriers that allow one component in a gas stream to pass through faster than the others. Figure 2.2(b) illustrates the process of these technologies. Selection or permeation of molecules are due to the relative molecule size (in porous membrane), or molecules solubilises and/or their diffusion coefficients (in dense membrane) [32]. CO_2 molecule, with radius 3.3 Å is smaller than lighter gases, such as O_2 (3.46 Å), N_2 (3.64 Å) and CH_4 (3.8 Å), and greater than H_2 (2.89 Å), thus, it is a fast diffusing gas in many membrane materials [33]. These separation processes have been widely used for CO_2 removal from natural gas, to separate air into N_2 and O_2, and separate hydrogen from ammonia synthesis [34]. Generally membrane permeation is pressure-driven, thus the low partial pressure of CO_2 in the flue gas raises a major challenge for deploying the technologies in post-combustion systems [32]. These technologies may be applied to high CO_2 partial pressure and concentration gas streams [10].

Recently, research has been carried out to develop an advanced membrane-based process that can be cost-effectively deployed to existing pulverized coal plants [33]. This project aims to capture more than 90% of CO_2 from flue gas with less than 35% increase in cost of electricity (by RTI: Research Triangle Institute and DOE/NETL: US Department of Energy/ National Energy Technology Laboratories, 2011) [33].

2.1.5 Cryogenic (phase separation)

This technology is based on the compression and liquefaction of CO_2 gas to distill and separate it. Gases with different boiling temperatures can be separated by cooling until they separate into different phases. Figure 2.2(c) shows the cryogenic separation process.

This technology has the advantage of enabling the direct production of very pure liquid CO_2, which can be readily transported [35]. Cryogenic processes consume large amounts of energy for refrigeration [36], and require steam removal (before cooling) to

avoid solid formation and the consequent disturbance to the process [34; 35]. These are both considered as disadvantages for the technology.

To lower the energy demand per unit of CO_2 avoided, phase separation process is limited to streams that contain high concentration of CO_2. The lower limit for CO_2 concentration has been stated of about 50%, although preferred concentration is more than 90% [35]. Furthermore, pressurised gases liquefy at higher temperature. Therefore, cryogenic separation technology is not suitable for separating CO_2 from flue gases in post-combustion systems, which contain low CO_2 concentration and low pressure.

2.2 Solid looping cycle for CO_2 separation

The problems and limitations discussed above, owing to CO_2 capturing technologies, have directed research and investigation towards the use of different reversible reactions by solid oxide. A solid looping cycle can be defined as a technology that uses solid oxides in a circulating mode between two reactors to produce a pure stream of CO_2. This can take place by two different processes. CO_2 looping cycles (solid sorption-looping cycles) and O_2 looping cycles (chemical-looping combustion) are these two types of solid looping processes for CO_2 separation. In CO_2 cycles, oxide reacts with CO_2 in the gas stream and yields the carbonate (carbonation step); this carbonate can then be thermally decomposed to the solid oxide and CO_2 by heating it beyond decomposition temperature (regeneration step). In O_2 cycle, metal oxide transfers the oxygen from the air (oxidation step) to the fuel for combustion (reduction step). The circulation of solid sorbents between two different chemical reactors with fluidised bed combustion (FBC) is the common element in the two technologies [17]. Owing to the variety of deployed solids and the types of processes, solid looping cycles can be categorised in different technologies, as illustrated in Figure 2.3.

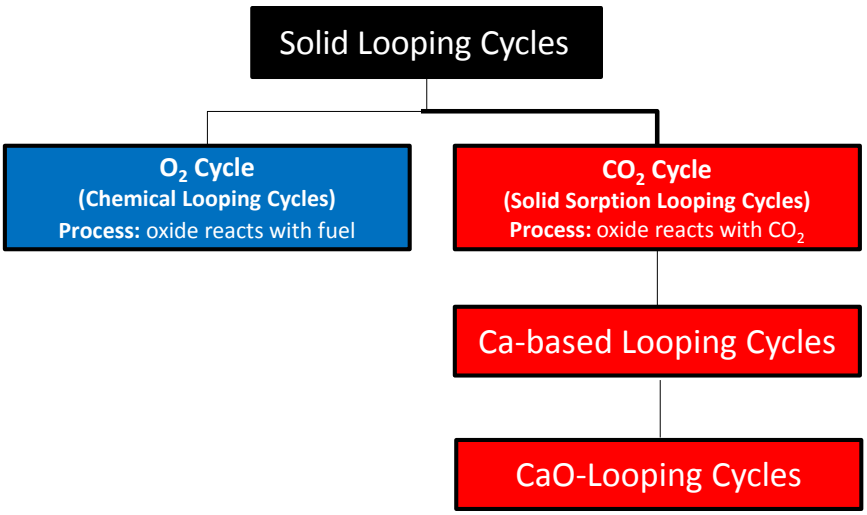

Figure 2.3: Categories of solid looping technologies for CO_2 capturing classified by types of processes and solid sorbents.

Solid looping cycles offer the advantage of application of fluidised bed combustion (FBC). This provides circulation of the solid between two reactors, which is a well-developed technology in large-scale that provides a good gas-solid contacting. FBC also enables the process to set a uniform temperature across the reactor beds [26; 37].

Furthermore, they are capable of producing a pure CO_2 stream at the end of the process [17]. These technologies will be reviewed in more detail in section 3.1.3.

2.2.1 Chemical looping combustion (CLC)

CLC is based on the use of an oxygen carrier typically a metal oxide (Me_xO_y), and the process unit consists of two interconnected fluidised bed reactors, an air- reactor and a fuel-reactor. The metal oxide transfers oxygen from the air reactor to the fuel reactor, and circulates between them. A schematic picture of CLC is presented in Figure 2.4.

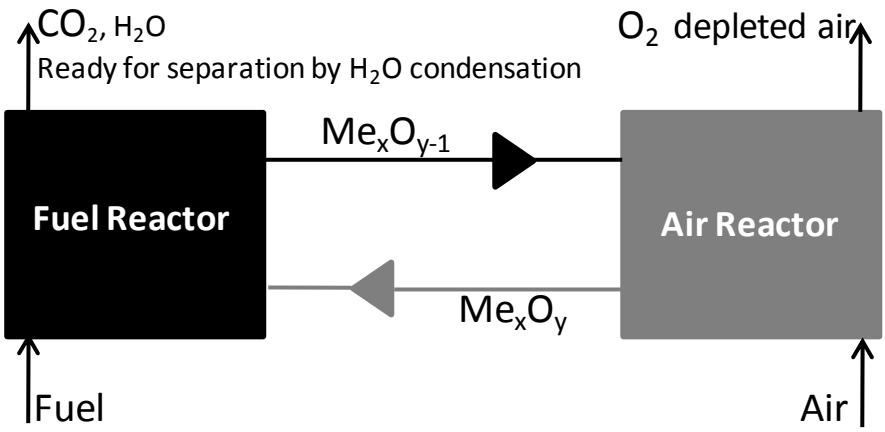

Figure 2.4: Chemical-looping cycle for CO_2 separation.

The reactions taking part in the different reactors are:

$$(2n + m)Me_xO_y + C_nH_{2m} \rightarrow (2n + m)\ Me_xOy_{-1} + nCO_2 + mH_2O \qquad (2.1)$$

$$Me_xO_{y-1} + ½O_2 \rightarrow Me_xO_y \qquad (2.2)$$

The oxides in the fuel-reactor are reduced due to combustion of the fuel with the oxygen from this oxygen carrier (Equation 2.1). The reduced oxygen carriers are then oxidised in the air-reactor by taking up oxygen from the air for the new cycle (Equation 2.2).

Reaction (2.1) is either endothermic or exothermic, depending on the type of oxygen carrier and fuel, whereas reaction (2.2) is always exothermic [17]. The fuel may be syngas from gasification or natural gas, and it has been shown that the combustion of solid fuel such as coal is possible in CLC system [38; 39]. Similar to oxy-fuel combustion, the flue gas stream contains almost only CO_2 and steam, which can be separated by steam condensation.

2.2.2 Solid sorption-looping cycle

Several investigations have been carried out to study the performance of different solid oxides for CO_2 separation, such as the Na-based sorbent Na_2CO_3 [40], dolomite, potassium-based, CaO-based, and Li-based sorbents [10].

Table 2.2: CO_2 capacity and regeneration energy of metal oxides.

Metal oxide	Density (g/cm^3)	CO_2 capacity (g of CO_2 of oxide)	Regeneration energy (kJ/g of CO_2)
Ag_2O	7.14	0.189	1.865
BaO	5.72	0.287	6.081
CaO	2.62	0.785	4.042
Cs_2O	4.36	0.156	9.279
K_2O	2.32	0.468	8.895
Li_2O	2.01	1.471	5.146
MgO	3.65	1.092	2.681
Na_2O	2.27	0.709	7.309
Rb_2O	3.72	0.235	9.172
SrO	4.70	0.425	5.249
ZnO	5.47	0.540	1.616

In a study of several CO_2 sorbents, as summarised in Table 2.2 [41], Feng concluded that most of the sorbents being developed for CO_2 adsorption are not suitable for zero emission schemes in power plants, because of having low capacity at high temperatures [41]. Solid sorption separation processes offer some advantages as:

Solid sorption-looping technologies (unlike other technologies in section 2.1) provide CO_2 separation under flue gas conditions. The temperature of flue gas generated from fossil-fuelled combustion sources can be up to 800 °C before heat recovery [42]. Flue gas temperature after heat recovery, either by Heat Recovery Steam Generation, HRSG [8] or through Air Pre-Heater, APH [10; 43] is held at more than 100 °C if it is necessary to prevent water formation. Therefore, required heat for carbonation can be provided by transferring the flue gas to the carbonator before heat recovery, or partially by CaO particles leaving the calciner [44]. The flue gas pressure is atmospheric. The CO_2 concentration in power plant flue gas ranges 3% - 15% (for a NGCC and a coal-fired plant respectively) [8; 10; 45], and 15% - 30% for cement industries [10]. The remainder of flue gas contains mainly N_2, O_2, steam, and SO_2 (in case of coal-firing). Therefore, any process that involves a high system pressure and/or a low temperature (such as chemical and physical absorption, adsorption, and membrane) requires compression and/or cooling of the entire flue gas stream, which can be expensive. High temperature (100 °C or more) will cause degradation in MEA solubility of CO_2 [46]. Furthermore, any amount of SOx, NOx, fly ash, and high amount of O_2 results in degradation and loss in MEA [46].

In general, sorbents used for solid sorption-looping CO_2 separation processes have high sorption capacities. Table 2.3 compares capacities for the sorbent/solvent used in several technologies. These quantities reveal the advantage of employment of a solid sorption-looping process, which is the lower sorbent requirement owing significantly higher CO_2 sorption capacity. This consequently leads to further advantages such as smaller reactor sizes and lower pressure drop across the reactor.

Table 2.3: CO_2 sorption capacity for some materials [47]; [42].

Sorbent/ Solvent	**CO_2 sorption capacity** (g of CO_2/kg of material)
MEA (absorption)	60 under ideal conditions
Silica gel (adsorption)	13.2
Activated carbon (adsorption)	88
Limestone ($CaCO_{3)}$	790
Dolomite ($CaCO_3.MgCO_3$)	490
Huntite ($CaCO_3.3MgCO_3$)	250
Hydrotalcite, promoted K_2CO_3 [a]	29
Lithium orthosilicate (Li_4SiO_4)	370
Lithium zirconate (Li_2ZrO_3)	290
Sodium zirconate (Na_2ZrO_3)	240

[a:] Reported as 0.65 molCO_2/kg equivalent to 29 g of CO_2/kg of material; regeneration temperature 400 °C; sorption capacity is stable after many cycles (45 cycles reported) [47]

The equilibrium partial pressure of gaseous species (or solid decomposition pressure) that results from the dissociation of solid sorbents is low. Therefore, solid sorbents leave low concentrations of CO_2 in flue gases after the separation processes. In a reversible chemical reaction, such as chemisorption of CO_2, chemical equilibrium is the state in which the concentrations of the reactants (oxide and CO_2) and products (carbonate) have not yet changed with time. The desired absorbers should reach chemical equilibrium at a low CO_2 concentration so that CO_2 can be removed from flue gas to very low concentrations. Natural sorbents containing CaO and MgO have low equilibrium CO_2 concentrations, and hence they can react with atmospheric CO_2 at low concentrations in the 0.025% - 0.037% range, even at ambient temperature [42]. Therefore, these oxides are able to capture CO_2 at very low concentrations. The thermodynamic chemical equilibrium of $CaCO_3$ will be discussed in section 3.2.

Solid sorption-looping processes are capable of generating pure streams of CO_2 after separation. It is advantageous that only CO_2 released during the regeneration step. This can be achieved in solid sorbent technologies such as limestone looping processes, in which only $CaCO_3$ decomposes in the regeneration stage (~950 °C) and any present $CaSO_4$ will remain stable.

Solid sorbents can be simply separated from the gas stream, after capturing CO_2, and sent for regeneration in a different reactor [10].

2.2.3 Ca-based looping cycle

One essential aspect for the development of solid sorption separation processes is obviously the CO_2 absorption capacity of the sorbent, and also it's stability for long periods of operation in repeated cycles [10]. As can be seen in Tables 2.1 and 2.2 CaO-carrier sorbent appears to have a significantly higher CO_2 absorption capacity compared with other solid sorbents. Few studies have shown that CaO is thermodynamically and kinetically the best candidate among solid oxides for CO_2 captures in zero emission technologies [41; 48; 49]. Ca–based looping cycle, in particular limestone looping

cycles, represents a class of technology that may cost-effectively remove CO_2 from combustion or gasification syngases [37].

2.2.4 CaO-looping cycle

Among Ca-based sorbents, limestone as a CaO-carrier is one of the best options for CO_2 separation [17; 50], because despite the high sorption capacity of CaO [42; 44; 47], natural limestones are cheap [51], abundant, and high calcium content materials [45; 50]. The possibility of using the calcined purge as a cement feedstock is another potential advantage for limestone [52]. Chapter 3 focuses on this technology.

CHAPTER 3

Limestone in CaO-looping cycle technology for CO_2 capture

Chapter 3 : Limestone in CaO- looping cycle technology for CO_2 capture

3.1 Limestone in CaO-looping cycle

This section deals with the overall view of the technology, the process mechanisms, application of fluidised bed reactors in the technology, technical challenges and targets, and economic issues of the technology.

Application of limestone in CaO-looping cycle is founded on the reversible reaction between CaO and CO_2 to mitigate its emission to the atmosphere. The separation process begins with thermal decomposition of natural limestone particles (Equation 3.1), and then followed by CO_2 adsorption stage (Equation 3.2).

$$CaCO_3 \rightarrow CaO + CO_2 \qquad \Delta H°_r = +178 \text{ kJ mol}^{-1} \qquad (3.1)$$

$$CaO + CO_2 \rightarrow CaCO_3 \qquad \Delta H°_r = -178 \text{ kJ mol}^{-1} \qquad (3.2)$$

The technology was first initiated and simulated by Shimizu et al., in order to capture CO_2 from combustion flue gases, but the experimental validation and sorbent performance were not considered in their study [53]. Later, this process was experimentally investigated by other researchers such as Lu et al. [54]. Further to the basic development, four different processes using CaO in combustion systems have been proposed by Abanades et al. [44]. The use of CaO in petroleum coke combustion systems for power generation has also been investigated [55]. In further applications, CaO has also been considered for H_2 production [50; 56-59].

The process unit consists of two interconnected fluidized bed reactors. One is operated in the temperature range 600 -700 °C [60] acting as carbonator (absorber), and the other in the temperature range 750-950 °C [60] performing calcination (regeneration). Solids are circulated between these two reactors through valves and cyclones. The process can be operated under atmospheric or pressurised conditions. Calcination of limestone is a highly endothermic reaction. Therefore, in the basic design of the process, the calciner reactor acts as an oxyfuel combustor to maintain the required heat for sorbents decomposition. The heat then can also be used for power generation after the being transferred from the calciner.

CO_2 looping cycle can be deployed in both post-combustion and pre-combustion systems [61; 62]. However, it follows the similar principles for CO_2 removal in both systems. Figure 3.1 illustrates the block diagram of the basic principles of the process to be integrated in to coal-fuelled power plants as post-combustion systems.

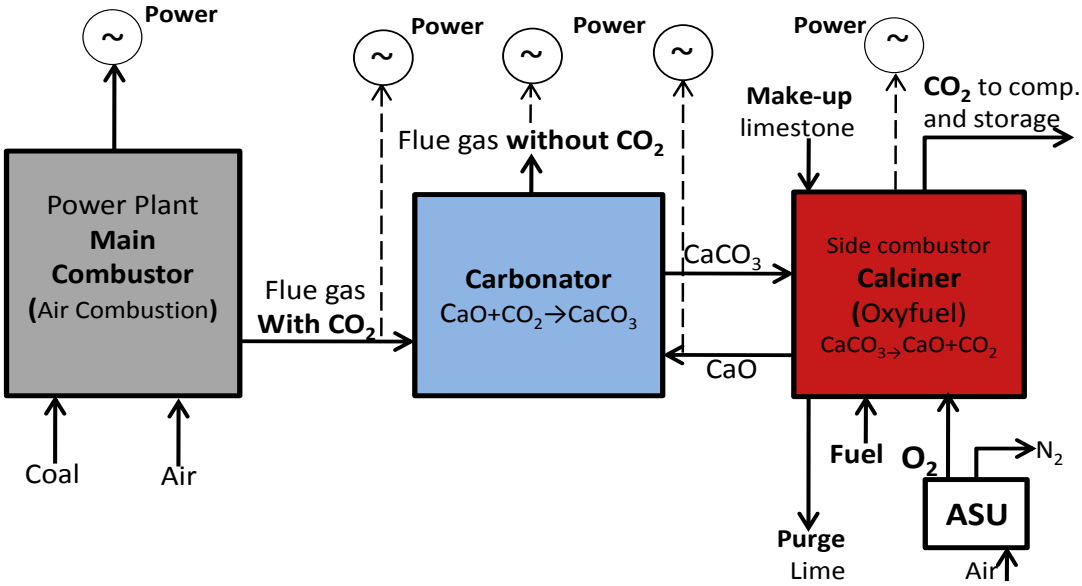

Figure 3.1: CaO-looping cycle for post-combustion CO_2 capture in coal-fuelled power plants.

A potential application of limestone looping cycles for pre-combustion systems is the gasification process as represented by Figure 3.2. In this process, the carbonation reaction takes place in the reformer simultaneously. However, as this project aims to investigate the application of limestone looping cycle in CO_2 removal from flue gas streams, the rest of the chapter focuses on post-combustion systems.

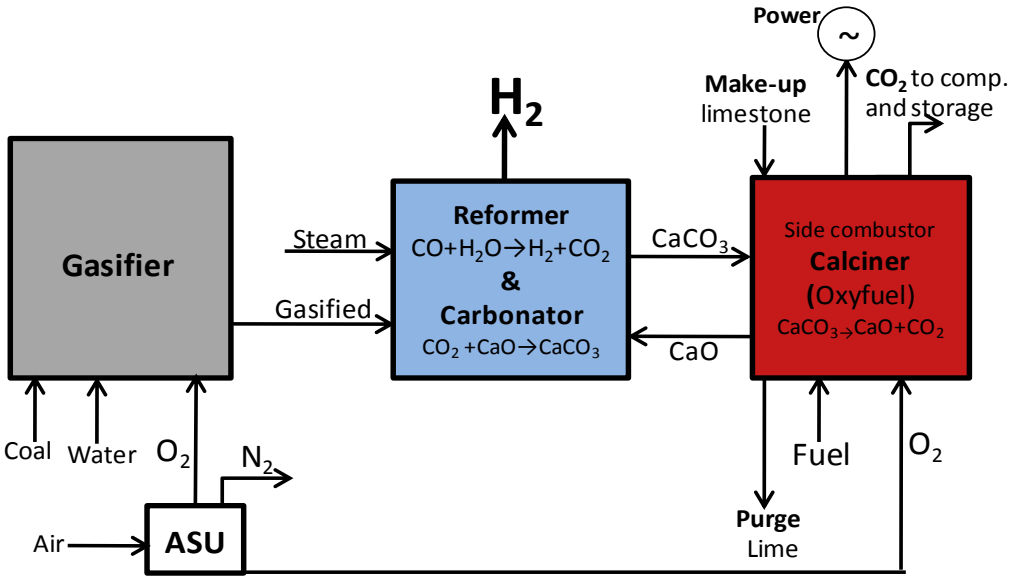

Figure 3.2: CaO-looping cycle for pre-combustion CO_2 capture in gasification process [61; 62].

3.1.1 Process of CaO-looping cycle using limestone

The CO_2 present in the flue gas coming from the main combustion of power plant, contacts with a flux of CaO in the carbonator. The gas-solid contact leads to the formation of $CaCO_3$, and hence CO_2 is being captured. The solids leaving the carbonator ($CaCO_3$ and non-converted CaO) are directed to a second fluidised bed, where

calcination (regeneration) takes place. In order to maintain the necessary heat for decomposition of $CaCO_3$ in the second fluidised reactor, a fuel burns with O_2/CO_2 mixture. In fact the calciner acts as a side oxy-fuel combustor. The required oxygen is supplied by an air separation unit that consumes power. In the heated calciner, solid $CaCO_3$ (coming from carbonator) is decomposed to CaO and CO_2. Then the captured CO_2 from the flue gas and the CO_2 resulting from the oxy-fired combustion of coal leave the calciner, and is recovered in concentrated form, suitable for final purification, compression, transport and storage in a geological formation or other applications. The calciner requires a large fraction (35-50%) of the total energy entering the system in order to heat up the calciner system for the decomposition of $CaCO_3$ [63]. However, the energy leaves the system in this streams of CO_2 gas (to purification and compression) or CaO particles (to carbonator) at high temperature (at T > 900 °C), which then can be recovered (i.e. as heat in the carbonator at around 650 °C) [64].

3.1.2 Fluidised bed combustion in CaO-looping cycle

Interconnected fluidised bed systems have such characteristics that make them suitable for this process. Generally, they are widely used in various applications to carry out simultaneous dual reactions in one process such as CO_2 capture, gas desulphurisation, chemical-looping combustion, chemical-looping H_2 production, and so on [65]. Most of these process necessitate two or more reactors, and require non-mechanical valves for solid conveying and gas sealing between two reactors such as loop seal, seal pot, J-valve, L-valve, U-valve, and so on [66-68]. Circulating fluidised bed systems are particularly suitable for handling large amounts of solids [66]. For instance, the flow rate of flue gas from a typical 1000 MWt power plant is about 300 $Nm^3\ s^{-1}$, and carrying the contact of this huge flow of gas with required CaO particles is only possible with reactors that have a very high gas throughput per unit area such as CFB reactors [64]. In addition, lowering the make-up flow of limestone, which improves the technology's economic efficiency, requires higher circulation rates between calciner and carbonator [69]. Incorporating CFBs provides excellent material circulation and mixing, which significantly enhances the reaction between solids and gases, and maximizes mass/heat transfer and reaction rates [53]. CFBs using limestone sorbent also offer the potential advantage of sulphur removal when burning sulphur-containing fuels [55; 70] via the sulphation and carbonation reactions likely in separated reactors [71; 72]. Another potential advantage of CFBs-limestone process is the mechanical similarity between the carbonator and the commercial CFB combustors, which operate with gas velocities, solid circulation rates, and solid types similar to conditions required for limestone looping process [64]. It is worth noting that the use of fluidised bed combustors in power generation industries are increasing because the technology offers fuel flexibility, competitive cost, environmental performance, high reliability, and efficiency in energy conversion [44].

3.1.3 Economic issues and technical targets of CaO-looping cycle

Economics of limestone looping cycle, for CO_2 removal from flue gases, have been explored in several studies [28; 73-75]. Investigations led to estimations of the cost at about \$20/tCO_2 avoided for atmospheric processes. Abanades et.al (2007) predicted the

cost of CaO looping cycle for post-combustion systems at \$15/tCO_2 avoided [73]. Romeo et.al (2009) estimated it at less than €20/tCO_2 avoided [75].

Economic studies of deploying the Cao looping cycle with pressurised fluidized beds indicated that Ca-based sorbents would be economically attractive option for CO_2 capture [28]. The cost of this technology for pressurised systems has been estimated (2007) at €12/tCO_2 [76].

However, the above average estimated cost of atmospheric-pressure, limestone looping cycles, of ~\$20/tCO_2 avoided, is low when compared to other systems like MEA at range \$40-\$74/tCO_2 avoided, or oxy-fuel combustion with range \$35-\$72/tCO_2 avoided (Table 1.2 [19]).

The heat required for supplying adequate temperature for calcination in the hot CaO-looping cycle, can be reused for more power generation. The heat can be recovered through CO_2 stream leaving the calciner, or by CaO particles stream from the calciner to the carbonator. In addition, the required oxygen for the calciner is only about 1/3 to 1/2 of oxygen needed for oxyfuel combustion. Therefore, the estimated net efficiency penalty of limestone looping cycle, $\eta < 6\%$ [76], is very low compared to other systems like MEA or oxy-fuel combustion, which reveal values at 10.4% and 8.4% average percentage points, respectively (Table 1.2). This efficiency penalty includes CO_2 compression to 100 bars as well; furthermore, it will be even lower than 4% if considering the energy saved in the integrated cement plant due to the access to pre-calcined lime particles [76].

It has been projected that the technology is capable of removing more than 90% of CO_2 for new power plants and more than 60% for retrofitted existing plants [76].

Reactions and influencing factors in CaO-looping cycle using limestone are described here. Adding the limestone at a high temperature to a reactor, in which the flue gases contain CO_2, steam, and SO_2, promotes a series of interlinked reactions. First the fresh limestone is calcined to lime (CaO), which can then react with both CO_2 (carbonation) and SO_2 (sulphation). Meanwhile, the structure of the lime initially formed during calcination, is changed by sintering. The progress of these reactions, which include calcination, sintering, sulphation- carbonation, depends on the limestone type and the reaction conditions [60]. The sorbents in a circulating fluidised bed will experience all these processes, and research is required on the prospect of, and effect of their simultaneous occurring.

3.2 Calcination

Calcination, $CaCO_3 \rightarrow CaO + CO_2$, is a highly endothermic reaction. The limestone decomposition will proceed only if the partial pressure of CO_2 in the gas surrounding the solid surface is less than the equilibrium thermodynamic decomposition pressure of limestone, which can be expressed as Equation 3.3 [77].

$$P_{eq} = 4.137 \times 10^{7} \exp\left(-\frac{20474}{T}\right) atm \qquad (3.3)$$

Decomposition pressure of limestone (CO_2 partial pressure over the sorbent at equilibrium) can be obtained by computing the Gibbs free energy changes over the calcination reaction.

Gibbs free energy change of the system at constant temperature and pressure can be computed using Equation 3.4. Here, it is assumed that the reaction takes place at atmospheric pressure.

$$\Delta G_{sys}\,(\mathrm{T}) = \Delta G^{o}_{reac}(\mathrm{T}) + RT\ ln\ Q_p \qquad (3.4)$$

Here $Q_p = \frac{\prod_i [Products]^{v_i}}{\prod_i [Reactants]^{v_i}}$ and:

ΔG_{sys} : Gibbs free energy change of the system (T, 1bar)

ΔG^{o}_{reac}: Gibbs free energy change on the reaction at standard state (T, 1bar)

Q_p: reaction quotient

T: temperature (°K)

R: gas constant (J mol^{-1} K)

v_i: stoichiometric coefficients

Limestone decomposition involves only CO_2 as gas species, hence $Q_p = [CO_2]$ that is CO_2 partial pressure. At equilibrium $\Delta G_{sys} = 0$ and $Q_p = K_p = P_{eq}(CO_2) / P$; where K_p is the equilibrium constant, and P is reaction pressure (here is 1 bar). Therefore:

$$\Delta G^{o}_{reac}(\mathrm{T}) = -RT\ ln\ K_p$$

$$K_p = \exp\left(-\frac{\Delta G_{reac}}{RT}\right)$$

At standard temperature T_0 = 25°C:

$$\Delta G^{o}_{reac}(T_0{=}25°C) = \sum_i v_i \Delta G^{o}_{f_i}$$

where $\Delta G^{o}_{f_i}$ denotes Gibbs energies of formation at 25°C for one mole of each substance, and are presented by thermodynamics quantities tables. Thus:

$\Delta G^{o}_{reac}(T_0{=}25°C)$ =

$= \sum v_i \Delta G^{o}_{f_i}$(Products at T_0=25°C) - $\sum v_i \Delta G^{o}_{f_i}$(Reactants at T_0=25°C) =

$= \Delta G^{o}_{f_{CO_2}}(T_0{=}25°C) + \Delta G^{o}_{f_{CaO}}(T_0{=}25°C) - \Delta G^{o}_{f_{CaCO_3}}(T_0{=}25°C) = -RT\ ln\ K_p$

Therefore:

$$K_p(T_0=25°C) = \exp\left(-\frac{-394400-604000+1128800\ (\frac{J}{mol})}{8.314\left(\frac{J}{mol\,K}\right)\ \mathrm{X}\ 298.15(K)}\right) = 1.424\times10^{-23}\ \text{bar}$$

Equilibrium partial pressures of CO_2, $K_p(T_i)$, have also been computed for various temperatures up to 1150 °C based on $K_p(T_0=25°C)$. The results are presented in Table3.1. Details of the calculations are described in Appendix D.

Table 3.1: Equilibrium partial pressures of CO_2 at different temperature during calcination of limestone

	^{0}C	Kp = P_{CO_2} (bar) / P (1 bar) at equilibrium	ΔG^o_{reac} (kJ/mol)
T_0	25	1.42E-23	130.401
T_1	150	2.3403E-14	110.418
T_2	250	3.58355E-10	94.599
T_3	350	2.41858E-07	78.930
T_4	450	2.62936E-05	63.406
T_5	550	0.0009	48.025
T_6	650	0.01	32.785
T_7	750	0.12	17.689
T_8	850	0.75	2.741
T_9	950	3.27	-12.054
T_{10}	1050	11.32	-26.691
T_{11}	1150	32.43	-41.164

The results confirm low equilibrium partial pressures of CO_2 during limestone decomposition. It means, for instance, that carbonation at temperature 650 °C could remove CO_2 flue gases up to 1 vol %.

Different factors affect the kinetics and extent of calcination including: total pressure, CO_2 partial pressure (CO_2 concentration), reaction temperature, particle size, presence of other impurities (like SO_2) and gas content (like steam). The effect of some of these conditions will be reviewed in this section.

3.2.1 Effect of particles size on calcination

The rate of calcination increases with decreasing particle size, because smaller $CaCO_3$ particles yield more amount of CaO in shorter times relative to larger particles [27; 77]. The calcination rate of very small particles (1-90 μm) is controlled by chemical reaction [78], while for particles above 6000 μm it is controlled by heat transfer process [21]. For sizes in between, the rate is controlled by chemical reaction and internal mass transfer [27]. Particles are not recommended to be milled finer than 5 μm owing to the associated destruction of pore volume [79]. Furthermore, a decrease in particles size below 1–2 μm does not demonstrate a significant effect on calcination [60]. Figure 3.3

shows the effect of particle size on the calcination rate. The calcination conditions are presented in the figure caption.

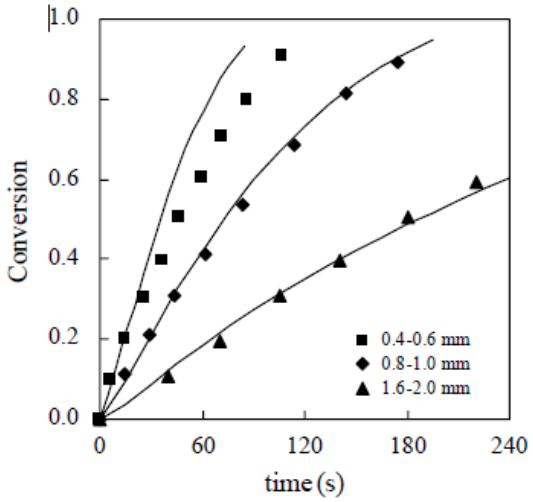

Figure 3.3: Effect of particle size on the calcination conversion: (symbols) experimental data; (continuous line) model predictions; 850°C; 1 MPa; 0% CO_2 [80].

3.2.2 Effect of impurities and gas contents on calcination

Huang and Daugherty investigated the influence of flue gas impurities on calcination reaction [81; 82]. They concluded that fly ash and V_2O_5 reduce calcination rate, Al_2O_3 and CaO have no effect, but Li_2CO_3 accelerates the particle decomposition. Effects of other impurities and gas contents, such as SO_2 and steam, on calcination will be reviewed and investigated in chapters 4 and 7.

3.2.3 Effect of temperature on calcination

It is expected that temperature influences the calcination rate, as it defines the equilibrium decomposition pressure of $CaCO_3$ at any given pressure. Figure 3.4 presents calcination conversion over reaction time for a certain type of limestone at 800, 850, and 900 ºC of temperature, pressure of 0.6 MPa, and in an atmosphere with no CO_2 present [27].

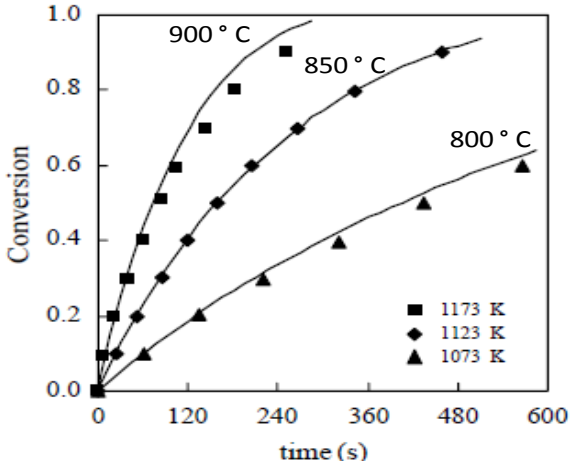

Figure 3.4: Effect of temperature on the calcinations conversion: (symbols) experimental data; (continuous line) model predictions; 0.6 MPa; 0% CO_2; dp = 0.8–1 μm [27].

A plot of different calcination rate equations is presented by Stanmore and Gilot [60] in the form of an Arrhenius diagram (Figure 3.5).

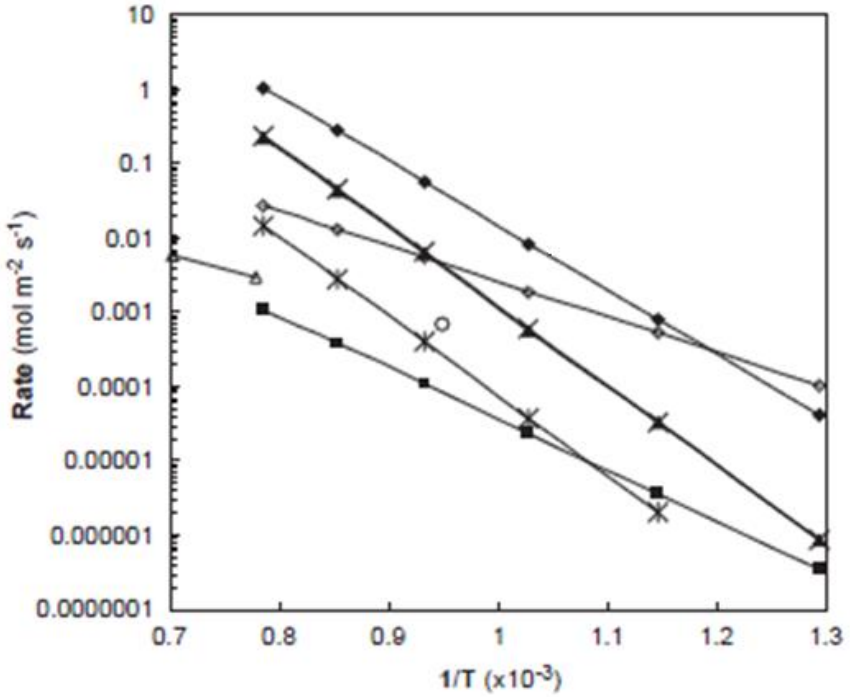

Figure 3.5: The influence of temperature on the calcination rate of limestone, measured by a number of investigators [60].

3.3 Sintering

High temperature, required for reactions in fluidised bed reactors, provides a suitable environment for sintering of CaO particles. Sintering results in a decrease in both the porosity and surface area of CaO particles. The surface area of a sorbent is a function of its calcination and sintering rates, and their comparative rates dictate the evolution of surface area [83].

Schmalzried [84] expressed sintering by distinguishing a three stages schematic model, from the view point of limiting cases, as shown in Figure 3.6. During sintering, if no molten phase appears, decrease in number and size of pores (through mass transfer in solid phase), decrease in porosity, and growing of grains take place.

In the first stage of sintering (a), the width of the contact area between grains, *x*, increases, but the porosity remains constant. In the second stage (b), material is transported from grains boundaries and surfaces to the pores. During the sintering of compounds such as CaO (or in a general form as AX), there will also be a flux of coupled ions as Ca^{2+} and O^{2-} (in a general form A^{+} and X^{-}) toward grains boundaries, in this stage. Finally, in the third stage (c), the large pores inside the crystallites will grow at the expense of the smaller pores (namely parasitic pore growth). At the end of this stage the grain boundaries act as an opening sink or source for ions.

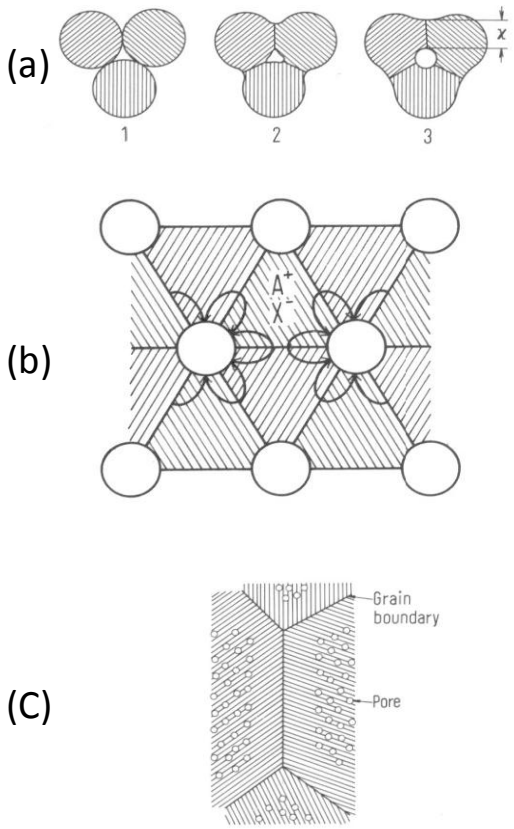

Figure 3.6: Schematic model illustrating the sintering in three stages [84].

3.3.1 Effect of Sintering

Sintering of CaO particles is reported to be the major cause of deactivation and decrease in CO_2 sorption capacity, as is evident by the change in sorbent surface texture after multiple cycles [45; 48; 51; 85; 86]. The effects of sintering on porosity and surface area for 15 minutes at various temperatures, and under inert gas atmosphere, are shown in Figure 3.7 by Borgwardt [87]. The study claimed that significant fall in surface area is the predominant change influencing initial sorption rate.

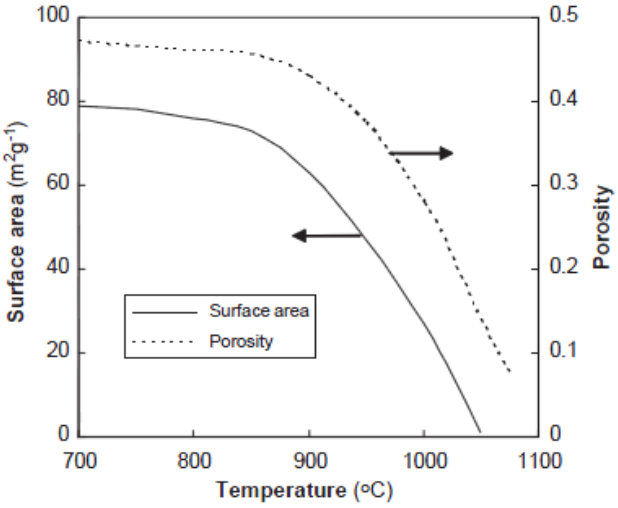

Figure 3.7: The effect of temperature on the porosity and surface area of lime after 15 min exposure.

3.3.2 Effect on Sintering

Sintering is favoured both by high temperatures and time at temperature, and is greatly facilitated by the presence of CO_2 and H_2O in gas phase [49; 50; 60]. Experimental data show that sintering in the presence of CO_2 and H_2O is much faster than in N_2 atmosphere [83].

3.4 Carbonation

Carbonation, $CaO + CO_2 \rightarrow CaCO_3$, is the reverse of the calcination reaction, and hence is exothermic. The carbonation reaction can proceed within a range of temperature. The lower temperature limit is set by the effect of reaction. The upper limit is the maximum temperatures (according to Equation 3.3) at any given CO_2 partial pressure, at which decomposition of $CaCO_3$ cannot proceed. This temperature range is shown in Figure 3.8 [60], which is the plot of various equations presenting thermodynamic equilibrium decomposition pressure for $CaCO_3$ (including Equation 3.3).

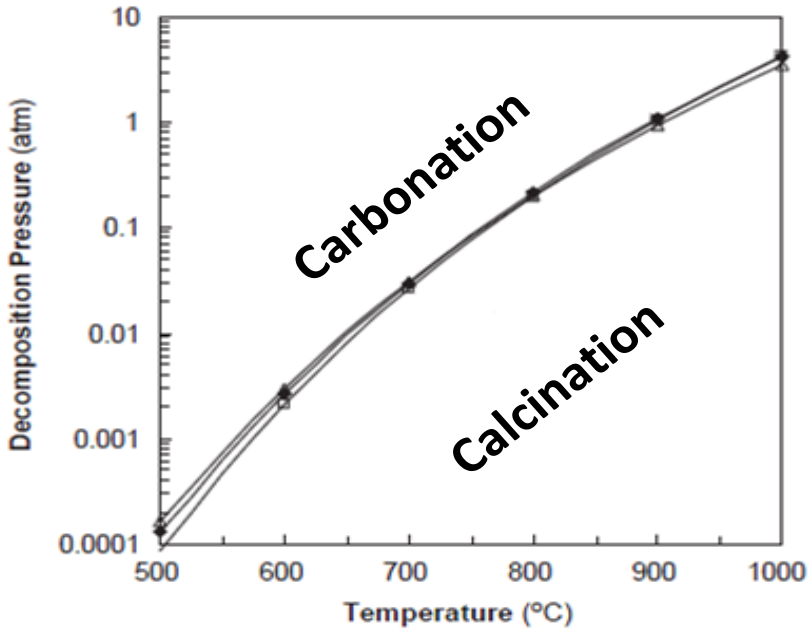

Figure 3.8: Equilibrium thermodynamic decomposition pressure of CO_2 over CaO, outlined from different equations including Equation 3.3.

3.4.1 Slow and fast stage carbonation

Carbonation takes place in two steps of reaction rate that have been confirmed in most of the studies [48; 53; 88-90]. Figure 3.9 shows these two stages in multi-cycles process. These investigations claimed that the faster step is chemically controlled carbonation, due to the interface reaction, which occurs on the surface of the CaO particles as the main rate-determining factor. Meanwhile, over the second step, CaO converts slower because the formed product layer of $CaCO_3$ restricts and controls the gas diffusion towards the internal surface of CaO.

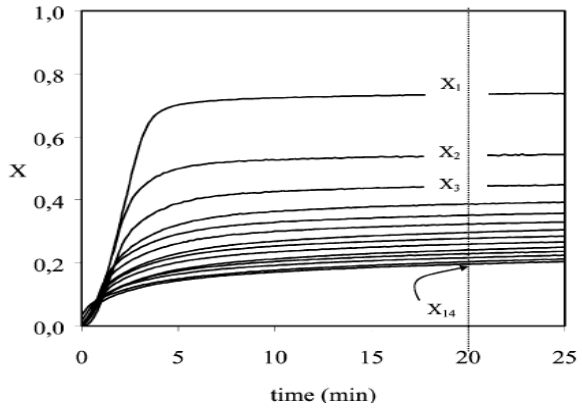

Figure 3.9: Evolution of the carbonation conversion with an increasing number of carbonation/calcination cycles [48].

The drop in carbonation rate is attributed to the formation of $CaCO_3$ product layer surrounding the CaO, which by reaching a certain thickness, resists CO_2 diffusion toward inner surfaces [89; 91; 92].

3.4.2 Decay in sorbent reactivity for CO_2 capture

Despite the advantages in using limestone looping cycles to remove CO_2 from gas streams, this technology suffers from the decay in sorption capability of sorbents in multiple cycles. This is a key factor, which negatively influences the economics of the process [93]. Abanades showed that carbonation conversion declines from initial extent of 60% - 80% to 20% after 10 cycles [94]. Later, Grasa and Abanades showed that an extent of 7.5% is the conversion limit for carbonation after 500 cycles [69]. The decay behaviour of the sorption capacity of CaO sorbent during cyclic carbonation-calcination has been studied by numerous investigations. These investigations can be classified as: **(I)** modelling of the deactivation, **(II)** effect of process variables on deactivation, **(III)** reactivation methods for used sorbents. This section reviews the literatures findings on sorbent deactivation.

(I). Data obtained in carbonation-calcination cycles have been subject to curve fitting to develop empirical models describing X_N, the extent of conversion of CaO to $CaCO_3$ in the N^{th} cycle, as a function of number of cycles, N. First, Abanades [94] fitted an empirical model as:

$$X_N = f^{N+1} + b \qquad (3.5)$$

With constants values at f=0.782 and b=0.174, Equation (3.5) demonstrates a strong correlation between two variables, of coefficient 0.982. This empirical equation does not result in unity (X_N=1) for N=0. Therefore, later, Abanades and Alavarez [48] developed an analytical model in terms of change in porosity, as:

$$X_N = f_m^{\,N}(1 - f_w) + f_w \qquad (3.6)$$

where two parameters, f_m and f_w, can be obtained for each process. However, several series of data from previous works covering a wide range of conditions (particle diameter 20-1000 μm and temperature 750-1060 °C [51]) were used to correlate them around values of 0.77 and 0.17, respectively. Afterwards, Wang and Anthony [95] presented a simpler model based on only one parameter, $a_N=1/(1+kN)$, initially to predict activity in the N^{th} cycle, a_N, which is the ratio of X_N to the maximum conversion. By assuming the initial activity of CaO to be unity ($X_0 = 1$), the value of a_N will be the estimation of X_N, thus it gives the following equation,

$$X_N = \frac{1}{1+kN} \qquad (3.7)$$

where k is the model parameter. Finally, considering a residual conversion (minimum limit), X_r, of about 7% - 8%, Grasa and Abanades [69] developed a semi-empirical model based on one parameter:

$$X_N = \frac{1}{\frac{1}{1-X_r}+kN} + X_r \qquad (3.8)$$

Figure 3.10 demonstrates the decay in performance of CaO in cyclic CO_2 capture, demonstrating a comparison of the previous experimental results and predictive model by Equations (3.6) and (3.7).

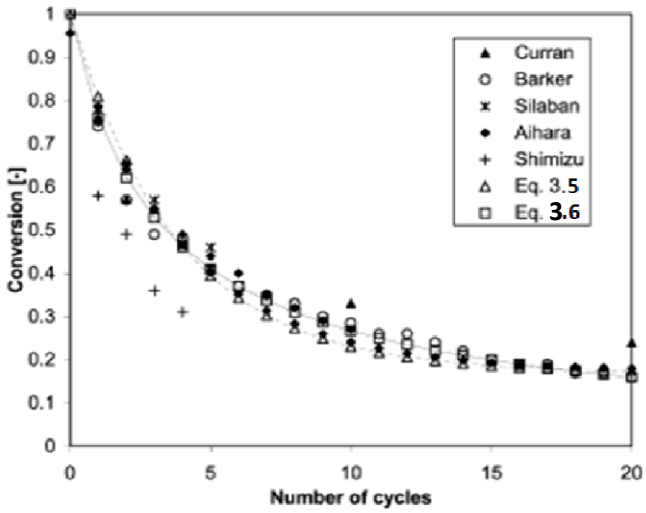

Figure 3.10: Decay in carbonation conversion with an increasing number of cycles. The open symbols represent calculated conversion [95].

(II). As described in section 3.4.1, the drop in carbonation rate from fast to slow stage, is stated to be the result of $CaCO_3$ product layer formation to a certain thickness, which then resists the CO_2 diffusion toward reacting surface. Further, Mess et al., in a description of CaO deactivation, also attributed the sorbent decay to the diffusional obstruction of CO_2 in reaching CaO surface [89]. However, Bathia and Perlmutter [92] showed that the first calcined particles reached 70% carbonation conversion, because of limitations in pore volume related to adequately small pores (smaller than 100 nm in diameter). It shows that even in sorbents with high surface area (such as the first

calcined), carbonation is limited due to shortage of void space for the development of product layer.

Figure 3.11 shows a schematic of carbonation according to the mechanism presented by Bathia and Perlmutter [92]. Based on this mechanism, during the reaction, $CaCO_3$ formed in all of the voids made up of small pores, and furthermore, it occupies a small portion of large voids, limited by the certain thickness of $CaCO_3$ layer at the inception of slow carbonation.

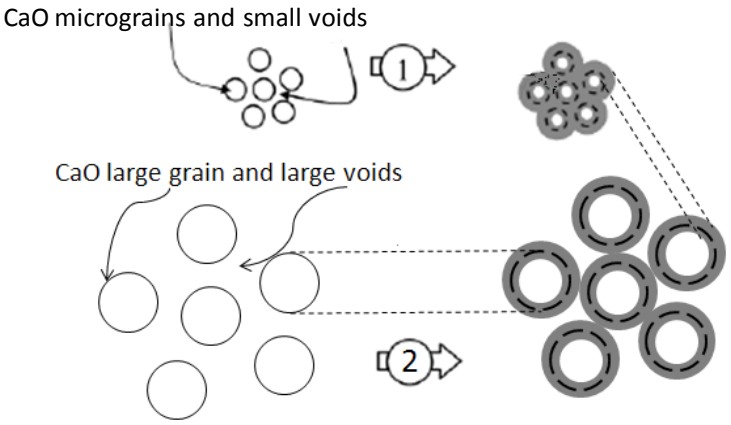

Figure 3.11: Carbonation mechanism and its different implications to small and large grains. Similar thicknesses of product layers formed, which leaves high unreacted space in the case of large pores. The dashed lines in 1 and 2 (right) indicate the boundary zone of CaO before carbonation. The grey parts indicate the maximum zone occupied by the product layer after carbonation, modified from [48; 92].

Sintering of particles during multiple cycles, results in larger grains, larger voids, and (based on this mechanism) a product layer that prevents CO_2 diffusion toward a large unreacted part of the grains. Figure 3.12 demonstrates the increase in pores and grains size in sorbents, which experienced more carbonation/calcination cycles. This situation, which is caused by sintering, is believed to be the major contributor to the decay of capture capacity [51]

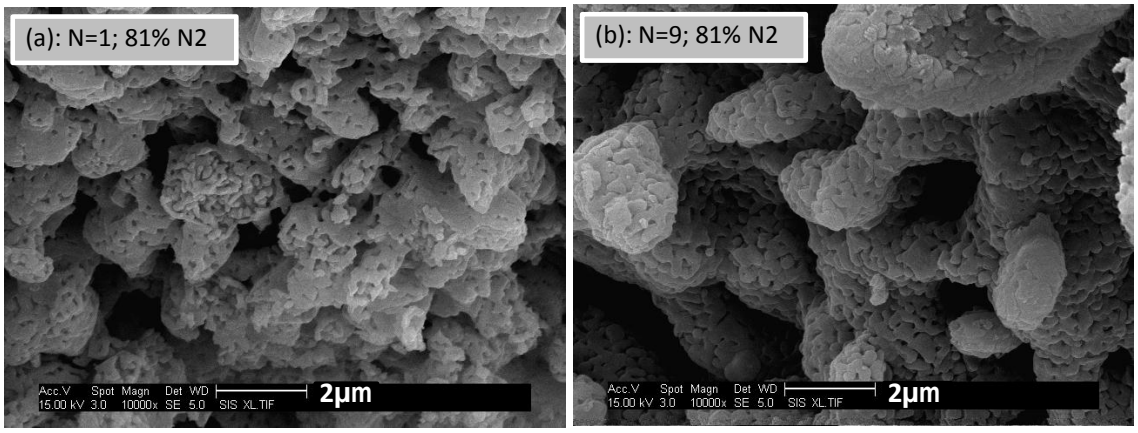

Figure 3.12: SEM images illustrating the continuous decay of microporosity and the parallel increase of microporosity in CaO particles: **(a)** the sorbent, after the 1st calcination, and **(b)** after the 9th carbonation-calcination. **(calcination)** at 950 °C in 15% CO_2, 3% O_2, and N_2 balance; **(carbonation)** at 650 °C in 15% CO_2, 4% O_2, and N_2 balance.

Alvarez and Abanades, [51] investigated the effects of internal morphology of CaO particles on their CO_2 adsorption capability. They concluded that the maximum extent of carbonation conversion by a CaO sorbent not only depends on the amount of its surface area, but also on the geometry of this free surface. This pores texture has to be able to accommodate a product layer with a maximum thickness possible for gas penetration over the reaction time.

Abanades and Alvarez [48] in their investigation of the conversion limit in carbonation reaction, stated that the gas penetration into the wall of large pores is limited to the thickness of about 0.2 µm. Beyond this point, the limiting factor for further carbonation in the large pores is not the lack of voidage, but the restriction of the product layer against gas diffusion. It has also been claimed that the product layer thickness that marks the beginning of the slow stage carbonation is around 0.1 µm [48].

Figure 3.13 shows the relationship between pore volumes, product layer formed, and CaO conversion. As can be seen in Figure 3.13a, the fast stage carbonation lasted about 5 min, where 75% of total conversion (11% out of 14%) occurred. About half of the pore blockage (~30% out of ~60%) occurred during this 5 min time of fast stage carbonation, Figure 3.13b. As expected, the two curves in (a) and (b) show the same pattern versus time, which shows the linear correlation between the extent of carbonation and the presence of void space. The correlation has been demonstrated by the linear curve in Figure 3.13c as well. The product layer reached to a maximum thickness of 0.16 µm over the entire reaction time and to 0.14 µm thickness marks the onset of slow stage carbonation.

However, in order to improve the capabilities of limestone-based technology for CO_2 separation, Alvarez and Abanades, [51] suggested further efforts as: (i) Using sorbents with the highest surface area, and pore diameter no smaller than 150 nm (0.15 µm), (ii) Avoid sintering by milder calcination conditions, as it causes occlusion of pores and shrinkage of CaO during cycling, (iii) Avoiding the use of extended carbonation times, which might lead to the blockage of pores.

Other investigation also showed that very long calcination times and calcination temperature over 950 °C, which can cause more sintering, accelerate the decay in sorption capacity [69].

(III). Different reactivation methods have already been studied to improve the activity of cycled sorbent. These include steam reactivation [80; 96; 97], thermal and self-reactivation [97], and reactivation using chemical additive such as Na_2CO_3 and NaCl [98].

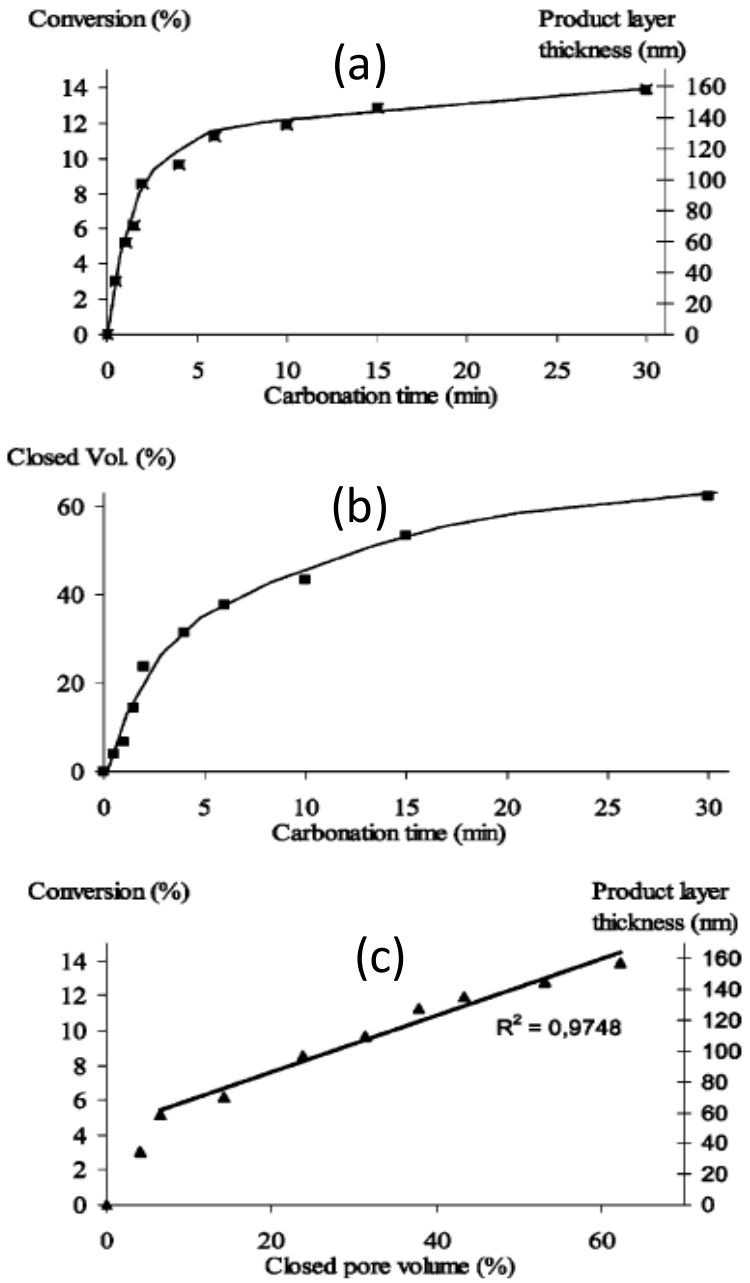

Figure 3.13: Structural transformations of a calcined particles (30 cycles; recarbonation time, 30 min; no pre-sintering) with carbonation conversion/time. (a): variation of carbonation conversion and product layer thickness with time. (b): variation of the percentage of occluded pore volume with carbonation time. (c): variation of conversion and product layer thickness with the percentage of pore closure [51].

3.4.3 Effect of particle size on carbonation

To study the likely effect of limestone particle size on carbonation, several groups, covering short ranges of particle diameter, have been subjected to multiple cycles of calcination/carbonation by Grasa et al [52], shown in Figure 3.14. The carbonation conversions of CaO were compared for different limestone sizes after 1 cycle (left), and 20 cycles (right). It has been concluded that the particle size did not influence the

sorption capacity, as there are modest differences in the slopes of the curves for the first cycle, which have disappeared after 20 cycles.

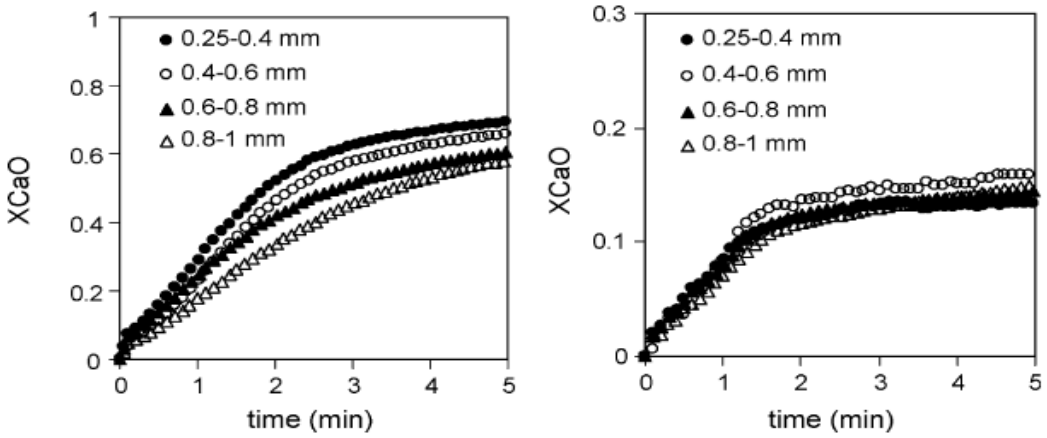

Figure 3.14: Conversion rates for different particle size in atmospheric conditions; $T_{carbonation}$ 650 ◦C, for 20 min; $T_{calcination}$ 850 ◦C, for 15 min. (Left) cycle 1, (right) cycle 20. Note that the Y-axis scale is different for both figures [52].

These authors have also concluded that for the first calcined particles, larger particles have more resistance to gas diffusion towards inside the sorbents (according to the results in the first cycle depicted in left figure). Later, unlike this conclusion, a similar investigation [69] confirmed that particle size does not affect the carbonation reaction. This can be seen in Figure 3.15, which compares the maximum achieved conversion of different particle size in multiple cycles.

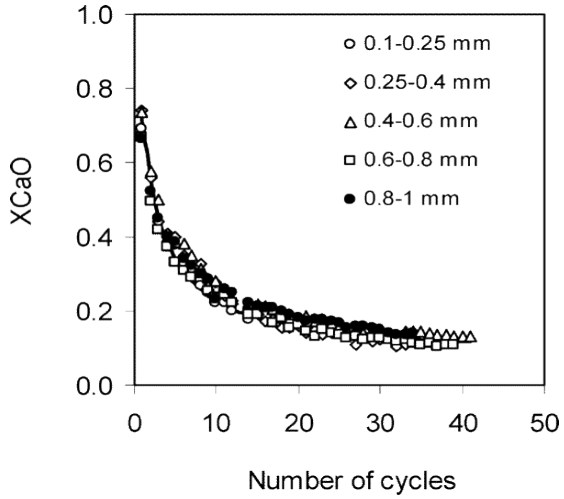

Figure 3.15: Cyclic conversion for different particle size calcination at 850 °C, 20 min; carbonation at 650 °C, 20 min; p_{CO2} of 0.01 MPa. The solid line corresponds to the data sketched based on Equation (3.7) with: k=0.52 and Xr = 0.075.

3.4.4 Effect of limestone type on carbonation

The study of carbonation of different limestones shows that there are no appreciable differences in reactivity between them. Figure 3.16 shows the carbonation conversions over reacting time for four different limestone types [86]. All the samples (with a slight

difference in type A) achieved almost the maximum conversion in the same time. Other investigation also reported the similar slopes for the fast stage carbonation, and claimed that the slight difference occurred in slow stages are controlled by gas diffusion through product layer [52].

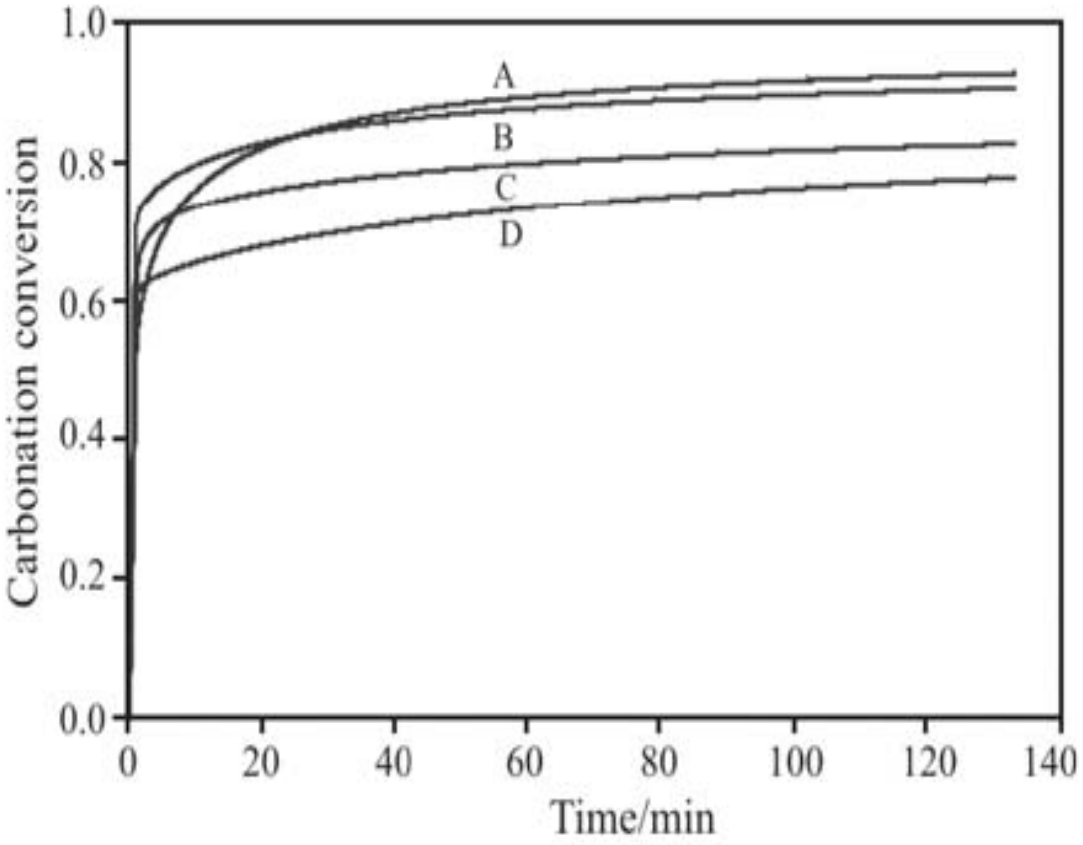

Figure 3.16: Carbonation conversion for the four different limestones.

Therefore, selection of the sorbent should be based on other factors such as availability, cost and mechanical stability [69].

3.4.5 Effect of CO_2 partial pressure on carbonation

The carbonation reaction rate of CaO particles, in the fast stage, has been described as a first-order reaction with respect to the CO_2 partial pressure [92], and independent to it in the slow stage [53; 92][53; 92], except when p_{CO_2} is close to equilibrium [52]. The carbonation conversion of calcined particles under different CO_2 partial pressure, up to 0.1 MPa, was investigated by Grasa et al. [52], and the results are depicted in Figure 3.17. It can be seen that the slopes of the fast carbonation reaction stage are strongly affected by the concentration of the reactant.

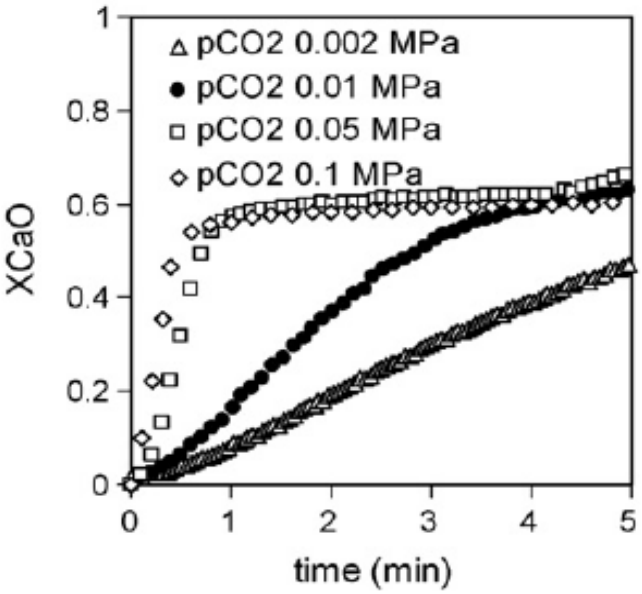

Figure 3.17: Conversion curves vs. time for different PCO_2, cycle 1. $T_{carbonation:}$ 650 ◦C, 20 min [52].

The study showed the correlation as first-order between carbonation reaction rates ($\Delta X/\Delta t$ in min^{-1}) and the CO_2 concentration over fast stage carbonation, in Figure 3.18.

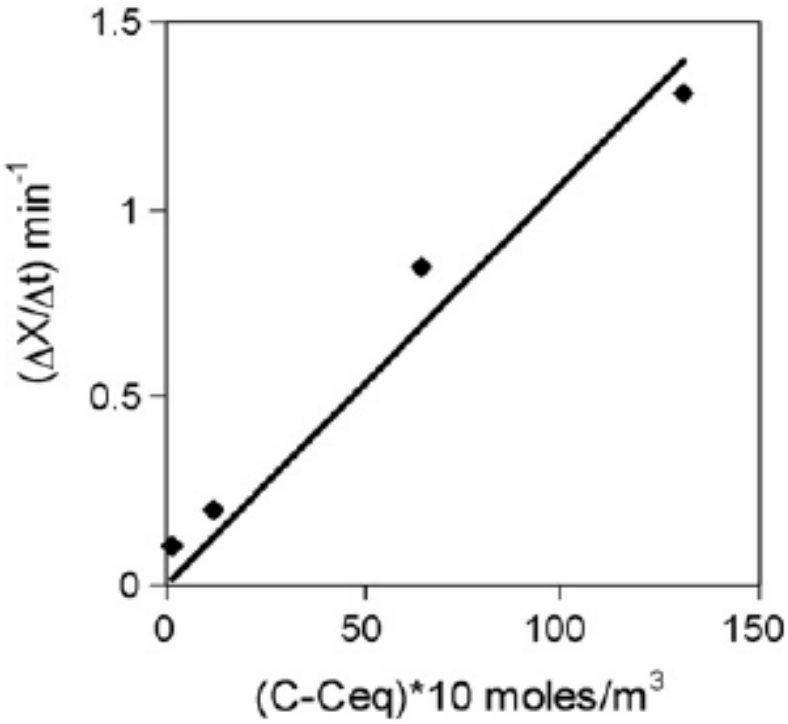

Figure 3.18: The reaction rate vs. CO_2 concentration in cycle 1 and over fast stage carbonation [52].

Figure 3.19 [52] represents the conversion curves for cycle 10 (left) and cycle 40 (right), respectively; in which the observed trends are in agreement with the first cycle (Figure 3.17).

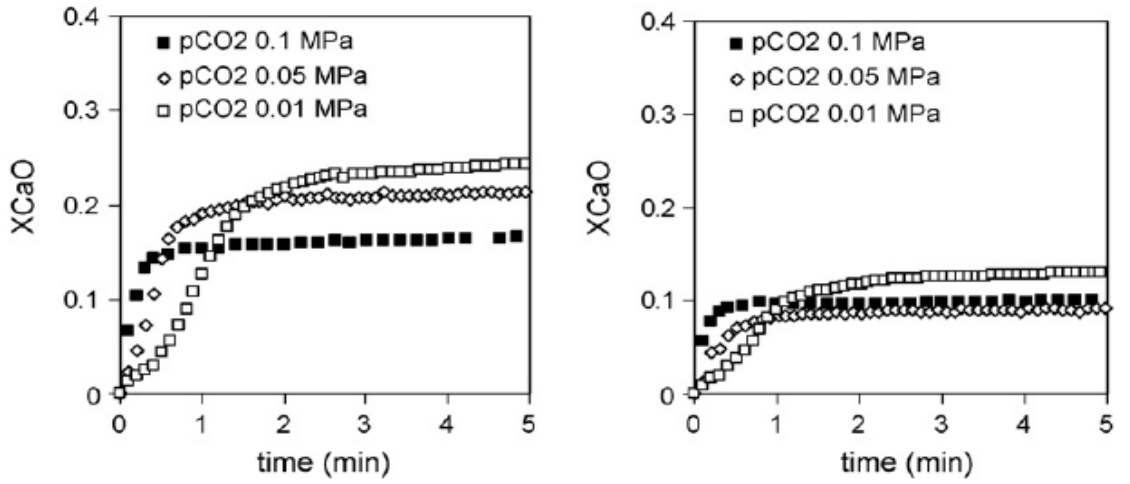

Figure 3.19: Carbonation conversion for different P_{CO2}. $T_{carbonation}$ 650 ◦C, 20 min; $T_{calcination}$ 900 ◦C, 15 min. (Left): cycle 10; (right): cycle 40.

The carbonation conversion under pressure higher than atmospheric has been compared to the atmospheric and subatmospheric pressures [69], as shown in Figure 3.20. It can be seen that higher CO_2 partial pressure results in more conversion when the cycle number is increased.

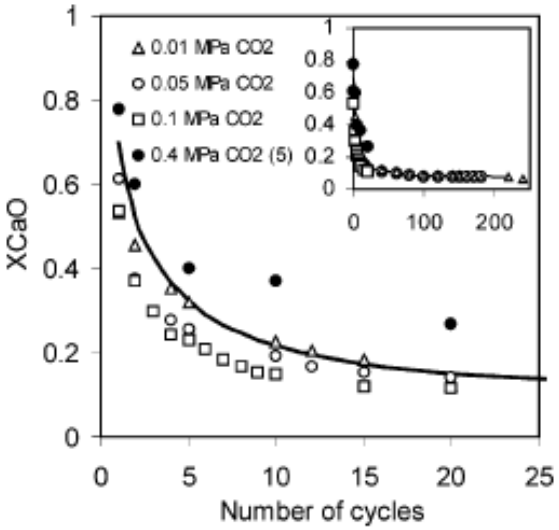

Figure 3.20: Cyclic carbonation conversion for different PCO_2; calcination temperature 950 °C; carbonation temperature 650 °C, 5 min. The solid line corresponds to the data sketched based on Equation (3.7) with: k=0.52 and Xr = 0.075.

3.4.6 Effect of reaction temperature on carbonation

The carbonation reaction was studied in a range of temperatures from 450 to 850 °C [52; 69; 99-101]. The extent of conversion is affected by temperature over this wide range. However, in a shorter sub-range like 600-730 °C, which is close to the operation conditions in the proposed capture process, curves demonstrate similar slopes corresponding to the fast stage of the carbonation. This indicates the poor dependency of the kinetic parameter on temperatures [52]. Figure 3.21 shows the conversion curves

over the range of 450-730°C, in which the results are in agreement with the described role of temperature in conversion gradients.

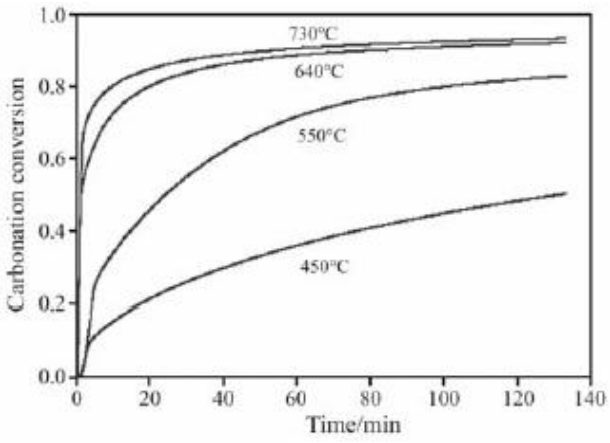

Figure 3.21: Carbonation conversion vs. time for initial carbonation in pure CO_2 at different temperatures. Limestone was 100% calcined before initial first carbonation in pure N_2[86].

3.5 Sulphation

In presence of SO_2 and O_2 in the flue gas stream, SO_2 can react with CaO (sulphation) or with the $CaCO_3$ (direct sulphation). Direct sulphation of limestone can take place if the partial pressure of CO_2 is above the decomposition pressure of $CaCO_3$ (otherwise limestone decomposition to CaO and CO_2 occurs).

The possible sulphation during carbonation/calcination process, the likely effects of it on carbonation reaction and sorbent performance will be reviewed with details in chapters 4 and 7.

CHAPTER 4

Review the role of steam, SO_2, and pressure in CaO-looping cycle

Chapter 4 : Review the role of steam, SO_2, and pressure in CaO-looping cycle

4.1 Introduction

CO_2 capture using CaO-looping cycle is affected by a number of reacting and operating conditions. Presence of different possible impurities such as steam, SO_2 and O_2 in the CO_2 gas stream will influence the performance of the separation process. The process is also affected by operating conditions such as temperature, pressure and reacting gas flow rates. The roles of a part of these factors have been reviewed in chapter 3. This chapter reviews the literatures on the effects of steam, SO_2, and pressure on the limestone looping technology.

4.2 The effect of steam on calcination-carbonation cycles

Burning fuels always results in steam production. Fuels are burned in the main combustor, or in calciner to maintain the required heat for calcination. Furthermore, in case of using the process for a pre-combustion system, the reformer will contain steam as a part of reacting conditions. The percentage of steam in different reacting conditions of the process depends on the type of fuel, and type of combustion (air or oxyfuel combustion).

4.2.1 Presence of steam in carbonation

The use of calcium-based sorbents to remove CO_2 has received increasing attention, not only for CO_2 reduction from flue gases, but also directly from reactors in combination with the main reaction. Using CaO and dolomite to enhance hydrogen production in steam reforming process [57; 102-105], steam gasification process, and water gas shift reaction [58; 59] has been investigated. CO_2 removal from combustion flue gases by Ca-based sorbent has also been studied by using either the main combustor as the carbonator [44; 98; 106], or by means of a separate carbonator [42; 44; 45; 53]. However, in all of these cases carbonation takes place in presence of different amount of steam.

4.2.2 Presence of steam in calcination

The desired temperature for the decomposition step of $CaCO_3$ (calcination) can be provided by a range of processes: (i) using separated carbonation-calcination reactors from the main combustor; (ii) with direct heat transfer from main combustor to calciner; (iii) or with indirect heat transfer from main combustor to calciner, which have been proposed by Abanades et al. [44]. However, calcination could occur with steam present; because regeneration in case (i) takes place in an oxy-fuel combustor and in other cases (in which heat is being transferred from combustor to calciner) steam could be added to dilute the reactor atmosphere.

4.2.3 Different effects of steam on limestone looping cycle

Steam could be considered to influence the CO_2 separation by means of Ca-based sorbent in different ways such as: effect on carbonation, effect on calcination, and the effect of steam hydration reactivation [80].

4.2.4 The effect of steam on carbonation

The carbonation of calcium-based sorbent in presence of steam has been investigated by several researchers. Sun et al. [80] and Han et al [107] studied cyclic CaO carbonation in gas atmosphere with steam present; and stated that no appreciable enhancement occurred. Dobner et al. [108], studied the effect of steam on cyclic carbonation of dolomite. They claimed that the addition of steam results in a two order of magnitude increase in recarbonation rate. Figure 4.1 shows the results of carbonation with steam present. As can be seen, replacing 50% N_2 by steam during the carbonation in the 10^{th} cycle significantly enhanced carbonation conversion. Yang and Xiao [109] investigated the effect of steam on single carbonation under pressurised conditions, and found that steam increased capture performance significantly. Most of the investigations to date have been performed in a pure CO_2 atmosphere and/or using thermogravimetric reactor (TGR). The study of the effects of steam (1 – 20%) on cyclic carbonation with low concentration of CO_2 (15%) shows that steam enhances the carbonation conversion[110].

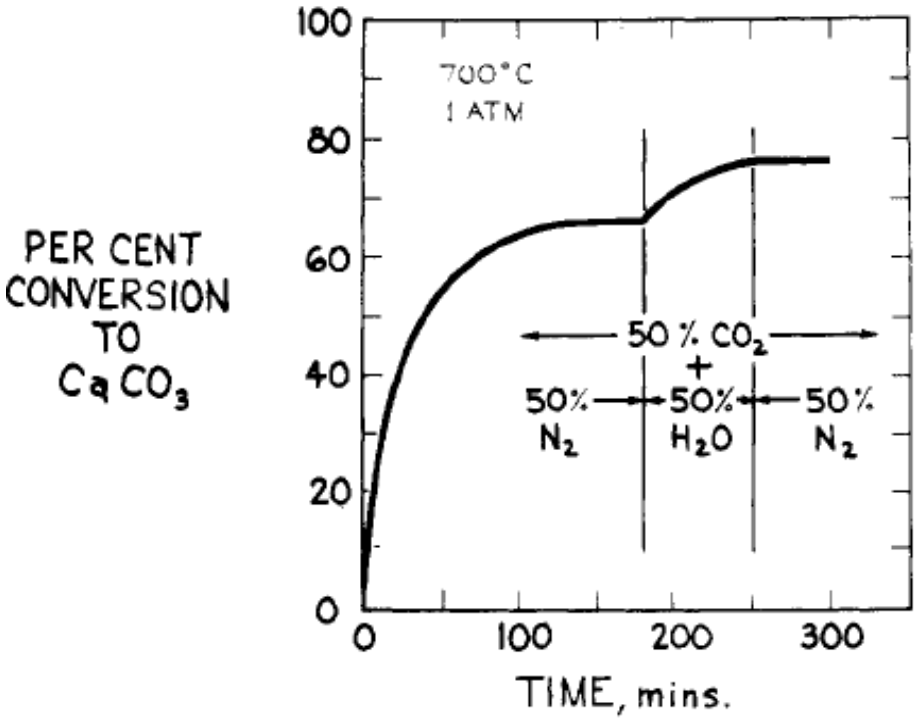

Figure 4.1: Effect of steam addition during recarbonation of dolomite at 700 °C in 0.5 atm of CO_2 at atmospheric pressure (tenth cycle) [108].

4.2.5 The effect of steam on calcination

Regeneration step in different calcination-carbonation processes occurs with steam present, because it takes place in either an oxy-fuel combustor or steam-diluted reactor atmosphere. In addition, decomposition of sorbents in a pure CO_2 and/or steam environment could lead the process to obtain a nearly pure CO_2 stream (after drying the flue gases). Steam-diluted atmosphere reduces CO_2 partial pressure in calciner, so lowers the required calcination heat and reduces sintering. Steam can also adsorb on the CaO surface faster than CO_2, and acts to weaken the CaO-CO_2 bond [111], thus lowering the incipient calcination temperature [80]. On the other hand, sintering of the newly formed CaO that takes place during the calcination of the limestone particles and driven by temperature [78; 112], is believed to be the major cause of the decay in sorption capacity after multiple cycles [45; 48; 85; 86; 91] The presence of steam (and CO_2) have been reported to facilitate sintering [83; 113]. Therefore, it is worth studying the effects of steam calcination on the cyclic capturing process.

Wang et al. [114] studied the behavior of limestone decomposition in a pure CO_2 atmosphere and indicated that the bed temperature had to be raised above 1020 °C for calcination. They also claimed that the capture reactivity of the CaO produced at higher temperature (>1020 °C) was lower, due to the sintering of CaO. Limestone decomposition with steam present has been investigated by several authors for a single cycle [111; 115-117], or during a multi-cycles run [80; 107].Yin Wang et al. [115] studied the single-cycle calcite decomposition in elevated steam dilution up to 100 vol.%, and claimed that calcination conversion increased with increasing the steam concentration. They also stated that the carbonation conversion of calcite increased with increasing the steam concentration in decomposition step, as shown in Figure 4.2. Their opinion on calcination step was consistent with the findings of Burnham et al [117] in the study of oil shade calcination with steam present.

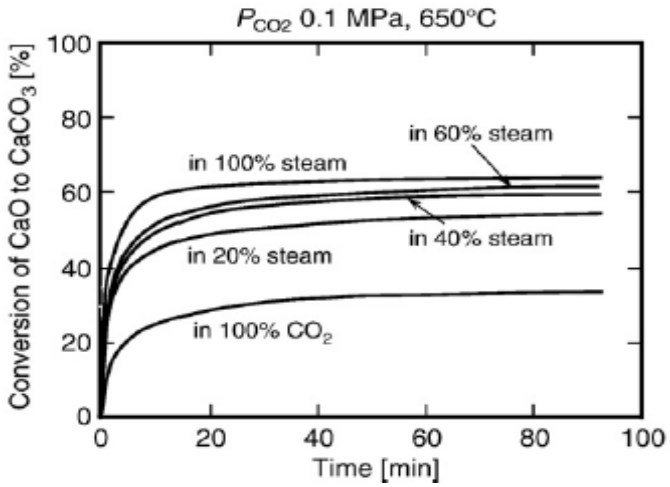

Figure 4.2: Carbonation conversions of CaO, which have been calcined with elevated steam percentages [115].

Khraisha and Dugwell [116], and Yong Wang and Thompson [111] calcined limestone in gas atmosphere with a small amount of steam. Both groups claimed increase in

decomposition (conversion and rate respectively) with small steam pressure, but their opinions were not consistent about the effect of increased steam dilution. Sun et al. [80] cyclically calcined a limestone with 95% steam presence, using thermogravimetric reactor (TGR), and found no appreciable effect on capture capacity, compared to sample calcined in 100% N_2 atmosphere. They also claimed no enhancement of sintering by steam detected based on pore size distributions, which is not consistent with the findings of above mentioned investigations on sintering. However, no information about the effect of steam/CO_2 environment on multicycle calcination-carbonation under realistic combustion conditions, and using operating fluidized bed reactors has been reported.

4.3 The effect of SO_2 on calcination-carbonation cycles

Sulphur dioxide, as one of the potential flue gas impurities, can affect the performance of Ca-based sorbents in CO_2 capture processes. SO_2 will always exist in the flue gases if heavy hydrocarbons or solid fossil fuels, such as coal, are burned in the main combustion unit. Burning sulphur containing fuels to maintain the required heating for sorbents decomposition will also result in presence of SO_2 in calcination step. Therefore, the effect of SO_2 on CO_2 capture capacity of the sorbent will be one of the challenges for Ca-based looping cycle technology, if it is to be deployed for the separation step.

In presence of SO_2 and O_2 in the reacting gas stream, SO_2 can react with CaO (sulphation) or with the $CaCO_3$ (direct sulphation), which can be represented as Equations (4.1) and (4.2) respectively. Direct sulphation takes place under conditions such that the $CaCO_3$ does not decompose to CaO prior to sulphation. Oxy-fuel combustion systems [118] or carbonation atmosphere, in which CO_2 partial pressure is higher than its thermodynamic equilibrium pressure, are suitable conditions for direct sulphation.

$$CaO + SO_2 + ½\ O_2 \rightarrow CaSO_4 \qquad (4.1)$$

$$CaCO_3 + SO_2 + ½\ O_2 \rightarrow CaSO_4 + CO_2 \qquad (4.2)$$

4.3.1 Carbonation in presence of SO_2

The recommended temperature range for carbonation step of CaO particles is 650-700°C [37; 44; 53; 54; 99; 119]. $CaSO_4$ actively forms at temperatures above 580°C [120] hence, sulphation can occur together with the carbonation reaction. Formation of $CaSO_4$ at the reacting surface results in development of a product layer resistant to reactant gases, which prevents any further gas-solid reaction [121]. Furthermore, $CaSO_4$ is thermodynamically stable at temperature region around 950°C [119; 122], which is the typical temperature for Ca-based sorbent decomposition in the cyclic carbonation-calcination. Therefore, presence of SO_2 can deactivate the sorbent capacity to capture CO_2 in cyclic separation processes, although the SO_2 concentrations are several orders of magnitude lower than CO_2 concentrations.

Li et al. [119] studied the function of CO_2 in improving the ability of limestone for sulphur capture using a cycle split into three steps as calcination/sulphation/carbonation, and stated that CO_2 can promote the activity of partially sulphated sorbent to capture SO_2, while the effect of SO_2 on the CO_2 capture capacity was reversed. A schematic sequence was presented to illustrate the mechanism of CO_2 in enhancing the sulphation of unreacted core sorbent, shown in Figure 4.3.

Here, after the sulphation step, which results in the formation of a layer of $CaSO_4$ at the outer surface of the particle, some CO_2 penetrates through this layer during carbonation step, as it has smaller molecular volume than SO_2. This CO_2 then reacts with unreacted CaO to form $CaCO_3$. The $CaCO_3$ has larger molecular volume than that of CaO, causing fracture in the sulphated shell, thus exposing unreacted CaO in the core for further sulphation. However, this study did not investigate the simultaneous presence of CO_2 and SO_2 during the separation and regeneration process.

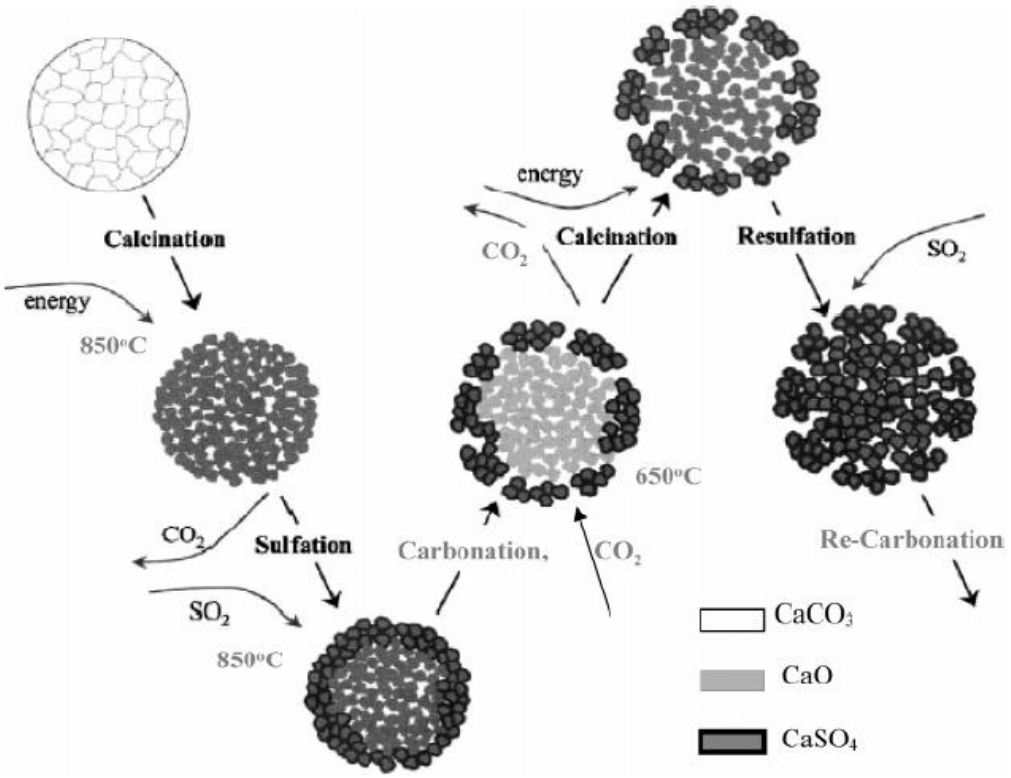

Figure 4.3: Schematic of unreacted core type of limestone over a sequential calcination, sulphation, and carbonation [119].

Later, the tendency of spent sorbent (in cyclic CO_2 separation) to react with SO_2 has also been confirmed by Grasa and others [123], in a TGA study. The results demonstrated that sulphation of CaO increases with increasing the number of carbonation/calcination cycles, as shown in Figure 4.4 (left). Conversely, as can be seen in Figure 4.4 (right), with increased extent of presulphation of CaO sorbent, the extent of carbonation decreases.

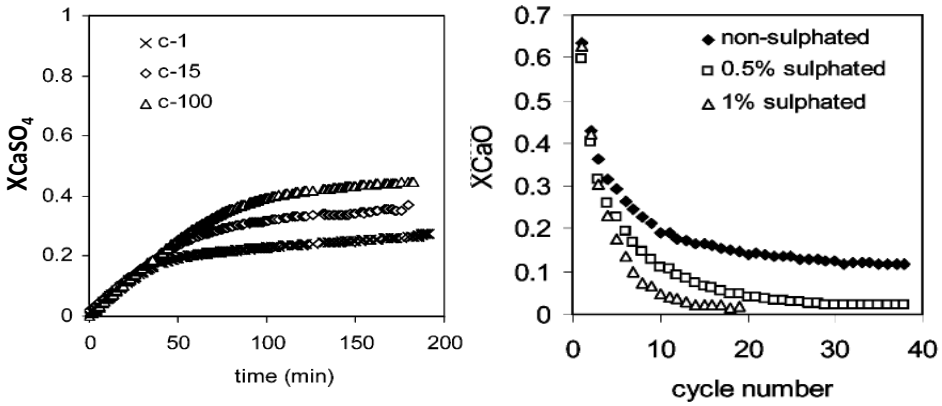

Figure 4.4: (Left) Sulphation of CaO after experiencing 1, 15, and 100 carbonation/calcination cycles. Sulphation atmosphere was air containing 2200 ppm of SO_2 at 900 °C. (Right) Cyclic carbonation of CaO sorbents after experiencing sulphation up to 0%, 0.5%, and 1% molar conversion. Both tests carried out by the same limestone type [123].

Simultaneous presence of CO_2 and SO_2 in limestone looping cycles has also been studied in a few investigations. Ryu [124] and others in the co-capture investigation using FBC demonstrated that CO_2 capture capacity of the sorbent decreased faster with SO_2 present, and proportional to SO_2 concentrations, while cumulative SO_2 capture increased with number of cycles and SO_2 concentrations. Their findings are demonstrated in Figure 4.5.

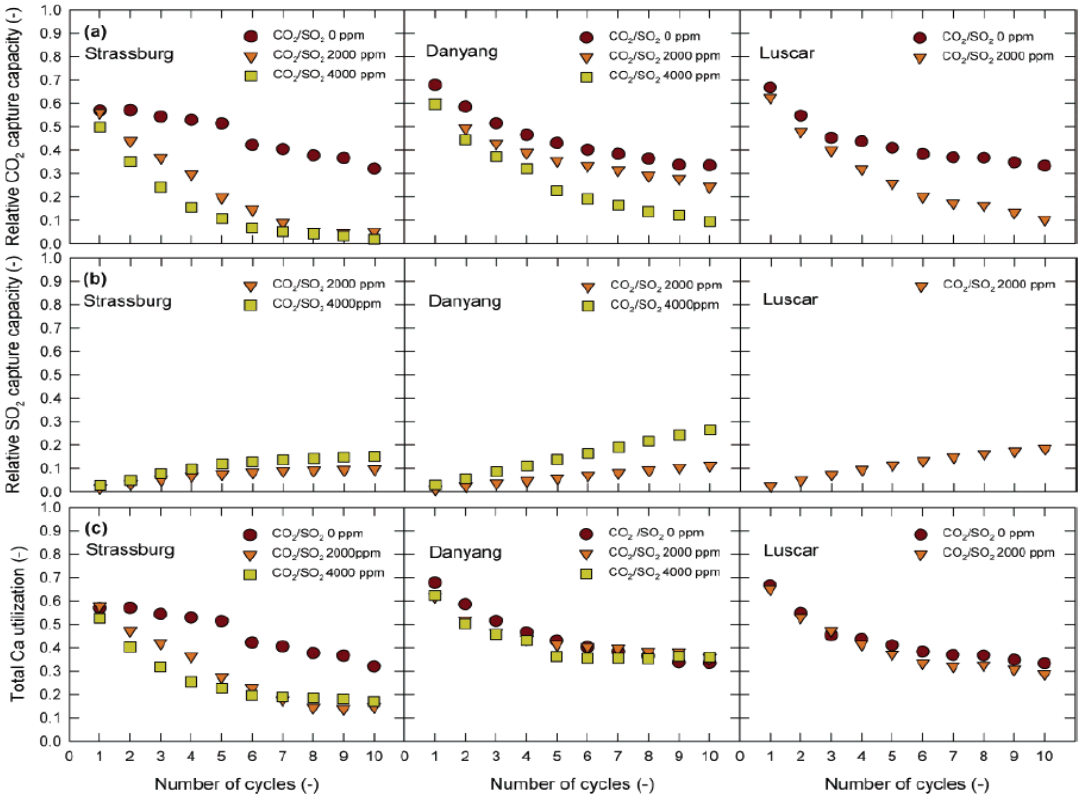

Figure 4.5: Cyclic carbonation and sulphation conversion in a co-capture process. Carbonation in 700 °C and 16% CO_2, elevated SO_2 percentage, 5% O_2, and N_2 balance. Calcination carried out in 850 °C and air [124].

In a thermogravimetric study of several types of limestones, Sun et al. [85], showed that the carbonation conversion of sorbent decayed faster with SO_2 present. They have investigated the performance of seven different sorbents including five types of limestone and two types of dolomite, as shown in Figure 4.6.

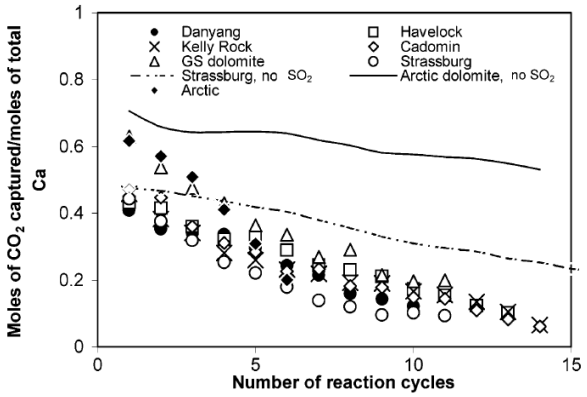

Figure 4.6: Cyclic carbonation and sulphation conversion of seven different sorbents in co-capture processes. Carbonation made in 850 °C and 80% CO_2, 2900 ppm of SO_2, 3% O_2, and N_2 balance. Calcination carried out in 850 °C and pure N_2 [85].

In another co-capture study, Manovic and Anthony [122] investigated the competition of sulphation and carbonation using TGA, and confirmed the findings of Sun and others. Their results on co-capture investigation with elevated SO_2 concentrations for two types of sorbent (natural and artificial limestone) are presented in Figure 4.7. They finally concluded that changes in particles morphology during the CaO carbonation cause a higher sorbent reactivity with SO_2.

4.3.2 Calcination in presence of SO_2

Manovic and Anthony [125] investigated the performance of an artificial type of limestone (calcium aluminate cement) for SO_2 capture at temperature range of 900 °C by TGA experiments. It has been found out that the reaction of these pellets with SO_2 at calcination temperature can reduce their capability in carbonation/ calcination cycles. However, no information on the performance of natural limestone in cyclic carbonation/calcination, when calcination atmosphere contains SO_2, has been reported.

4.4 Cyclic CO_2 capture with pressurised calcination

Performance of the CaO-looping process is influenced by CO_2 partial pressure in reaction conditions. At any given temperature, the limestone decomposition reaction, $CaCO_3 \rightarrow CaO + CO_2$, will proceed if the CO_2 partial pressure surrounding the particles is lower than the thermodynamic equilibrium pressure of limestone. Similarly, the proper operating conditions for the reverse reaction, $CaO + CO_2 \rightarrow CaCO_3$, are identified by comparing CO_2 partial pressure and the equilibrium pressure at any given temperature. More details and the temperature ranges for the two reactions have been described in section 3.4. Therefore, operating pressure and CO_2 partial pressure are influencing both reactions.

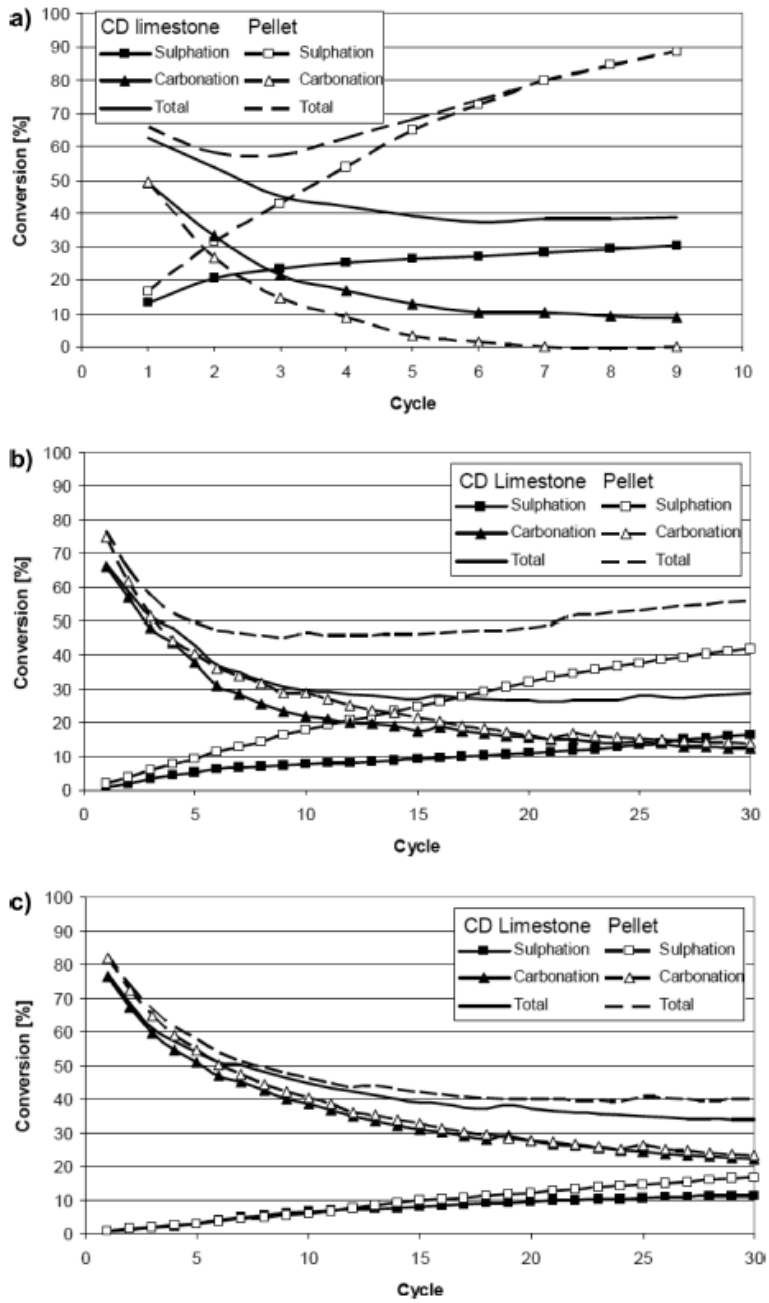

Figure 4.7: Cyclic carbonation and sulphation conversion of two different sorbents in co-capture processes. Carbonation/sulphation made in 650-700 °C and 15% CO_2, elevated SO_2 percentage, 3% O_2, and N_2 balance. Calcination carried out in 950 °C and pure N_2. Elevated SO_2 at (a): 5000 ppm, (b): 500 ppm, and (c): 100 ppm [122].

4.4.1 Pressurised carbonation and cyclic CO_2 capture process

Investigating the potential ways to enhance the CO_2 capture capacity of Ca-based sorbents led to study the pressurised carbonation [126]. Further to this motivation, according to the thermodynamics of CaO-CO_2 reaction, efficient CO_2 capture in FBC in which temperature ranges 850-900 °C can only be obtained by pressurised carbonation

[85]. These investigations were both carried out in pressurised thermogravimetric analysers (PTGA).

4.4.2 Pressurised calcination and cyclic CO_2 capture process

Pressurised calcination has been studied in some investigations. Thermodynamically, calcium-based sorbent will be calcined under pressurised conditions of a gasifier, such as integrated gasification combined cycle (IGCC) process, if CO_2 equilibrium pressure exceeds the CO_2 partial pressure surrounding the sorbents. All researchers concluded that a lower partial pressure of CO_2 increases the calcination rate by providing a higher driving force for the removal of CO_2 from calcined sorbent [27; 127; 128]. Barker stated that CO_2 concentration has no influence on calcination rate if it is well below the decomposition pressure [91]. Figure 4.8 shows the influence of CO_2 partial pressure on calcination rate.

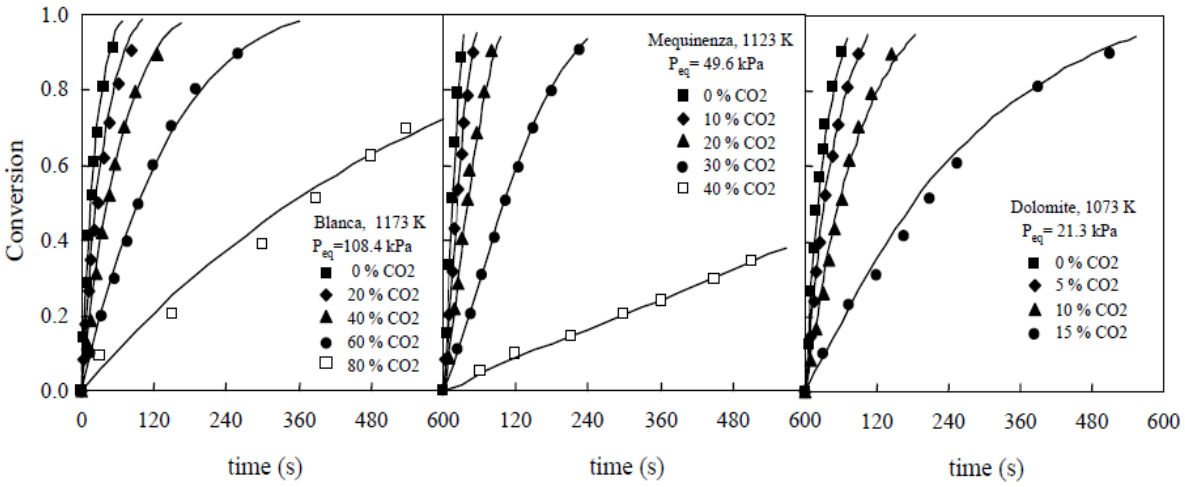

Figure 4.8: Effect of CO_2 partial pressure on atmospheric carbonation conversion. Continues lines demonstrate the model predictions [27].

In an investigation on pressurised calcination, Dennis and Hayhurst [128] found that an increase in pressure gave a decrease in calcination rate, even in absence of CO_2 in the reaction conditions. Prior to this study, investigations on the effect of CO_2 partial pressure on calcination led to raise different views on modelling. Several investigations about the effect of CO_2 partial pressure on calcination considered the reaction rate as a linear function of $(p_{CO_2} - p_{eq})$ to fit the results [77; 129; 130]. Later, Khinast et al. [131] presented an exponential decay in the calcination rate constant with p_{CO_2}. Sun et al. [50] studied the effect of pressurised calcination and carbonation on the cyclic sorption process using PTGA. They concluded that the pressurised calcination, with no CO_2 present, did not change the sorbent reversibility. However, there is no information on cyclic CO_2 capture ability of sorbents involving pressurised calcination/atmospheric carbonation in presence of CO_2.

So far most of the investigations have been made by thermogravimetric analyzer (TGA), or in case of pressurised test, by means of pressurised thermogravimetric analyzer (PTGA). Carrying experiments out by means of TGA can lead to erroneous reading of the results due to the system limitations such as low gas throughput, and dependency on weight change as the sole measured factor [132]. Therefore, taking care in extrapolating the results from TGA has also been suggested by Anthony [37]. Furthermore, there is a lack of results in practical calcination atmosphere, and in cyclic mode processes.

CHAPTER 5

Experimental

Chapter 5 : Experimental

5.1 Experimental apparatus

The experimental facilities used to carry out these tests consist of two main parts: (i) the reactor, and (ii) the apparatus used to maintain required conditions, analyse the off-gases, and acquire the process data.

5.1.1 Pressurised fluidised bed reactor

The multi-cycles split calcination and carbonation experiments with elevated pressure, different steam and SO_2 percentages were carried out in a fluidised bed reactor. A schematic of the system is presented in Figure 5.1. The experiments conducted by the test unit were run batch wise for the solids, so no particles were added during the runs.

The major components consist of the outer pressurised tube, a preheating zone which is the lower space between the rector and the outer tube (Figure 5.2), the fluidised reactor, a hot gas filter on the flue stream, a gas dryer, a water pump, and two gas-analyser units (ADC 7000 GAS ANALYSER) to measure CO_2 and SO_2 concentrations. The outer tube has a height of 1180mm and internal diameter of 37mm. A quartz reactor at 550mm height and 32mm internal diameter was used for the atmospheric tests. For the pressurised tests, the quartz reactor was replaced with a stainless steel (310) reactor, in order to be able to operate under higher pressure. The pre-heater zone therefore has a height of 630mm. A sintered plate was placed at the bottom of the reactor as gas-distributor, while its holes separate the pre-heater zone and the reactor, so that the limestone and lime particles remain inside the reaction column.

An electrical heater surrounding the outer tube maintained the required reaction temperature in the reactor, and provided preheating of gases. The heater can maintain the reactor region at a maximum temperature of 1200°C. Reactor temperature, from K-type thermocouple measurement, and the differential pressure across the bed have been recorded by a data acquisition system.

Water and reactant gases, CO_2, O_2, SO_2, and N_2, were fed to the system via bottom flange of the outer tube, and passed through the pre-heater zone prior to entering the reactor. These gases have been supplied by gas bottles. The flow rates of introduced gases were manipulated using highly accurate Mass Flow Controllers (MFC), (Bronkhorst; EL-FLOW Series), Figure 5.3.

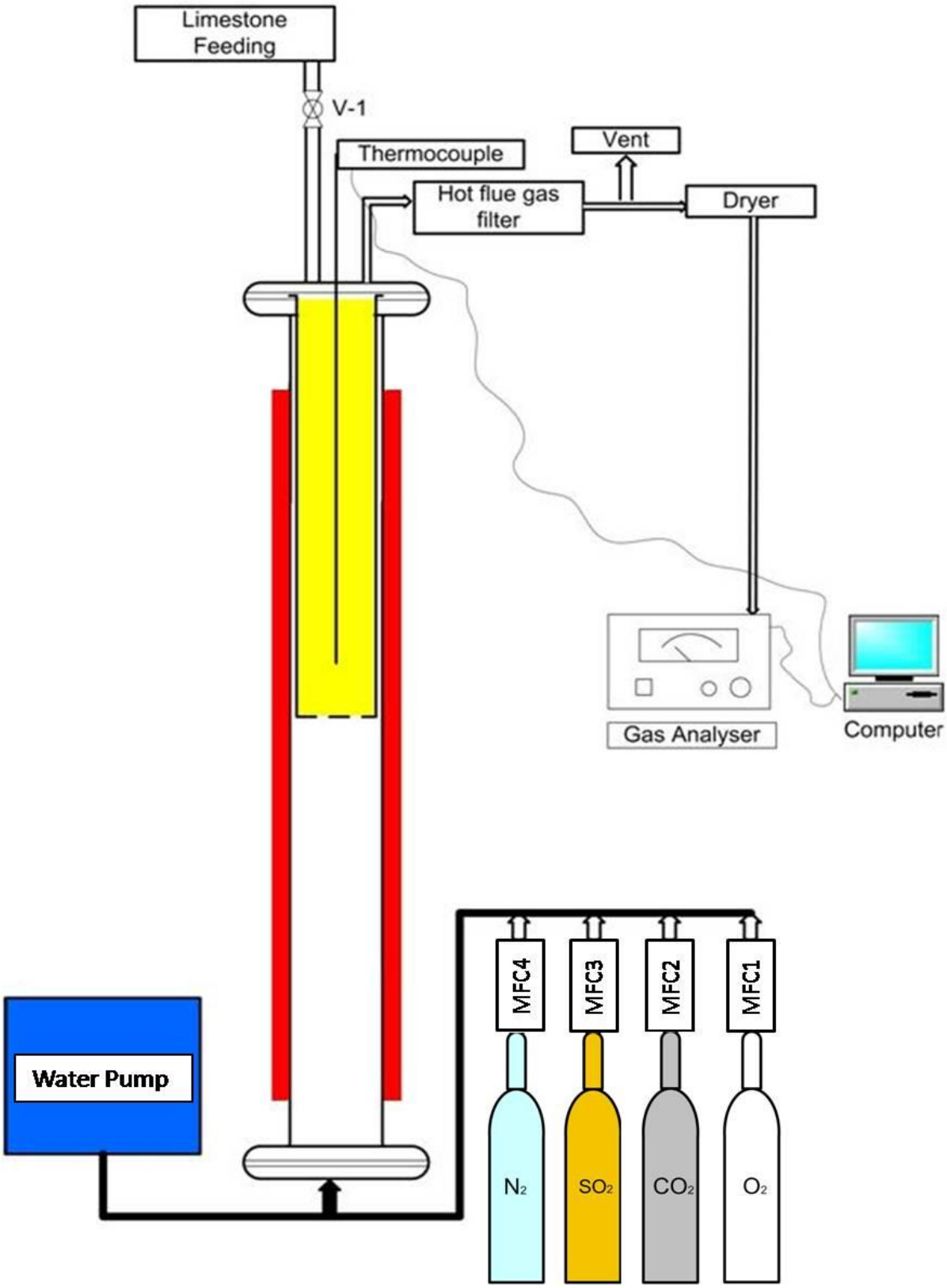

Figure 5.1: Schematic of pressurised system (fluidised bed reactor

Figure 5.2: Pressurised vessel and the preheating zone of the tests facilities.

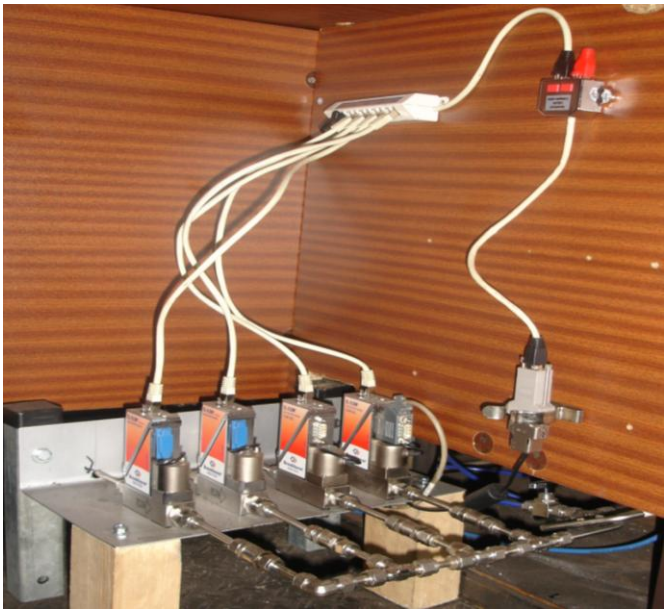

Figure 5.3: Mass Flow Controllers (MFC) system for CO_2 capture.

Water was fed to the preheating zone using a HPLC pump at an appropriate flow rate so that produces the required amount of steam for each set of tests. High temperature and volume of the preheating zone compared to the flow rate of injected water prevented any disturbance to the temperature profile inside the reactor. The stability in the reactor temperature has been evidenced by plotting the temperature versus time of carbonation, as isothermal reactions. Figure 5.4 depicts temperature against time of carbonation in presence of 20% steam.

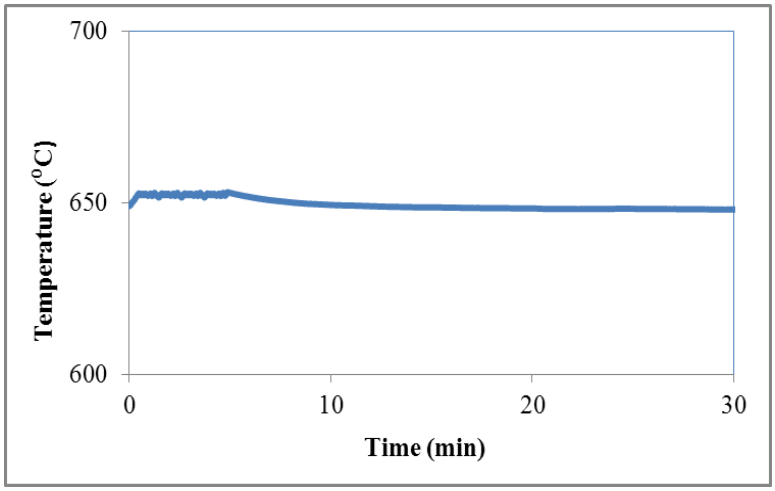

Figure 5.4: Reactor temperature over the carbonation time in a test cycle. Carbonation conditions: 20% steam, 15% CO_2, 4% O_2, and balance N_2.

The exit stream from the fluidised bed reactor was dried before being analysed at the gas analyser. The CO_2 and SO_2 concentrations were measured using the gas analysers on the flue stream, and logged continuously by the data acquisition system. Continuous production of steam was evidenced by plotting the exit CO_2 concentrations versus time before commencing and after completing the calcination reactions. The steady state dried CO_2 concentration curves verified that the steam has been provided continuously. Figure 5.5 demonstrates CO_2 traces against time of calcination in presence of 78% steam.

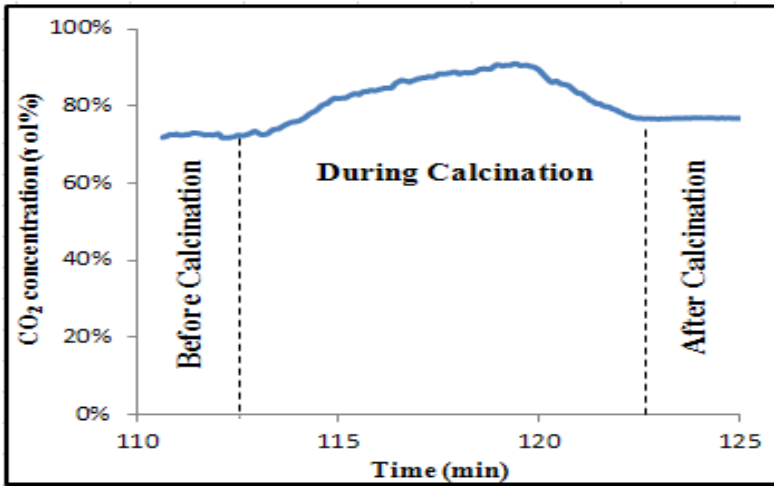

Figure 5.5: CO_2 concentrations in off-gases before, during and after calcination in a test cycle. Calcination conditions: 78% steam, 15% CO_2, 3% O_2, and balance N_2.

5.1.2 Solid analysis and characterisation

In order to observe the changes in sorbent morphology and pore structure, to aid the interpretation of results, calcined samples were collected after the first and final cycles for each run of set conditions. Some of the samples were slightly crushed to study their morphology for both the outer shell and interior of the particles. The samples were gold-coated prior to the imaging, to make them conductive and to obtain high-resolution reflection. They were then subjected to scanning electron microscope imaging (SEM) by a PHILIPS XL30SFEG instrument. A SIEMENS D5005 X-ray diffractometer has been used to produce a diffraction patterns (XRD) of particles after different number of test cycles. Other morphological characteristics of the CaO particles including specific surface area, pore volume, porosity, and pore size distribution have been also measured. TriStar micrometrics pressure measurement has been used by volumetric gas adsorption analysis. Different mathematical models have been applied for the calculations. Pore volume and surface area were measured using BET, Longmuir and BJH models. The t-plot and BJH models were used to obtain pore size distribution.

5.2 Experimental material

In this study, Longcliffe calcium carbonate (Longcal SP52) with minimum 98.25% of $CaCO_3$ content, and specific gravity 2.65 g/cm^3, was used for the experimental sample. The limestone was ground and sieved to 125-250 microns for the experiments. Table 5.1 shows the chemical composition of the used limestone.

Table 5.1: Specification of the used limestone

Composition	Calcium as $CaCO_3$	Calcium as CaO	CO_2	others
Amount	98.25%	55%	43.25%	1.75%

5.3 Experimental procedures

Prior to heat-up for the calcination step, the quartz reactor was preloaded with 10g of limestone. Temperatures of the fluidised bed reactor and the gas pre-heater zone then were ramped at a constant rate. Therefore, the calcinations were carried out in non-isothermal conditions. The reactor bed was fluidised with a total inlet gas flow of 1.2 Nl/min in all calcination cases, to provide a bubbling fluidised bed in gas-solid contact. In the reverse reaction the reactor was cooled down at a constant rate. The reactor bed was fluidised with a total inlet gas flow of 1.6 Nl/min in all carbonation steps. The required steam content in the reacting gases was maintained by continues pumping of deionised water. The U/U_{mf} were about 2 for both calcination and carbonations steps. Higher levels of the U/U_{mf} could cause that some amounts of smaller particles to leave the system, considering the height of the reactor. Selection of gas flow rates and other reaction conditions are described in chapter 6. More details on minimum bubbling gas flow rates will be presenting in and Appendix A.

5.3.1 Test runs with steam present in calcination-carbonation cycles

Temperatures of the fluidised bed reactor and the gas pre-heater zone then were raised at the rate 20°C/min to the target values of 950°C. Calcination steps were ended once the limestone was fully decomposed. Complete calcination is reached when the decomposed CO_2 vol% drops to a negligible level in the exit stream. Therefore, the reactor was cooled-down to 650 °C at the rate of 7.5 °C/min and the produced lime was exposed to gas mixtures containing a certain percentage of CO_2 and a flow at 1.6 Nl/min. The carbonation step was also continued until the reaction was completed, which corresponds to CO_2 vol% reaching a constant level in the exit gas stream, that is almost equal to the feed level. After a complete carbonation, the bed temperature was increased again to 950 °C to regenerate the lime. These sequential processes were repeated about 10 cycles for each set of operating conditions.

Taking the various recommended process integrations into account [44], the oxy-fuel combustion conditions were simulated for calcination steps. The simulated decomposition sweep gas contained 3% O_2, 2% N_2, and elevated amount of steam/CO_2 starting from 28% / 67% as the base. The basic conditions for steam/CO_2 were estimated by oxy-fuel combustion calculation for coal. The recent calculation was carried out based on the composition analysis of daw mill coal [133]. The flue gas calculations for a few fuels in different combustion conditions are presented in the Appendix B. The calcination conditions were then followed with 20% and 50% added steam, which finally reached to oxy-fuel of natural gas.

The carbonation steps were carried out in the real air-fuel flue gas composition. The simulated flue gas contained 15% CO_2 and 4% O_2, and two levels of steam (6 and 20%), for all sorption tests. Nitrogen was introduced as balance in carbonation steps. Two runs were also carried out with no steam present in decomposition conditions. The experimental conditions are summarized in Table 5.2.

Table 5.2: Experimental conditions in tests run with steam present.

Run Set	Calcination						Carbonation					
	Conditions	Steam	CO_2	O_2	SO_2	N_2	Conditions	Steam	CO_2	O_2	SO_2	N_2
Steam01	Air-fuel	-	15%	4%	-	balance	Air-fuel	20%	15%	4%	-	balance
Steam02	Air-fuel	-	15%	4%	-	balance	Air-fuel	-	15%	4%	-	balance
Steam1	Oxy-fuel	28%	67%	3%	-	2%	Air-fuel	6%	15%	4%	-	balance
Steam2	Oxy-fuel	28%	67%	3%	-	2%	Air-fuel	20%	15%	4%	-	balance
Steam3	Oxy-fuel	48%	47%	3%	-	2%	Air-fuel	6%	15%	4%	-	balance
Steam4	Oxy-fuel	48%	47%	3%	-	2%	Air-fuel	20%	15%	4%	-	balance
Steam5	Oxy-fuel	78%	17%	3%	-	2%	Air-fuel	6%	15%	4%	-	balance
Steam6	Oxy-fuel	78%	17%	3%	-	2%	Air-fuel	20%	15%	4%	-	balance

5.3.2 Test runs with SO_2 present in calcination-carbonation cycles

Temperatures of the fluidised bed reactor were raised at the rate 25°C/min to the target values of 950°C. Direct sulphation of limestone has been reported that takes place at 610, 720, 800, and 850°C, resulting in 10%, 15%, 25%, and 40% conversion, respectively, in presence of about 1900 ppm of SO_2 and 80% CO_2 during 5000s reacting time [132]. Therefore, in order to avoid direct sulphation during the heating-up and before the start of decomposition, SO_2 was supplied when the reactor reached incipient calcination temperature. Calcination steps were stopped once the limestone was fully decomposed. Complete calcination is obtained when the decomposed CO_2 vol% drops to a negligible level in the exit stream. After the complete calcination the reactor was cooled-down to 650 °C at the rate of 10 °C/min. The literature [97] suggests that the range 850-900 °C is the optimal temperature for CaO sulphation. Therefore, in order to provide the co-capture conditions and predict CaO-sulphation during the cooling-down, SO_2 feeding was ceased after the complete decomposition.

After the temperature reached 650 °C, the produced lime was exposed to carbonating gas mixtures containing a certain percentage of CO_2 and SO_2 at a flow of 1.6 Nl/min. The carbonation step was also continued until the reaction was completed, which corresponds to CO_2 vol% reaching a constant level in the exit gas stream, that is almost equal to the feed level. On average the capturing step lasted about 30 minutes. After complete carbonation, the bed temperature was increased again to 950 °C to regenerate the lime. These sequential processes were repeated about 10 cycles for each set of operating conditions.

Taking the recommended processes integrations into account [44], the oxy-fuel combustion conditions were supposed to be simulated for calcination steps. However, in order to study the effects of a single factor (SO_2), the other influencing factor (steam) was omitted from the reaction conditions. Therefore, N_2 was used to replace the minimum amount of steam in oxy-coal conditions, and also for more dilution in calcination. In fact, N_2 was used to replace the steam in conditions simulating oxy-coal with 52% added steam (set Steam 5 and 6 in Table 5.2). The simulated decomposition sweep gas contained 15% CO_2, 3% O_2, 0 or 1500 ppm simulate SO_2, and N_2 balance. The considered 1500 ppm is a realistic flue gas value for low sulphur coal containing ~0.6% sulphur, such as Brown coal [133]. More examples of SO_2 produced in different coal and gas combustion are presented in the Appendix B.

The carbonation steps were carried out in the real air-fuel flue gas composition. The simulated flue gas contained 15% CO_2 and 4% O_2, three levels of SO_2 (200, 2500, and 5000 ppm), for all sorption tests. Nitrogen was introduced as balance in carbonation steps. The experimental conditions are summarized in Table 5.3.

Table 5.3: Experimental conditions in tests run with SO_2 present

Run No.	Calcination					Carbonation					
	Steam	CO_2	O_2	SO_2(ppmv)	N_2	Condition	Steam	CO_2	O_2	SO_2(ppmv)	N_2
Sulph 1	-	15%	3%	-	balance	Air-fuel	-	15%	4%	200	balance
Sulph 2	-	15%	3%	-	balance	Air-fuel	-	15%	4%	2500	balance
Sulph 3	-	15%	3%	-	balance	Air-fuel	-	15%	4%	5000	balance
Sulph 4	-	15%	3%	1500	balance	Air-fuel	-	15%	4%	200	balance
Sulph 5	-	15%	3%	1500	balance	Air-fuel	-	15%	4%	2500	balance
Sulph 6	-	15%	3%	1500	balance	Air-fuel	-	15%	4%	5000	balance

5.3.3 Test runs with pressurised calcination

Temperatures of the fluidised bed reactor were raised at the rate 25 °C/min to the target values of 950°C. The reactor bed was fluidised with a sweep gas at flow rates of 1.2, 6.0, and 12.0 Nl/min in decomposition steps, to provide a bubbling regime during gas-solid reaction under elevated pressures. Calcination steps were carried out once the CO_2 detected in the outlet flue gases dropped to a constant level over a significant period, and almost equal to that for the initial amount. After the calcination the reactor was cooled-down to 650 °C at the rate of 10 °C/min.

After the temperature reached 650 °C, the produced lime was exposed to carbonating gas mixtures containing a certain percentage of CO_2 at a flow of 1.6 Nl/min. The carbonation step was also continued until the reaction was completed, which corresponds to CO_2 vol% reaching a constant level in the exit gas stream, that is almost equal to the feed level. The capturing step lasted about 30 minutes. After a complete carbonation, the bed temperature was increased again to 950 °C to regenerate the lime. These sequential processes were repeated about 8-10 cycles for each set of operating pressure.

Taking the recommended process integrations into account [44], the oxy-fuel combustion conditions were supposed to be simulated for calcination steps. However, in order to study the effects of a single factor (pressure), other influencing factors (steam and SO_2) were omitted from the reaction conditions. Therefore, N_2 was used to replace the minimum amount of steam and SO_2 in oxy-coal conditions, and also for more dilution in calcination. In fact, N_2 was used to replace SO_2 and steam in conditions simulating oxy-coal with 52% added steam (set Steam 5 and 6 in Table 5.2). The simulated decomposition sweep gas contained 15% CO_2, 3% O_2, and N_2 balance.

The carbonation steps were carried out in the real air-fuel flue gas composition. The simulated flue gas contained 15% CO_2 and 4% O_2 for all sorption tests. Nitrogen was introduced as balance in carbonation steps. The experimental conditions are summarized in Table 5.4.

Table 5.4: Experimental conditions in tests run with pressurised calcination

Test Run / Pressure	**Calcination** CO_2	O_2	N_2	**Carbonation** Condition	CO_2	O_2	N_2
Press1 (0.1 MPa)	15%	3%	balance	Air-fuel	15%	4%	balance
Press2 (0.5 MPa)	15%	3%	balance	Air-fuel	15%	4%	balance
Press3 (1.0 MPa)	15%	3%	balance	Air-fuel	15%	4%	balance

CHAPTER

6

Optimising the tests operating conditions

Chapter 6 : Optimising the tests operating conditions

6.1 Introduction

A number of single cycle experiments were primarily performed to select the operating conditions. Figures 6.1 to Figure 6.5 show the calcination and carbonation conversion curves versus time obtained at different level of operating factors. All of these initial experiments were carried out in N_2 for calcination, and then followed by carbonation reaction in conditions containing 15% CO_2 and N_2 balance.

Statistical analysis of the experiments has also been carried out by investigating the repeatability of tests in cyclic runs, shown in Figure 6.6. The tests conditions are given in the figure caption.

6.2 Isothermal and non-isothermal calcination

The limitation on the time period required for the entire experimental set governes the process arrangement in terms of the sorbent feeding. This section deals with the calcination process. Practically keeping the sorbents in the reactor at the end of calcination and during cooling down the system, provides a cyclic process in a shorter time. To investigate any likely effect of the two arrangements on calcination and carbonation, they are compared in this section.

Isothermal reaction corresponds to a run where sorbents are added to the system after the reactor reached the target temperature for calcination, 950°C. Non-isothermal run corresponds to the process in which sorbents were fed to the reactor prior the heating up.

Both calcinations have been carried out and, in order to compare their perfomances, the calcinations were followed by recarbonation. The results are shown in Figure 6.1. These results reveal the similar extent in conversion for both processes , but faster rate for the isothermal calcination. The equations used in calculating these results are given in chapter 7.

6.3 Effect of particles size

Three different sorbent sizes were used for calcination and carbonation to understand the effect of particle size on the capture performance. The sorbent sizes were: (1) smaller than 125μm, (2) between 125 μm and 250μm, and (3) bigger than 800 μm. The calcination and carbonation conversions are depicted in Figure 6.2. The calcination curves show slightly better conversion for the medium size range.

As discussed in section 3.2.1 a higher conversion rate and extent was expected for smaller particles. These results also confirmed the same effect and the only exception for particles smaller than 125μm may be interpreted as the adhering of fine particles, and lowering their decomposition. The carbonation conversion curves also prove that a better decomposition has been carried out for the particles of medium size.

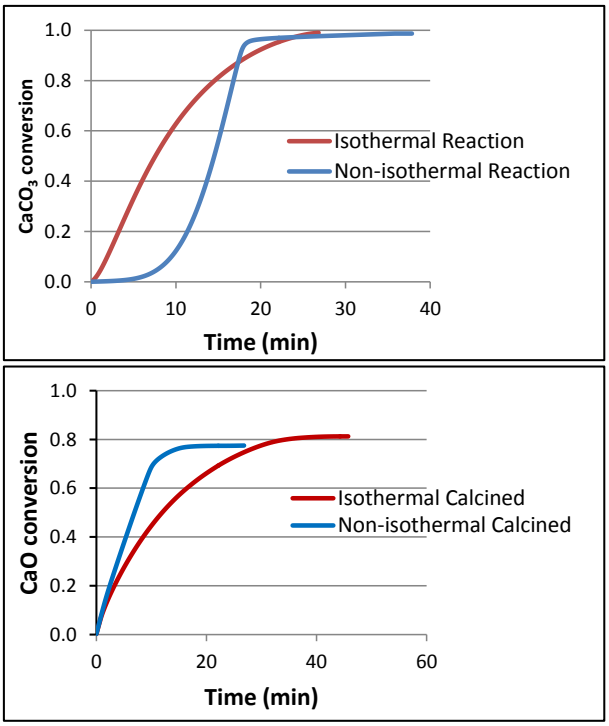

Figure 6.1: Effect of sorbent feeding in calcination step. **(top)** shows calcination and **(bottom)** demonstrates carbonations; **(calcination)** in N_2; **(carbonation)** 15% CO_2, 4% O_2, balances N_2.

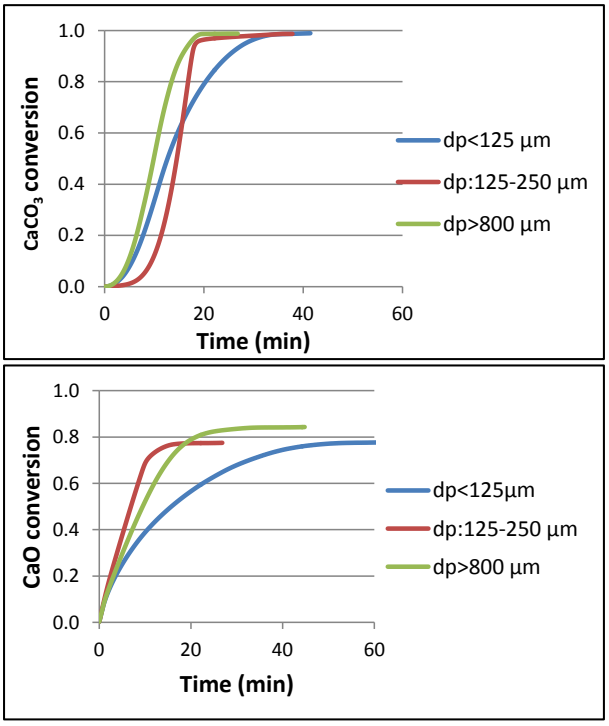

Figure 6.2: Effect of particle size on the performance of the calcite **(top)** shows calcination and **(bottom)** demonstrates carbonations; **(calcination)** in N_2; **(carbonation)** 15% CO_2, 4% O_2, balances N_2.

6.4 Effect of gas flow rate

The input gases flow rate, $Q_{gas,}$ to maintain a bubbling regime in the fluidised bed has been set at about 1.2 l.min^{-1} and 1.6 l.min^{-1} for calcination and carbonation steps, respectively. The minimum superfacial gas velocities (U_{mf}), required to fluidise the bed, were calculated based on reactions temperature [134]. The U/U_{mf} were about 2 for both calcination and carbonation steps. However, in order to investigate the likely influence of the flow rate on the process, the calcination and carbonation of the particles have been carried out at two levels of flow rate. These flow rates were applied equally as sweeping gas in calcination step, and as reacting gas in carbonation step. The results are depicted in Figure 6.3. As can be seen, sorbents demonstrates better performance when they are fluidised by lower flow rates of gas.

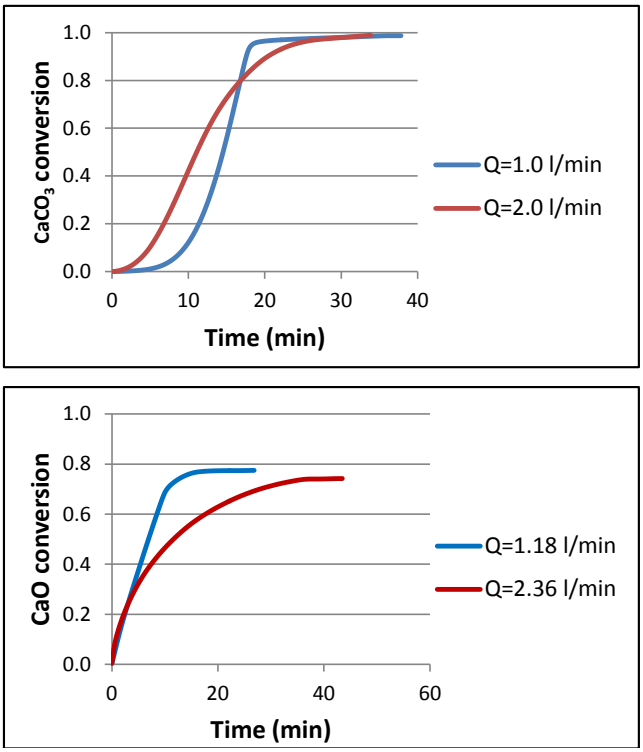

Figure 6.3: Effect of gas flow rate on the performance of the process; **(top)** shows calcination and **(bottom)** demonstrates carbonations; **(calcination)** in N_2; **(carbonation)** 15% CO_2, 4% O_2, balances N_2.

6.5 Effect of bed inventory

Three different bed inventories at 20, 10, and 5g were used in calcination/carbonation process, to observe the effect of sample quantity. As can be seen in Figure 6.4, both calcination and carbonation rate for 20g is slower than other quantities of samples, although after a long reaction rate all samples achieved almost equal conversions

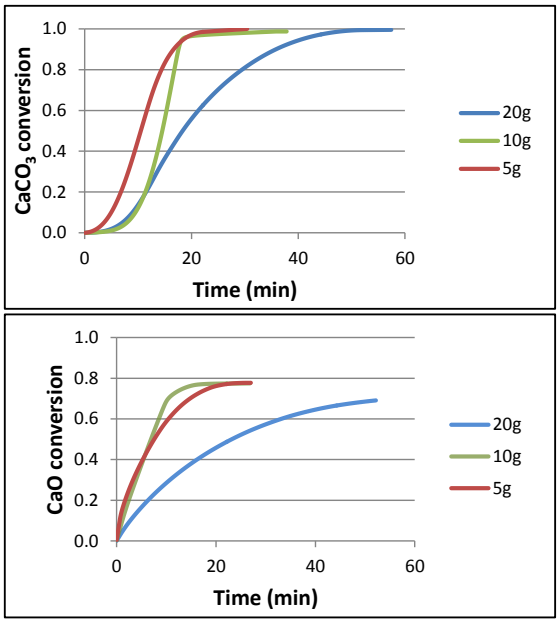

Figure 6.4: Effect of bed inventory on calcination–carbonation; **(top)** shows calcination and **(bottom)** demonstrates carbonations; **(calcination)** in N_2; **(carbonation)** 15% CO_2, 4% O_2, balances N_2.

6.6 Effect of reaction temperature

The calcination/carbonation reactions have been carried out and compared in two levels of temperature. Calcination was made at 950 °C, which was then followed by carbonation at 650 °C. Another experiment includes decomposition at 850 °C and sorption at 700 °C. As can be seen in Figure 6.5 calcination in 950 °C results in higher conversions for both calcination and carbonation steps.

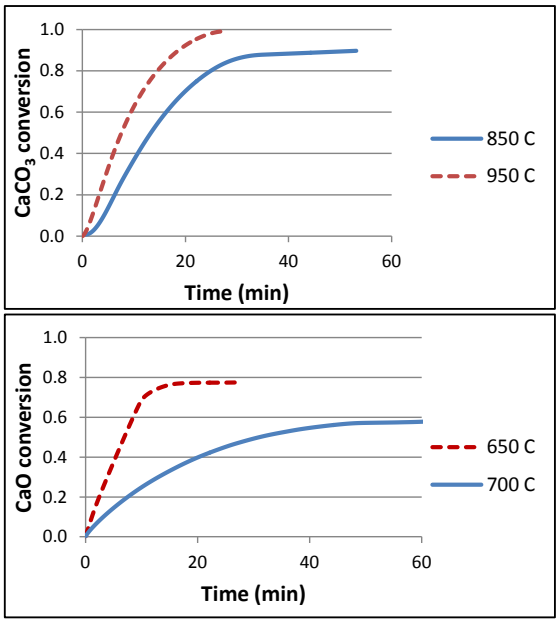

Figure 6.5: Effect of reaction temperature on calcination **(top)**, and carbonation **(bottom)**; Carbonation in 650 °C corresponds to the sorbent which have been calcined at 950 °C.; **(calcination)** in N_2; **(carbonation)** 15% CO_2, 4% O_2, balances N_2.

6.7 Optimising operating conditions

The operating conditions which eventually used to perform the experiments are summarised in Table 6.1. In order to lower the reaction period and to prevent the subsequent troubles in the steel rector; the pressurised test at 1.0 MPa were carried out using 5g of sample, as the single exemption in test conditions.

Table 6.1: Optimised operating conditions applied in test runs

Limestone		**Calcination**		**Carbonation**	
Bed inventory	Particle size	Temperature	gas flow rate	**Temper**ature	gas flow rate
10(g)	120-250(µm)	950(°C)	$1.2(\mathrm{l.min^{-1}})$	650(°C)	$1.6(\mathrm{l.min^{-1}})$

6.8 Repeatability of the tests (statistical analysis)

The repeatability of the experiments has been investigated by comparing three cyclic runs, which were carried out in similar conditions, as shown in Figure 6.6. As can be seen the results demonstrate quite close values of carbonation conversions over corresponding cycle numbers. The results show that about 94% of the conversion values lie in within one standard deviation around the mean (Ave ± 1S), in each cycle. All the conversion values, 100%, are placed within two standard deviation around the mean (Ave ± 2S).

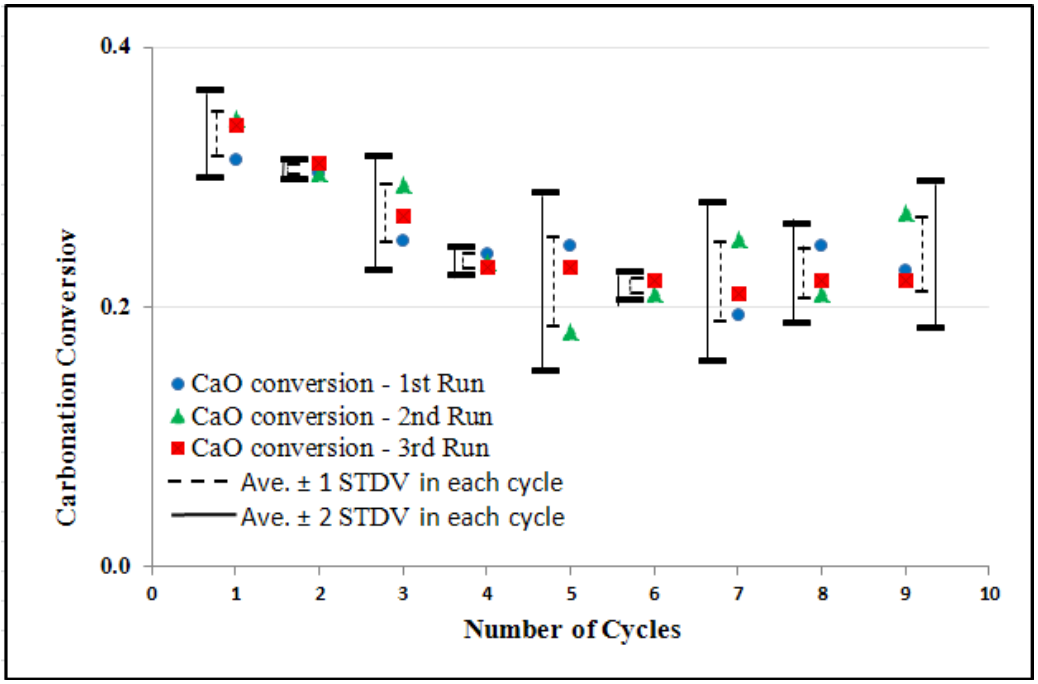

Figure 6.6: Repeatability of the tests by comparing three cyclic runs in the same conditions; **(calcination)** 47% CO_2, 3% O_2, 48% steam, balance N_2; **(carbonation)** 15% CO_2, 4% O_2, 20% steam, balance N_2.

6.9 Data recording in cyclic calcination-carbonation

A typical raw data recording of CO_2 concentration and temperature against time, collected over a cyclic process of calcination-carbonation, is illustrated in Figure 6.7. The number of test cycles per day was restricted by the total time required to complete one cycle (approximately 1.5 h or more); hence, total cycles in a test set lasted for several days. Discontinuity points in the curves indicate the portion of test conducted in each day.

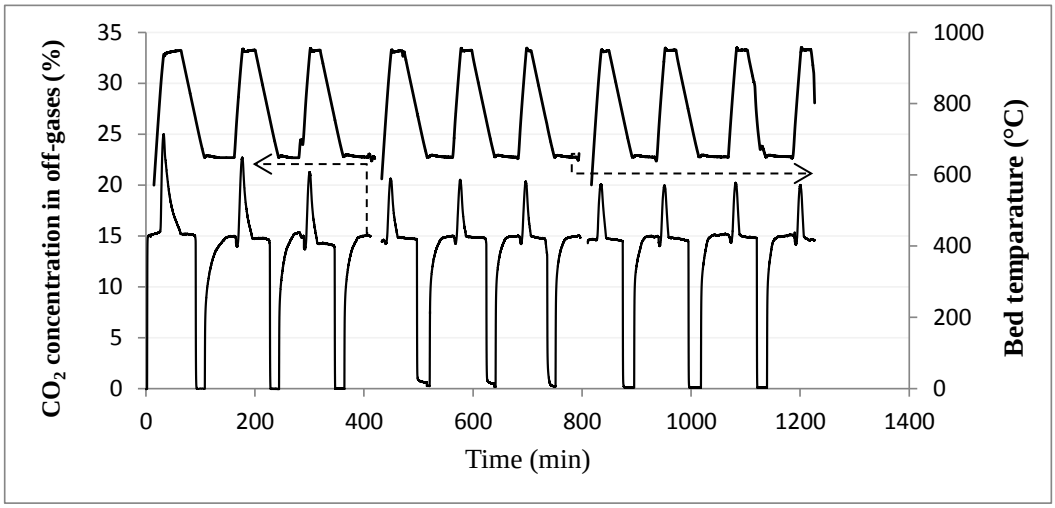

Figure 6.7: A typical raw process data acquisied over a cyclic calcination-carbonation

CHAPTER 7

Results and Discussion

Chapter 7 : Results and Discussion

This chapter comprises results obtained from experiments, and the subsequent discussion. The extent of conversion for each reaction was considered as the key dependent variable to evaluate the performance of the sorbent. The gas concentration was measured as the base of conversion calculation.

Carbonation and sulphation conversions were calculated by integrating the CO_2 and SO_2 concentration over the reaction time. Figure 7.1 illustrates the mathematical method to calculate carbonation and sulphation conversion based on the measurement of the species in off-gases. Similarly calcination conversion was calculated, but using the area under the concentration curve. The time interval, dt, corresponds to the sampling interval of data acquisition system. The sensitivity analysis shows that a reliable calculation is provided by this method, considering the likely error in concentration measurement.

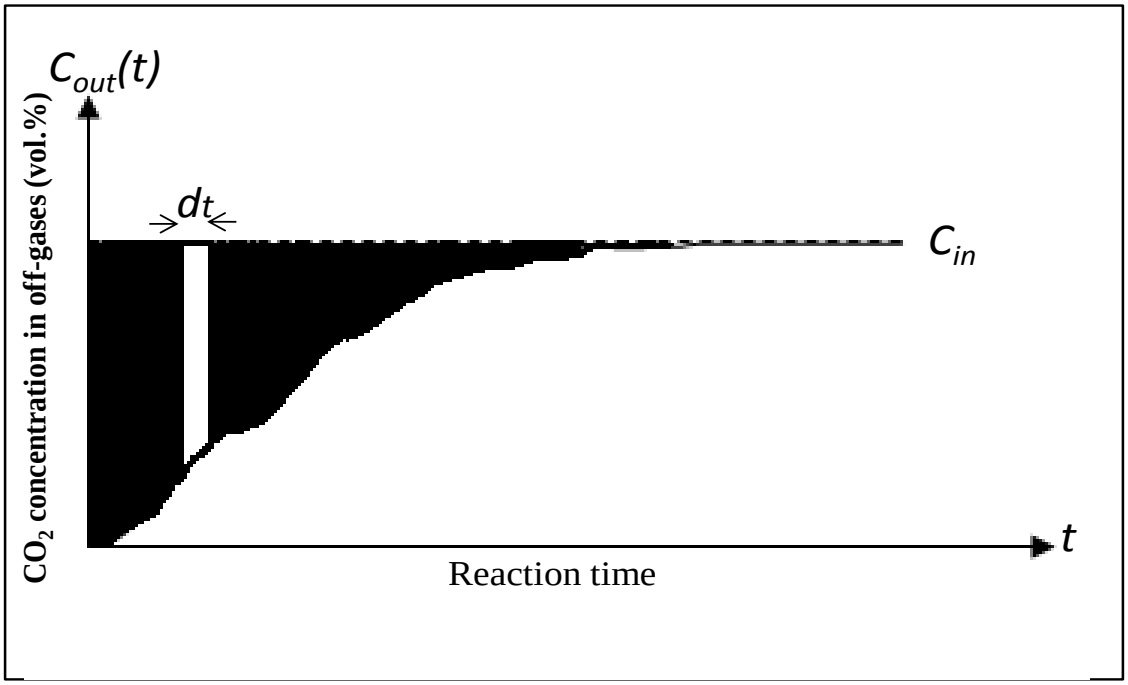

Figure 7.1: Mathematical method to calculate the carbonation and sulphation conversion based on off-gas measurement.

The volume flow rate of CO_2 captured during carbonation can be calculated as:

$$Q_{CO_2\ captured} = Q_{in} - Q_{out} \quad (7.1)$$

Symbols are defined at the end of this section. Since only CO_2 is being captured, [(a)]

$$Q_{in} - Q_{out} = Q_{in} . C_{CO_2\ in} - Q_{out} . \ C_{CO_2\ out} \quad (7.2)$$

$$Q_{out} = \frac{1-C_{CO_2\,in}}{1-C_{CO_2\,out}} Q_{in} \quad (7.3)$$

Then combining (7.1) and (7.3) gives:

$$Q_{CO_2 captured} = Q_{in} - Q_{out} = Q_{in} - \frac{1-C_{CO_2\,in}}{1-C_{CO_2\,out}} Q_{in} = \frac{C_{CO_2\,in} - C_{CO_2\,out}}{1-C_{CO_2\,out}} Q_{in}$$

$$V_{CO_2\,captured} = Q_{in} \int \frac{C_{CO2\,in} - C_{CO2\,out}}{1-C_{CO2\,out}} dt$$

Therefore, carbonation conversion can be calculated using:

$$\boldsymbol{X_{Carb}(t) = \frac{Q_{in} M_{CaCO_3}}{m_0 V_{m_{CO_2}}(T,p)} \int_0^t \frac{C_{CO_2\,in} - C_{CO_2\,out}(t)}{1-C_{CO_2\,out}(t)}\, dt} \quad (7.4)$$

Conversely, over calcination reaction Q_{out} *is greater than* Q_{in}. Therefore, a similar approach gives:

$$Q_{CO_2\,released} = Q_{out} - Q_{in} \quad (7.5)$$

Since only CO_2 is being released: *(b)*

$$Q_{out} - Q_{in} = Q_{out} \cdot C_{CO_2\,out} - Q_{in} \cdot C_{CO_2\,in} \quad (7.6)$$

$$Q_{out} = \frac{1-C_{CO_2\,in}}{1-C_{CO_2\,out}} Q_{in} \quad (7.7)$$

Then combining (7.5) and (7.7) gives:

$$Q_{CO_2\,released} = Q_{out} - Q_{in} = \frac{1-C_{CO_2\,in}}{1-C_{CO_2\,out}} Q_{in} - Q_{in} = \frac{C_{CO_2\,out} - C_{CO_2\,in}}{1-C_{CO_2\,out}} Q_{in}$$

$$V_{CO_2\,released} = Q_{in} \int \frac{C_{CO2\,out} - C_{CO2\,in}}{1-C_{CO2\,out}} dt$$

Therefore, if volume fraction of off-gas species is being measured, calcination conversion can be calculated using:

$$\boldsymbol{X_{Calc}(t) = \frac{Q_{in} M_{CaCO_3}}{m_0 V_{m_{CO_2}}(T,p)} \int_0^t \frac{C_{CO_2\,out}(t) - C_{CO_2\,in}}{1-C_{CO_2\,out}(t)}\, dt} \quad (7.8)$$

In a co-capture process, two reactions (sulphation and carbonation) are taking place simultaneously, unlike the situation in part (a) and (b). For a single sulphation reaction the flow rate of captured SO_2 can be calculated as:

$$Q_{SO_2\ captured} = Q_{in}\ .C_{SO_2\ in} - Q_{out}\ .\ C_{SO_2\ out} \quad (7.9)$$

However, Q_{out} in equation (7.9) is also affected (reduced) as a result of simultaneous carbonation. This means Q_{out} during carbonation can be considered as equation (7.3):

$$Q_{out} = \frac{1-C_{CO2\ in}}{1-C_{CO2\ out}} Q_{in}$$

Substituting the corrected Q_{out} in equation (7.9) gives:

$$Q_{SO_2\ captured} = Q_{in}[C_{SO_2\ in} - \frac{1-C_{CO_2\ in}}{1-C_{CO_2\ out}}\ C_{SO_2\ out}]$$

$$V_{SO_2\ captured} = Q_{in} \int [C_{SO_2\ in} - \frac{1-C_{CO_2\ in}}{1-C_{CO_2\ out}}\ C_{SO_2\ out}]dt$$

Therefore, sulphation during carbonation can be calculated using:

$$\boldsymbol{X_{Sulph}(t) = \frac{Q_{in}M_{CaCO_3}}{m_0 V_{m_{SO_2}}(T,p)} \int_0^t [C_{SO_2\ in} - \frac{1-C_{CO_2\ in}}{1-C_{CO_2\ out}}\ C_{SO_2\ out}]\ dt} \quad (7.10)$$

Similarly, carbonation during sulphation (in co-capture process) can be calculated using:

$$Q_{CO_2 captured} = Q_{in}\ .C_{CO_2\ in} - Q_{out}\ .\ C_{CO_2\ out}$$

Here, unlike equation (7.9), the amount of reduction in Q_{out} as a result of sulphation can be ignored, due to very low concentration of SO_2. Therefore, carbonation in co-capture process can be calculated by equation (7.4).

Sulphation during calcination can be calculated using an approach similar to the co-capture calculation. Here, two reactions are taking place simultaneously. Calcination results in increasing Q_{out}, while sulphation causes a decrease in Q_{out}. For a single sulphation reaction the flow rate of captured SO_2 can be calculated using equation (7.9), since it causes a reduction in Q:

$$Q_{SO_2\ captured} = Q_{in}\ .C_{SO_2\ in} - Q_{out}\ .\ C_{SO_2\ out}$$

However, Q_{out} in equation (7.9) is also affected (increased) as a result of simultaneous calcination. It means Q_{out} after the calcination can be considered based on equation (7.3):

$$Q_{out} = \frac{1-C_{CO_2\ in}}{1-C_{CO_2\ out}} Q_{in}$$

Substituting the corrected Q_{out} in equation (7.9) gives:

$$Q_{SO_2\ captured} = Q_{in}[C_{SO_2\ in} - \frac{1-C_{CO_2\ in}}{1-C_{CO_2\ out}}\ C_{SO_2\ out}]$$

$$V_{SO_2\ captured} = Q_{in} \int [C_{SO_2\ in} - \frac{1-C_{CO_2\ in}}{1-C_{CO_2\ out}}\ C_{SO_2\ out}]dt$$

Therefore, sulphation during calcination can also be calculated using equation (7.10), similar to that for sulphation during carbonation. The reason that equation (7.10) can be used for sulphation calculation during both carbonation and calcination is the magnitude of the ratio $\frac{1-C_{CO2\ in}}{1-C_{CO2\ out}}$ as:

$$\frac{1-C_{CO2\ in}}{1-C_{CO2\ out}} \begin{cases} < 1 \text{ during Carbonation} \\ > 1 \text{ during Calcination} \end{cases}$$

The extent of calcination conversion can also be calculated using equation (7.11), if the change in the mass of solid sample is being measured.

$$X_{Calc}(t) = \frac{M_{CaCO_3}(m_0 - m_t)}{m_0 M_{CO_2}(T,p)} \qquad (7.11)$$

Here:

X_{carb} (t): Carbonation conversion at any given time [ ]

X_{sulph} (t): Sulphation conversion at any given time [ ]

X_{Calc} (t): Calcination conversion at any given time [ ]

Q: Gas flow rates [l /min]

C: Volume fractions of gas species [ ]

V: Volume [l]

Vm_{CO2} (T, p): Molar volumes of CO_2 at given temperature and pressure [l/mol]

Vm_{SO2} (T, p): Molar volumes of SO_2 at given temperature and pressure [l/mol]

m_0: Initial sample mass [g]

M_{CaCO3}: The relative molar mass of limestone [g/mol]

7.1 The effect of steam on calcination-carbonation cycles

This investigation aimed to study the calcination of limestone in different steam/CO_2 atmosphere and the subsequent effects on the CO_2 capturing performance in cyclic processes. An experimental programme was carried out to investigate the role of presence of steam in cyclic calcination-carbonation during CO_2 capture by means of limestone looping cycle process, using the bubbling fluidised bed reactor.

In the main part of the experiments, the decomposition of limestone in simulated oxy-fuel conditions and elevated steam dilution (up to 50% added to steam volume) was investigated. Thereafter, capturing capacity of the produced CaO has been tested in simulated air-fuel combustion conditions, and with an added amount of steam percentage (up to 20 vol. %), to study the effects of steam on carbonation.

7.1.1 The effect of steam on calcination

The influence of steam dilution during calcination has been investigated on both decomposition and sorption stages. Figure 7.2 shows the average bed temperature and initial decomposition temperature in elevated steam calcination respectively. The average bed temperatures were 940°C, 930°C, and 915°C with 28%, 48%, and 78% (vol%) steam dilution respectively; while the corresponding initial decomposition temperature were about 870 °C, 850 °C, and 810 °C. It can be seen that the average bed temperature required for calcination to reach the maximum conversion decreased with increasing steam dilution percentage. The result is consistent with the findings of Yin Wang et al [115], although their investigation was in a non-cyclic mode. In addition, the curve reveals that increasing steam dilution lowers the initial decomposition temperature. The role of steam dilution in lowering calcination temperature agrees with literature [80].

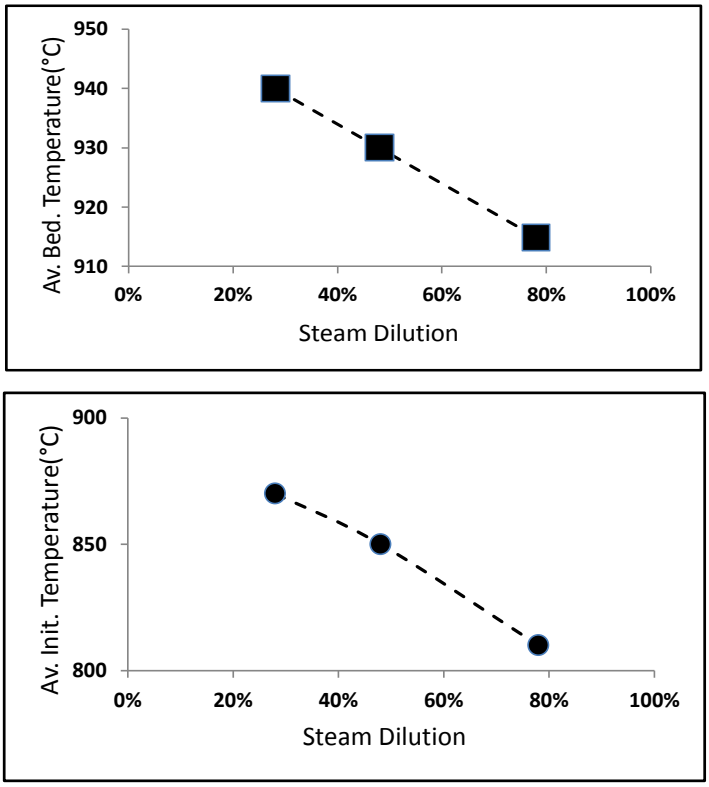

Figure 7.2: Effect of steam/CO_2 ratio in terms of steam dilution on the average bed temperature over calcination (up), and on the initial bed temperature for calcination in different sets (down).

Average bed temperature and initial decomposition temperature with 15% CO_2, 4% O_2, and balance N_2 (runs Steam01 and Steam02) were also in the same range as that of the set conditions Steam5 and Steam6 (78% steam, 15% CO_2 and 4% O_2). Therefore, lowering these values may not be attributed to the type of the dilutant (steam or N_2), identified in Table 5.2. Decomposition rate and conversion of limestone are dependent on CO_2 partial pressure. Reducing P_{CO_2} provides decomposition conditions for limestone with a lower thermodynamic equilibrium partial pressure, P^*_{CO2}, and consequently with a lower temperature. Milder calcination conditions could minimize the effect of sintering [51], which could be provided by steam dilution.

After limestone decomposition in presence of three different levels of steam (28%, 48%, and 78%), reactivity of the calcined samples were performed in an atmosphere with steam present at two levels: 6% (Figure 7.3a) and 20% (Figure 7.3b). It can be seen from each figure that the capture capacity of the CaO produced in higher steam dilution atmosphere were better than those of the CaO produced in lower steam dilution atmosphere. This agrees with the findings of Yin Wang et al. [115]; [135] in their single-cycle study.

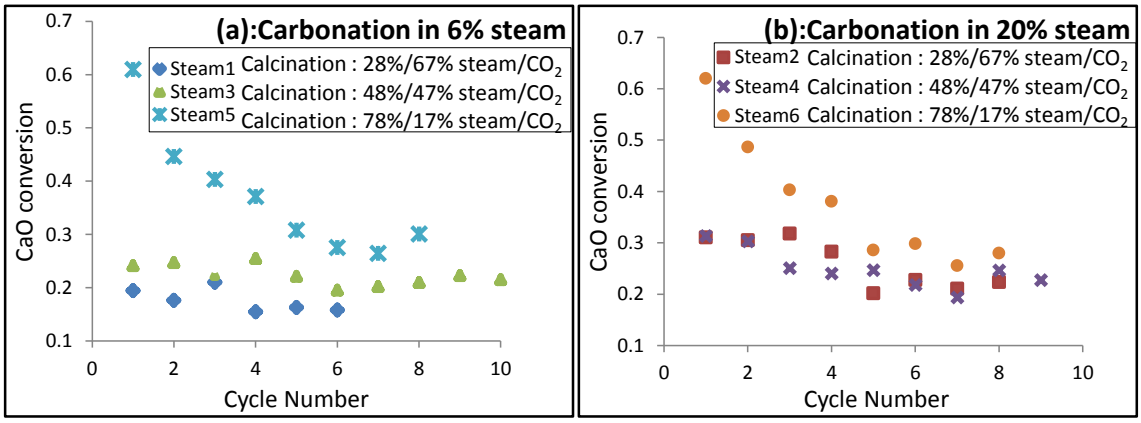

Figure 7.3: Effect of steam diluted calcination on cyclic CO_2 captures performance. Test conditions: *carbonation* at 650°C, (a): in 6% steam, 15% CO_2, 4% O_2, and balance N_2; (b): in 20% steam, 15% CO_2, 4% O_2, and balance N_2; *calcination* at 950°C and Steam1 and Steam2: 28% steam, 67% CO_2, 3% O_2, 2% N_2; Steam3 and Steam4: 48% steam, 47% CO_2, 3% O_2, 2% N_2; Steam5 and Steam6:78% steam, 17% CO_2, 3% O_2.

The enhancement in sorption capacity of calcined particles produced in steam diluted atmosphere may be attributed to the sorbents specific surface area and pore structure. The surface area of CaO particles is dependent on comparative rates of limestone calcination and sintering, and both of these rates are dependent on temperature [83]. Increasing in dilution (i.e. by steam) decreases decomposition temperature, and consequently increases the calcination rate. Therefore, calcination rate could seriously affect the evolution of surface area, and reduces the relative rate of sintering.

The results demonstrated in Figure 7.3 were also illustrated by scanning electron microscopy (SEM) images of particles after first calcination under different experimental conditions, shown in Figure 7.4. It is obvious that higher surface area of CaO particles provides a better gas-solid contact and yields greater carbonation conversion. Alvarez and Abanades [51] confirmed that capture capacity of calcined sorbent as well as the surface area, depends on the geometry of the surface and the ability of pores to accommodate the maximum layer of forming carbonate. Thus, their recommendation was using CaO sorbents with pores of diameter no smaller than 150 nm, which is identified by the thickness of developed product layer. Figure 7.4.a shows the surface texture of particles calcined in 28 % steam diluting. It can be observed that there are a number of homogenous pores (about 200-500 nm diameters) and some large pores (~1 μm diameter) on the outer surface of the particles. With the increase of steam dilution for limestone calcination, the amount of pores with medium size diameter increased (Figures 7.4.b and 7.4.c). Finally, pore structure and surface texture of

particles that can be observed for the N_2 diluted calcination (Figure 7.4.d), is similar to the equivalent dilution by steam (Figure 7.4.c).

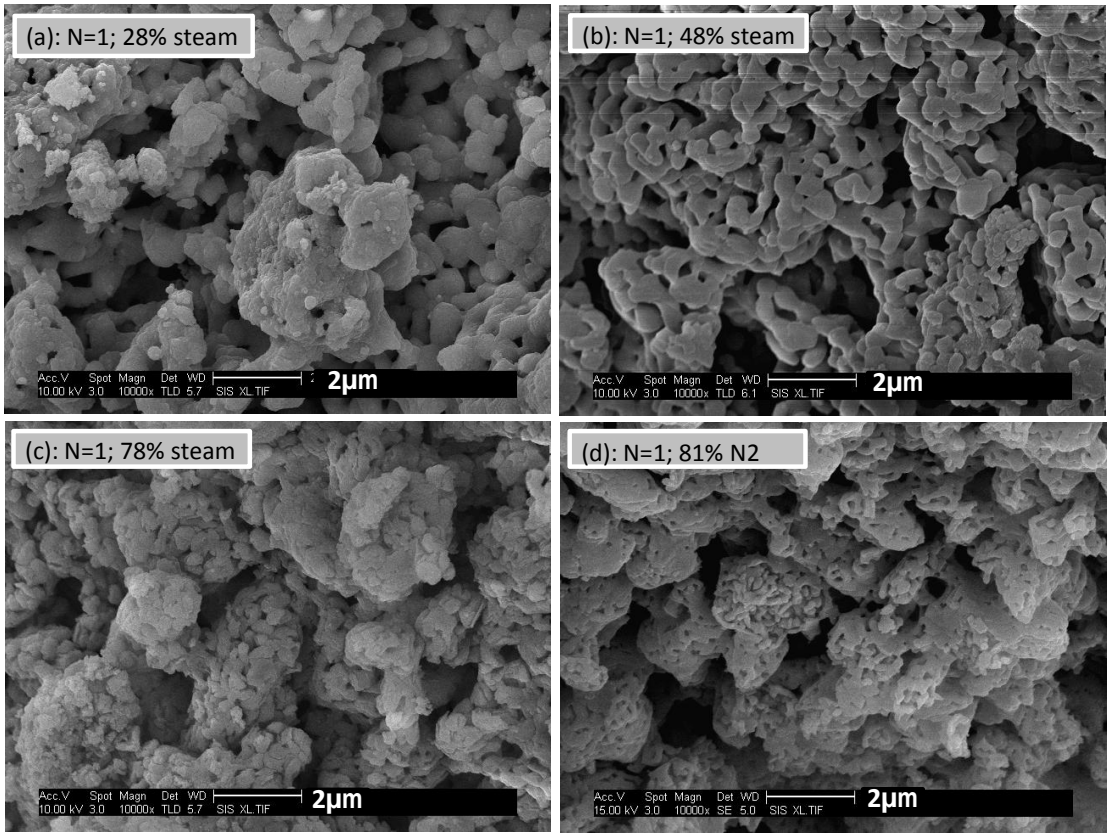

Figure 7.4: SEM micrographs of CaO particles after the first calcination. Decomposition in **(a):** 28% steam, 67% CO_2, 3% O_2, 2% N_2; **(b):** 48% steam, 47% CO_2, 3% O_2, 2% N_2; **(c):** 78% steam, 17% CO_2, 3% O_2, 2% N_2; **(d):** 15% CO_2, 4% O_2, and balance N_2.

Further to SEM images, samples were characterised for the porous structural properties of the particles in different stages. Specific surface area and pore volume of particles are given in Table 7.1.

Pore volumes are attributed to small to medium-size pores (~60-300 nm). The values are calculated based on the difference between cumulative volume of pores with diameter ranging from 1.7nm to 300nm, and the pore volume measured for smaller and micropores with diameter less than about 60 nm. Therefore, these pore volumes correspond to pores with diameters of about 60nm-300nm. As described earlier, further to high surface area, pore size of the sorbents is a key factor in sorption capacity, which geometrically is supposed to be able to accommodate the forming product layer. As presented in Table 7.1, BET specific surface areas were measured as 5, 5.3, and 12m^2/g for samples after the first calcination in presence of 28%, 48%, and 78% steam dilution, respectively. The corresponding volumes of small pores were 0.01, 0.01, 0.018 cm^3/g in the three steam calcination, respectively. Therefore, these results confirmed that steam dilution enhances the sorbents properties for CO_2 capture.

Table 7.1: Porous structural properties of calcined samples after the first steam calcination.

Calcined Sample [a]	S_{BET} (m^2/g)	Pore Volume (cm^3/g)
28% Steam, 1st cycle	5	0.01
48% Steam, 1st cycle	5.3	0.01
78% Steam, 1st cycle	12	0.018
81% N_2, 1st cycle	18	0.022

a. Details of the reaction conditions are given in Table 5.2.

Although sorbent calcination with N_2 diluting results in a better surface area ($18m^2/g$) than that for almost equivalent steam diluted ($12m^2/g$), their effective pore volumes are close. The pore size distributions, plotted in Figure 7.5, reveal that the amount of mesopores greater than 85 nm are higher in CaO particles which were calcined under steam diluted conditions. This situation results in almost similar carbonation performances of steam and N_2 calcined particles, which will be focused in section 7.1.2. However, all of the steam calcined sorbents appear to have more micropores and small mesopores (<25nm) than N_2 diluted ones.

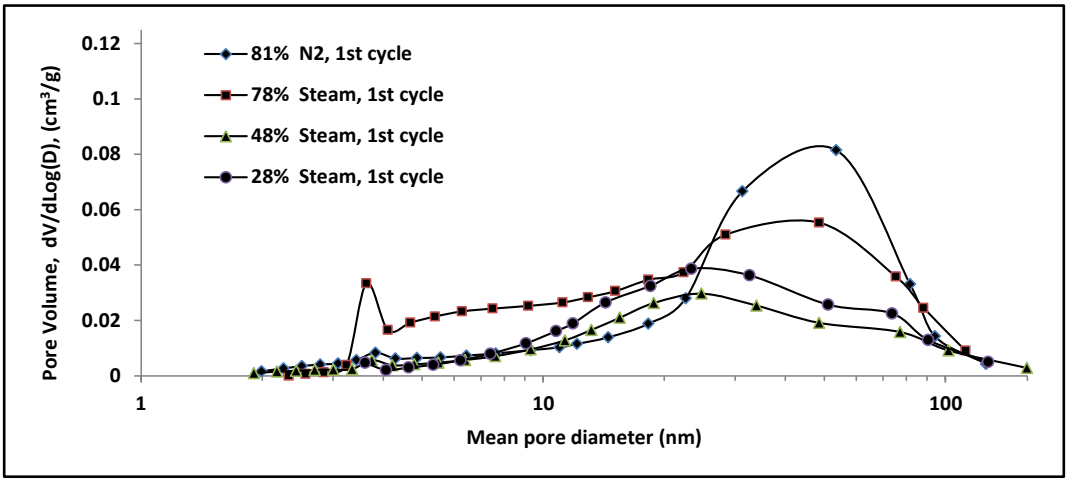

Figure 7.5: Pore-size distribution of CaO particles after the first calcination. Decomposition in **(28% steam):** 67% CO_2, 3% O_2, 2% N_2; **(48% steam):** 47% CO_2, 3% O_2, 2% N_2; **(78% steam):** 17% CO_2, 3% O_2, 2% N_2; **(81% N_2):** 15% CO_2, 4% O_2.

The results depicted in Figure 7.3 also reveal a better enhancement in capture capacity for the sorbents produced in high steam diluted (78%) atmosphere in the first few cycles. Thereafter, these steam calcined particles experienced higher rates of decay in sorption capacity, and the capture capacity of sorbents calcined in different diluting conditions became closer, with increasing number of cycles. The carbonation conversions were 0.67 and 0.30 for the CaO produced in 78% steam dilution and

carbonated in a 6% steam atmosphere, which were obtained in cycles 1 and 8 respectively. While, in the same cycles and similar sorption conditions, the carbonation conversions were 0.34 and 0.24 for the CaO produced in 28% steam.

This outcome was also supported by SEM images of CaO particle surfaces after experiencing a number of cyclic carbonation-calcination, in varying conditions of decomposition and sorption stages, Figure 7.6. General appearance of calcined particles, after experiencing several cycles under different conditions, reveal close status in their surface texture. As can be seen in Figures 7.6 -a, b, c and d, the porous textures of the particles mostly consist of large pores (>~1 μm diameter) and micropores, which are not as efficient as small pores in CO_2 capture. Nevertheless, the SEM images demonstrated that there are higher amounts of surface exposed large pores on the outer shell of particles calcined in more diluted atmosphere, which could provide a better gas-solid contact in the internal voids.

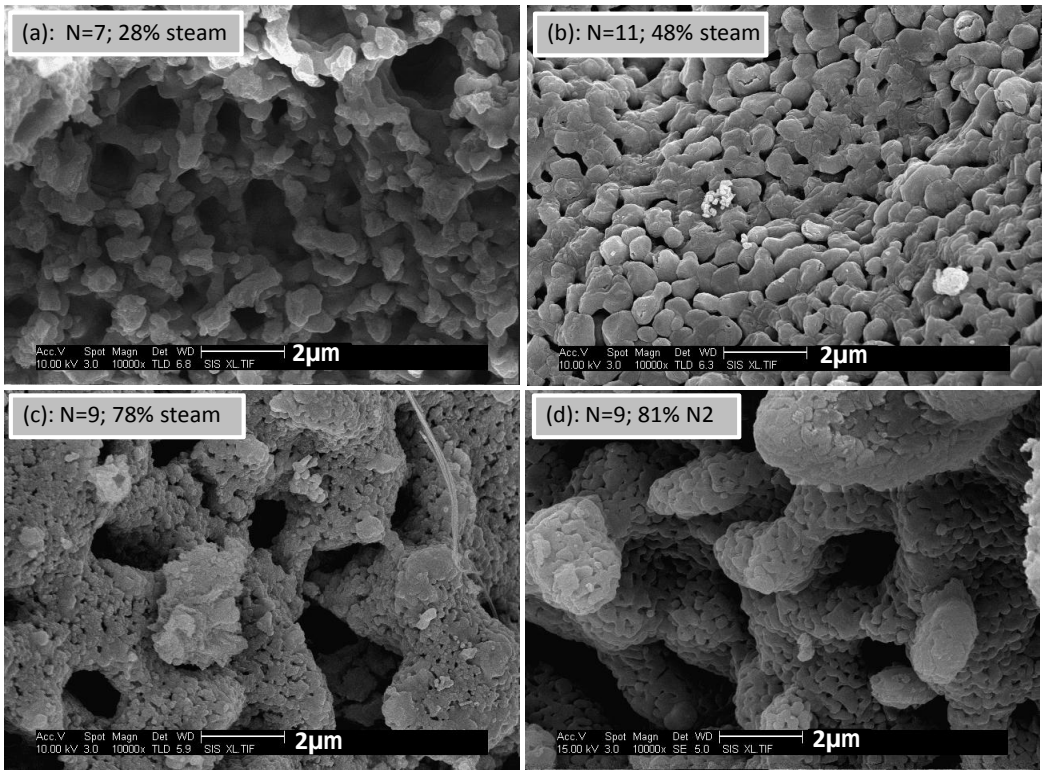

Figure 7.6: SEM micrographs of CaO particles after different cyclic calcination-carbonation. **(a):** decomposition in 28% steam, 67% CO_2, 3% O_2, 2% N_2; sorption in 6% steam, 15% CO_2, 4% O_2, balance N_2. **(b):** decomposition in 48% steam, 47% CO_2, 3% O_2, 2% N_2; sorption in 20% steam, 15% CO_2, 4% O_2, balance N_2. **(c):** decomposition in 78% steam, 17% CO_2, 3% O_2, 2% N_2; ; sorption in 6% steam, 15% CO_2, 4% O_2, balance N_2. **(d):** decomposition in 15% CO_2, 4% O_2, balance N_2; sorption in 20% steam, 15% CO_2, 4% O_2, balance N_2.

The recent deduction is also supported by comparing the porous structural properties of CaO particles after experiencing several sorption/decomposition cycles in different reaction conditions. As can be seen in Table 7.2, the surface area of calcined particles varies from 3.9 to 6.5 m^2/g, unlike the wide variation for particles after the first calcination, which range from 5 to 18 m^2/g. Pore volumes, corresponding to small pores as calculated in Table 7.1, are also close, covering 0.006-0.010 cm^3/g range. In

contrast the pore volume after the first calcination covers a wide range of 0.10-0.022 cm^3/g.

Table 7.2: porous structural properties of calcined samples after cyclic calcination-carbonation.

Calcined Sample [a]	S_{BET} (m^2/g)	Pore Volume (cm^3/g)
28% Steam Cal., 6% Steam Carb., 7th Cycle	4.5	0.006
28% Steam Cal., 20% Steam Carb., 9th Cycle	3.9	0.008
78% Steam Cal., 6% Steam Carb., 9th Cycle	6.5	0.006
78% Steam Cal., 20% Steam Carb.,9th Cycle	5.3	0.006
81% N_2 Cal., 20% Steam Carb., 9th Cycle	5.7	0.010

a. Details of the reaction conditions are given in Table 5.2.

However, the presence of steam and CO_2 may facilitate sintering [83; 136; 137]. Figure 7.7 compares the cyclic capture capacity of calcined sorbent produced in steam diluted atmosphere to those formed in similar diluted N_2 atmosphere but carbonated in two conditions: with (Figure 7.7-a) and without (Figure 7.7-b) steam present. Limestone decomposed at 950°C in 78% steam**,** 17% CO_2**,** 3% O_2, balances N_2; and carbonated at 650°C in 20% steam, 15% CO_2, 4% O_2, and balances N_2, designated as Steam6; while the other two samples, Steam01 and Steam02 , calcined in 15% CO_2, 4% O_2, and balance N_2, and carbonated with 20% and 0% steam respectively. The curves depicted in Figure 7.7-a may give the impression that sintering of nascent CaO calcined in presence of steam is responsible for lower sorption capacity of steam calcined particles. But the results in Figure 7.7-b reveal that the difference may not be attributed to sintering of CaO particles. This somehow agrees with the findings of Sun et al [80] which claimed no enhancement of sintering by steam, compared to N_2 diluted atmosphere and based on pore size distribution of particles. Nevertheless, the difference observed in Figure 7.7-b shows the enhanced sorption capacity by steam carbonation, which will be more explained in section 7.1.2.

As a result, taking both potential effects of steam on calcination into account (enhancement in capturing capacity and possibly catalysing the sintering), it seems that steam can be used to dilute the calciner atmosphere, particularly considering its ease of separation from CO_2 compared to N_2 by condensation.

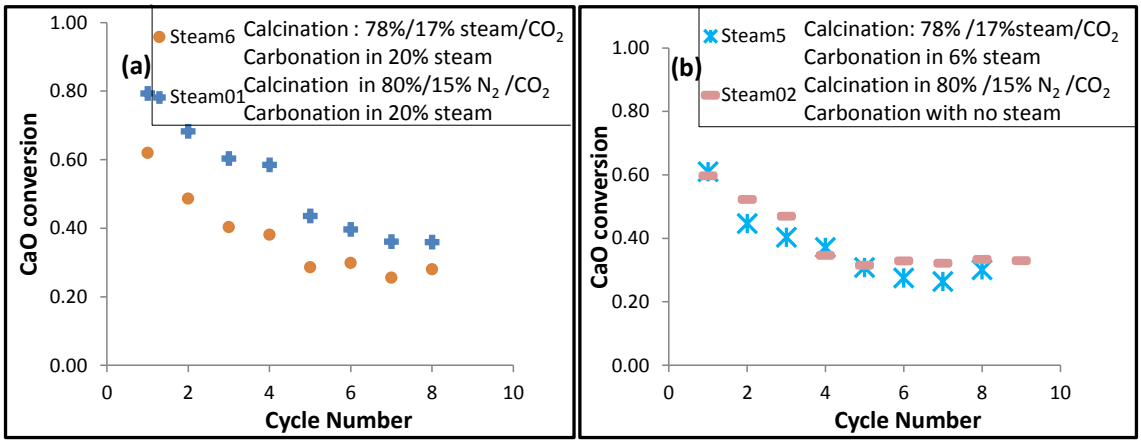

Figure 7.7: Effect of steam calcination on cyclic CO_2 captures performance. Test conditions: carbonation: at 650°C, Steam6 and Steam01 in 20% steam, 15% CO_2, 4% O_2, and balance N_2; Steam02 in 15% CO_2, 4% O_2, and balance N_2;. Steam5 in 6% steam, 15% CO_2, 4% O_2, and balance N_2; calcination: at 950°C, Steam01and Steam02 in 15% CO_2, 4% O_2, and balance N_2; Steam5 and Steam6 in 78% steam, 17% CO_2, 3% O_2.

7.1.2 The effect of steam on carbonation

Carbonation conversions of CaO particles produced in varying conditions were investigated with steam present in two levels: 6% and 20%. As shown in Figure 7.8 increasing the steam percentage in carbonation atmosphere improved the capture capacity of sorbents, which have been calcined in conditions with a lower steam dilution.

The highest level of enhancement in sorption capacity occurred for the sorbents that were calcined in atmosphere with no steam present, Figure 7.8-a. The amount of sorption enhancement (due to increasing the steam present in carbonation atmosphere) decreased with increasing the steam percentage in calcination (Figures 7.8-b and 7.8-c). Finally, sorbent decomposition with 78% steam dilution resulted in quite similar carbonation conversions with 6% and 20% steam present (Figure 7.8-d).

This result on the role of steam in carbonation is somewhat in agreement with the results reported by Yang and Xiao [109] for the effect of steam pre-treatment on carbonation, although they investigated for one cycle process. The catalytic effect of steam on carbonation has been proposed to be due to the reaction of CO_2 with surface hydroxyl groups (from H_2O dissociation to –OH on Ca, and -H on O during calcination) to form bicarbonates [109]. On the basis of these findings, here, it can be assumed that during calcination with lower steam dilution (and presence of CO_2) lower amount of hydroxyle groups, and hence, lower amount of bicarbonates were formed. Therefore, during the carbonation of these calcined particles with more steam present, more amount of steam could be adsorbed (by CaO) and dissociated to form hydroxyl groups. Thus, more CO_2 could react with them, and enhance the carbonation conversion. Sorbent hydration by steam or liquid water to obtain a hydroxide-derived CaO has also been reported to enhance CO_2 capture capacity [80; 109; 138].

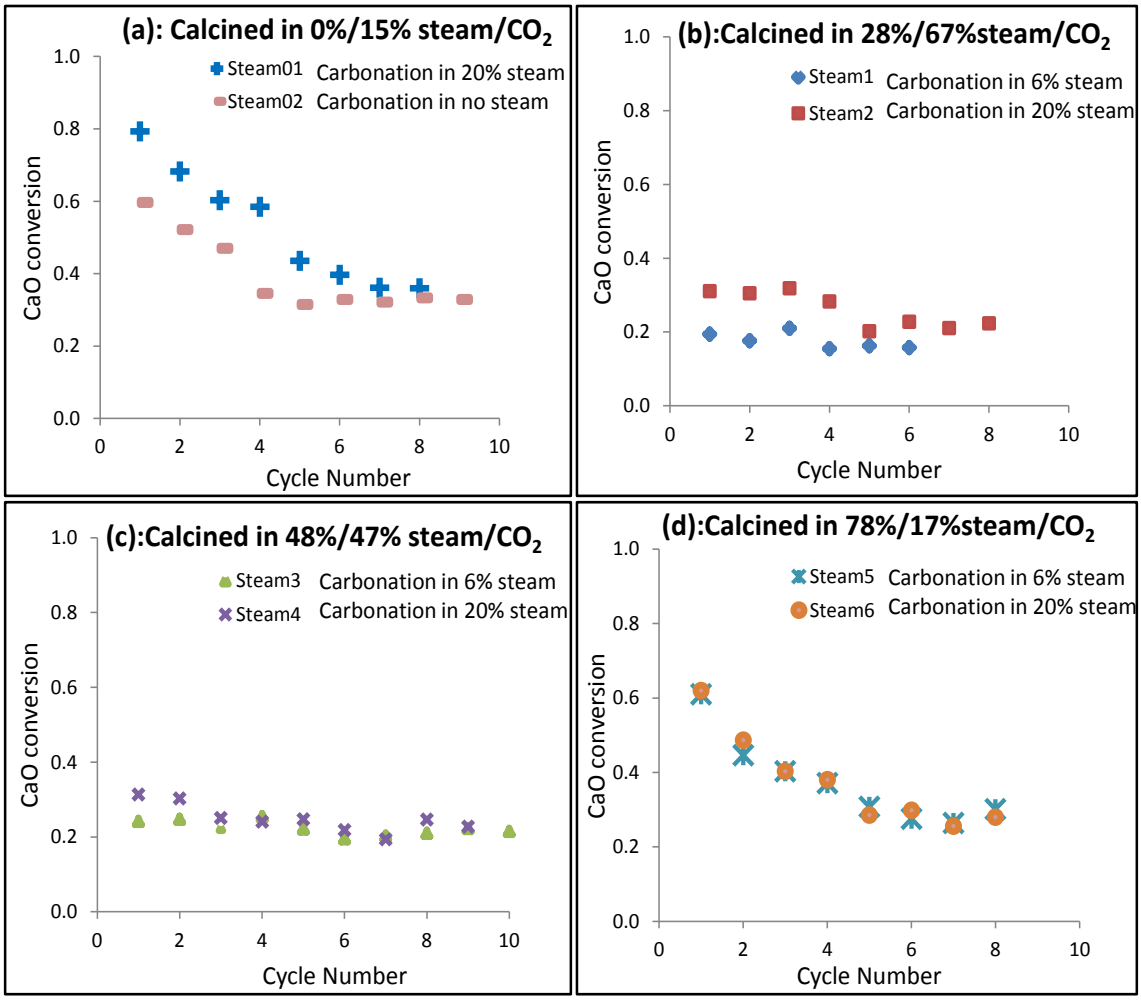

Figure 7.8: Effect of steam carbonation on cyclic CO_2 captures performance. Test conditions: *carbonation* at 650°C, (a): no steam and 20% steam, 15% CO_2, 4% O_2, and balance N_2; (b),(c), (d): in 6% and 20% steam, 15% CO_2, 4% O_2, and balance N_2; *calcination* at 950°C and (a): 15% CO_2, 4% O_2, and balance N_2; (b): in 28% steam, 67% CO_2, 4% O_2, and balance N_2; (c): 48% steam, 47% CO_2, 3% O_2, 2% N_2; (d): 78% steam, 17% CO_2, 3% O_2, 2% N_2.

However, the effect of steam on carbonation conversion in this investigation should not be attributed to sorbent hydration. Based on Equation (7.12) [139] thermodynamic equilibrium pressure of steam at 650°C is calculated as 1.14 MPa, while, the maximum partial pressure of steam in these experiments was 0.020 MPa, corresponding to the highest steam percentage in carbonation, which is lower than P^*_{H2O}.

$$P^*_{H2O} = 9 \times 10^{11} \exp(-12531.5 / T)\ \text{Pa}. \qquad (7.12)$$

Furthermore, using the same equation, sorbent hydration even with 78% steam present would be produced at a temperature lower than 500°C. The process was not operated under these operating conditions during the tests. This result was also supported by the XRD measurement, which confirmed the absence of $Ca(OH)_2$ both in the particles calcined after the calcination and in the carbonates after carbonation. Figure 7.9 demonstrates the X-ray diffraction patterns for one of the calcined samples.

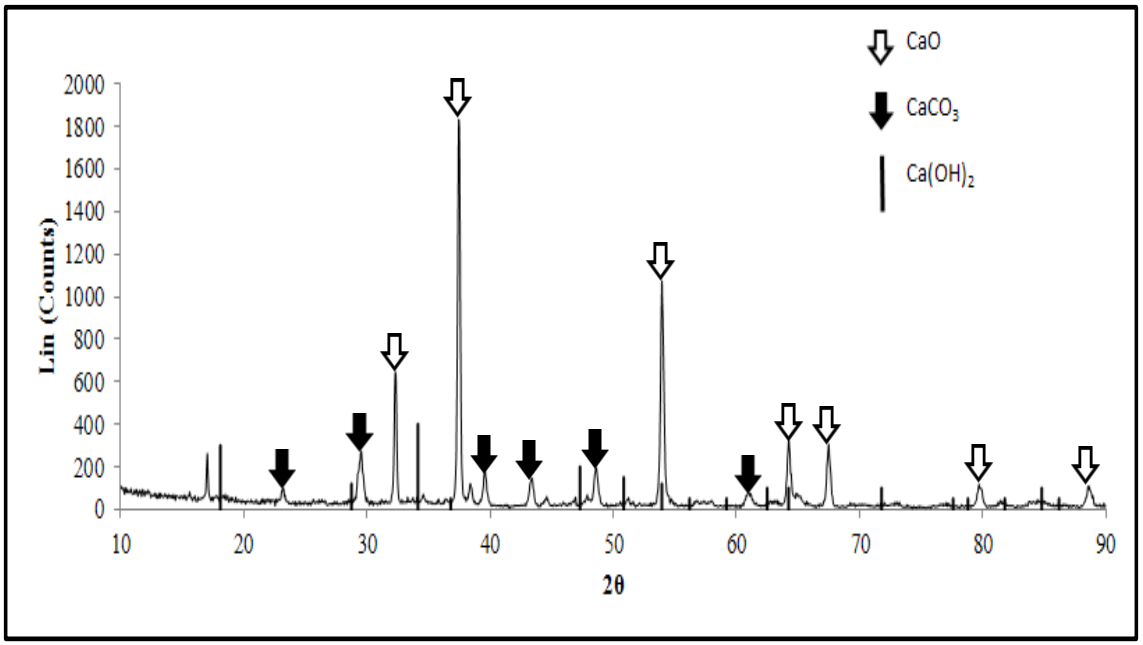

Figure 7.9: X-ray diffraction patterns of calcined after 10 cycles calcination-carbonation in presence of steam, which confirms no calcium hydroxide was formed.

7.2 The effect of SO_2 on calcination-carbonation cycles

This work investigates the effects of the presence of SO_2 in calcination, on CO_2 capturing performance in cyclic calcination-carbonation of limestone. Different series of test programmes were carried out to study the role of SO_2 presence. Reaction conditions were simulated at elevated SO_2 concentrations in cyclic calcination and carbonation of limestone.

7.2.1 Calcination in the presence of SO_2

After a complete calcination of limestone with (1500 ppm) and without SO_2 present, reactivity performances of the calcined sorbent were tested in different conditions in presence of SO_2 at three levels. Figure 7.10 compares the carbonation conversions, total sulphation conversions (during calcination and carbonation), and total calcium utilisation for different SO_2 concentrations. Carbonation atmosphere was provided with 200 ppm (Figures 7.10-1 and 7.10-4), 2500 ppm (Figures 7.10-2 and 7.10-5), and 5000 ppm of SO_2 (Figures 7.10-3 and 7.10-6). In contrast to $CaCO_3$ decomposition, $CaSO_4$ formed remains intact at the calcination temperature of 950 °C. Therefore the cumulative SO_2 retained were calculated.

The results depicted in each couple of figures in the same row of Figure 7.10 illustrate the effect of presence of SO_2 in calcination atmosphere. It can be seen that the CO_2 capture capacity of the CaO produced in presence of SO_2 was less than those of the CaO

produced with no SO_2 atmosphere. The averages of carbonation conversions of CaO (over the number of test cycles, Equation 7.13) produced in no SO_2 atmosphere were 0.32, 0.23, and 0.17 in presence of 200, 2500, and 5000 ppm of SO_2, respectively. The corresponding conversion values for sorbents produced with 1500 ppm SO_2 present were 0.30, 0.18, and 0.14. Sulphation during calcination resulted in lowering the capture capacity of sorbent. Therefore, the results indicate the necessity of removing SO_2 prior to both stages of the process. The economic performance of the technology will be negatively influenced by the presence of SO_2, as it increases the deactivation rate and make-up flow of CaO, which is in agreement with other investigations [28; 73-75]. Porous structural properties of the initial calcined samples with and without SO_2 present confirm the same outcome for calcination step. Specific surface area and pore volume of particles are given in Table 7.3.

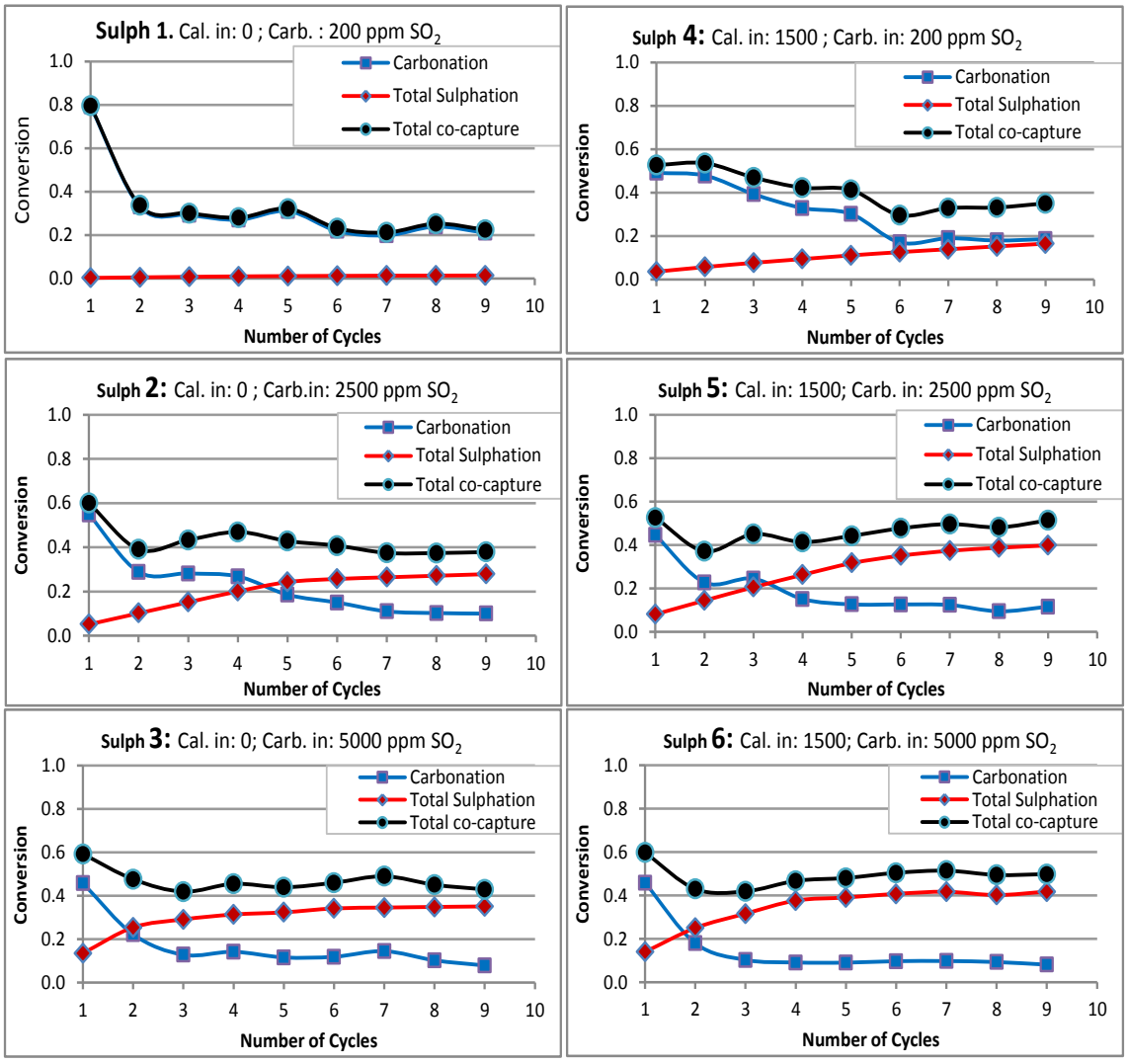

Figure 7.10: Effect of SO_2 on the performance of cyclic CO_2 capture. Test conditions: carbonation at 650°C, 15% CO_2, 4% O_2, and balance N_2; calcination at 950°C, 15% CO_2, 4% O_2, and balance N_2. The SO_2 concentrations in calcination and carbonation steps are shown in the figures for each test.

Table 7.3: Porous structural properties of calcined samples after the first calcination with SO_2.

Calcined Sample [a]	S_{BET} (m^2/g)	Pore Volume (cm^3/g)
0 ppm, 1th Cycle	18	0.022
1500 ppm, 1th Cycle	7.8	0.010

a. Details of the reaction conditions are given in Table 5.3.

Pore volumes in Table 7.3 are associated with small pores to medium-size pores (~60-300 nm). The volumes are calculated as the difference between cumulative volume of pores with diameter 1.7nm-300nm, and the pore volume measured for smaller pores with diameter less than about 60nm. Such pores can be a more effective size to accommodate the forming product layer. As presented in Table 7.3, BET specific surface areas were measured as 7.8 and 18m^2/g for samples after the first calcination without and with 1500 ppm SO_2 present, respectively. The corresponding volumes of small pores were 0.01 and 0.022 cm^3/g in the two calcinations, respectively. Pore size distributions of these calcined particles, depicted in Figure 7.11, confirm that the CaO particles produced in atmosphere with SO_2 present have more micropores (<20 nm), which results in less capture capacity. Therefore, these results confirmed that presence of SO_2 in calcination step lessens the sorbents properties for CO_2 capture.

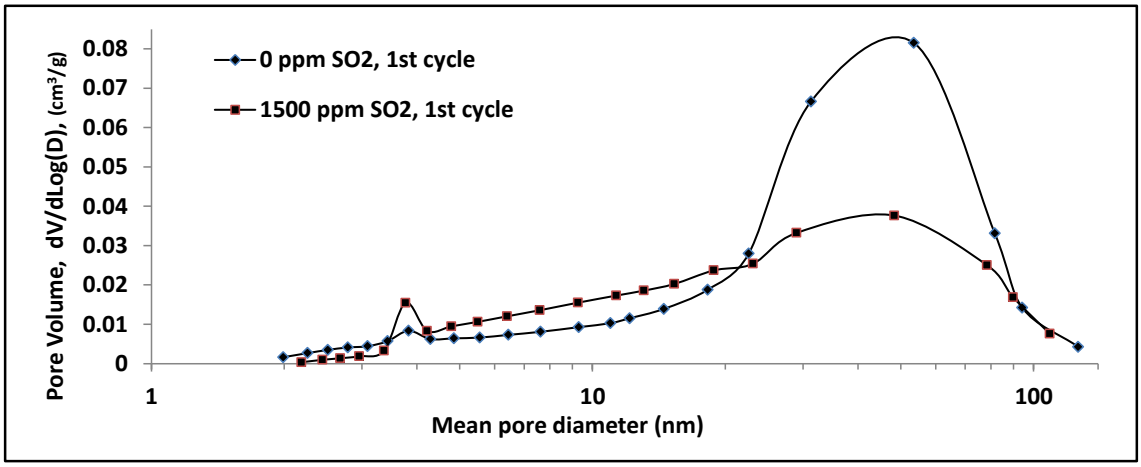

Figure 7.11: Pore-size distribution of CaO particles after the first calcination. Decomposition in **(0 ppm SO_2):** 15% CO_2, 4% O_2, balance N_2; **(1500 ppm SO_2):** 15% CO_2, 3% O_2, balance N_2.

The changes in results demonstrated in each set of data in the same column of Figure 7.10 exhibit the effect of presence of SO_2 in carbonation atmosphere. In similar calcination conditions, the results demonstrated lower CO_2 capture capacity for the CaO particles in presence of higher SO_2 concentrations during carbonation. This is simply due to the fact that competitive sulphation during carbonation utilises a fraction of the capture capacity of the sorbents. These outcomes are in agreement with findings of the previous investigations [85; 122-124]. As expected, these results also confirmed faster

decreasing rates of carbonation conversion with increasing SO_2 concentration in carbonating gases. This fact was clearly revealed by the comparison of the intercept of sulphation and carbonation curves, which occurred in earlier cycles when more SO_2 was presented.

CaO particle characterisation also confirmed that undergoing the cyclic process in an atmosphere containing more SO_2, results in greater reduction in particle porous structure. Specific surface areas and pore volumes (calculated as described in Table 7.3) for CaO particles, calcined in the 10^{th} cycle, are given in Table 7.4. As can be seen in Table 7.4, surface area and pore volume of calcined particles reduced drastically in the presence of SO_2 over the cyclic process.

Table 7.4: Porous structural properties of calcined samples after 10 cycle calcination-carbonation in the presence of SO_2.

Calcined Sample [a] SO_2 in calcination – SO_2 in carbonation	S_{BET} (m^2/g)	Pore Volume (cm^3/g)
0 ppm - 200 ppm, 10^{th} Cycle	2.3	0.0030
0 ppm- 2500 ppm , 10^{th} Cycle	0.3	0.0008
0 ppm - 5000 ppm, 10^{th} Cycle	0.08	0.0004
1500 ppm - 200 ppm, 10^{th} Cycle	1.3	0.0020
1500 ppm- 2500 ppm, 10^{th} Cycle	0.14	0.0006
1500 ppm- 5000 ppm, 10^{th} Cycle	0.02	Not reported

a. Details of the reaction conditions are given in Table 5.3.

These results were also supported by the images of sorbent particle morphology provided by scanning electron microscopy (SEM), shown in Figure 7.12. It is believed that the $CaSO_4$ layer formed, which will not be decomposed during calcination, is responsible for the sorbent deactivation. Therefore, it was interesting to compare the morphology of the surface and interior of the particles. In some cases (Figure 7.12-c, d, e, g, h) the figure shows these two areas. As can be seen, particles which experienced lower SO_2 concentrations over the cyclic process (such as a, b) have a greater number of small pores corresponding to higher surface area. In contrast, the images demonstrate reduction in small pores on the surface of particles which were exposed to a higher SO_2 atmosphere, compared to their interior texture. For some cases (such as g, h) in which particles experienced atmospheres containing 1500 ppm in calcination, and 2500 and 5000 ppm in carbonation, the SEM images demonstrate a denser layer formed on the surface.

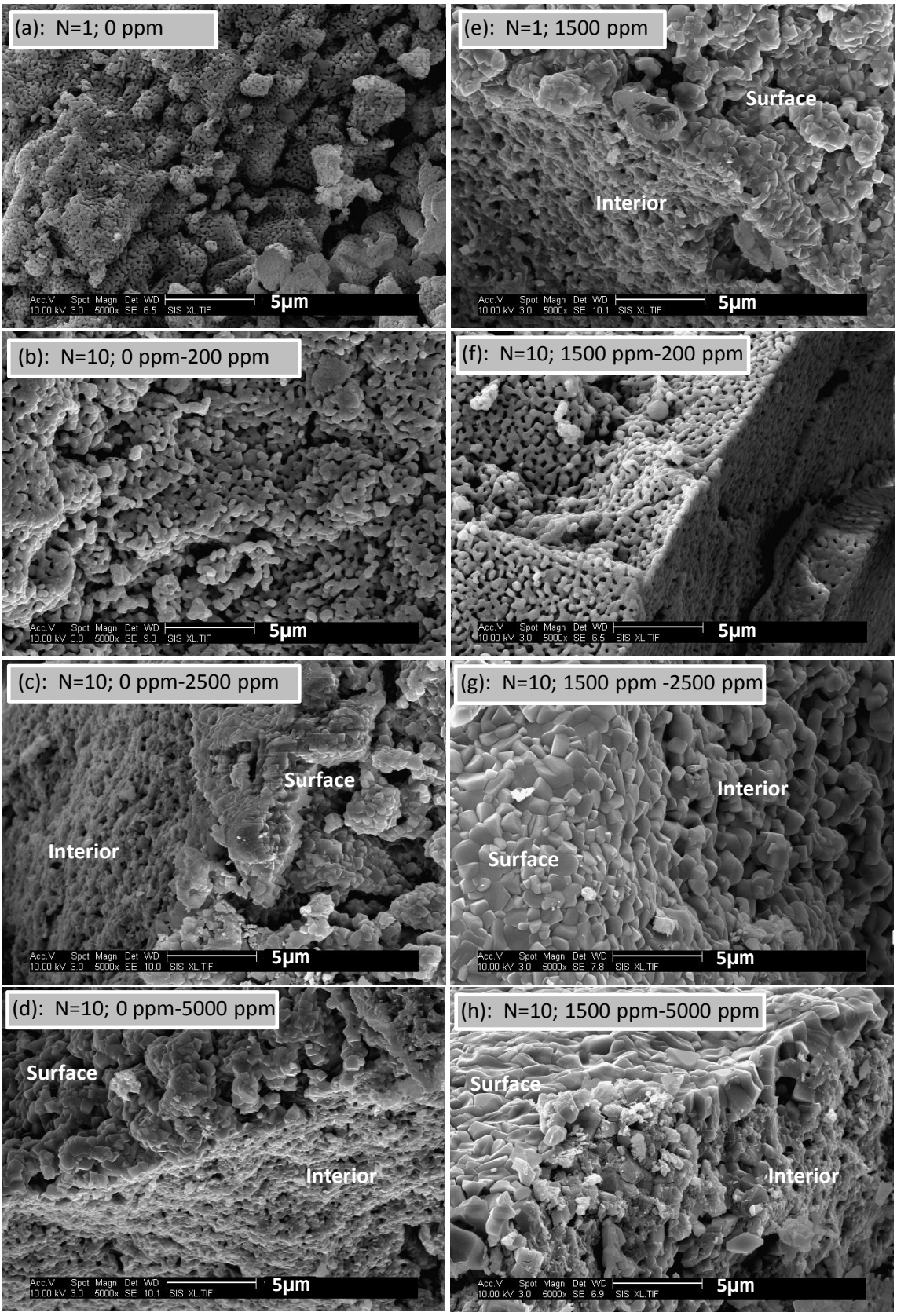

Figure 7.12: SEM images of the particles after the first calcination (a, e) and after the 10th calcinations (others) in different SO_2 concentrations. The two given SO_2 concentrations in images correspond to calcination and carbonation, respectively. **Calcinations:** at 950 °C; 15% CO_2, 3% O_2,

SO_2 as stated in images, and N_2 balance; **Carbonations:** at 650 °C; 15% CO_2, 4% O_2, SO_2 as stated in images, and N_2 balance.

7.2.2 The co-capture of CO_2 and SO_2

The idea of co-capturing process of CO_2 and SO_2 has been assessed in Figure 7.13. The trend of average total Ca utilization illustrates that a greater drop in co-capture capacity of the CaO occurred when higher SO_2 concentration was presented in both steps of calcination and carbonation, as portrayed by the blue line. The numbers in brackets in Figure 7.13 show the concentration of SO_2 in calcination and carbonation for each test set, respectively. Although calcination and carbonation were conducted for different periods, the total introduced SO_2 was used as the independent variable in Figure 7.13. The average total calcium utilization was 0.33 when particles were calcined with no SO_2 present and carbonated in presence of 200 ppm of SO_2. The average Ca utilization declined significantly when increasing the total concentrations of SO_2 in calcination and carbonation steps. It finally lessened to 0.19 when particles experienced calcination and carbonation in presence of 1500 and 5000 ppm SO_2, respectively. The average CO_2 capture in cycled process was also affected by SO_2 concentrations, as it was diminished from 0.32 to 0.14. In fact, presence of more amounts of SO_2 in the reaction atmosphere caused simultaneous loss in carbonation and increasing in sulphation of CaO particles. Consequently, the decrease in total Ca utilization simply reveals that the extent of loss in carbonation is larger than the extent of increasing in sulphation. These imbalanced adverse conversions are caused by the formation of voluminous calcium sulphate. $CaSO_4$ has a considerably larger molar volume (46 cm^3/mol) than that of CaO (17 cm^3/mol) and $CaCO_3$ (37 cm^3/mol). As a result, the occupied pores by a certain extent of sulphation cause a larger loss in the extent of carbonation. Therefore, the results do not advocate the co-capture process, as presence of SO_2 caused a decrease not only in CO_2 capture capacity but in total Ca utilization as well.

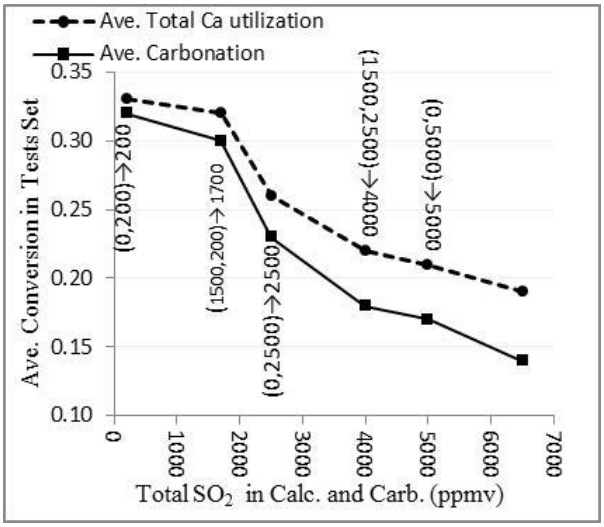

Figure 7.13: Trends of average carbonation conversions and average Ca utilisation in each test set, as a function of elevated total SO_2 concentrations in calcination and carbonation steps. The numbers in brackets show the concentrations of SO_2 in ppm during calcination and carbonation, respectively. The numbers after arrows demonstrate the total SO_2 concentrations introduced in each cycle.

The averages were calculated using Equations (7.13) and (7.14):

$$\overline{X_{CO_2}} = \frac{\Sigma_i X_{CO_{2_i}}}{N} \qquad (7.13)$$

$$Ave\ .total\ Ca\ utilisation = \overline{X_{CO_2}} + \frac{commulative\ X_{SO_2}}{N} \qquad (7.14)$$

, where $X_{CO_{2_i}}$ is the extent of carbonation conversion in the ith cycle, and N is the number of cycles in each test run.

The individual curves of sulphation during each single calcination and carbonation have been provided in Figure 7.14. The results confirm that sulphation took place during the calcination in presence of SO_2. The cumulative sulphation during calcination with 1500 ppm SO_2 present after 10 cycles resulted in 0.17, 0.15, and 0.12 conversion corresponding to test set in which sorbents were carbonated in presence of 200, 2500, and 5000 ppm SO_2, respectively. This part of sulphation mainly occurred via CaO-SO_2 reaction during calcination, because the SO_2 feeding was started at the time of starting sorbent regeneration and ended once decomposition had completed.

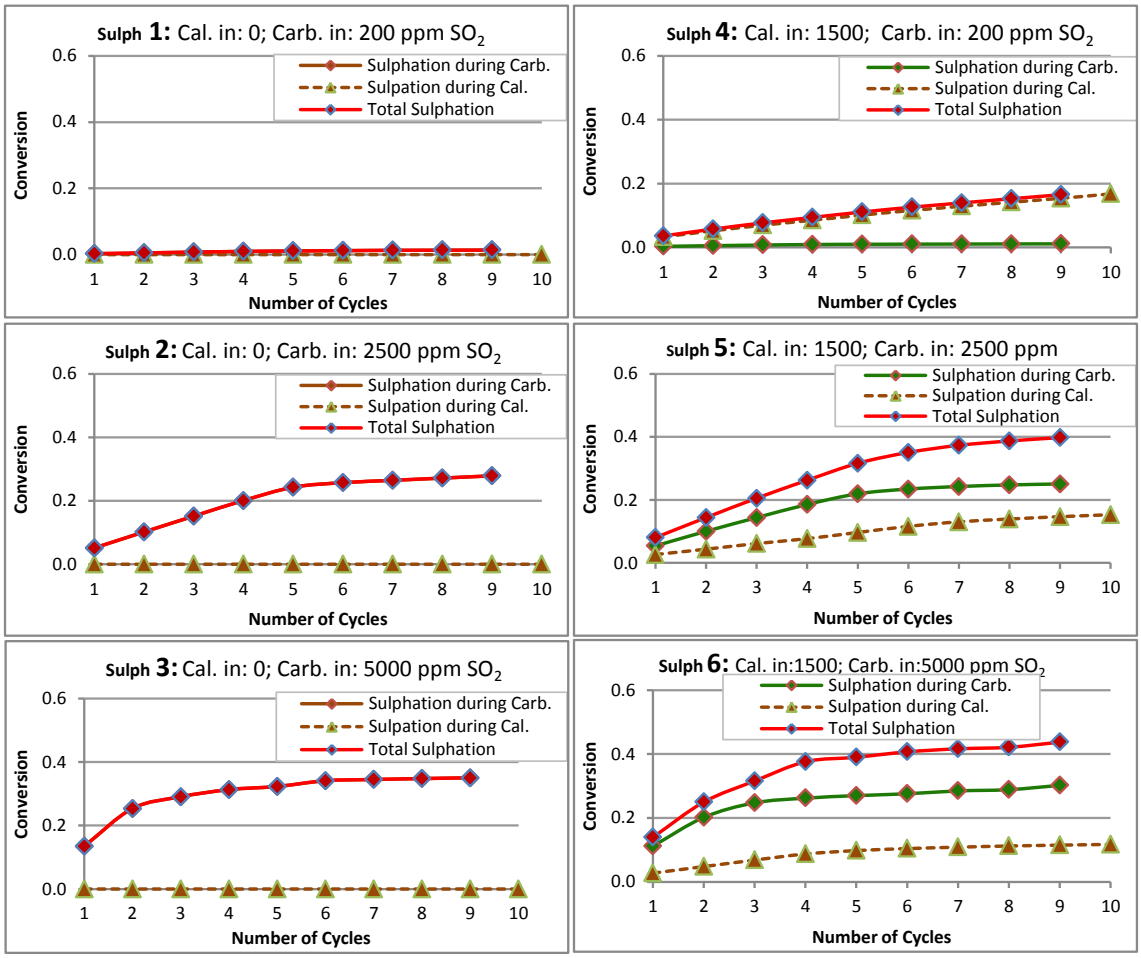

Figure 7.14: Total sulphation in each cycle; and individual sulphation conversion during calcination and carbonation. Test conditions: carbonation at 650°C, 15% CO_2, 4% O_2, and balance N_2; calcination at 950°C, 15% CO_2, 4% O_2, and balance N_2. The SO_2 concentrations in calcination and carbonation steps are shown in the figures for each tests set.

The extent of sulphation under different conditions is summarized in Figure 7.15. The total sulphation conversion was 0.01 when particles were calcined with no SO_2 present and carbonated in presence of 200 ppm of SO_2. Sulphation conversion significantly increased as the total concentrations of SO_2 in calcination and carbonation steps increased. It finally reached 0.44 when particles were calcined and carbonated in presence of 1500 and 5000 ppm SO_2, respectively.

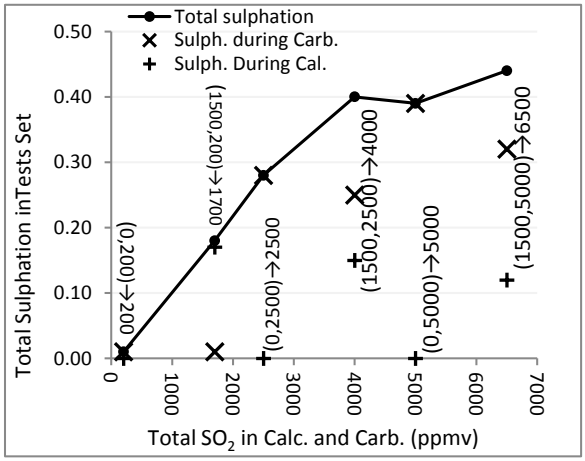

Figure 7.15: Trends of sulphation conversions as a function of total SO_2 concentrations in calcination and carbonation steps. The numbers in brackets show the concentrations of SO_2 in ppm during calcination and carbonation, respectively. The numbers after arrows demonstrate the total SO_2 concentrations introduced in each cycle.

Typical traces of SO_2 concentrations versus time during calcination of particles, which have already been carbonated at different SO_2 concentrations, are depicted in Figure 7.16. The SO_2 concentration in all calcination reactions was set at 1500 ppm. The particles have cyclically been carbonated with presence of 200 ppm (Figure 7.16a), 2500 ppm (Figure 7.16b), and 5000 ppm (Figure 7.16c) SO_2. It can clearly be seen that detected SO_2 in flue gases during calcinations increased by increasing the SO_2 presented in carbonation of the particles. This confirms that more SO_2 was captured during calcination of sorbents which have been carbonated at lower SO_2 concentration, consistent with Figures 7.10 and 7.14.

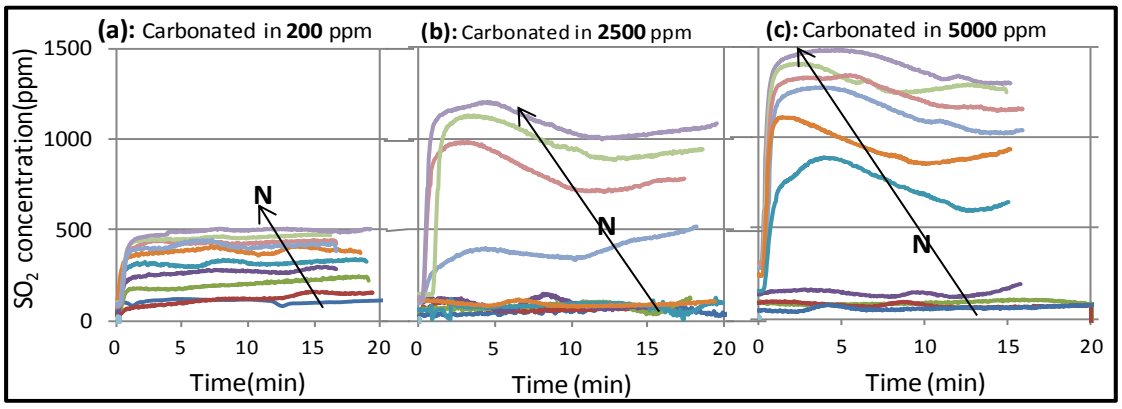

Figure 7.16: SO_2 concentrations during calcination with 1500 ppm SO_2 present in cyclic process, as a function of SO_2 concentration in carbonation steps of particles. N shows the increasing number of cycles.

7.2.3 Comparison of the effects of sulphation during calcination and carbonation

Figure 7.17 compares the SO_2 concentrations during calcination and carbonation over the reaction times. Figure 7.17-a1 and 7.17-a2 correspond to the tests runs with 1500 ppm and 2500 ppm SO_2 present in calcination and carbonation, respectively. Similarly, Figure 7.17-b1 and 7.17-b2 show the results of calcination with 1500 ppm and carbonation with 5000 ppm SO_2 present. A greater fraction of the input SO_2 was absorbed in earlier cycles, during both capturing and decomposition reactions. The detected SO_2 in the outlet gases increased in further cycles. This verifies that the ability of sorbent to capture SO_2, similar to their CO_2 capture capacity, decreased by cycling the sorbent in CO_2/ SO_2 atmosphere. The raise in accumulative sulphation conversions by increasing the number of cycles is caused by the irreversible sulphation reaction at calcination temperature.

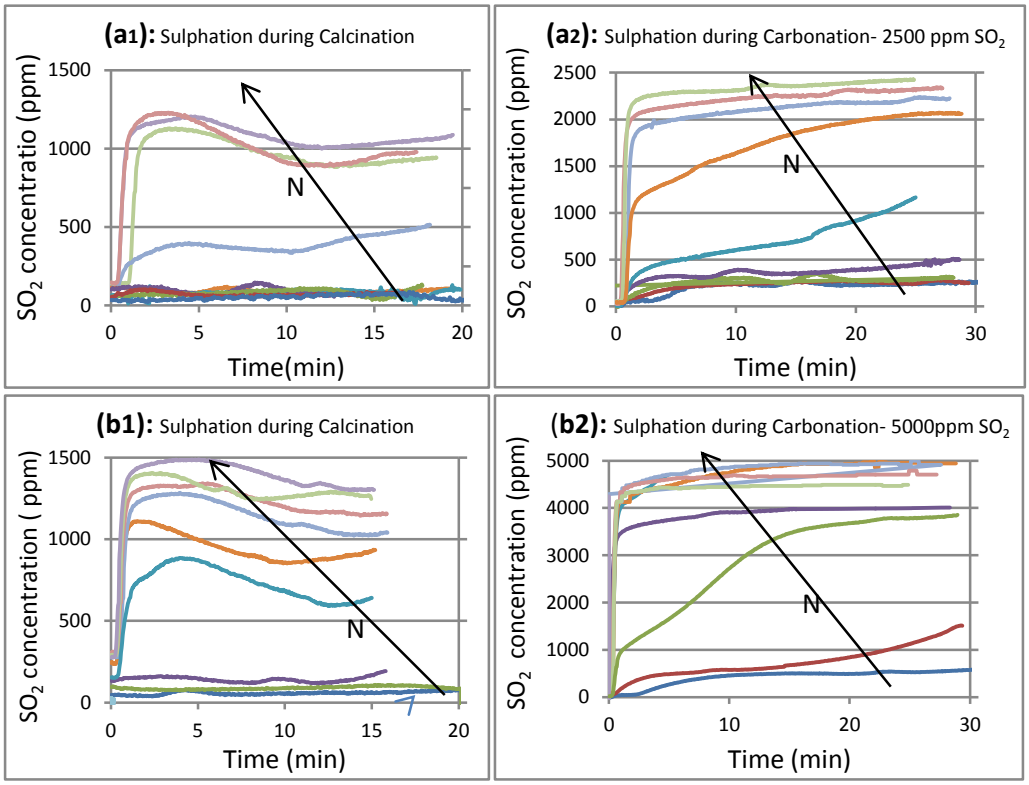

Figure 7.17: SO_2 concentrations during calcination with 1500 ppm SO_2 present (a1 and b1), and carbonation in presence of 2500 ppm (a2) and 5000 ppm SO_2 (b2). N shows the increasing number of cycles.

This can also be seen from the gradient of the sulphation curves depicted in Figure 7.17. In addition, the curves in Figure 7.17 reveal different approaches of sulphation during calcination and carbonation. Increase in detected SO_2 concentrations in exiting gases after being cycled, in early period of calcinations, verify that sulphation occurred (Figures 7.17-a1 and b1). In the beginning period of calcinations, during which not much CaO has been produced, SO_2 can be captured through direct sulphation. As decomposition progresses, and before complete calcination, SO_2 is absorbed through

both direct and CaO-sulphation simultaneously. Finally, after complete decomposition only CaO-sulphation takes place. The rate of $CaCO_3$ calcination is much faster than the rate of direct sulphation [140]. Thus, a brief exposure of limestone particles to calcination conditions will cause decomposition, which then leads to CaO-sulphation. Therefore, it can be concluded that CaO-sulphation is the main cause of sulphation during calcination. The counter-diffusion of produced CO_2 during direct sulphation reaction leads to form a porous product layer of calcium sulphate that presents less diffusion resistance than nonporous layer made during the CaO-sulphation [118; 140].

Moreover, during calcination in addition to the decomposed CaO, more CaO can be produced via solid-state ionic diffusion [84; 141-147]. As these results show, sulphation occurred during calcination in presence of SO_2. Ionic diffusion through the $CaSO_4$ layer requires a large activation energy, which could be achieved during calcination. During this process, Ca^{2+} and O^{2-} migrate (in a coupled manner to balance the local charge) through the $CaSO_4$ product layer towards the $CaSO_4$/gas interface. Afterwards, at the product layer surface more sulphation reaction takes place as Equation (7.15):

$$Ca^{2+} + O^{2-} + SO_{2\,(g)} + ½\ O_2 \rightarrow CaSO_4 \qquad (7.15)$$

It is clear that ionic diffusion during calcination can increase the concentration of CaO at the interface of $CaSO_4$ and gases, which contain both SO_2 and CO_2. However, thermodynamically at 950 °C, CaO will react with SO2 but not CO_2. Therefore, the $CaSO_4$ formed during calcination is mainly consists of nonporous CaO-sulphate layer, which consequently will cause more deactivation in sorbent ability to capture CO_2 in carbonation reaction. Furthermore, solid-state ionic diffusion, which can occur during calcination with SO_2 present, increases sulphation and consequently will cause more deactivation in CO_2 capture capacity of the sorbent. As a result, calcination of limestone in SO_2-free atmosphere seems to be the only solution to prevent the negative influence of sulphation during sorbent decomposition.

In order to describe the sulphation during calcination and carbonation, SO_2 concentrations and their gradients in a cycle are depicted in Figure 7.18. The higher specific surface area of porous CaO particles compared to $CaCO_3$ particles causes a faster rate of CaO-sulphation in comparison to direct sulphation [132]. This can be seen between the times B1 and B2 in Figure 7.18-a, over which a negative gradient indicates a significant decrease in SO_2 concentration associated with CaO-sulphation. After the time B2, a decrease in the amount of accessible CaO caused a decrease in CaO-sulphation. The trend of detected SO_2 concentrations in the outlet gases during cycles, depicted in Figure 7.17-a2 and b2, also confirms that sulphation occurred with the commencement of carbonation reactions. At the beginning of carbonation, and in presence of CaO particles, sulphation takes place through CaO-sulphation. As sorption progresses, and before the complete carbonation, SO_2 is adsorbed through both direct and CaO-sulphation simultaneously. Finally, following the complete carbonation, direct sulphation can take place. This can be seen in Figure 7.18-b as well. In the beginning of the sorption, which is concurrent to the fast stage carbonation (over the times A1 to A2),

detected SO_2 in the exhaust gases increased at a high constant rate and afterwards (A2 to A3) a decrease in the rate mainly attributes to direct sulphation.

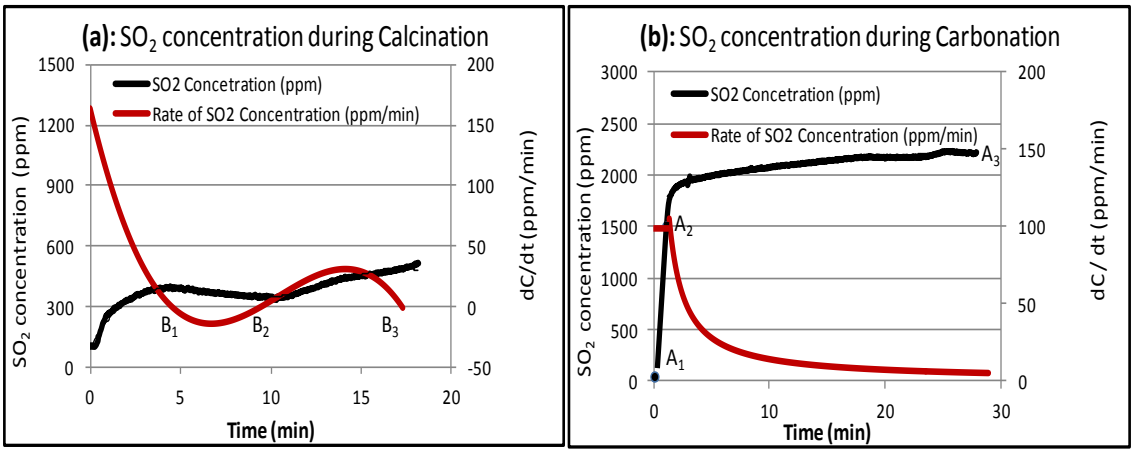

Figure 7.18: SO_2 concentrations and their gradients in a cycle: (a) during calcination with 1500 ppm SO_2 present, and (b) over carbonation in presence of 2500 ppm SO_2.

The rate of carbonation is much faster than the rate of CaO-sulphation [60], as this can be seen in Figure 7.19, which compares carbonation and sulphation conversions in one of the test sets. Depicted carbonation conversions (left) indicate that fast stage carbonations took place in 1 to 7 minutes depending on the number of cycle already undergone, and thereafter the rate of carbonation is very slow. Sulphation conversion curves (right) demonstrate almost a uniform rate over the carbonation time. On the other hand in presence of CaO particles in the beginning of carbonation, SO_2 capture can be mostly associated to CaO-sulphation, which inhibits more CO_2 diffusion. Therefore, flue gas desulphurisation prior to the carbonation reaction can be considered as an essential solution. However, in the absence of the desulphurisation process, restricting sorption to the fast stage carbonation will reduce the extent of sulphation.

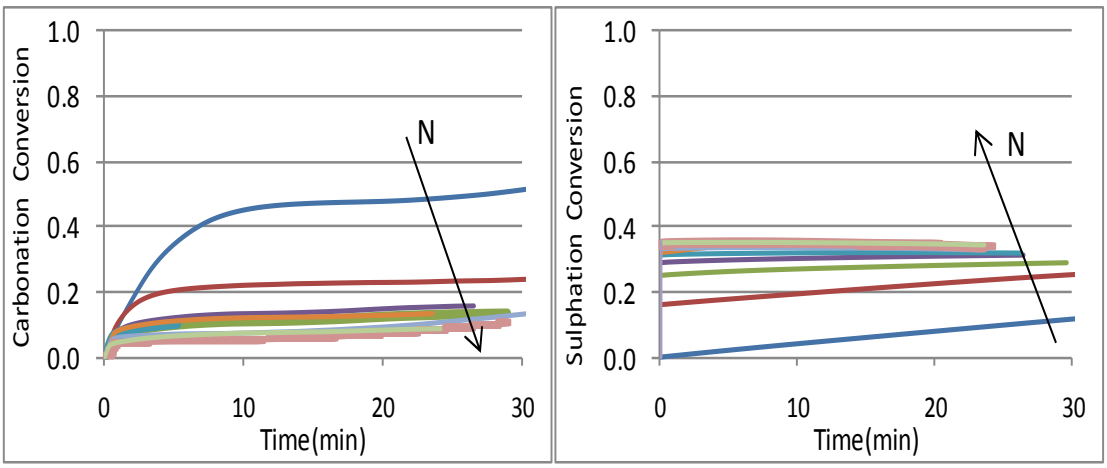

Figure 7.19: The reaction conversion curves for simultaneous carbonation (left) and sulphation (right) over a cyclic test.

7.3 Pressurised calcination of limestone in the CaO-looping cycle

The objective of this work is to study the CO_2 capture performance of limestone in atmospheric carbonations after pressurised calcinations in realistic flue gas conditions. Different series of test programmes were carried out to study the role of pressurised calcination using FBR. Operating conditions were simulated at elevated pressure in calcination during cyclic calcination and carbonation of limestone.

In this investigation, calcination of limestone particles was carried out at three levels of pressure: 0.1MPa, 0.5MPa, and 1.0MPa. The sorbent decomposition steps were performed once the CO_2 detected in the outlet flue gases dropped to a constant level over a significant period, and almost equal to that for the initial amount. After calcination reactivity, performances of the calcined sorbent were tested at atmospheric pressure. The carbonation conversion curves obtained from the cyclic process are depicted in Figure 7.20.

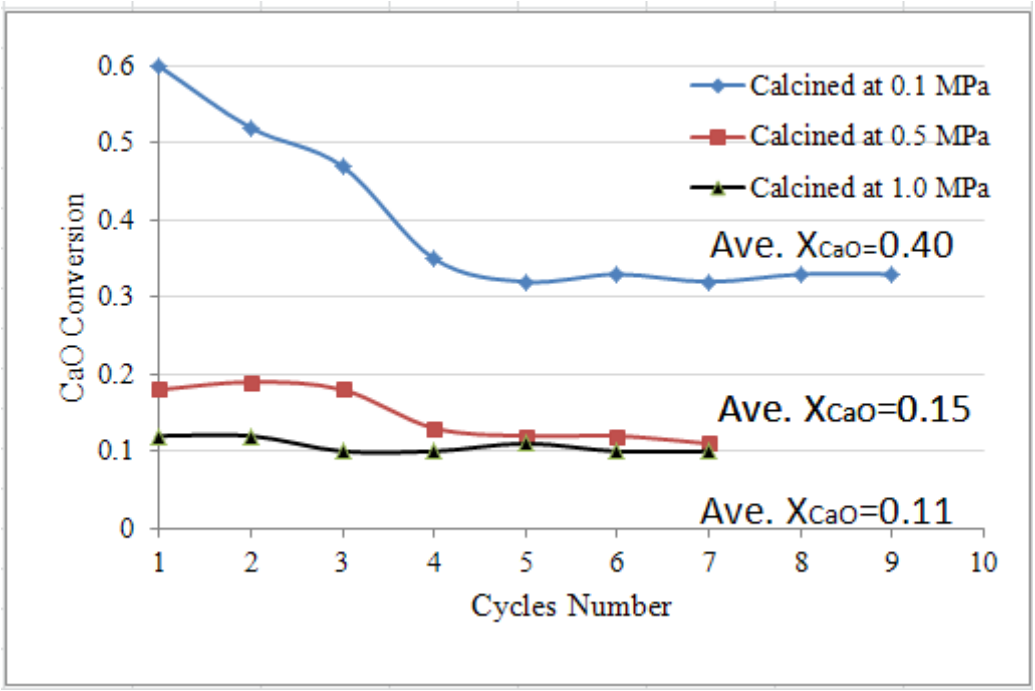

Figure 7.20: The carbonation conversion curves of calcined samples produced at elevated pressure and carbonated at atmospheric pressure. Calcination: at 950 °C, in 15% CO_2, 3% O_2 and N_2 balance. Carbonation: at 650 °C, in 15% CO_2, 4% O_2 and N_2 balance.

As can be seen, the carbonation conversions of calcined sorbent decrease significantly by increasing the level of pressure in calcination step. The average conversion for the CaO produced at atmospheric pressure was 0.42, while it declined to 0.12 and 0.09 for the sorbents calcined under 0.5 MPa and 1.0 MPa, respectively.

As expected, the incipient temperature of calcination increased by increasing the CO_2 partial pressure. As can be seen in Figure 7.21 the decomposition began at 790 °C, 870 °C and 940 °C at elevated pressures of 0.1MPa, 0.5 MPa, and 1.0 MPa, respectively. These are in agreement with models prediction for limestone calcination temperature, presented in Figure 3.8.

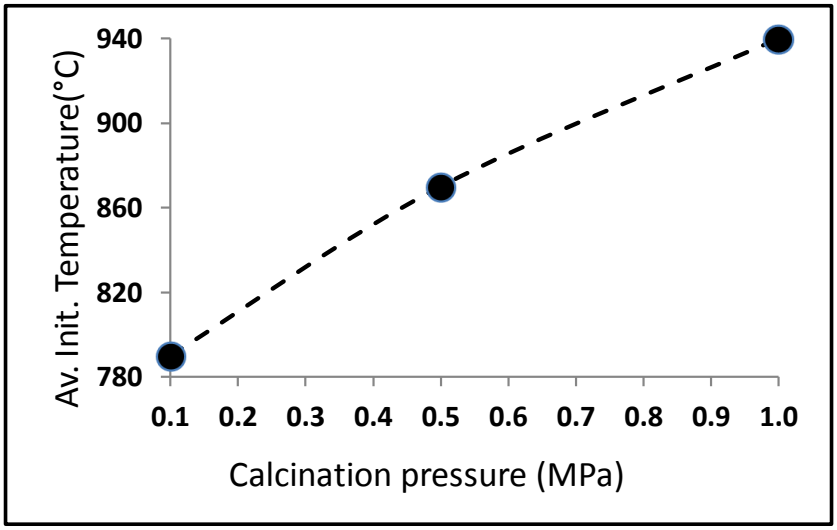

Figure 7.21: Effect of pressure on the incipient bed temperature for calcination.

It is clear that calcination reaction rate decreases with an increase in CO_2 partial pressure [27]. It has also been found that an increase in pressure results in the same effect on calcination rate even in the absence of CO_2 in reacting gases [128]. As expected, the time required for calcination raised significantly by increasing the pressure. The calcination periods lasted about 13 min, 40 min, and 110 min for decomposition under 0.1 MPa, 0.5 MPa, and 1.0 MPa pressure, respectively. It has been shown that sintering of CaO particles is favoured both by high temperatures and time at temperature [49; 50; 60]. Therefore, pressurised calcination, which requires higher temperature and longer time than those for lower pressure, causes the increase in sorbent sintering. Consequently, it can be confirmed that pressurised calcination results in reducing the capture capacity of sorbents (due to the extended time at temperature).

These results were also supported by the scanning electron microscopy (SEM) images of particles after the first and the last cycle of calcination at elevated pressure, as shown in Figure 7.22. The number of cycles and the calcination pressures are given on each SEM image. Figure 7.22-a shows the porous structure of initial calcined at 0.1 MPa, which clearly reveals a desirable sorbent texture consisting mainly of small pores. Existence of small pores increases the surface area and also enables sorbents to have a higher CO_2 capture. The series of images shown in Figures 7.22-a to 7.22-f illustrate the trend of surface texture of sorbents by increasing the calcination pressure and the number of cycles. As described earlier, particles calcined under higher pressure and after more cycles, have experienced higher temperature and longer time at temperature. Based on the SEM images, the occurrence of sintering in particles calcined under higher

pressure and after more cycles is obvious. SEM images clearly reveal the development of necks between the grains and increasing the pore sizes (as associated with sintering) by increasing the calcination pressure.

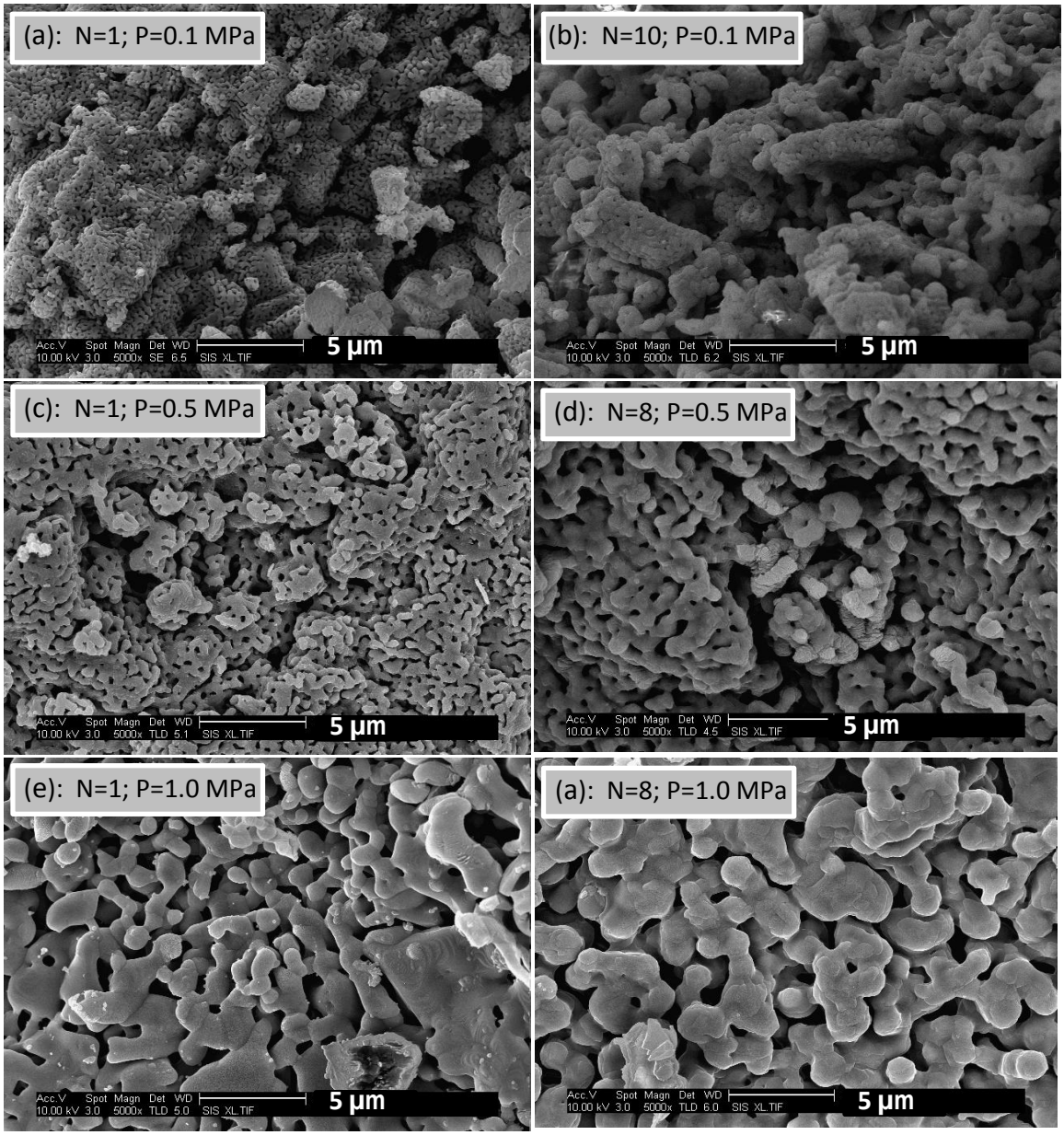

Figure 7.22: SEM images of the calcined particles produced at elevated pressure, after 1st or a number of cycle calcination-carbonation. **Calcinations:** 15% CO_2, 3% O_2, and N_2 balance; **Carbonations:** 15% CO_2, 4% O_2 and N_2 balance.

Further to SEM analysis, samples characterisations also confirmed the findings of this investigation. Particles characterisations were studied by measuring the porous structural properties of the calcined sorbent produced at elevated pressure and after different cycles. Specific surface area and pore volume of particles are given in Table 7.5. Pore volumes show the volumes of small pores and medium-size pores (~60-300 nm). The values are calculated as the difference between cumulative volume of pores

with diameters of 1.7nm-300nm, and the pore volume measured for smaller pores with diameter less than about 60 nm. These pores geometrically are able to accommodate a thicker forming product layer. As can be seen in Table 7.5, BET specific surface areas were measured at 18m^2/g for the initial calcined sorbent under 0.1 MPa pressure, which drastically fell to 2.5 and 1.1 m^2/g for those decomposed under 0.5 and 1.0 MPa, respectively. The corresponding volumes of small pores were 0.022, 0.004, and 0.001 cm^3/g for particles calcined at three levels of the calcination pressures.

Table 7.5: Porous structural properties of calcined particles after the first calcination at elevated pressure.

Calcined Sample [a]	S_{BET} (m^2/g)	Pore Volume (cm^3/g)
0.1 MPa, 1st cycle	18	0.022
0.5 MPa, 1st cycle	2.5	0.004
1.0 MPa, 1st cycle	1.1	0.001

a. Details of the reaction conditions are given in Table 5.4.

Pore size distributions, plotted in Figure 7.23, reveal that the number of small pores is higher in CaO particles, which were calcined at 0.1 MPa. Particles calcined at the same pressure but after the 10th cycle show more micropores (<30nm) than those were calcined in the 1st cycle, which is caused by a level of sintering over the cyclic process. It also indicate that the sorbents, which experienced pressurised calcination, even in the 1st cycle, contain a certain amount of micropores (<20nm), and after that the almost horizontal curves show the lack of small pores. This situation is more significant for the sorbents calcined under 1.0 MPa, which is caused by serious sintering.

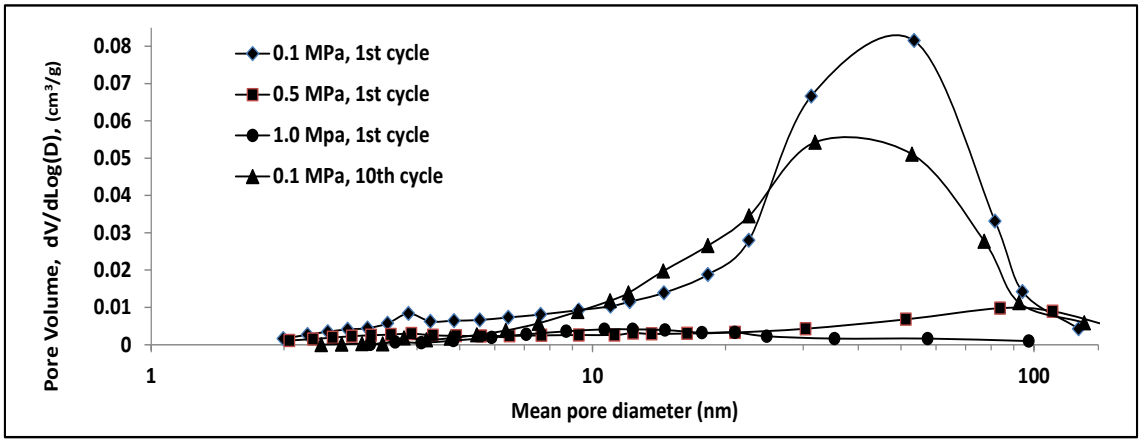

Figure 7.23: Pore-size distribution with the history of CaO particles at elevated pressure.

CaO particles characterisation also confirmed that experiencing the cyclic process with pressurised calcination results in greater reduction in particles porous structure. Specific surface areas and mesopores volumes (calculated as described in Table 7.5) for CaO particles, calcined in the 10^{th} or 8^{th} cycle, are given in Table 7.6. As can be seen in Table 7.6, the surface areas and pore volumes of calcined sorbent reduced drastically after pressurised calcination. This indicates that calcined sorbent produced under 0.1MPa (in the 10^{th} cycle) contains a surface area of 5.7 m^2/g, and pore volume of 0.010 cm^3/g. However, the corresponding values for CaO calcined under 0.5 MPa and 1.0 MPa (in the8^{th} cycle) have fallen to 1.2 and 0.25 m^2/g, and 0.002 and 0.0006 cm^3/g, respectively.

Table 7.6: Structural properties of calcined sorbent after cyclic process at elevated pressure.

Calcined Sample [a]	S_{BET} (m^2/g)	Pore Volume (cm^3/g)
0.1 MPa, 10^{th} cycle	5.7	0.010
0.5 MPa, 8^{th} cycle	1.2	0.002
1.0 MPa, 8^{th} cycle	0.25	0.0006

a. Details of the reaction conditions are given in Table 5.4.

So far it has been shown that a drop in the calcination rate under pressurised conditions, and the consequent sintering, results in the deactivation of sorbents. However, the extents of calcination conversions, based on the sorbents mass-change (Equation 7.16), have been provided, in order to investigate the appropriateness of the applied calcination time. The results of carbonation conversion at elevated pressure in the 1^{st} cycle are given in Table 7.7. The results showed that despite the applied long period for the pressurised calcinations, the extents of conversion are far less than those required for complete decompositions. This is more pronounced for calcination under higher pressure.

Table 7.7: The extent of calcination conversion at elevated pressure after the first cycle.

Pressure at Calcination	X_{CaCO_3} 1^{st} cycle
0.1 MPa	0.99
0.5 MPa	0.74
1.0 MPa	0.49

Meanwhile, investigating the applicability of pressurised calcination in industries requires studying both advantages and disadvantages. Sorbent deactivation is considered as the main disadvantage. Designing and operating fluidised valves (such as loop seal) to provide proper connection of the pressurised reactor (calciner) with the atmospheric reactor (carbonator) is more challenging than that for the same pressure reactors. Reduction in the energy required for CO_2 compression after separation is an initial advantage. Scaling down the equipments, due to possible process intensification could be considered as another advantage to this process.

The mass change of the solid sample was used for calculating the extent of calcination conversion using the equation

$$X_{Calc}(t) = \frac{M_{CaCO_3}(m_0 - m_t)}{m_0 V_{m_{CO_2}}(T,p)} \tag{7.16}$$

The symbols are as defined in the first part of chapter 7.

CHAPTER 8

Conclusions

Chapter 8 : Conclusions and Future Work

Limestone looping cycle is a promising capture technology to provide a cost-effective separation process to remove CO_2 content from power plants operations. The effects of three influencing factors (steam, SO_2, and pressure) on the performance of this technology, in post-combustion CO_2 capture system, have been studied. The investigations on the effects of these influencing factors led to the following conclusions:

8.1 The effects of steam on calcination-carbonation cycles

The performance of limestone calcination-carbonation for CO_2 removal from flue gases, in presence of steam, has been investigated. Experiments were conducted in three levels of steam percentage to investigate the applicability of steam for diluting the calcination atmosphere. Furthermore, steam-dilution has been compared to N_2-dilution, as the initial dilutant in industries. Subsequent to the calcination under elevated levels of steam, the performance of calcined particles was tested by sorbents carbonation in presence of two levels of steam. Therefore, the likely effects of steam in carbonation were investigated as well. As this project focuses on CO_2 capture from flue gases produced by existent power plants (post-combustion process), the corresponding real industrial conditions were simulated for carbonation atmosphere. This study led to the following conclusions:

1. Steam-diluting calcination could enhance the capacity of sorbents to capture CO_2. The sorption capacities of the CaO produced in higher steam dilution atmosphere were better than those of the CaO produced in lower steam dilution atmosphere. SEM images and particles characterisation confirmed an improvement in porous structural properties such as surface areas and pore volumes.

2. The sorbents produced in higher steam diluted atmosphere revealed a better enhancement in capture capacity in the first few cycles. Thereafter, these steam calcined particles experienced higher rates of decay in sorption capacity; and the capture capacity of sorbents calcined in different diluting conditions became closer, with increasing numbers of cycles. However, as a criterion, calcined sorbent produced under higher steam-dilution atmosphere, showed a higher level of average carbonation conversion.

3. The average bed temperature required for calcination to reach the maximum conversion, decreased with increasing the steam dilution percentage, as for N_2-dilution. In addition, increasing steam dilution lowers the initial decomposition temperature. Therefore, it can be concluded that steam dilution could result in

energy saving in the separation process. However, the overall energy of the system needs to be considered.

4. The almost equal percentage of steam and N_2 in calcination step resulted in almost similar improvements in the performance of calcined sorbent. Taking both potential effects of steam on calcination into account (enhancement in capturing capacity and possible catalysing the sintering), steam could be used to dilute the calciner atmosphere; particularly considering its ease of separation from CO_2 compared to N_2 by condensation.

5. Increasing the steam percentage in carbonation atmosphere improved the capture capacity of sorbents, which have been calcined in conditions with a lower steam dilution. This effect of steam on carbonation conversion should not be attributed to sorbent hydration.

8.2 The effects of SO_2 on calcination-carbonation cycles

Thermal decomposition of limestone in a combustion atmosphere of heavy fuels results in presence of SO_2. This work investigated the effects of calcination with SO_2 present on limestone looping technology for CO_2 capture. Different series of test programmes were carried out to study this effect of SO_2 presence, using FBR. The performances of calcined particles were tested by sorbents carbonation in presence of three levels of SO_2. Reaction conditions were simulated at elevated SO_2 concentrations to cover a wide range of power plants considering their combusting fuels and flue gas desulphurisation facilities. The idea of co-capturing process of CO_2 and SO_2 has also been assessed. The outcomes of the study are as follows:

1. The CO_2 capture capacity of the CaO produced in presence of SO_2 were less than those of the CaO produced with no SO_2 atmosphere. The particle characterisation and SEM images confirmed that presence of SO_2 in calcination step lessens the porous properties sorbents for CO_2 capture, such as surface area and pore volumes.

2. The presence of SO_2 in calcination sweep gas resulted in sulphation of sorbent. The $CaSO_4$ formed during calcination mainly consists of a non-porous CaO-sulphate layer, which consequently will cause more deactivation in sorbent ability to capture CO_2 in carbonation reaction. Furthermore, solid-state ionic diffusion, which can occur during calcination, with SO_2 present increases sulphation and consequently will cause more deactivation in CO_2 capture capacity of the sorbent. As a result, the use of very low sulphur fuels, or preferably SO_2-free atmosphere, to provide required heat in the calciner seems to be the only way to prevent the decay in sorbent capacity. However, it should be noted that long cycle times will lead to high sulphation per cycle and possibly extrapolate the effect.

3. The results show that more SO_2 was captured during calcination of sorbents, which have been carbonated at lower SO_2 concentration. Therefore, providing low sulphur calcination atmosphere is potentially desirable for plants facilitated by flue gas desulphurisation.

4. Carbonation of CaO particles in presence of SO_2 revealed that the ability of sorbent to capture CO_2 decreased at a higher rate, proportional to the SO_2 concentration. In presence of CaO particles in the beginning of carbonation, SO_2 capture can be mostly associated to CaO-sulphation, which inhibits more CO_2 diffusion. The particle characterisation and SEM images confirmed that carbonation with SO_2 present lowers the porous properties of sorbents for CO_2 capture, such as surface area and pore volumes. Reducing SO_2 concentrations in the flue gases prior to CO_2 capture process could lessen this type of decay in sorbent capacity. However, in the absence of flue gas desulphurisation process, restricting the sorption to the fast stage carbonation will reduce the extent of sulphation (considering the faster rate of carbonation than that of CaO-sulphation).

5. The total Ca utilization demonstrated a non-declining pattern after increasing cycle numbers. This fact could not be attributed to the tendency of SO_2 to react with particles which have already experienced numbers of carbonation and calcination cycles. The results verify that the ability of sorbent to capture SO_2, similar to their CO_2 capture capacity, decreased by cycling the sorbent in CO_2/SO_2 atmosphere. The rise in accumulative sulphation conversions by increasing the number of cycles is caused by the irreversible sulphation reaction at the calcination temperature.

6. The results do not advise the co-capture process, as presence of SO_2 caused a decrease not only in CO_2 capture capacity but in total Ca utilization as well. In fact, the presence of a higher amount of SO_2 in the reaction atmosphere causes simultaneous loss in carbonation and rise in sulphation of CaO particles. Consequently, the decrease in total Ca utilization simply reveals that the extent of the loss in carbonation is larger than the extent of the increase in sulphation. These imbalanced adverse conversions are caused by the formation of voluminous calcium sulphate. $CaSO_4$ has a considerably larger molar volume (46 cm^3/mol) than that of CaO (17 cm^3/mol) and $CaCO_3$ (37 cm^3/mol). As a result, the occupied pores by a certain extent of sulphation cause a larger loss in the extent of carbonation.

8.3 Pressurised calcination of limestone in the CaO-looping cycle

A study was carried out of the CO_2 capture performance of limestone under atmospheric carbonations after pressurised calcinations in practical gas conditions. Different series of test programmes were carried out to study the role of pressurised calcination by means of FBR. Operating conditions were simulated at elevated pressure in calcination during cyclic calcination and carbonation of limestone.

In this investigation, calcination of limestone particle was carried out at three levels of pressure: 0.1MPa, 0.5MPa, and 1.0MPa. After calcination, reactivity performance of the calcined sorbent was tested at atmospheric pressure. This investigation led to the following outcomes:

1. The results indicate that carbonation conversions of calcined sorbent decrease significantly by increasing the level of pressure in calcination step.

2. The incipient temperature of calcination increased by increasing the CO_2 partial pressure.

3. Pressurised calcination, which requires higher temperature and longer time than those for lower pressure, causes the increase in sorbent sintering. Consequently, it can be confirmed that pressurised calcination results in reducing the capture capacity of sorbents. Based on the SEM images, the occurrence of sintering in particles calcined under higher pressure and after more cycles is obvious. SEM images clearly reveal the development of necks between the grains and increasing the pore sizes (as associated with sintering) by increasing the calcination pressure. Specific surface area and pore volume of particles were studied by particle characterisation. BET specific surface areas, which were measured for the initial calcined particles under 0.1 MPa pressure, drastically fell for calcined particles decomposed under 0.5 and 1.0 MPa. The corresponding pore volumes experienced an extreme drop by increasing the calcination pressure.

4. Investigating the applicability of pressurised calcination in industries requires studying both advantages and disadvantages. Sorbent deactivation is considered the main disadvantage. Designing and operating fluidised valves (such as loop seal) to provide proper connection of the pressurised reactor (calciner) with the atmospheric reactor (carbonator) is a challenge to this process. Reduction in the energy required for CO_2 compression after separation is an initial advantage. Scaling down the equipments, due to possible process intensification could be considered as another advantage to this process.

8.4: Future work

Following the investigations described in this thesis, several lines of research could be taken up, involving influencing factors studied.

- During these investigations, in order to study the effects of each factor, other influencing factors were omitted from the reaction conditions. However, further understanding the effects requires investigating the effects of combination of the factors (steam, SO_2, and pressure) on the performance of limestone looping cycle.

- The results showed that increasing the steam percentage in carbonation atmosphere improved the capture capacity of sorbents, which have been calcined in conditions with a lower steam dilution. It was proposed that presence of CO_2 in calcination atmosphere may results in this effect. Investigating this effect requires conducting experiments in similar conditions with no CO_2 present in calcination.

- The results showed that an increase in CO_2 partial pressure and total pressure decreases the calcination rate, and causes an increase in reaction temperature, time, and the subsequent sintering. Therefore, it is interesting to study the techno-economic status of a process involving close-to-vacuum calcination.

Appendices

APPENDIX A

Gas flow rate calculation for bubbling fluidised bed

Increasing the gas flow rate in a fixed bed cause the rise in pressure drop across the bed, until superficial gas velocity reaches a value known as minimum fluidisation velocity, U_{mf}. Solid particles have been classified in four groups, based on their required gas flow rate to be fluidised [134].

The sorbent used in the tests with 125-250 μm size are in the range of Group B. Particles in Group B are normally in the range of 100 to 500 μm (for ρ_p = 2500 kg/m^3) size. They fluidise, and bubbles appear once the minimum fluidisation velocity is exceeded. Therefore in this group of particles minimum fluidisation velocity and bubbling velocity are at the same value ($U_{mb} = U_{mf}$). The minimum bubbling velocity, in these tests, was calculated based on the following equation [134].

$$U_{mf} = \frac{\mu\, Re_{mf}}{\rho_g\, d_p}$$

$$Re_{mf} = [C_1^2 + C_2\, Ar]^{0.5} - C_1$$

$$A_r = \frac{\rho_g(\rho_p - \rho_g)g d_p^3}{\mu^2}$$

A_r : Archimedes number
U_{mf}: Minimum fluidization velocity, m/sec
U_{mb} : Minimum bubbling velocity, m/sec
ρ_g : Density of gas, kg/m^3
ρ_p : Density of solids, kg/m^3
d_p : Surface-volume mean diameter of particles, m
Re_{mf}: Reynolds number at minimum fluidisation velocity
μ : Viscosity of gas, kg/m^2
$C_1 = 27.2$ and C_2 = 0.0408 both as taken from experiments

As can be seen in the calculation sheet, for the limestone used, the minimum gas flow rate calculated at around 0.6 and 0.8 l.min^{-1}, for calcination and carbonation, respectively. The results were entirely confirmed by fluidisation tests in a cold model (video and pictures were taken). It was found (theoretically and experimentally) that the transition between fluidisation regimes requires a wide gap. The effect of flow rate on the process was also studied, as given in chapter 6. Therefore, the minimum require flow rates were doubled for the experiments (1.2 and 1.6 l.min^1).

APPENDIX B

Minimum Bubling Fluidisation Gas Flowrate Calculation for Calcination and Carbonation- Masoud Kavosh	2				Ar calculation	Remf calculation	Umf calculation(m/s)
operating temperature-Calcination	950	C			C1=27.2 & C2=0.0408	equation(2.3)	equation(2.3)
operating temperature-Carbonation	650	C				for Limestone	
room temperature	20	C			35	0.0263	0.0148
gas density at op. temp.(CO2 @ 0.1MPa-950C)	0.44	kg/m3			75	0.0563	0.0189
gas density at op. temp.(CO2 @ 0.1MPa-650C)	0.58	kg/m3			22	0.0169	0.0149
gas density at op. temp.(N2 @ 0.1MPa-950C)	0.28	kg/m3			45	0.0335	0.0182
gas density at op. temp.(N2 @ 0.1MPa-650C)	0.37	kg/m3			734	0.5453	0.0413
gas density at room temp.(N2 @ 0.1MPa-20C)	1.16	kg/m3				for Limestone+Sand	
					188	0.1406	0.0454
mean particle diameter dp (mix Silica : Limestone= 4:1)	0.0003500	m			403	0.3003	0.0575
mean particle diameter dp (for Silica Sand 350-425 µm)	0.0003875	m			121	0.0902	0.0456
mean particle diameter dp (for Limstone 125-250 µm)	0.0002000	m			239	0.1790	0.0557
Globalspec equation for gas viscosity			Holman equation for viscosity		3936	2.8070	0.1214
dynamic viscosity of CO2 at 0.1 MPa. ;950C	0.0000495	Pa.s=s/m2	5.66919E-05	Pa.s			
dynamic viscosity of CO2 at 0.1 MPa. ;650C	0.0000389	Pa.s=s/m2	5.66919E-05	Pa.s			
dynamic viscosity of N2 at 0.1 MPa. ;950C	0.0000493	Pa.s=s/m2	4.5342E-05	Pa.s	Particles belonge to	group B so $U_{mb}=U_{mf}$	
dynamic viscosity of N2 at 0.1 MPa. ;650C	0.0000403	Pa.s=s/m2	4.5342E-05	Pa.s			
dynamic viscosity of N2 at 0.1 MPa. ;20C	0.0000176		1.80909E-05	Pa.s	pressurised gas densities for future calculatio		
fraction of particles smaller than 45 µm	0.05				gas density at op. temp.(CO2 @ 1MPa-950C	4.33	kg/m3
particle sphericity					gas density at op. temp.(CO2 @ 1MPa-650C	5.73	kg/m3
particle density	2500	kg/m3			gas density at op. temp.(N2 @ 1MPa-950C)	2.75	kg/m3
reactor diameter	0.03	m			gas density at op. temp.(N2 @ 1MPa-650C)	3.65	kg/m3
reactor height							
reactor area	0.00070650	m2					
flue gas pipe diameter	0.02500000	m	note: Masoud 1&2 calculation are almost the same except their dp.				
flue gas pipe area	0.00049063	m2					
					for Limestone+Sand		
	for Limestone				1.92		
Min. Bubling fluidisation CO2 flowrate at 0.1MPa- 950 C	0.63	l/min			2.44		
Min. Bubling fluidisation CO2 flowrate at 0.1MPa- 650 C	0.80	l/min			1.93		
Min. Bubling fluidisation N2 flowrate at 0.1MPa- 950 C	0.63	l/min			2.36		
Min. Bubling fluidisation N2 flowrate at 0.1MPa- 650 C	0.77	l/min			5.15		
Min. Bubling fluidisation N2 flowrate at 0.1MPa- 20 C	1.75	l/min					

		Combustion Calculation - General Program		Example: air/fuel of coal with 5% excess air;Analysis from fuel science book			
	INPUT						
Fuel Composition	wt %	kmol in 100 kg Fuel Burned	kmol Oxygen required	Product in Flue Gas	kmol	vol% wet	vol% dry
C	74.1	6.18	6.18	CO_2	6.18	**16.34**	**17.66**
H	5.1	2.55	1.28	Steam(including initial H2O)	2.83	**7.48**	
O	9.5	0.30	-0.30	O_2	0.36	**0.95**	**1.03**
N	1.35	0.05	0.00	N_2	28.41	**75.15**	**81.23**
S	0.95	0.03	0.03	SO_2	0.03	**0.08**	**0.08**
H_2O	5	0.28	0.00		0.00		
Ash	4		0.00		0.00		
Total	100	**al kmol Oxygen required=**	**7.18**	Σwet=	37.80	**100.00**	**100.00**
				Σdry=	34.97		

		Combustion Calculation - General Program		Example: oxyfuel of coal with no excessO2;Analysis from fuel science book			
	INPUT						
Fuel Composition	wt %	kmol in 100 kg Fuel Burned	kmol Oxygen required	Product in Flue Gas	kmol	vol% wet	vol% dry
C	74.1	6.18	6.18	CO_2	6.18	**68.00**	**98.75**
H	5.1	2.55	1.28	Steam(including initial H2O)	2.83	**31.14**	
O	9.5	0.30	-0.30	O_2	0.00	**0.00**	**0.00**
N	1.35	0.05	0.00	N_2	0.05	**0.53**	**0.77**
S	0.95	0.03	0.03	SO_2	0.03	**0.33**	**0.47**
H_2O	5	0.28	0.00		0.00		
Ash	4		0.00		0.00		
Total	100	**al kmol Oxygen required=**	**7.18**	Σwet=	9.08	**100.00**	**100.00**
				Σdry=	6.25		

		Combustion Calculation		Example: oxyfuel of coal with 5% excessO2;Analysis from fuel science book			
	INPUT						
Fuel Composition	wt %	kmol in 100 kg Fuel Burned	kmol Oxygen required	Product in Flue Gas	kmol	vol% wet	vol% dry
C	74.1	6.18	6.18	CO_2	6.18	**65.41**	**93.39**
H	5.1	2.55	1.28	Steam(including initial H2O)	2.83	**29.96**	
O	9.5	0.30	-0.30	O_2	0.36	**3.80**	**5.43**
N	1.35	0.05	0.00	N_2	0.05	**0.51**	**0.73**
S	0.95	0.03	0.03	SO_2	0.03	**0.31**	**0.45**
H_2O	5	0.28	0.00		0.00		
Ash	4		0.00		0.00		
Total	100	**al kmol Oxygen required=**	**7.18**	Σwet=	9.44	**100.00**	**100.00**
				Σdry=	6.61		

		Combustion Calculation		Oxyfuel of daw mill coal with 5% excessO2;Analysis from Phyllis			
	INPUT						
Fuel Composition	wt %	kmol in 100 kg Fuel Burned	kmol Oxygen required	Product in Flue Gas	kmol	vol% wet	vol% dry
C	67.1	5.59	5.59	CO_2	5.59	**67.58**	**93.26**
H	4.2	2.10	1.05	Steam(including initial H_2O)	2.28	**27.53**	
O	10.3	0.32	-0.32	O_2	0.32	**3.85**	**5.31**
N	1.16	0.04	0.00	N_2	0.04	**0.50**	**0.69**
S	1.43	0.04	0.04	SO_2	0.04	**0.54**	**0.75**
H_2O	3.2	0.18	0.00		0.00		
Ash	12.4		0.00		0.00		
Total	99.79	**al kmol Oxygen required=**	**6.36**	Σwet=	8.27	100.00	100.00
				Σdry=	6.00		

		Combustion Calculation - General Program		Natural gas example run; analysis from Phylis site;Oxyfuel with no exess O2			
	INPUT						
Fuel Composition	wt %	kmol in 100 kg Fuel Burned	kmol Oxygen required	Product in Flue Gas	kmol	vol% wet	vol% dry
C	58.2	4.85	4.85	CO_2	4.85	**32.38**	**86.30**
H	18.72	9.36	4.68	Steam(including initial H_2O)	9.36	**62.48**	
O	1.5	0.05	-0.05	O_2	0.00	**0.00**	**0.00**
N	21.56	0.77	0.00	N_2	0.77	**5.14**	**13.70**
S	0	0.00	0.00	SO_2	0.00	**0.00**	**0.00**
H_2O	0	0.00	0.00		0.00		
Ash	0		0.00		0.00		
Total	99.98	**Total kmol Oxygen required=**	**9.48**	Σwet=	14.98	100.00	100.00
				Σdry=	5.62		

		Combustion Calculation - General Program		Natural gas example run; analysis from Phylis site;Oxyfuel with 5% exess O2			
	INPUT						
Fuel Composition	wt %	kmol in 100 kg Fuel Burned	kmol Oxygen required	Product in Flue Gas	kmol	vol% wet	vol% dry
C	58.2	4.85	4.85	CO_2	4.85	**31.38**	**79.58**
H	18.72	9.36	4.68	Steam(including initial H_2O)	9.36	**60.57**	
O	1.5	0.05	-0.05	O_2	0.47	**3.07**	**7.78**
N	21.56	0.77	0.00	N_2	0.77	**4.98**	**12.64**
S	0	0.00	0.00	SO_2	0.00	**0.00**	**0.00**
H_2O	0	0.00	0.00		0.00		
Ash	0		0.00		0.00		
Total	99.98	**al kmol Oxygen required=**	**9.48**	Σwet=	15.45	100.00	100.00
				Σdry=	6.09		

		Combustion Calculation		Natural gas example (Groningen) analysis from Phyllis site ; Oxyfuel with 5% exess O2			
	INPUT						
Fuel Composition	wt %	kmol in 100 kg Fuel Burned	kmol Oxygen required	Product in Flue Gas	kmol	vol% wet	vol% dry
C	58.2	4.85	4.85	CO_2	4.85	**31.38**	**79.58**
H	18.72	9.36	4.68	Steam(including initial H_2O)	9.36	**60.57**	
O	1.5	0.05	-0.05	O_2	0.47	**3.07**	**7.78**
N	21.56	0.77	0.00	N_2	0.77	**4.98**	**12.64**
S	0	0.00	0.00	SO_2	0.00	**0.00**	**0.00**
H_2O	0	0.00	0.00		0.00		
Ash	0		0.00		0.00		
Total	99.98	**kmol Oxygen required=**	**9.48**	Σwet=	15.45	100.00	100.00
				Σdry=	6.09		

APPENDIX C

Surface areas, pore volume, and pore size distribution sample

Full Report Set

TriStar 3000 V6.08 A | Unit 1 Port 2 | Serial #: 1001 | Page 1

Sample: Sample_4
Operator: ZS
Submitter: Masoud Kavosh Bedford Uni.
File: C:\...\003-50~1\003-870.SMP

Started: 16/12/2011 13:08:24PM
Completed: 16/12/2011 18:12:49PM
Report Time: 19/12/2011 14:57:00PM
Warm Free Space: 8.4430 cm³ Measured
Equilibration Interval: 5 s
Sample Density: 1.000 g/cm³

Analysis Adsorptive: N2
Analysis Bath Temp.: -195.800 °C
Sample Mass: 0.5431 g
Cold Free Space: 25.7302 cm³ Measured
Low Pressure Dose: None
Automatic Degas: No

Isotherm Tabular Report

Relative Pressure (P/Po)	Absolute Pressure (mmHg)	Quantity Adsorbed (cm³/g STP)	Elapsed Time (h:min)	Saturation Pressure (mmHg)
			00:41	741.98938
0.011064954	8.22036	2.8507	00:51	
0.031770494	23.61470	3.5466	00:55	
0.062678453	46.60575	4.0149	00:58	
0.078870142	58.66005	4.1875	01:00	
0.099639050	74.12554	4.3767	01:02	
0.119574429	88.96739	4.5379	01:03	
0.139453674	103.78413	4.6892	01:05	
0.159367967	118.63435	4.8338	01:07	
0.179294693	133.48457	4.9745	01:08	
0.199236564	148.36829	5.1123	01:10	
0.246730304	183.78197	5.4400	01:12	
0.298891147	222.69055	5.8098	01:14	
0.349004093	260.09235	6.1843	01:16	
0.396862927	295.83249	6.5664	01:18	
0.446179880	332.67761	6.9936	01:20	
0.495449831	369.50601	7.4692	01:22	
0.544493225	406.18372	8.0225	01:24	
0.593432689	442.85724	8.6830	01:27	
0.642189832	479.42194	9.4925	01:30	
0.690460333	515.71454	10.5188	01:34	
0.738610045	551.95276	11.8585	01:38	
0.794710117	594.31860	13.9768	01:44	
0.813139201	608.40289	14.8813	01:48	
0.838747966	627.95343	16.3376	01:53	
0.861280070	645.22290	17.9272	01:58	
0.890456226	667.82471	20.7528	02:07	
0.908727653	682.03455	23.2800	02:13	
0.937824205	705.09259	30.1595	02:27	
			02:42	753.23254
0.956765445	720.66687	39.9778	02:42	
0.960767172	723.80182	42.5068	02:48	
0.991830980	747.32861	52.0049	02:54	
0.991914766	747.43329	53.6830	02:56	
0.973654153	733.75500	53.2938	03:00	
0.955295782	720.06000	48.5913	03:07	
0.927837607	699.75183	36.0490	03:27	
0.901913534	680.46497	27.4295	03:41	
0.870834089	657.23535	22.4189	03:53	
0.846648195	639.14136	19.9438	04:02	
0.819210594	618.54858	17.9740	04:09	
0.791257185	597.55823	16.3963	04:16	
0.754444888	569.82074	14.7524	04:20	
0.699388681	528.32550	12.8620	04:26	
0.636383566	480.82407	11.1654	04:33	
0.603965183	456.36807	10.4251	04:36	
0.552864560	417.79016	9.3935	04:39	
			04:42	755.74548
0.501645031	379.11597	8.4939	04:43	
0.453384570	342.64334	7.1532	04:49	
0.403108180	304.64719	6.5212	04:51	
0.339013857	256.20819	5.9962	04:54	

Sample: Sample_4
Operator: ZS
Submitter: Masoud Kavosh Bedford Uni.
File: C:\...\003-50~1\003-870.SMP

Started: 16/12/2011 13:08:24PM
Completed: 16/12/2011 18:12:49PM
Report Time: 19/12/2011 14:57:00PM
Warm Free Space: 8.4430 cm³ Measured
Equilibration Interval: 5 s
Sample Density: 1.000 g/cm³

Analysis Adsorptive: N2
Analysis Bath Temp.: -195.800 °C
Sample Mass: 0.5431 g
Cold Free Space: 25.7302 cm³ Measured
Low Pressure Dose: None
Automatic Degas: No

Isotherm Tabular Report

Relative Pressure (P/Po)	Absolute Pressure (mmHg)	Quantity Adsorbed (cm³/g STP)	Elapsed Time (h:min)	Saturation Pressure (mmHg)
0.303906782	229.67618	5.7340	04:55	
0.252240304	190.62947	5.3680	04:58	
0.202373759	152.94305	5.0274	05:00	
0.143147548	108.18311	4.6203	05:02	

Sample: Sample_4
Operator: ZS
Submitter: Masoud Kavosh Bedford Uni.
File: C:\...\003-50~1\003-870.SMP

Started:	16/12/2011 13:08:24PM	Analysis Adsorptive:	N2
Completed:	16/12/2011 18:12:49PM	Analysis Bath Temp.:	-195.800 °C
Report Time:	19/12/2011 14:57:00PM	Sample Mass:	0.5431 g
Warm Free Space:	8.4430 cm³ Measured	Cold Free Space:	25.7302 cm³ Measured
Equilibration Interval:	5 s	Low Pressure Dose:	None
Sample Density:	1.000 g/cm³	Automatic Degas:	No

Isotherm Linear Plot

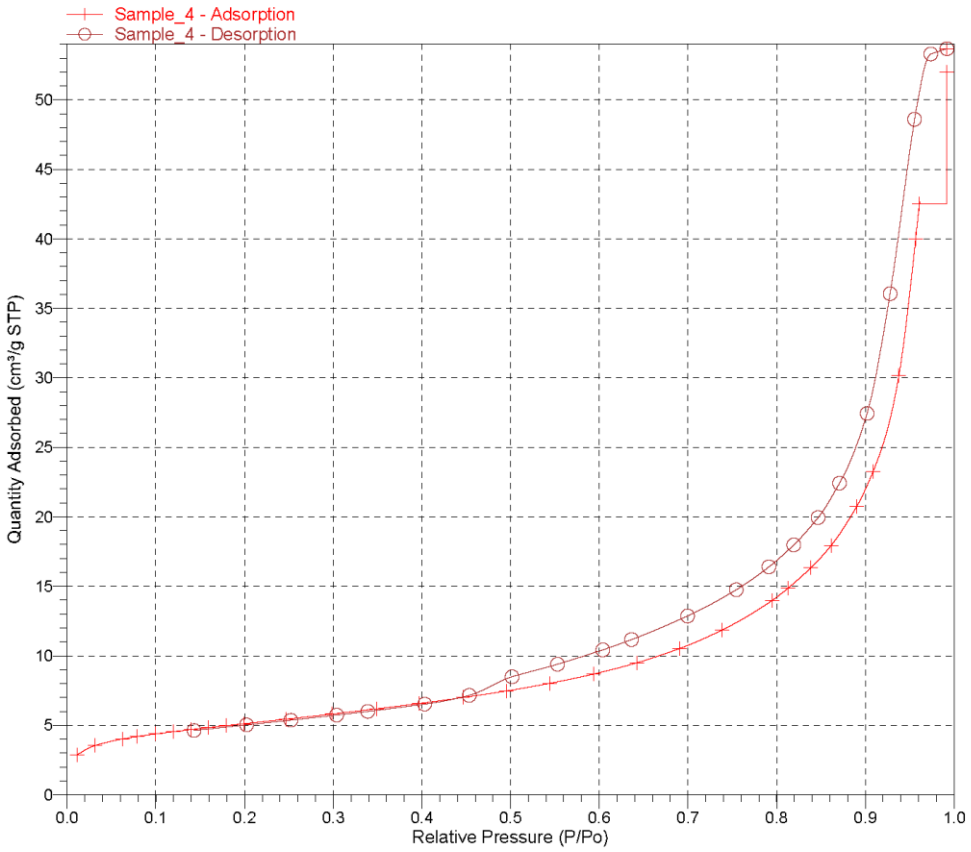

Sample: Sample_4
Operator: ZS
Submitter: Masoud Kavosh Bedford Uni.
File: C:\...\003-50~1\003-870.SMP

Started:	16/12/2011 13:08:24PM	Analysis Adsorptive:	N2
Completed:	16/12/2011 18:12:49PM	Analysis Bath Temp.:	-195.800 °C
Report Time:	19/12/2011 14:57:00PM	Sample Mass:	0.5431 g
Warm Free Space:	8.4430 cm³ Measured	Cold Free Space:	25.7302 cm³ Measured
Equilibration Interval:	5 s	Low Pressure Dose:	None
Sample Density:	1.000 g/cm³	Automatic Degas:	No

Isotherm Log Plot

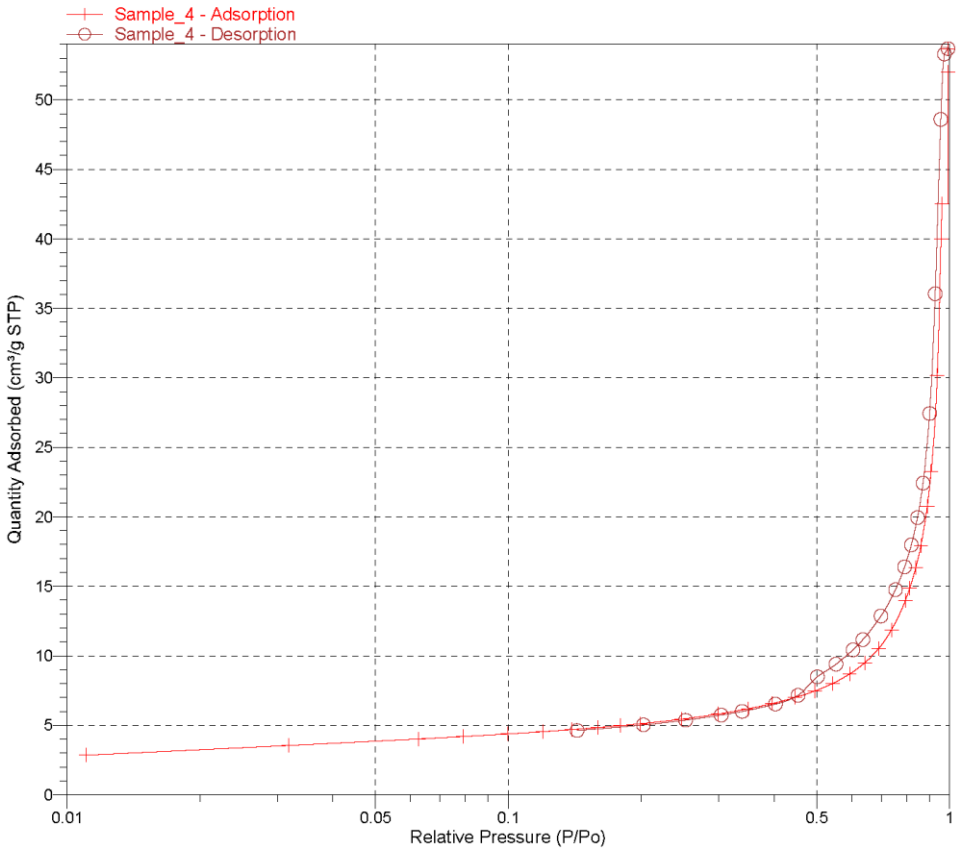

Sample: Sample_4
Operator: ZS
Submitter: Masoud Kavosh Bedford Uni.
File: C:\...\003-50~1\003-870.SMP

Started: 16/12/2011 13:08:24PM
Completed: 16/12/2011 18:12:49PM
Report Time: 19/12/2011 14:57:00PM
Warm Free Space: 8.4430 cm³ Measured
Equilibration Interval: 5 s
Sample Density: 1.000 g/cm³

Analysis Adsorptive: N2
Analysis Bath Temp.: -195.800 °C
Sample Mass: 0.5431 g
Cold Free Space: 25.7302 cm³ Measured
Low Pressure Dose: None
Automatic Degas: No

BET Surface Area Report

BET Surface Area: 18.3086 ± 0.0682 m²/g
Slope: 0.236104 ± 0.000879 g/cm³ STP
Y-Intercept: 0.001664 ± 0.000108 g/cm³ STP
C: 142.885003
Qm: 4.2058 cm³/g STP
Correlation Coefficient: 0.9999446
Molecular Cross-Sectional Area: 0.1620 nm²

Relative Pressure (P/Po)	Quantity Adsorbed (cm³/g STP)	1/[Q(Po/P - 1)]
0.011064954	2.8507	0.003925
0.031770494	3.5466	0.009252
0.062678453	4.0149	0.016655
0.078870142	4.1875	0.020447
0.099639050	4.3767	0.025285
0.119574429	4.5379	0.029929
0.139453674	4.6892	0.034559
0.159367967	4.8338	0.039220
0.179294693	4.9745	0.043917
0.199236564	5.1123	0.048668

Sample: Sample_4
Operator: ZS
Submitter: Masoud Kavosh Bedford Uni.
File: C:\...\003-50~1\003-870.SMP

Started:	16/12/2011 13:08:24PM	Analysis Adsorptive:	N2
Completed:	16/12/2011 18:12:49PM	Analysis Bath Temp.:	-195.800 °C
Report Time:	19/12/2011 14:57:00PM	Sample Mass:	0.5431 g
Warm Free Space:	8.4430 cm³ Measured	Cold Free Space:	25.7302 cm³ Measured
Equilibration Interval:	5 s	Low Pressure Dose:	None
Sample Density:	1.000 g/cm³	Automatic Degas:	No

BET Surface Area Plot

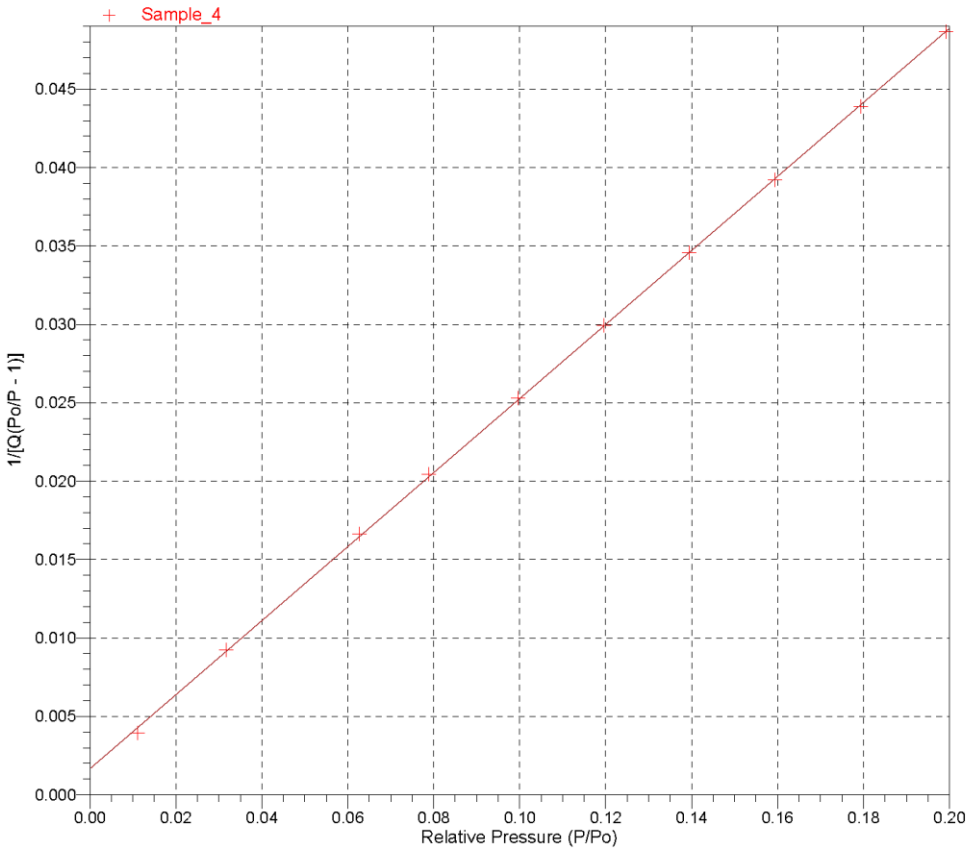

Sample: Sample_4
Operator: ZS
Submitter: Masoud Kavosh Bedford Uni.
File: C:\...\003-50~1\003-870.SMP

Started: 16/12/2011 13:08:24PM
Completed: 16/12/2011 18:12:49PM
Report Time: 19/12/2011 14:57:00PM
Warm Free Space: 8.4430 cm³ Measured
Equilibration Interval: 5 s
Sample Density: 1.000 g/cm³

Analysis Adsorptive: N2
Analysis Bath Temp.: -195.800 °C
Sample Mass: 0.5431 g
Cold Free Space: 25.7302 cm³ Measured
Low Pressure Dose: None
Automatic Degas: No

Langmuir Surface Area Report

Langmuir Surface Area: 23.5571 ± 0.6527 m²/g
Slope: 0.184793 ± 0.005120 g/cm³ STP
Y-Intercept: 2.557111 ± 0.470165 mmHg·g/cm³ STP
b: 0.072266 1/mmHg
Qm: 5.4115 cm³/g STP
Correlation Coefficient: 0.996943
Molecular Cross-Sectional Area: 0.1620 nm²

Pressure (mmHg)	Quantity Adsorbed (cm³/g STP)	P/Q (mmHg·g/cm³ STP)
8.22036	2.8507	2.884
23.61470	3.5466	6.658
46.60575	4.0149	11.608
58.66005	4.1875	14.008
74.12554	4.3767	16.936
88.96739	4.5379	19.605
103.78413	4.6892	22.133
118.63435	4.8338	24.543
133.48457	4.9745	26.834
148.36829	5.1123	29.022

Sample: Sample_4
Operator: ZS
Submitter: Masoud Kavosh Bedford Uni.
File: C:\...\003-50~1\003-870.SMP

Started: 16/12/2011 13:08:24PM
Completed: 16/12/2011 18:12:49PM
Report Time: 19/12/2011 14:57:00PM
Warm Free Space: 8.4430 cm³ Measured
Equilibration Interval: 5 s
Sample Density: 1.000 g/cm³

Analysis Adsorptive: N2
Analysis Bath Temp.: -195.800 °C
Sample Mass: 0.5431 g
Cold Free Space: 25.7302 cm³ Measured
Low Pressure Dose: None
Automatic Degas: No

Langmuir Surface Area Plot

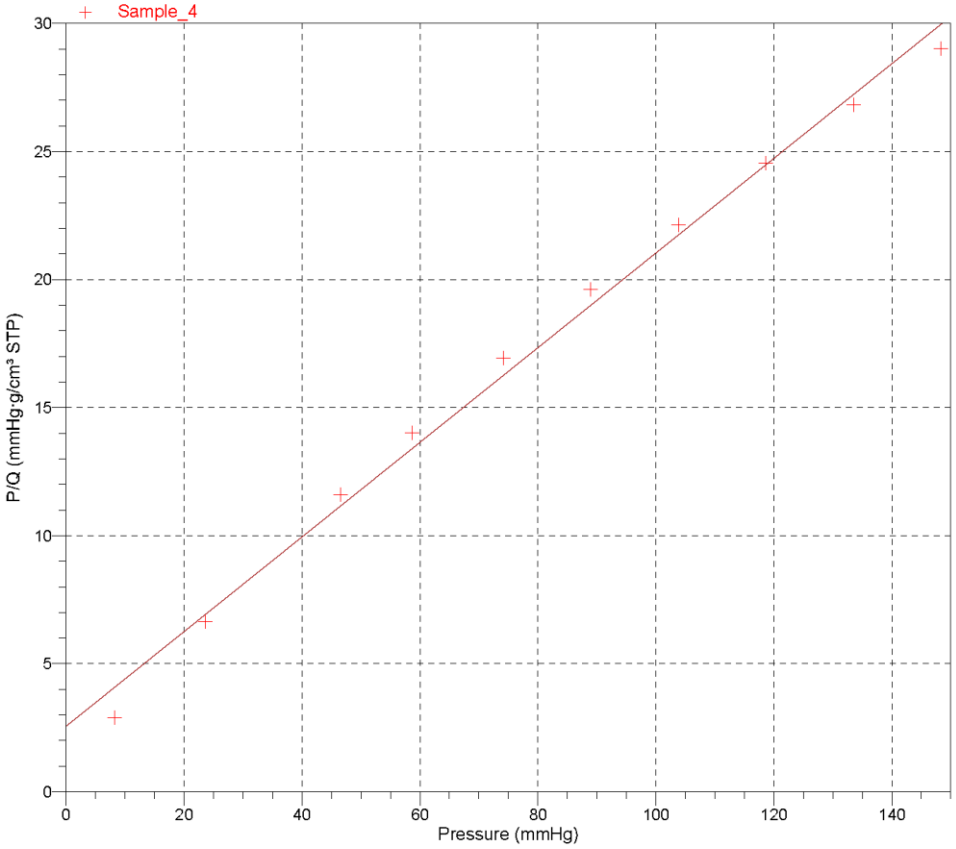

Sample: Sample_4
Operator: ZS
Submitter: Masoud Kavosh Bedford Uni.
File: C:\...\003-50~1\003-870.SMP

Started: 16/12/2011 13:08:24PM
Completed: 16/12/2011 18:12:49PM
Report Time: 19/12/2011 14:57:00PM
Warm Free Space: 8.4430 cm³ Measured
Equilibration Interval: 5 s
Sample Density: 1.000 g/cm³

Analysis Adsorptive: N2
Analysis Bath Temp.: -195.800 °C
Sample Mass: 0.5431 g
Cold Free Space: 25.7302 cm³ Measured
Low Pressure Dose: None
Automatic Degas: No

t-Plot Report

Micropore Volume: 0.000657 cm³/g STP
Micropore Area: 1.6866 m²/g
External Surface Area: 16.6220 m²/g
Slope: 10.746035 ± 0.035160 cm³/g·nm STP
Y-Intercept: 0.424676 ± 0.014269 cm³/g STP
Correlation Coefficient: 0.999968
Surface Area Correction Factor: 1.000
Density Conversion Factor: 0.0015468
Total Surface Area (BET): 18.3086 m²/g
Thickness Range: 0.35000 nm to 0.50000 nm
Thickness Equation: Harkins and Jura

$$t = [\ 13.99 / (\ 0.034 - \log(P/Po)\ )\ ]\ ^{\wedge}\ 0.5$$

Relative Pressure (P/Po)	Statistical Thickness (nm)	Quantity Adsorbed (cm³/g STP)
0.011064954	0.26514	2.8507
0.031770494	0.30219	3.5466
0.062678453	0.33631	4.0149
0.078870142	0.35076	4.1875
0.099639050	0.36755	4.3767
0.119574429	0.38247	4.5379
0.139453674	0.39657	4.6892
0.159367967	0.41016	4.8338
0.179294693	0.42339	4.9745
0.199236564	0.43639	5.1123
0.246730304	0.46689	5.4400
0.298891147	0.50050	5.8098
0.349004093	0.53370	6.1843
0.396862927	0.56687	6.5664
0.446179880	0.60321	6.9936
0.495449831	0.64240	7.4692
0.544493225	0.68517	8.0225
0.593432689	0.73265	8.6830
0.642189832	0.78620	9.4925

Sample: Sample_4
Operator: ZS
Submitter: Masoud Kavosh Bedford Uni.
File: C:\...\003-50~1\003-870.SMP

Started: 16/12/2011 13:08:24PM
Completed: 16/12/2011 18:12:49PM
Report Time: 19/12/2011 14:57:00PM
Warm Free Space: 8.4430 cm³ Measured
Equilibration Interval: 5 s
Sample Density: 1.000 g/cm³

Analysis Adsorptive: N2
Analysis Bath Temp.: -195.800 °C
Sample Mass: 0.5431 g
Cold Free Space: 25.7302 cm³ Measured
Low Pressure Dose: None
Automatic Degas: No

t-Plot

Harkins and Jura

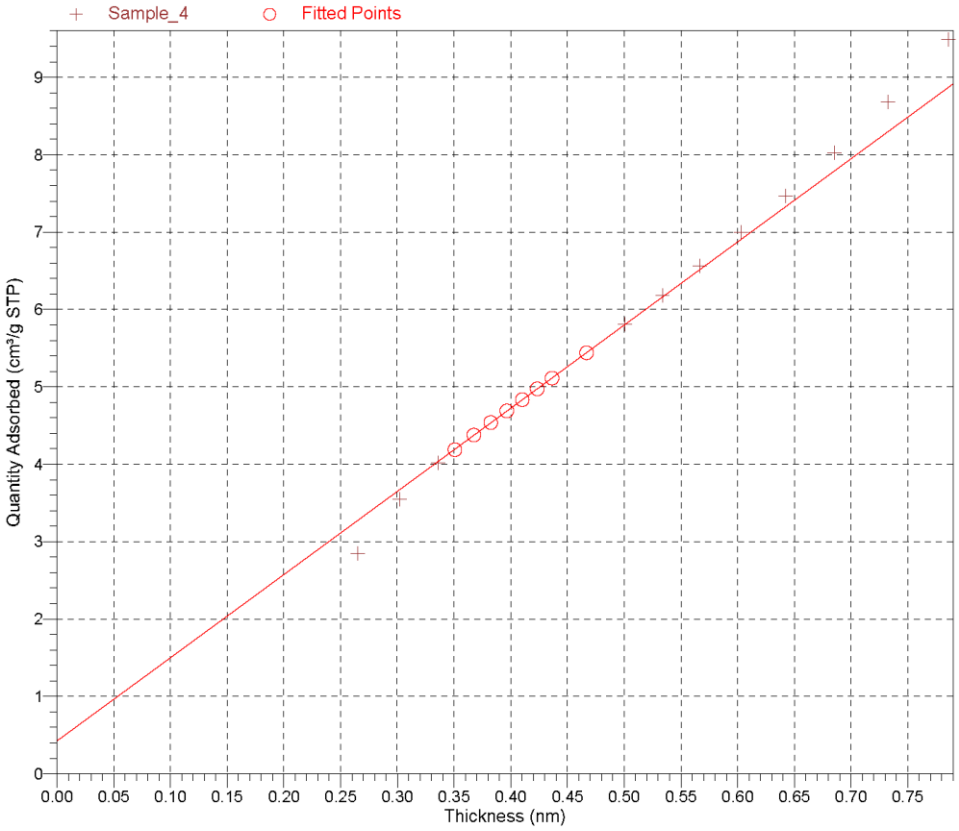

Sample: Sample_4
Operator: ZS
Submitter: Masoud Kavosh Bedford Uni.
File: C:\...\003-50~1\003-870.SMP

Started: 16/12/2011 13:08:24PM
Completed: 16/12/2011 18:12:49PM
Report Time: 19/12/2011 14:57:00PM
Warm Free Space: 8.4430 cm³ Measured
Equilibration Interval: 5 s
Sample Density: 1.000 g/cm³

Analysis Adsorptive: N2
Analysis Bath Temp.: -195.800 °C
Sample Mass: 0.5431 g
Cold Free Space: 25.7302 cm³ Measured
Low Pressure Dose: None
Automatic Degas: No

BJH Adsorption Pore Distribution Report

t = 3.54 [-5 / ln(P/Po)] ^ 0.333

Diameter Range: 1.7000 nm to 300.0000 nm
Adsorbate Property Factor: 0.95300 nm
Density Conversion Factor: 0.0015468
Fraction of Pores Open at Both Ends: 0.00

Pore Diameter Range (nm)	Average Diameter (nm)	Incremental Pore Volume (cm³/g)	Cumulative Pore Volume (cm³/g)	Incremental Pore Area (m²/g)	Cumulative Pore Area (m²/g)
240.6 - 238.2	239.4	0.002727	0.002727	0.046	0.046
238.2 - 51.0	58.6	0.016483	0.019210	1.125	1.170
51.0 - 46.4	48.5	0.004424	0.023634	0.365	1.535
46.4 - 32.6	37.0	0.017502	0.041136	1.891	3.426
32.6 - 22.4	25.6	0.012319	0.053454	1.927	5.354
22.4 - 18.8	20.2	0.004468	0.057922	0.883	6.237
18.8 - 14.9	16.3	0.005009	0.062931	1.226	7.463
14.9 - 12.8	13.7	0.002802	0.065734	0.818	8.281
12.8 - 11.1	11.8	0.002576	0.068310	0.871	9.152
11.1 - 10.1	10.6	0.001612	0.069922	0.610	9.762
10.1 - 7.9	8.7	0.003794	0.073716	1.737	11.499
7.9 - 6.7	7.2	0.002363	0.076079	1.316	12.815
6.7 - 5.7	6.1	0.001747	0.077826	1.141	13.956
5.7 - 5.0	5.3	0.001301	0.079127	0.980	14.936
5.0 - 4.4	4.7	0.000994	0.080121	0.853	15.789
4.4 - 3.9	4.1	0.000768	0.080889	0.744	16.532
3.9 - 3.5	3.7	0.000598	0.081487	0.649	17.181
3.5 - 3.2	3.3	0.000499	0.081986	0.604	17.785
3.2 - 2.8	3.0	0.000415	0.082401	0.557	18.342
2.8 - 2.6	2.7	0.000369	0.082770	0.550	18.892
2.6 - 2.3	2.4	0.000314	0.083084	0.522	19.414
2.3 - 2.1	2.2	0.000224	0.083308	0.415	19.829
2.1 - 2.0	2.0	0.000077	0.083385	0.153	19.981
2.0 - 1.9	1.9	0.000074	0.083459	0.154	20.136
1.9 - 1.8	1.8	0.000069	0.083527	0.150	20.286

Sample: Sample_4
Operator: ZS
Submitter: Masoud Kavosh Bedford Uni.
File: C:\...\003-50~1\003-870.SMP

Started: 16/12/2011 13:08:24PM
Completed: 16/12/2011 18:12:49PM
Report Time: 19/12/2011 14:57:00PM
Warm Free Space: 8.4430 cm³ Measured
Equilibration Interval: 5 s
Sample Density: 1.000 g/cm³

Analysis Adsorptive: N2
Analysis Bath Temp.: -195.800 °C
Sample Mass: 0.5431 g
Cold Free Space: 25.7302 cm³ Measured
Low Pressure Dose: None
Automatic Degas: No

BJH Adsorption Cumulative Pore Volume

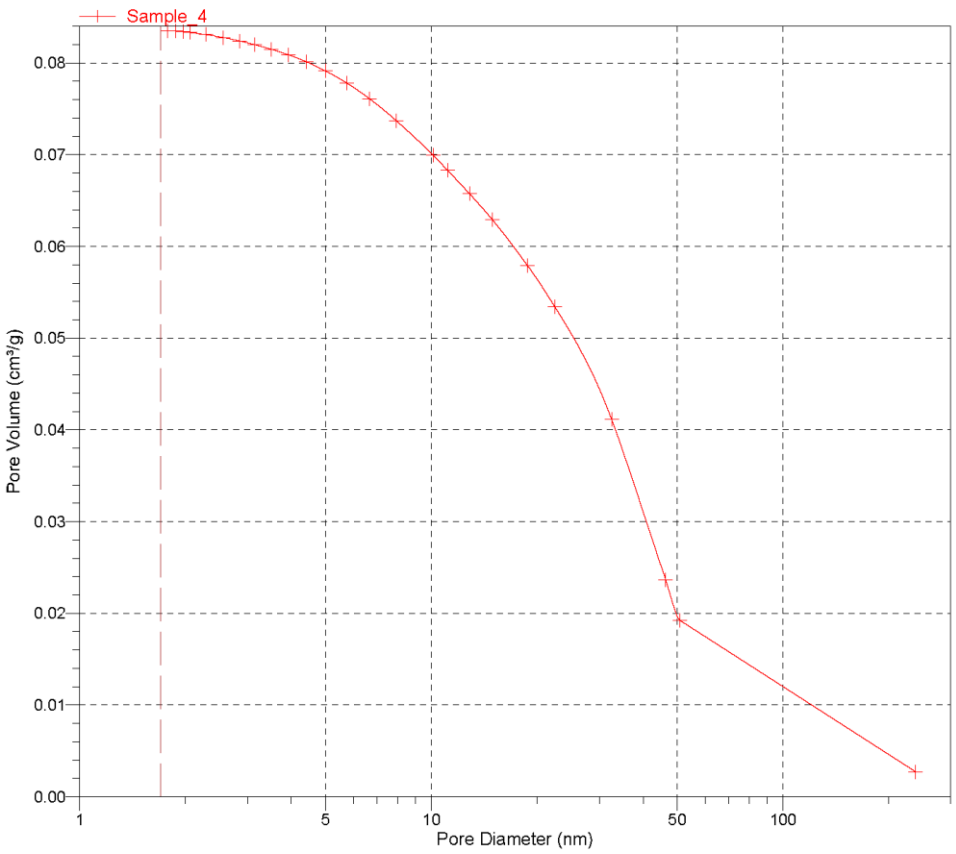

Sample: Sample_4
Operator: ZS
Submitter: Masoud Kavosh Bedford Uni.
File: C:\...\003-50~1\003-870.SMP

Started: 16/12/2011 13:08:24PM
Completed: 16/12/2011 18:12:49PM
Report Time: 19/12/2011 14:57:00PM
Warm Free Space: 8.4430 cm³ Measured
Equilibration Interval: 5 s
Sample Density: 1.000 g/cm³

Analysis Adsorptive: N2
Analysis Bath Temp.: -195.800 °C
Sample Mass: 0.5431 g
Cold Free Space: 25.7302 cm³ Measured
Low Pressure Dose: None
Automatic Degas: No

BJH Adsorption dV/dD Pore Volume

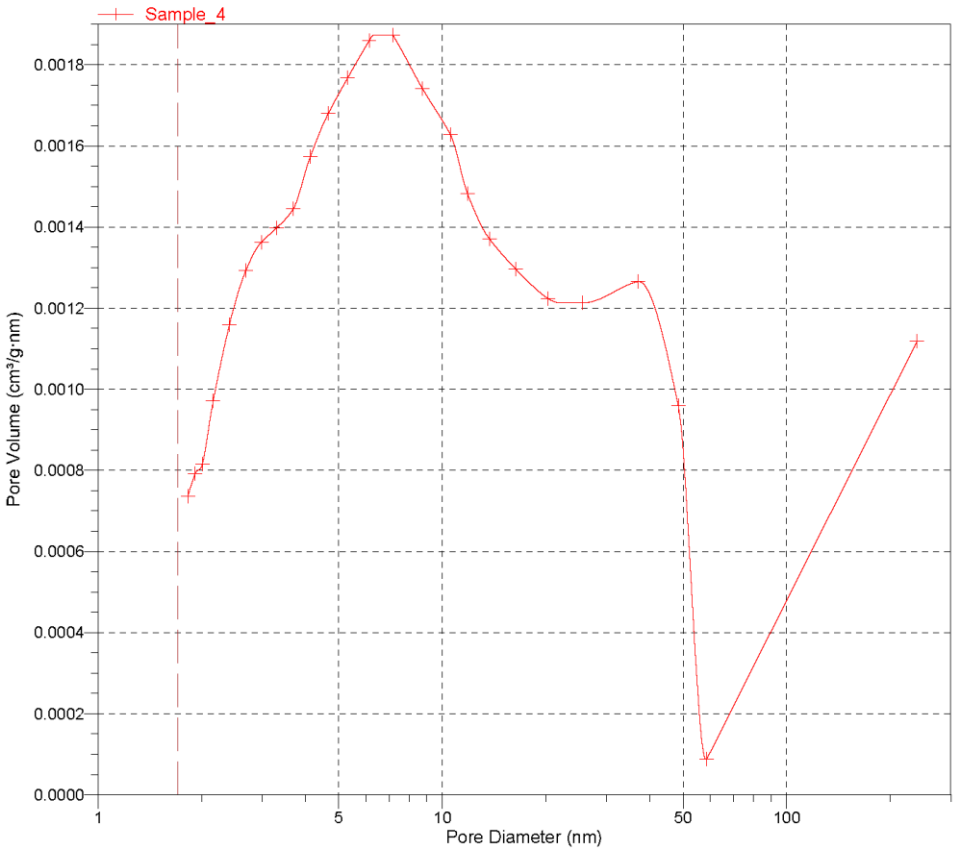

Sample: Sample_4
Operator: ZS
Submitter: Masoud Kavosh Bedford Uni.
File: C:\...\003-50~1\003-870.SMP

Started: 16/12/2011 13:08:24PM
Completed: 16/12/2011 18:12:49PM
Report Time: 19/12/2011 14:57:00PM
Warm Free Space: 8.4430 cm³ Measured
Equilibration Interval: 5 s
Sample Density: 1.000 g/cm³

Analysis Adsorptive: N2
Analysis Bath Temp.: -195.800 °C
Sample Mass: 0.5431 g
Cold Free Space: 25.7302 cm³ Measured
Low Pressure Dose: None
Automatic Degas: No

BJH Adsorption dV/dlog(D) Pore Volume

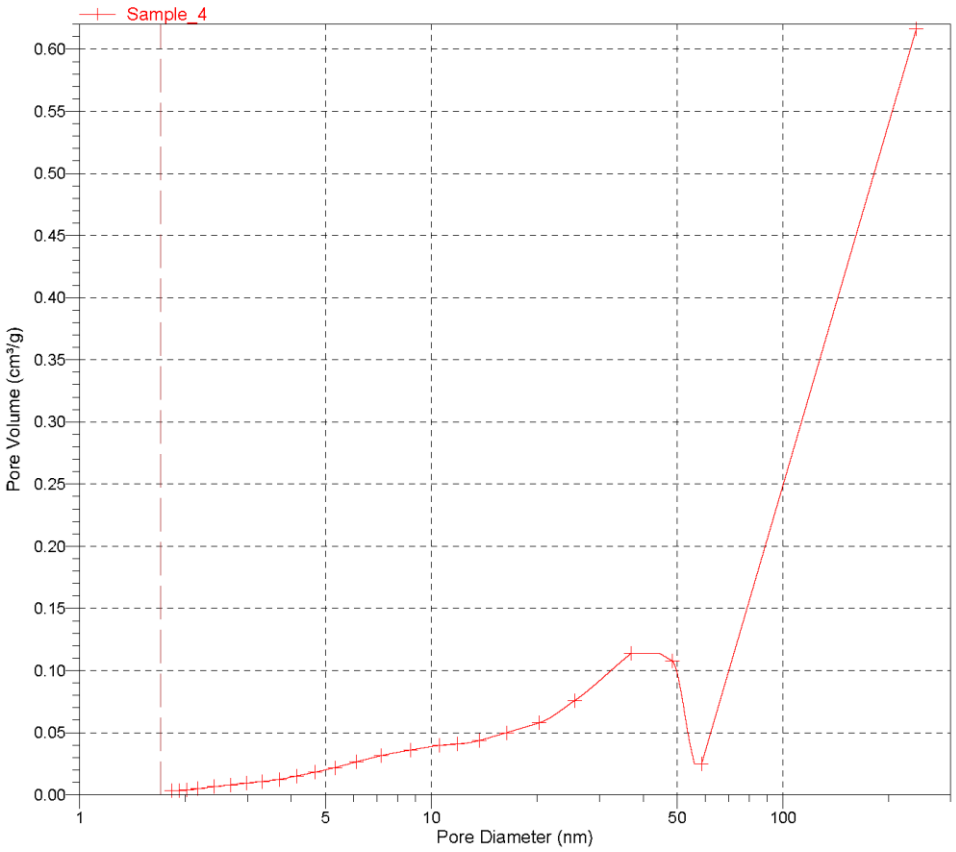

Sample: Sample_4
Operator: ZS
Submitter: Masoud Kavosh Bedford Uni.
File: C:\...\003-50~1\003-870.SMP

Started:	16/12/2011 13:08:24PM	Analysis Adsorptive:	N2
Completed:	16/12/2011 18:12:49PM	Analysis Bath Temp.:	-195.800 °C
Report Time:	19/12/2011 14:57:00PM	Sample Mass:	0.5431 g
Warm Free Space:	8.4430 cm³ Measured	Cold Free Space:	25.7302 cm³ Measured
Equilibration Interval:	5 s	Low Pressure Dose:	None
Sample Density:	1.000 g/cm³	Automatic Degas:	No

BJH Adsorption Cumulative Pore Area

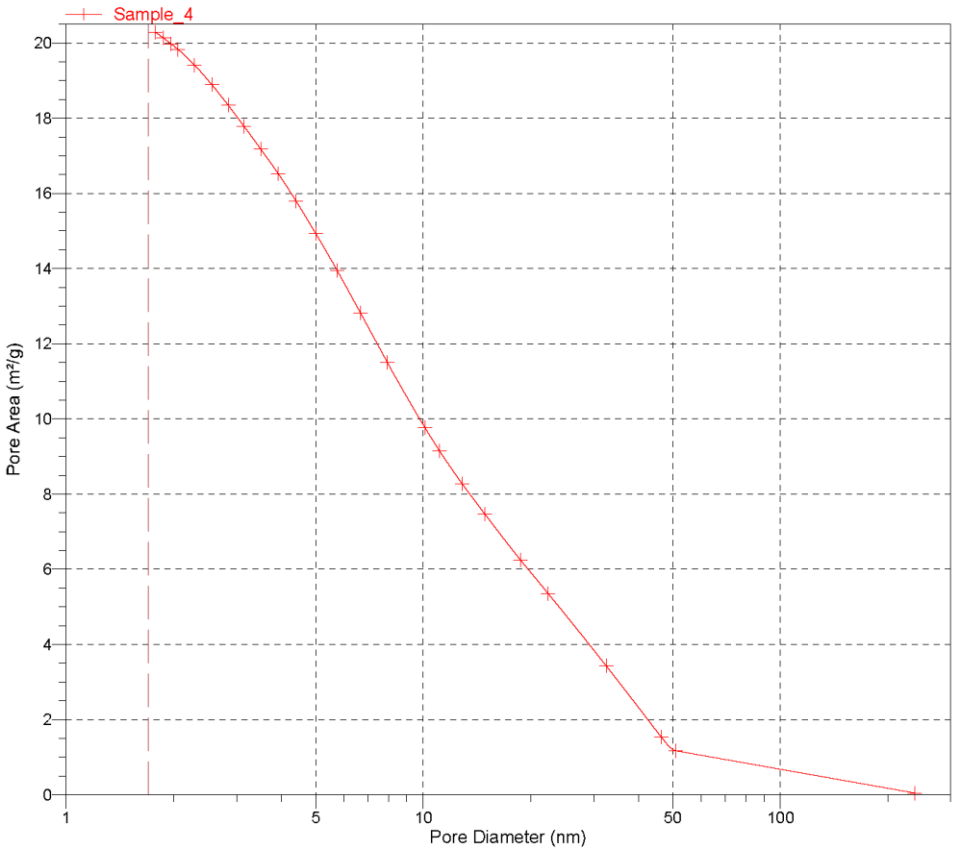

Sample: Sample_4
Operator: ZS
Submitter: Masoud Kavosh Bedford Uni.
File: C:\...\003-50~1\003-870.SMP

Started: 16/12/2011 13:08:24PM
Completed: 16/12/2011 18:12:49PM
Report Time: 19/12/2011 14:57:00PM
Warm Free Space: 8.4430 cm³ Measured
Equilibration Interval: 5 s
Sample Density: 1.000 g/cm³

Analysis Adsorptive: N2
Analysis Bath Temp.: -195.800 °C
Sample Mass: 0.5431 g
Cold Free Space: 25.7302 cm³ Measured
Low Pressure Dose: None
Automatic Degas: No

BJH Adsorption dA/dD Pore Area

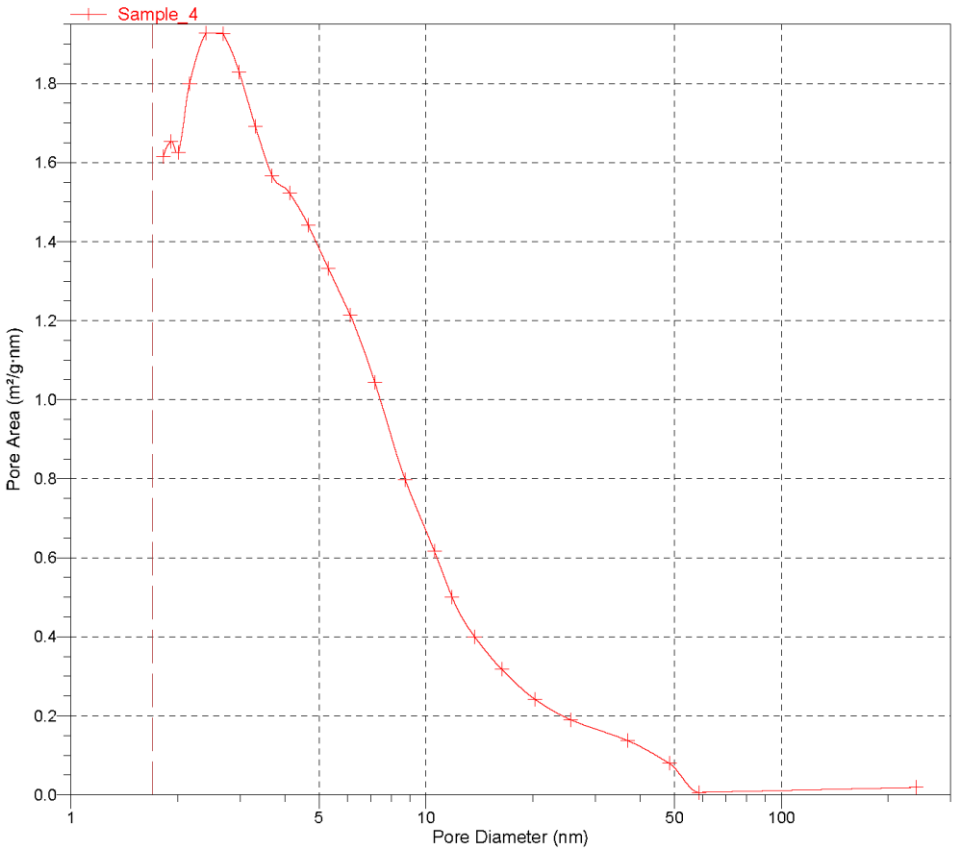

Sample: Sample_4
Operator: ZS
Submitter: Masoud Kavosh Bedford Uni.
File: C:\...\003-50~1\003-870.SMP

Started:	16/12/2011 13:08:24PM	Analysis Adsorptive:	N2
Completed:	16/12/2011 18:12:49PM	Analysis Bath Temp.:	-195.800 °C
Report Time:	19/12/2011 14:57:00PM	Sample Mass:	0.5431 g
Warm Free Space:	8.4430 cm³ Measured	Cold Free Space:	25.7302 cm³ Measured
Equilibration Interval:	5 s	Low Pressure Dose:	None
Sample Density:	1.000 g/cm³	Automatic Degas:	No

BJH Adsorption dA/dlog(D) Pore Area

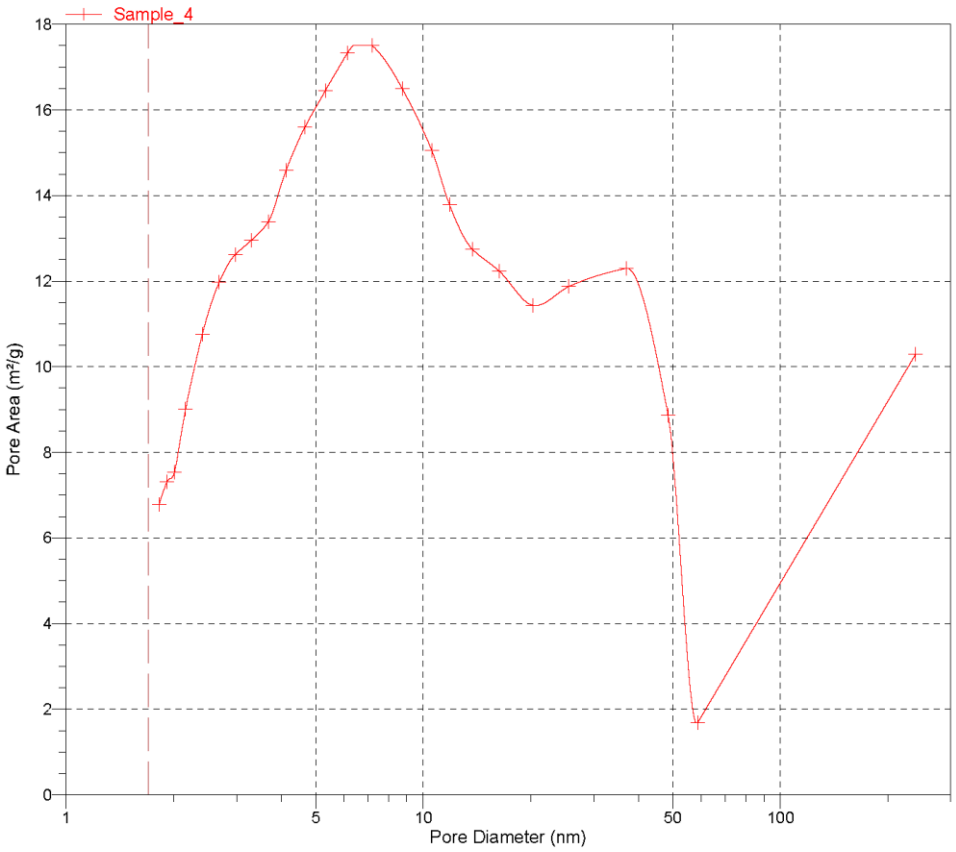

Sample: Sample_4
Operator: ZS
Submitter: Masoud Kavosh Bedford Uni.
File: C:\...\003-50~1\003-870.SMP

Started: 16/12/2011 13:08:24PM
Completed: 16/12/2011 18:12:49PM
Report Time: 19/12/2011 14:57:00PM
Warm Free Space: 8.4430 cm³ Measured
Equilibration Interval: 5 s
Sample Density: 1.000 g/cm³

Analysis Adsorptive: N2
Analysis Bath Temp.: -195.800 °C
Sample Mass: 0.5431 g
Cold Free Space: 25.7302 cm³ Measured
Low Pressure Dose: None
Automatic Degas: No

BJH Desorption Pore Distribution Report

t = 3.54 [-5 / ln(P/Po)] ^ 0.333

Diameter Range: 1.7000 nm to 300.0000 nm
Adsorbate Property Factor: 0.95300 nm
Density Conversion Factor: 0.0015468
Fraction of Pores Open at Both Ends: 0.00

Pore Diameter Range (nm)	Average Diameter (nm)	Incremental Pore Volume (cm³/g)	Cumulative Pore Volume (cm³/g)	Incremental Pore Area (m²/g)	Cumulative Pore Area (m²/g)
240.4 - 75.1	89.2	0.000655	0.000655	0.029	0.029
75.1 - 44.7	52.5	0.008183	0.008839	0.624	0.653
44.7 - 28.0	32.5	0.022610	0.031449	2.780	3.433
28.0 - 20.7	23.2	0.015749	0.047198	2.714	6.148
20.7 - 15.8	17.5	0.008996	0.056194	2.052	8.199
15.8 - 13.3	14.3	0.004352	0.060546	1.216	9.416
13.3 - 11.3	12.1	0.003385	0.063932	1.118	10.534
11.3 - 9.8	10.4	0.002689	0.066621	1.034	11.568
9.8 - 8.3	8.9	0.002778	0.069399	1.252	12.821
8.3 - 6.7	7.3	0.003166	0.072565	1.736	14.557
6.7 - 5.4	5.9	0.002825	0.075391	1.907	16.464
5.4 - 5.0	5.2	0.001212	0.076603	0.938	17.401
5.0 - 4.3	4.6	0.001674	0.078277	1.462	18.863
4.3 - 3.8	4.0	0.001422	0.079699	1.419	20.282
3.8 - 3.4	3.6	0.002859	0.082559	3.221	23.504
3.4 - 3.0	3.2	0.000722	0.083281	0.914	24.418
3.0 - 2.6	2.8	0.000110	0.083391	0.160	24.578
2.6 - 2.4	2.5	0.000001	0.083392	0.001	24.579

Sample: Sample_4
Operator: ZS
Submitter: Masoud Kavosh Bedford Uni.
File: C:\...\003-50~1\003-870.SMP

Started:	16/12/2011 13:08:24PM	Analysis Adsorptive:	N2
Completed:	16/12/2011 18:12:49PM	Analysis Bath Temp.:	-195.800 °C
Report Time:	19/12/2011 14:57:00PM	Sample Mass:	0.5431 g
Warm Free Space:	8.4430 cm³ Measured	Cold Free Space:	25.7302 cm³ Measured
Equilibration Interval:	5 s	Low Pressure Dose:	None
Sample Density:	1.000 g/cm³	Automatic Degas:	No

BJH Desorption Cumulative Pore Volume

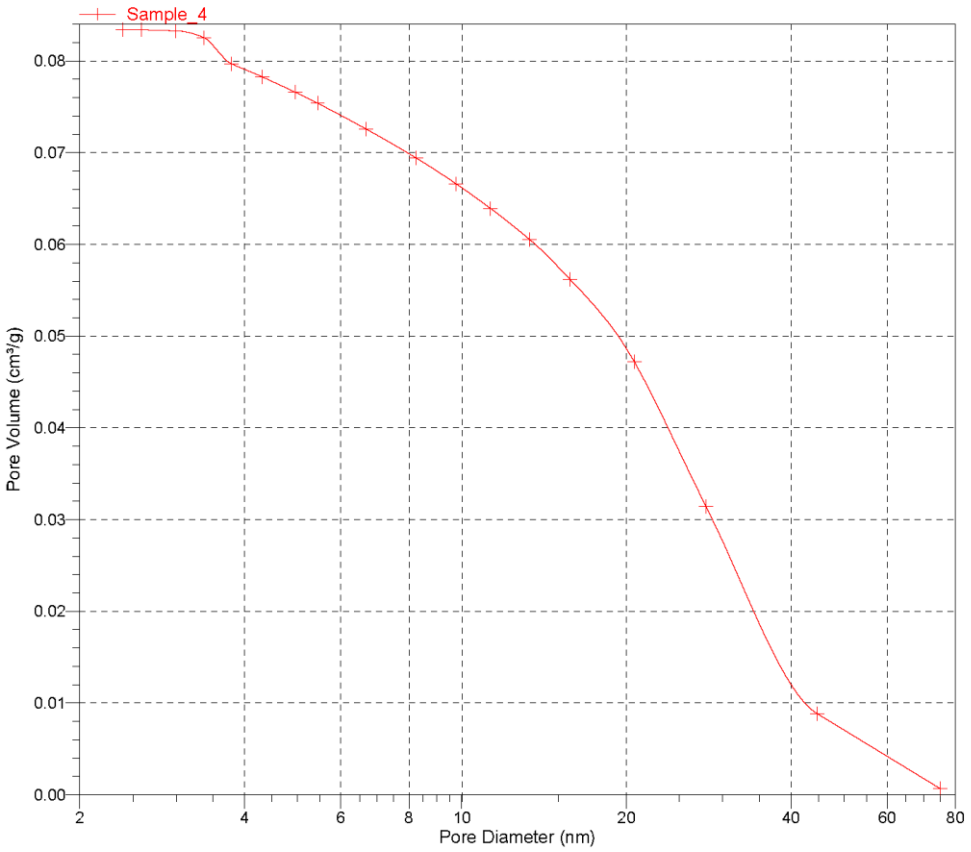

Sample: Sample_4
Operator: ZS
Submitter: Masoud Kavosh Bedford Uni.
File: C:\...\003-50~1\003-870.SMP

Started: 16/12/2011 13:08:24PM
Completed: 16/12/2011 18:12:49PM
Report Time: 19/12/2011 14:57:00PM
Warm Free Space: 8.4430 cm³ Measured
Equilibration Interval: 5 s
Sample Density: 1.000 g/cm³

Analysis Adsorptive: N2
Analysis Bath Temp.: -195.800 °C
Sample Mass: 0.5431 g
Cold Free Space: 25.7302 cm³ Measured
Low Pressure Dose: None
Automatic Degas: No

BJH Desorption dV/dD Pore Volume

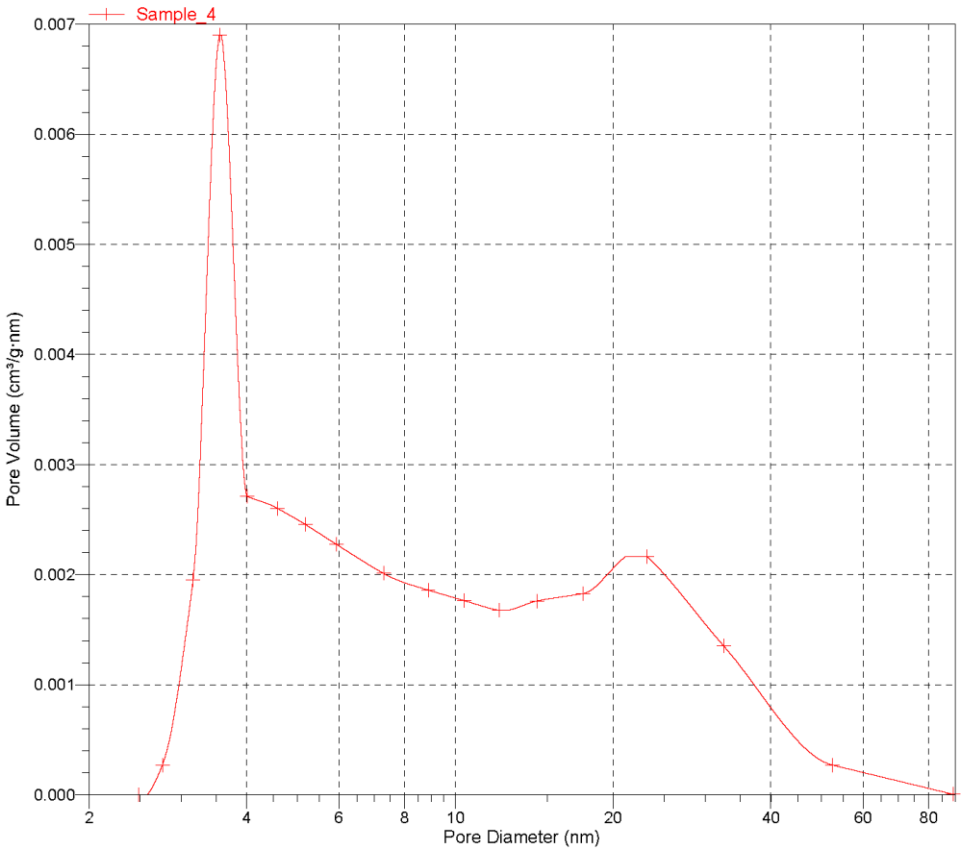

Sample: Sample_4
Operator: ZS
Submitter: Masoud Kavosh Bedford Uni.
File: C:\...\003-50~1\003-870.SMP

Started: 16/12/2011 13:08:24PM
Completed: 16/12/2011 18:12:49PM
Report Time: 19/12/2011 14:57:00PM
Warm Free Space: 8.4430 cm³ Measured
Equilibration Interval: 5 s
Sample Density: 1.000 g/cm³

Analysis Adsorptive: N2
Analysis Bath Temp.: -195.800 °C
Sample Mass: 0.5431 g
Cold Free Space: 25.7302 cm³ Measured
Low Pressure Dose: None
Automatic Degas: No

BJH Desorption dV/dlog(D) Pore Volume

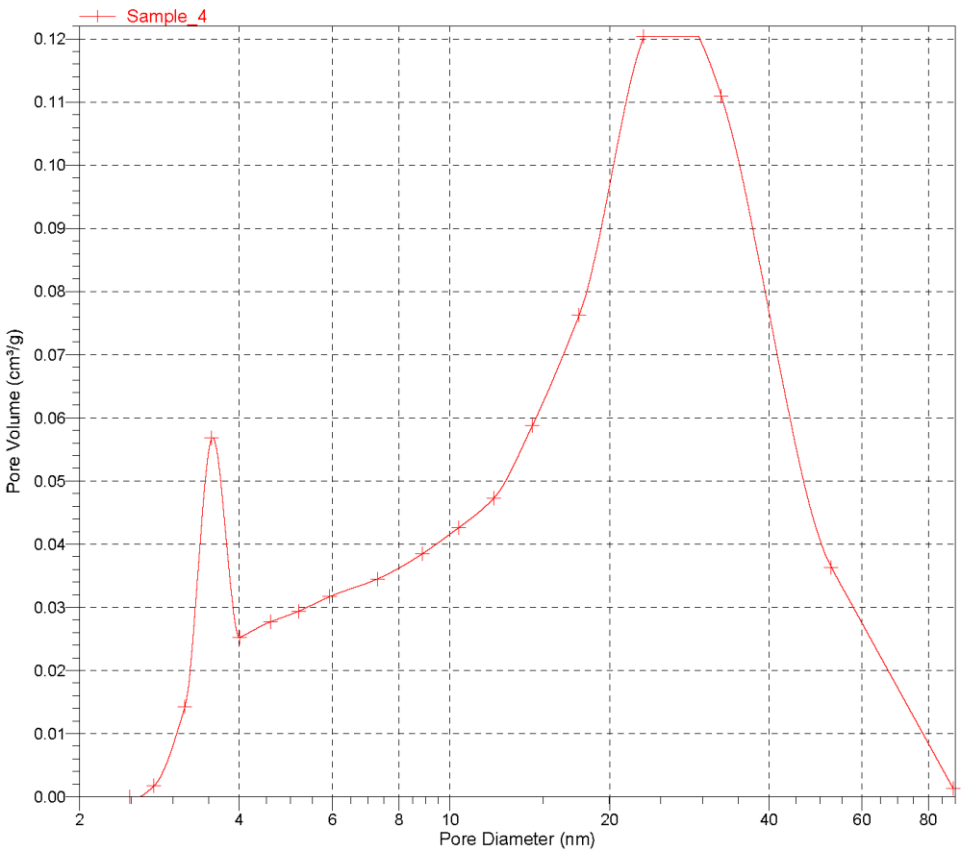

Sample: Sample_4
Operator: ZS
Submitter: Masoud Kavosh Bedford Uni.
File: C:\...\003-50~1\003-870.SMP

Started: 16/12/2011 13:08:24PM
Completed: 16/12/2011 18:12:49PM
Report Time: 19/12/2011 14:57:00PM
Warm Free Space: 8.4430 cm³ Measured
Equilibration Interval: 5 s
Sample Density: 1.000 g/cm³

Analysis Adsorptive: N2
Analysis Bath Temp.: -195.800 °C
Sample Mass: 0.5431 g
Cold Free Space: 25.7302 cm³ Measured
Low Pressure Dose: None
Automatic Degas: No

BJH Desorption Cumulative Pore Area

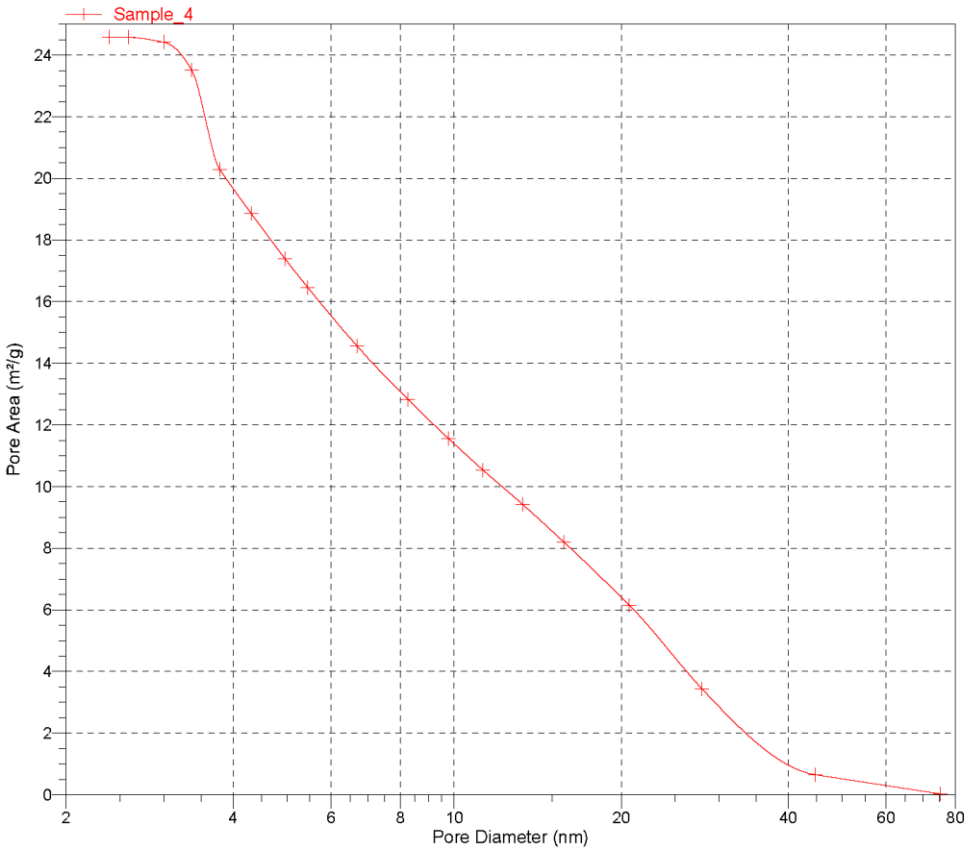

Sample: Sample_4
Operator: ZS
Submitter: Masoud Kavosh Bedford Uni.
File: C:\...\003-50~1\003-870.SMP

Started:	16/12/2011 13:08:24PM	Analysis Adsorptive:	N2
Completed:	16/12/2011 18:12:49PM	Analysis Bath Temp.:	-195.800 °C
Report Time:	19/12/2011 14:57:00PM	Sample Mass:	0.5431 g
Warm Free Space:	8.4430 cm³ Measured	Cold Free Space:	25.7302 cm³ Measured
Equilibration Interval:	5 s	Low Pressure Dose:	None
Sample Density:	1.000 g/cm³	Automatic Degas:	No

BJH Desorption dA/dD Pore Area

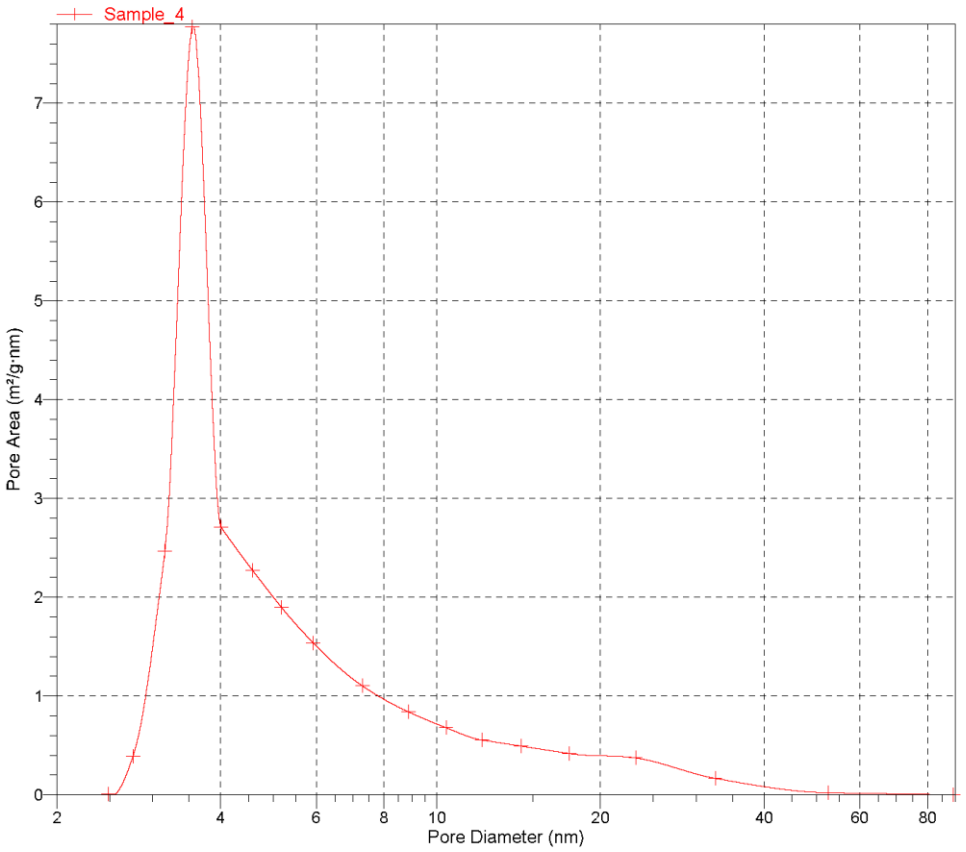

Sample: Sample_4
Operator: ZS
Submitter: Masoud Kavosh Bedford Uni.
File: C:\...\003-50~1\003-870.SMP

Started: 16/12/2011 13:08:24PM
Completed: 16/12/2011 18:12:49PM
Report Time: 19/12/2011 14:57:01PM
Warm Free Space: 8.4430 cm³ Measured
Equilibration Interval: 5 s
Sample Density: 1.000 g/cm³

Analysis Adsorptive: N2
Analysis Bath Temp.: -195.800 °C
Sample Mass: 0.5431 g
Cold Free Space: 25.7302 cm³ Measured
Low Pressure Dose: None
Automatic Degas: No

BJH Desorption dA/dlog(D) Pore Area

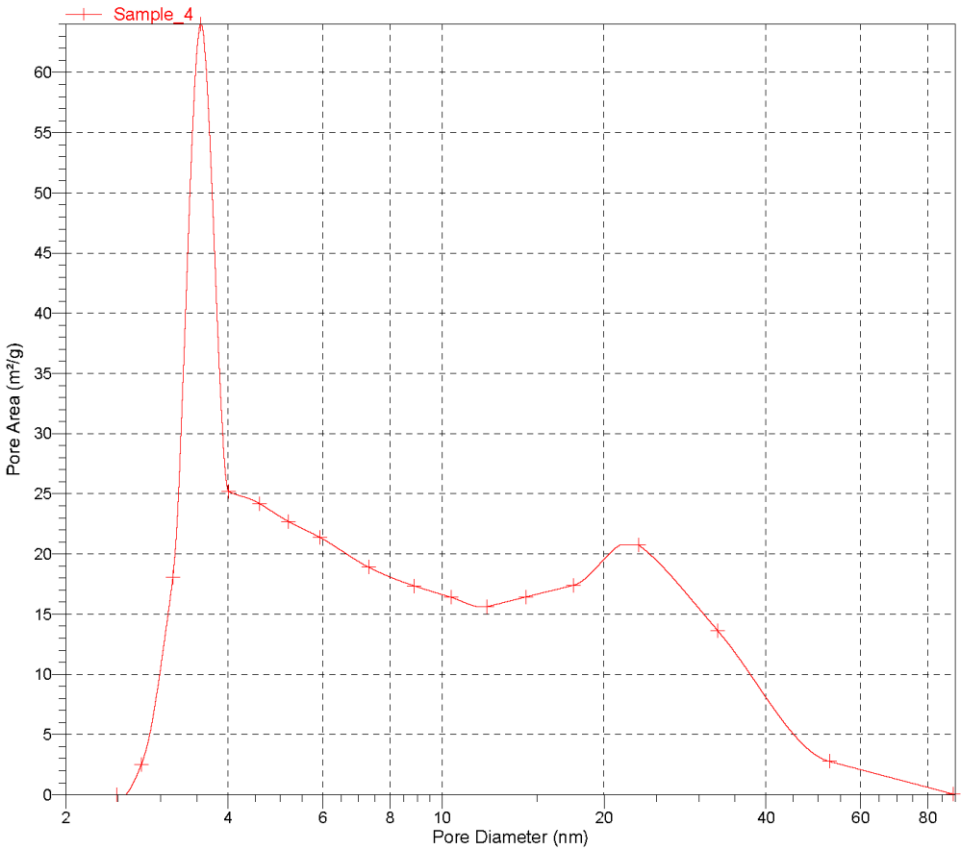

Sample: Sample_4
Operator: ZS
Submitter: Masoud Kavosh Bedford Uni.
File: C:\...\003-50~1\003-870.SMP

Started:	16/12/2011 13:08:24PM	Analysis Adsorptive:	N2
Completed:	16/12/2011 18:12:49PM	Analysis Bath Temp.:	-195.800 °C
Report Time:	19/12/2011 14:57:01PM	Sample Mass:	0.5431 g
Warm Free Space:	8.4430 cm³ Measured	Cold Free Space:	25.7302 cm³ Measured
Equilibration Interval:	5 s	Low Pressure Dose:	None
Sample Density:	1.000 g/cm³	Automatic Degas:	No

Options Report

Sample Tube

Sample Tube: Sample Tube3
Stem Diameter: 1/2 inch
Physical volume below mark: 1.0000 cm³
Use Isothermal Jacket: Yes
Use Filler Rod: Yes

Analysis Conditions

Preparation

Fast evacuation: Yes
Evacuation time: 0.10 h
Leak test: No

Free Space

Free-space type: Measured
Lower dewar for evacuation: No
Evacuation time: 0.10 h
Outgas test: No

Po and Temperature

Po and T type: Measure Po at intervals during analysis. Enter the Analysis Bath Temperature below.
Po and T type: Measure Po at intervals during analysis. Enter the Analysis Bath Temperature below.
Temperature: -195.800 °C
Measurement interval: 120 min

Dosing

Use first pressure fixed dose: No
Use maximum volume increment: No
Target tolerance: 5.0% or 5.000 mmHg

Equilibration

Equilibration interval: 5 s
Minimum equilibration delay at P/Po >= 0.995: 600 s

Adsorptive Properties

Adsorptive: Nitrogen
Maximum manifold pressure: 1050.00 mmHg
Non-ideality factor: 0.0000620
Density conversion factor: 0.0015468
Molecular cross-sectional area: 0.162 nm²

Sample: Sample_4
Operator: ZS
Submitter: Masoud Kavosh Bedford Uni.
File: C:\...\003-50~1\003-870.SMP

Started:	16/12/2011 13:08:24PM	Analysis Adsorptive:	N2
Completed:	16/12/2011 18:12:49PM	Analysis Bath Temp.:	-195.800 °C
Report Time:	19/12/2011 14:57:01PM	Sample Mass:	0.5431 g
Warm Free Space:	8.4430 cm³ Measured	Cold Free Space:	25.7302 cm³ Measured
Equilibration Interval:	5 s	Low Pressure Dose:	None
Sample Density:	1.000 g/cm³	Automatic Degas:	No

Summary Report

Surface Area

Single point surface area at P/Po = 0.199236564:	17.8210 m²/g
BET Surface Area:	18.3086 m²/g
Langmuir Surface Area:	23.5571 m²/g
t-Plot Micropore Area:	1.6866 m²/g
t-Plot External Surface Area:	16.6220 m²/g
BJH Adsorption cumulative surface area of pores between 1.7000 nm and 300.0000 nm diameter:	20.2861 m²/g
BJH Desorption cumulative surface area of pores between 1.7000 nm and 300.0000 nm diameter:	24.5787 m²/g

Pore Volume

Single point adsorption total pore volume of pores less than 46.5439 nm diameter at P/Po = 0.956765445:	0.061838 cm³/g
t-Plot micropore volume:	0.000657 cm³/g
BJH Adsorption cumulative volume of pores between 1.7000 nm and 300.0000 nm diameter:	0.083527 cm³/g
BJH Desorption cumulative volume of pores between 1.7000 nm and 300.0000 nm diameter:	0.083392 cm³/g

Pore Size

Adsorption average pore width (4V/A by BET):	13.51007 nm
BJH Adsorption average pore diameter (4V/A):	16.4699 nm
BJH Desorption average pore diameter (4V/A):	13.5714 nm

APPENDIX D

Thermodynamic equilibrium partial pressure of CO_2 during calcination-carbonation of limestone

Chemical reactions are in the form of: Reactants ⟶ Products. Reactants are those components which decrease in quantity during reaction, while products are those increase in quantity.

Chemical equilibrium is an state (temperature and pressure) in the reactor that rates of the forward and the reverse are equal. Therefore, equilibrium is macroscopicaly static, but is microscopicaly dynamic (no change in quantity is obsereved, but exists and equal).

In a reversible reaction as $\Sigma \nu_i R_i \leftrightarrow \Sigma \nu_i P_i$, according to the law of mass action, the rate of forward and reverse reactions are defined as $K_f \prod_i [Products]^{\nu_i}$ and $K_r \prod_i [Reactants]^{\nu_i}$, respectively. K_f and K_r denote the rate constants for the forward and the reverse reaction, respectively. The reaction quotient is also expressed by the ratio as $Q = \frac{\prod_i [Products]^{\nu_i}}{\prod_i [Reactants]^{\nu_i}}$. At equilibrium, the rates of both reactions are equal. Therefore, at equilibrium:

$$K_f \prod_i [Products]^{\nu_i} = K_r \prod_i [Reactants]^{\nu_i}$$

$$\frac{K_f}{K_r} = \frac{\prod_i [Products]^{\nu_i}}{\prod_i [Reactants]^{\nu_i}} = Q$$

The equilibrium constant, K, is expressed as $\frac{K_f}{K_r}$. Therefore, K is the special value that Q has when the reaction is at equilibrium. The terms [Products] and [Reactants] can show either partial pressure or concentration of each species; hence equilibrium constant can be denoted as K_p or K_c.

The values of K_p (or Q_p) at different temperatures, in chapter 3, were computed from [148]

$$ln\frac{K_p(T_i)}{K_p(T_0)} = \frac{\Delta a}{R}\, ln\frac{T_i}{T_o} + \frac{\Delta b}{2R}(T_i - T_0) + \frac{\Delta c}{6R}(T_i^2 - T_0^2) + \frac{\Delta d}{12R}(T_i^3 - T_0^3) + \frac{\Delta e}{2R}(T_i^{-2} - T_0^{-2}) + \frac{1}{R}\left[-\Delta H^0_{reac}(T_0) + \Delta a T_0 + \frac{\Delta b}{2}T_0^2 + \frac{\Delta c}{3}T_0^3 + \frac{\Delta d}{4}T_0^4 - \frac{\Delta e}{T_0}\right] X \left[\frac{1}{T_i} - \frac{1}{T_0}\right]$$

Here ΔH^0_{reac} shows the standard state heat of reaction at 25°C and 1 bar. $\Delta a = \Sigma \nu_i a_i$, $\Delta b = \Sigma \nu_i b_i$ and so on, where ν_i are stoichiometric coefficients and a_i, b_i, c_i, d_i and e_i are the

coefficients in the calculation of constant-pressure heat capacity of the species i, from the equation

$$C_{P,i} = a_i + b_i T + c_i T^2 + d_i T^3 + e_i T^{-2}$$

The coefficients and calculation for species which are involved in limestone calcination (CaO, CO_2, and $CaCO_3$) are presented in following tables.

	ai	bi*10^2	ci*10^5	di*10^9	ei	ΔH_f^o(kJ/mol)	ΔG_f^o(kJ/mol)
CaO	41.84	2.025	0	0	-451870	-635.1	-604
CO2	22.243	5.977	-3.499	7.464	0	-393.5	-394.4
CaCO3	82.34	4.975	0	0	-1E+06	-1206.9	-1128.8
Δ	-18.257	3.027	-3.499	7.464	835130		
T0	298.15						
ΔH_{T0}^o (J/mol)	178300						
ΔG_{T0}^o (J/mol)	130400						
R (J/molK)	8.314						
Kp(T0)	1.42E-23						

	°K	°C	ln[Kp(Ti)/Kp(T1)]	Kp(Ti)=P_{CO2} (bar)	ΔG_{Ti}^o (kJ/mol)
T0	298.15	25	0	1.424E-23	130.401
	400	126.85	18.29586008	1.2569E-15	114.102
	423.15	150	21.2200731	2.3403E-14	110.418
	523.15	250	30.85649164	3.58355E-10	94.599
	600	326.85	36.05873435	6.51057E-08	82.544
	623.15	350	37.37107221	2.41858E-07	78.930
	723.15	450	42.05980279	2.62936E-05	63.406
	800	526.85	44.85203081	0.000429042	51.573
	823.15	550	45.58857722	0.000896143	48.025
	923.15	650	48.33437328	0.013959234	32.785
	1000	726.85	50.05959133	0.07836358	21.171
	1023.15	750	50.52650806	0.124995285	17.689
	1123.15	850	52.31245022	0.745621552	2.741
	1200	926.85	53.47229338	2.378110006	-8.643
	1223.15	950	53.79133979	3.271839833	-12.054
	1323.15	1050	55.03229664	11.31703725	-26.691
	1400	1126.85	55.85595518	25.78951088	-37.828

References

[1] Yang, H., Xu, Z., Fan, M., Gupta, R., Slimane, R. B., Bland, A. E. and Wright, I. (2008), "Progress in carbon dioxide separation and capture: A review", *Journal of Environmental Sciences*, vol. 20, no. 1, pp. 14-27.

[2] Earth System Research Laboratory (2011), *Trends in Atmospheric Carbon Dioxide,Global Monitoring Division*, available at: E:\Paper-C SET\D15 - ESRL - 2011 - [6] in D11 - Trends in Carbon Dioxide.mht (accessed 12th Nov).

[3] Song, C. (2006), "Global challenges and strategies for control, conversion and utilization of CO2 for sustainable development involving energy, catalysis, adsorption and chemical processing", *Catalysis Today*, vol. 115, no. 1-4, pp. 2-32.

[4] Stewart, C. and Hessami, M. (2005), "A study of methods of carbon dioxide capture and sequestration—the sustainability of a photosynthetic bioreactor approach", *Energy Conversion and Management*, vol. 46, no. 3, pp. 403-420.

[5] Parry, M. L., Canziani, O. F., Palutikof, J. P., van der Linden, P. J. and Hanson, C. E. (2007), *The Fourth Assessment Report of the Intergovernmental Panel on Climate Change*, 4, Cambridge University Press, Cambridge, United Kingdom and New York, NY, USA.

[6] Allison, N. L., Bindoff, R. A., Bindschadler, P. M., Cox, N., de Noblet, M. H., England, J. E. and Francis, N. (2009), *The Copenhagen Diagnosis: Updating the World on the Latest Climate Science*, The University of New South Wales, Sydney, Australia.

[7] International Energy Agency, I. (2011), *CO_2 EMISSIONS FROM FUEL COMBUSTION - Highlights*, , IEA, France.

[8] Rackley, S. A. (2010), *Carbon Capture and Storage*, Elsevier.

[9] *EIA, International Energy Outlook*, (2011), DOE/ELA-0484(2011). http//www.eia.doe.gov/oiaf/ieo/index.html, U.S. Energy Information Administration.

[10] Metz, B., Davidson, O., de Coninck, H., Loos, M. and Meyer, L. (2005), *Special Report on Carbon Dioxide Capture and Storage. In Intergovernmental Panel on Climate Change*, , Cambridge University Press, New York.

[11] Rubin, E. S. (2005), "IPCC Special Report on Carbon Dioxide Capture and and Storage", November 14, 2005, Washington, DC, U.S. Climate Change Science Program Workshop, .

[12] Dooley, J. J., Dahowski, R. T., Davidson, C. L., Wise, M. A., Gupta, N., Kim, S. H. and Malone, E. L. (2006), *Carbom Dioxide Capture and Geologic Storage;*

Global Energy Technology Strategy Program (GTSP) report, , Battle Memorial Institute, USA.

[13] Feron, P. H. M. and Hendriks, C. A. (2005), "CO2 capture process principles and costs", *Oil and Gas Science and Technology*, vol. 60, no. 3, pp. 451-459.

[14] Iyer, M. V., Gupta, H., Sakadjian, B. B. and Fan, L. -. (2004), "Multicyclic study on the simultaneous carbonation and sulfation of high-reactivity CaO", *Industrial and Engineering Chemistry Research*, vol. 43, no. 14, pp. 3939-3947.

[15] Figueroa, J. D., Fout, T., Plasynski, S., McIlvried, H. and Srivastava, R. D. (2008), "Advances in CO2 capture technology—The U.S. Department of Energy's Carbon Sequestration Program", *International Journal of Greenhouse Gas Control*, vol. 2, no. 1, pp. 9-20.

[16] Elwell, L. C. and Grant, W. S. (2006), *Technology options for capturing CO_2*, available at: E:\Paper-A SET\A111-Technology options for capturing CO2.mht (accessed 4th Nov, 2011).

[17] Manovic, V. and Anthony, E. J. (2009), "Improvement of CaO-based sorbent performance For CO2 looping cycles", *Thermal Science*, vol. 13, no. 1, pp. 89-104.

[18] Murai, S. and Fujioka, Y. (2008), "Challenges to the Carbon dioxide Capture and Storage (CCS) technology", *IEEJ Transactions on Electrical and Electronic Engineering*, vol. 3, no. 1, pp. 37-42.

[19] Finkenrath, M. (2011), *Cost and Performance of Carbon Dioxide Capture from Power Generation*, , International Energy Agency (IEA), France.

[20] Gibbins, J. and Chalmers, H. (2008), "Carbon capture and storage", *Energy Policy*, vol. 36, no. 12, pp. 4317-4322.

[21] Rao, A. B. and Rubin, E. S. (2002), "A technical, economic, and environmental assessment of amine-based CO2 capture technology for power plant greenhouse gas control", *Environmental Science and Technology*, vol. 36, no. 20, pp. 4467-4475.

[22] Steeneveldt, R., Berger, B. and Torp, T. A. (2006), "CO2 Capture and Storage: Closing the Knowing–Doing Gap", *Chemical Engineering Research and Design*, vol. 84, no. 9, pp. 739-763.

[23] Bailey, D. W. and Feron, P. H. M. (2005), "Post-combustion decarbonisation processes", *Oil and Gas Science and Technology*, vol. 60, no. 3, pp. 461-474.

[24] Alie, C., Backham, L., Croiset, E. and Douglas, P. L. (2005), "Simulation of CO2 capture using MEA scrubbing: A flowsheet decomposition method", *Energy Conversion and Management*, vol. 46, no. 3, pp. 475-487.

[25] Pellegrini, G., Strube, R. and Manfrida, G. (2010), "Comparative study of chemical absorbents in postcombustion CO2 capture", *Energy*, vol. 35, no. 2, pp. 851-857.

[26] MacDowell, N., Florin, N., Buchard, A., Hallett, J., Galindo, A., Jackson, G., Adjiman, C. S., Williams, C. K., Shah, N. and Fennell, P. (2010), "An overview of CO2 capture technologies", *Energy and Environmental Science*, vol. 3, no. 11, pp. 1645-1669.

[27] García-Labiano, F., Abad, A., de Diego, L. F., Gayán, P. and Adánez, J. (2002), "Calcination of calcium-based sorbents at pressure in a broad range of CO2 concentrations", *Chemical Engineering Science*, vol. 57, no. 13, pp. 2381-2393.

[28] MacKenzie, A., Granatstein, D. L., Anthony, E. J. and Abanades, J. C. (2007), "Economics of CO2 capture using the calcium cycle with a pressurized fluidized bed combustor", *Energy and Fuels*, vol. 21, no. 2, pp. 920-926.

[29] Supap, T., Idem, R., Tontiwachwuthikul, P. and Saiwan, C. (2006), "Analysis of monoethanolamine and its oxidative degradation products during CO2 absorption from flue gases: A comparative study of GC-MS, HPLC-RID, and CE-DAD analytical techniques and possible optimum combinations", *Industrial and Engineering Chemistry Research*, vol. 45, no. 8, pp. 2437-2451.

[30] Goff, G. S. and Rochelle, G. T. (2004), "Monoethanolamine degradation: O2 mass transfer effects under CO2 capture conditions", *Industrial and Engineering Chemistry Research*, vol. 43, no. 20, pp. 6400-6408.

[31] Belmabkhout, Y., Serna-Guerrero, R. and Sayari, A. (2009), "Adsorption of from dry gases on MCM-41 silica at ambient temperature and high pressure. 1: Pure adsorption", *Chemical Engineering Science*, vol. 64, no. 17, pp. 3721-3728.

[32] Herzog, H., Meldon, J. and Hatton, A. (2009), *Advanced Post-Combustion CO_2 Capture*
, Clean Air Task Force.

[33] Toy, L., Kataria, A., Akunuri, N., Gupta, R., Amin-Sanayei, R., Airaud, C., Lin, C., Schmidhauser, J., Jensvold, J., Coan, F., Chan, R. and Straub, M. (2011), " CO_2 Capture Membrane Process for Power Plant Flue Gas", 22th August, NETL CO2Capture Technology Meeting, Pittsburgh, PA, .

[34] Hermann, W., Bosshard, P., Hung, E., Hunt, R. and Simon, A. J. (2005), *An Assessment of Carbon Capture Technology and Research Opportunities*, , Global Climate and Energy Project, STANFORD UNIVERSITY.

[35] Vision, 2. (2007), *Carbon Dioxide Separation Technology: R&D Needs For the Chemical and Petrochemical Industries*, 2.

[36] Cavenati, S., Grande, C. A. and Rodrigues, A. E. (2006), "Removal of carbon dioxide from natural gas by vacuum pressure swing adsorption", *Energy and Fuels*, vol. 20, no. 6, pp. 2648-2659.

[37] Anthony, E. J. (2008), "Solid looping cycles: A new technology for coal conversion", *Industrial and Engineering Chemistry Research*, vol. 47, no. 6, pp. 1747-1754.

[38] Shen, L., Wu, J. and Xiao, J. (2009), "Experiments on chemical looping combustion of coal with a NiO based oxygen carrier", *Combustion and Flame*, vol. 156, no. 3, pp. 721-728.

[39] Berguerand, N. and Lyngfelt, A. (2008), "Design and operation of a 10 kWth chemical-looping combustor for solid fuels - Testing with South African coal", *Fuel*, vol. 87, no. 12, pp. 2713-2726.

[40] Liang, Y., Harrison, D. P., Gupta, R. P., Green, D. A. and McMichael, W. J. (2004), "Carbon dioxide capture using dry sodium-based sorbents", *Energy and Fuels*, vol. 18, no. 2, pp. 569-575.

[41] Feng, B., An, H. and Tan, E. (2007), "Screening of CO2 adsorbing materials for zero emission power generation systems", *Energy and Fuels*, vol. 21, no. 2, pp. 426-434.

[42] Gupta, H. and Fan, L. -. (2002), "Carbonation-calcination cycle using high reactivity calcium oxide for carbon dioxide separation from flue gas", *Industrial and Engineering Chemistry Research*, vol. 41, no. 16, pp. 4035-4042.

[43] Sarunac, N. (2010), *Flue Gas Heat Recovery in Power Plants, Part I (Power 101)*, available at: E:\Paper-C SET\D41 - Flue gas temperature.mht (accessed 5th Nov., 2011).

[44] Abanades, J. C., Anthony, E. J., Wang, J. and Oakey, J. E. (2005), "Fluidized bed combustion systems integrating CO2 capture with CaO", *Environmental Science and Technology*, vol. 39, no. 8, pp. 2861-2866.

[45] Abanades, J. C., Anthony, E. J., Lu, D. Y., Salvador, C. and Alvarez, D. (2004), "Capture of CO2 from combustion gases in a fluidized bed of CaO", *AICHE Journal*, vol. 50, no. 7, pp. 1614-1622.

[46] Aaron, D. and Tsouris, C. (2005), "Separation of CO2 from flue gas: A review", *Separation Science and Technology*, vol. 40, no. 1-3, pp. 321-348.

[47] Barelli, L., Bidini, G., Gallorini, F. and Servili, S. (2008), "Hydrogen production through sorption-enhanced steam methane reforming and membrane technology: A review", *Energy*, vol. 33, no. 4, pp. 554-570.

[48] Abanades, J. C. and Alvarez, D. (2003), "Conversion limits in the reaction of CO2 with lime", *Energy and Fuels*, vol. 17, no. 2, pp. 308-315.

[49] Hughes, R. W., Macchi, A., Lu, D. Y. and Anthony, E. J. (2009), "Changes in limestones sorbent morphology during CaO-CaCO3 looping at pilot scale", *Chemical Engineering and Technology*, vol. 32, no. 3, pp. 425-434.

[50] Sun, P., Grace, J. R., Lim, C. J. and Anthony, E. J. (2007), "The effect of CaO sintering on cyclic CO2 capture in energy systems", *AIChE Journal*, vol. 53, no. 9, pp. 2432-2442.

[51] Alvarez, D. and Abanades, J. C. (2005), "Pore-size and shape effects on the recarbonation performance of calcium oxide submitted to repeated calcination/recarbonation cycles", *Energy and Fuels*, vol. 19, no. 1, pp. 270-278.

[52] Grasa, G. S., Abanades, J. C., Alonso, M. and González, B. (2008), "Reactivity of highly cycled particles of CaO in a carbonation/calcination loop", *Chemical Engineering Journal*, vol. 137, no. 3, pp. 561-567.

[53] Shimizu, T., Hirama, T., Hosoda, H., Kitano, K., Inagaki, M. and Tejima, K. (1999), "A twin fluid-bed reactor for removal of CO2 from combustion processes", *Chemical Engineering Research and Design*, vol. 77, no. 1, pp. 62-68.

[54] Lu, D. Y., Hughes, R. W. and Anthony, E. J. (2008), "Ca-based sorbent looping combustion for CO2 capture in pilot-scale dual fluidized beds", *Fuel Processing Technology*, vol. 89, no. 12, pp. 1386-1395.

[55] Wang, J., Anthony, E. J. and Abanades, J. C. (2004), "Clean and efficient use of petroleum coke for combustion and power generation", *Fuel*, vol. 83, no. 10, pp. 1341-1348.

[56] Han, C. and Harrison, D. P. (1994), "Simultaneous shift reaction and carbon dioxide separation for the direct production of hydrogen", *Chemical Engineering Science*, vol. 49, no. 24, Part 2, pp. 5875-5883.

[57] Ortiz, A. L. and Harrison, D. P. (2001), "Hydrogen production using sorption-enhanced reaction", *Industrial and Engineering Chemistry Research*, vol. 40, no. 23, pp. 5102-5109.

[58] Lin, S. -., Suzuki, Y., Hatano, H. and Harada, M. (2001), "Hydrogen production from hydrocarbon by integration of water-carbon reaction and carbon dioxide removal (HyPr-RING method)", *Energy and Fuels*, vol. 15, no. 2, pp. 339-343.

[59] Lin, S. -., Suzuki, Y., Hatano, H. and Harada, M. (2002), "Developing an innovative method, HyPr-RING, to produce hydrogen from hydrocarbons", *Energy Conversion and Management*, vol. 43, no. 9-12, pp. 1283-1290.

[60] Stanmore, B. R. and Gilot, P. (2005), "Review—calcination and carbonation of limestone during thermal cycling for CO2 sequestration", *Fuel Processing Technology,* vol. 86, no. 16, pp. 1707-1743.

[61] Manovic, V., Anthony, E. J. and Loncarevic, D. (2009), "SO2 Retention by CaO-based sorbent spent in CO2 looping cycles", *Industrial and Engineering Chemistry Research,* vol. 48, no. 14, pp. 6627-6632.

[62] Blamey, J., Anthony, E. J., Wang, J. and Fennell, P. S. (2010), "The calcium looping cycle for large-scale CO2 capture", *Progress in Energy and Combustion Science,* vol. 36, no. 2, pp. 260-279.

[63] Rodriguez, N., Alonso, M., Grasa, G. and Abanades, J. C. (2008), "Heat requirements in a calciner of CaCO3 integrated in a CO2 capture system using CaO", *Chemical Engineering Journal,* vol. 138, no. 1-3, pp. 148-154.

[64] Alonso, M., Rodríguez, N., Grasa, G. and Abanades, J. C. (2009), "Modelling of a fluidized bed carbonator reactor to capture CO2 from a combustion flue gas", *Chemical Engineering Science,* vol. 64, no. 5, pp. 883-891.

[65] Ryu, H. -., Park, Y. -., Jo, S. -. and Park, M. -. (2008), "Development of novel two-interconnected fluidized bed system", *Korean Journal of Chemical Engineering,* vol. 25, no. 5, pp. 1178-1183.

[66] Davidson, J. F., Clift, R. and Harrison, D. (1985), *Fluidization,* 2nd ed, Academic Press, London.

[67] Geldart, D. (2008), "Use of non-mechanical valves at high temperature - A case study", *Canadian Journal of Chemical Engineering,* vol. 86, no. 3, pp. 605-607.

[68] Yang, W. (2003), *Hand book of Fluidization and Fluid-particle Systems,* 3th ed, CRC Press.

[69] Grasa, G. S. and Abanades, J. C. (2006), "CO2 capture capacity of CaO in long series of carbonation/calcination cycles", *Industrial and Engineering Chemistry Research,* vol. 45, no. 26, pp. 8846-8851.

[70] Anthony, E. J. and Granatstein, D. L. (2001), "Sulfation phenomena in fluidized bed combustion systems", *Progress in Energy and Combustion Science,* vol. 27, no. 2, pp. 215-236.

[71] Sun, P., Grace, J. R., Lim, C. J. and Anthony, E. J. (2007), "Sequential capture of CO2 and SO2 in a pressurized TGA simulating FBC conditions", *Environmental Science and Technology,* vol. 41, no. 8, pp. 2943-2949.

[72] Hughes, R. W., Lu, D. Y., Anthony, E. J. and MacChi, A. (2005), "Design, process simulation and construction of an atmospheric dual fluidized bed

combustion system for in situ CO2 capture using high-temperature sorbents", *Fuel Processing Technology,* vol. 86, no. 14-15, pp. 1523-1531.

[73] Abanades, J. C., Grasa, G., Alonso, M., Rodriguez, N., Anthony, E. J. and Romeo, L. M. (2007), "Cost structure of a postcombustion CO2 capture system using CaO", *Environmental Science and Technology,* vol. 41, no. 15, pp. 5523-5527.

[74] Romeo, L. M., Lara, Y., Lisbona, P. and Martínez, A. (2009), "Economical assessment of competitive enhanced limestones for CO2 capture cycles in power plants", *Fuel Processing Technology,* vol. 90, no. 6, pp. 803-811.

[75] Romeo, L. M., Lara, Y., Lisbona, P. and Escosa, J. M. (2009), "Optimizing make-up flow in a CO2 capture system using CaO", *Chemical Engineering Journal,* vol. 147, no. 2-3, pp. 252-258.

[76] Schuster, A. (. (2007), *C3-Capture; Calcium Cycle for Efficient and Low-cost CO_2 Capture using Fluidised Bed System,* available at: http://ec.europa.eu/research/energy/pdf/synopses_co2_en.pdf (accessed Nov. 2011).

[77] Silcox, G. D., Kramlich, J. C. and Pershing, D. W. (1989), "A mathematical model for the flash calcination of dispersed CaCO3 and Ca(OH)2 particles", *Industrials Engineering Chemistry Research®,* vol. 28, no. 2, pp. 155-160.

[78] Borgwardt, R. H. (1985), "CALCINATION KINETICS AND SURFACE AREA OF DISPERSED LIMESTONE PARTICLES.", *AIChE Journal,* vol. 31, no. 1, pp. 103-111.

[79] Ye, Z., Wang, W., Zhong, Q. and Bjerle, I. (1995), "High temperature desulfurization using fine sorbent particles under boiler injection conditions", *Fuel,* vol. 74, no. 5, pp. 743-750.

[80] Sun, P., Grace, J. R., Lim, C. J. and Anthony, E. J. (2008), "Investigation of attempts to improve cyclic CO2 capture by sorbent hydration and modification", *Industrial and Engineering Chemistry Research,* vol. 47, no. 6, pp. 2024-2032.

[81] Huang, J. and Daugherty, K. E. (1988), "Inhibition of the calcination of calcium carbonate", *Thermochimica Acta,* vol. 130, no. 0, pp. 173-176.

[82] Huang, J. and Daugherty, K. E. (1987), "Lithium carbonate enhancement of the calcination of calcium carbonate: proposed extended-shell model", *Thermochimica Acta,* vol. 118, no. 0, pp. 135-141.

[83] Agnew, J., Hampartsoumian, E., Jones, J. M. and Nimmo, W. (2000), "Simultaneous calcination and sintering of calcium based sorbents under a combustion atmosphere", *Fuel,* vol. 79, no. 12, pp. 1515-1523.

[84] Schmalzried, H. (1974), *Solid State Reactions*, 1th ed, Academic Press, New York.

[85] Sun, P., Grace, J. R., Lim, C. J. and Anthony, E. J. (2007), "Removal of CO2 by calcium-based sorbents in the presence of SO2", *Energy and Fuels*, vol. 21, no. 1, pp. 163-170.

[86] Chrissafis, K. and Paraskevopoulos, K. M. (2005), "The effect of sintering on the maximum capture efficiency of CO 2 using a carbonation/calcination cycle of carbonate rocks", *Journal of Thermal Analysis and Calorimetry*, vol. 81, no. 2, pp. 463-468.

[87] H. Borgwardt, R. (1989), "Sintering of nascent calcium oxide", *Chemical Engineering Science*, vol. 44, no. 1, pp. 53-60.

[88] Silaban, A. and Harrison, D. P. (1995), "High temperature capture of carbon dioxide: characteristics of the reversible reaction between CaO(s) and CO2(g)", *Chemical Engineering Communications*, vol. 137, pp. 177-190.

[89] Mess, D., Sarofim, A. F. and Longwell, J. P. (1999), "Product layer diffusion during the reaction of calcium oxide with carbon dioxide", *Energy and Fuels*, vol. 13, no. 5, pp. 999-1005.

[90] Aihara, M., Nagai, T., Matsushita, J., Negishi, Y. and Ohya, H. (2001), "Development of porous solid reactant for thermal-energy storage and temperature upgrade using carbonation/decarbonation reaction", *Applied Energy*, vol. 69, no. 3, pp. 225-238.

[91] Barker, R. (1973), "REVERSIBILITY OF THE REACTION CaCO//3 reversible reaction CaO plus CO//2.", *J Appl Chem Biotechnol*, vol. 23, no. 10, pp. 733-742.

[92] Bhatia, S. K. and Perlmutter, D. D. (1983), "Effect of the product layer on the kinetics of the CO2-lime reaction", *AIChE Journal*, vol. 29, no. 1, pp. 79-86.

[93] Abanades, J. C., Rubin, E. S. and Anthony, E. J. (2004), "Sorbent cost and performance in CO2 capture systems", *Industrial and Engineering Chemistry Research*, vol. 43, no. 13, pp. 3462-3466.

[94] Abanades, J. C. (2002), "The maximum capture efficiency of CO2 using a carbonation/calcination cycle of CaO/CaCO3", *Chemical Engineering Journal*, vol. 90, no. 3, pp. 303-306.

[95] Wang, J. and Anthony, E. J. (2005), "On the decay behavior of the CO2 absorption capacity of CaO-based sorbents", *Industrial and Engineering Chemistry Research*, vol. 44, no. 3, pp. 627-629.

[96] Góra, D., Anthony, E. J., Bulewicz, E. M. and Jia, L. (2006), "Steam reactivation of 16 bed and fly ashes from industrial-scale coal-fired fluidized bed combustors", *Fuel*, vol. 85, no. 1, pp. 94-106.

[97] Manovic, V. and Anthony, E. J. (2008), "Sequential SO2/CO2 capture enhanced by steam reactivation of a CaO-based sorbent", *Fuel*, vol. 87, no. 8-9, pp. 1564-1573.

[98] Salvador, C., Lu, D., Anthony, E. J. and Abanades, J. C. (2003), "Enhancement of CaO for CO2 capture in an FBC environment", *Chemical Engineering Journal*, vol. 96, no. 1-3, pp. 187-195.

[99] Chrissafis, K. (2007), "Multicyclic study on the carbonation of CaO using different limestones", *Journal of Thermal Analysis and Calorimetry*, vol. 89, no. 2, pp. 525-529.

[100] Reddy, E. P. and Smirniotis, P. G. (2004), "High-temperature sorbents for CO2 made of alkali metals doped on CaO supports", *Journal of Physical Chemistry B*, vol. 108, no. 23, pp. 7794-7800.

[101] Chen, Z., Song, H. S., Portillo, M., Lim, C. J., Grace, J. R. and Anthony, E. J. (2009), "Long-term calcination/carbonation cycling and thermal pretreatment for CO2 capture by limestone and dolomite", *Energy and Fuels*, vol. 23, no. 3, pp. 1437-1444.

[102] Reijers, H., Elzinga, G. D., Cobden, P. D., Haije, W. G. and van den Brink, R. W. (2011), "Tandem bed configuration for sorption-enhanced steam reforming of methane", *International Journal of Greenhouse Gas Control*, vol. 5, no. 3, pp. 531-537.

[103] Barelli, L., Bidini, G., Corradetti, A. and Desideri, U. (2007), "Production of hydrogen through the carbonation-calcination reaction applied to CH4/CO2 mixtures", *Energy*, vol. 32, no. 5, pp. 834-843.

[104] Solieman, A. A. A., Dijkstra, J. W., Haije, W. G., Cobden, P. D. and van den Brink, R. W. (2009), "Calcium oxide for CO2 capture: Operational window and efficiency penalty in sorption-enhanced steam methane reforming", *International Journal of Greenhouse Gas Control*, vol. 3, no. 4, pp. 393-400.

[105] Johnsen, K., Ryu, H. J., Grace, J. R. and Lim, C. J. (2006), "Sorption-enhanced steam reforming of methane in a fluidized bed reactor with dolomite as CO2-acceptor", *Chemical Engineering Science*, vol. 61, no. 4, pp. 1195-1202.

[106] Hughes, R. W., Lu, D., Anthony, E. J. and Wu, Y. (2004), "Improved long-term conversion of limestone-derived sorbents for in situ capture of CO2 in a fluidized bed combustor", *Industrial and Engineering Chemistry Research*, vol. 43, no. 18, pp. 5529-5539.

[107] Han, C., Silaban, A., Narcida, M. and Harrison, D. P. (1994), *Calcium oxide sorbent process for bulk separation of carbon dioxide,* Technical report; DE95011399, Technical report to Department of Energy, US.

[108] Dobner, S., Sterns, L., Graff, R. A. and Squires, A. M. (1977), "Cyclic calcination and recarbonation of calcined dolomite", *Industrial and Engineering Chemistry Process Design and Development,* vol. 16, no. 4, pp. 479-486.

[109] Shaojun, Y. and Yunhan, X. (2008), "Steam catalysis in CaO carbonation under low steam partial pressure", *Industrial and Engineering Chemistry Research,* vol. 47, no. 12, pp. 4043-4048.

[110] Donat, F., Florin, N. H., Anthony, E. J. and Fennell, P. S. (2012), "Influence of high-temperature steam on the reactivity of CaO sorbent for CO 2 capture", *Environmental Science and Technology,* vol. 46, no. 2, pp. 1262-1269.

[111] Wang, Y. and Thomson, W. J. (1995), "The effects of steam and carbon dioxide on calcite decomposition using dynamic X-ray diffraction", *Chemical Engineering Science,* vol. 50, no. 9, pp. 1373-1382.

[112] Fuertes, A. B., Alvarez, D., Rubiera, F., Pis, J. J. and Marban, G. (1991), "Surface Area and Pore Size Changes during Sintering of Calcium Oxide Particles", vol. 109, no. Chem. Eng. Commun., pp. 73-88.

[113] Borgwardt, R. H. (1989), "Calcium oxide sintering in atmospheres containing water and carbon dioxide", *Industrial and Engineering Chemistry Research®,* vol. 28, no. 4, pp. 493-500.

[114] Wang, Y., Lin, S. and Suzuki, Y. (2007), "Study of limestone calcination with CO2 capture: Decomposition behavior in a CO2 atmosphere", *Energy and Fuels,* vol. 21, no. 6, pp. 3317-3321.

[115] Wang, Y., Lin, S. and Suzuki, Y. (2010), "Experimental study on CO2 capture conditions of a fluidized bed limestone decomposition reactor", *Fuel Processing Technology,* vol. 91, no. 8, pp. 958-963.

[116] Khraisha, Y. H. and Dugwell, D. R. (1991), "Effect of water vapour on the calcination of limestone and raw meal in a suspension reactor", *Chemical Engineering Research and Design,* vol. 69, no. 1, pp. 76-78.

[117] Burnham, A. K., Stubblefield, C. T. and Campbell, J. H. (1980), "EFFECTS OF GAS ENVIRONMENT ON MINERAL REACTIONS IN COLORADO OIL SHALE.", *Fuel,* vol. 59, no. 12, pp. 871-877.

[118] Jia, L., Tan, Y., Wang, C. and Anthony, E. J. (2007), "Experimental study of oxy-fuel combustion and sulfur capture in mini-CFBC", *Energy and Fuels,* vol. 21, no. 6, pp. 3160-3164.

[119] Li, Y., Buchi, S., Grace, J. R. and Lim, C. J. (2005), "SO2 removal and CO2 capture by limestone resulting from calcination/sulfation/carbonation cycles", *Energy and Fuels,* vol. 19, no. 5, pp. 1927-1934.

[120] Hartman, M. and Trnka, O. (1993), "Reactions between calcium oxide and flue gas containing silfur dioxide at lower temperatures", vol. 39, no. A.I.Ch.E.J., pp. 615-624.

[121] Duo, W., Sevill, J. P. K., Kirkby, N. F. and Clift, R. (1994), "Formation of product layers in solid-gas reactions for removal of acid gases", *Chemical Engineering Science,* vol. 49, no. 24 PART A, pp. 4429-4442.

[122] Manovic, V. and Anthony, E. J. (2010), "Competition of sulphation and carbonation reactions during looping cycles for CO2 capture by cao-based sorbents", *Journal of Physical Chemistry A,* vol. 114, no. 11, pp. 3997-4002.

[123] Grasa, G. S., Alonso, M. and Abanades, J. C. (2008), "Sulfation of CaO particles in a carbonation/calcination loop to capture CO2", *Industrial and Engineering Chemistry Research,* vol. 47, no. 5, pp. 1630-1635.

[124] Ryu, H. -., Grace, J. R. and Lim, C. J. (2006), "Simultaneous CO2/SO2 capture characteristics of three limestones in a fluidized-bed reactor", *Energy and Fuels,* vol. 20, no. 4, pp. 1621-1628.

[125] Manovic, V. and Anthony, E. J. (2010), "Sulfation performance of CaO-based pellets supported by calcium aluminate cements designed for high-temperature CO2 capture", *Energy and Fuels,* vol. 24, no. 2, pp. 1414-1420.

[126] Chen, H., Zhao, C., Li, Y. and Chen, X. (2010), "CO2 capture performance of calcium-based sorbents in a pressurized carbonation/calcination loop", *Energy and Fuels,* vol. 24, no. 10, pp. 5751-5756.

[127] Sakadjian, B. B., Iyer, M. V., Gupta, H. and Fan, L. -. (2007), "Kinetics and structural characterization of calcium-based sorbents calcined under subatmospheric conditions for the high-temperature CO2 capture process", *Industrial and Engineering Chemistry Research,* vol. 46, no. 1, pp. 35-42.

[128] Dennis, J. S. and Hayhurst, A. N. (1987), "the effect of CO2 on the kinetics and extent of calcination of limestone and dolomite particles in fluidised beds", *Chemical Engineering Science,* vol. 42, no. 10, pp. 2361-2372.

[129] Khraisha, Y. H. and Dugwell, D. R. (1989), "Thermal decomposition of limestone in a suspension reactor", *Chemical Engineering Research and Design,* vol. 67, no. 1, pp. 52-57.

[130] Fuertes, A. B., Marban, G. and Rubiera, F. (1993), "Kinetics of thermal decomposition of limestone particles in a fluidized bed reactor", *Chemical Engineering Research and Design,* vol. 71, no. A4, pp. 421-428.

[131] Khinast, J., Krammer, G. F., Brunner, C. and Staudinger, G. (1996), "Decomposition of limestone: The influence of CO2 and particle size on the reaction rate", *Chemical Engineering Science,* vol. 51, no. 4, pp. 623-634.

[132] Liu, H., Katagiri, S., Kaneko, U. and Okazaki, K. (2000), "Sulfation behavior of limestone under high CO2 concentration in O2/CO2 coal combustion", *Fuel,* vol. 79, no. 8, pp. 945-953.

[133] ECN, P. (2011), *The composition of biomass and waste*, available at: http://www.ecn.nl/phyllis/ (accessed Jan,2010).

[134] Basu, P. (2006), *Combustion and Gasification in Fluidized Beds,* CRC Press.

[135] Kim, H. T. and Kwon, H. B. (1998), "Kinetic Study of Limestone Calcination and Sulfation Reaction Under AFBC Environment", vol. 3, no. Environ. Eng. Res., pp. 105-113.

[136] Ewing, J., Beruto, L. and Searcy, A. (1979), "The nature of CaO produced by calcite powder decomposition in vacuum and in CO_2", vol. 62, no. J. Am. Ceram. Soc., pp. 580-584.

[137] Beruto, D., Barco, L. and Searcy, A. W. (1984), "CO_2-catalyzed surface area and porosity changes in high-surface area CaO aggregates", vol. 67, no. J. Am. Ceram. Soc., pp. 512-515.

[138] Shaojun, Y. and Yunhan, X. (2008), "Steam catalysis in CaO carbonation under low steam partial pressure", *Industrial and Engineering Chemistry Research,* vol. 47, no. 12, pp. 4043-4048.

[139] Fujimoto, S., Bilgen, E. and Ogura, H. (2002), "CaO/Ca(OH)2 chemical heat pump system", *Energy Conversion and Management,* vol. 43, no. 7, pp. 947-960.

[140] Snow, M. J. H., Longwell, J. P. and Sarofim, A. F. (1988), "Direct sulfation of calcium carbonate", *Industrial and Engineering Chemistry Research,* vol. 27, no. 2, pp. 268-273.

[141] Borgwardt, R. H., Bruce, K. R. and Blake, J. (1987), "An investigation of product-layer diffusivity for CaO sulfation", *Industrial and Engineering Chemistry Research,* vol. 26, no. 10, pp. 1993-1998.

[142] Borgwardt, R. H. and Bruce, K. R. (1986), "EFFECT OF SPECIFIC SURFACE AREA ON THE REACTIVITY OF CaO WITH SO//2.", *AIChE Journal,* vol. 32, no. 2, pp. 239-246.

[143] Hsia, C., St. Pierre, G. R. and Fan, L. -. (1995), "Isotope study on diffusion in CaSO4 formed during sorbent-flue-gas reaction", *AIChE Journal,* vol. 41, no. 10, pp. 2337-2340.

[144] Hsia, C., St. Pierre, G. R., Raghunathan, K. and Fan, L. -. (1993), "Diffusion through CaSO4 formed during the reaction of CaO with SO2 and O2", *AIChE Journal*, vol. 39, no. 4, pp. 698-700.

[145] Bhatia, S. K. and Perlmutter, D. D. (1981), "EFFECT OF PORE STRUCTURE ON FLUID-SOLID REACTIONS: APPLICATION TO THE SO//2-LIME REACTION.", *AIChE Journal*, vol. 27, no. 2, pp. 226-234.

[146] Borgwardt, R. H., Bruce, K. R. and Blake, J. (1984), "EPA Experimental Stydies of the Mechanisms of Sulfur Capture by Limestone", Sandiego, Symp. on Dry SO2 and Simutaneous SO2/NOx Control Technology, .

[147] Milne, C. R. and Pershing, D. W. (1987), "Time resolved sulfation rate measurements for sized sorbents", *In Proceedings of the 4th Annual Pittsburgh Coal Conference*, pp. 109.

[148] Sandler, S. I. (ed.) (1999), *Chemical and Engineering Thermodynamics*, Third ed, John Wiley and Sons, USA.